frontiers | Research Topics

Women in lens and cataract

Edited by
Catherine Cheng and Barbara Pierscionek

Published in
Frontiers in Ophthalmology

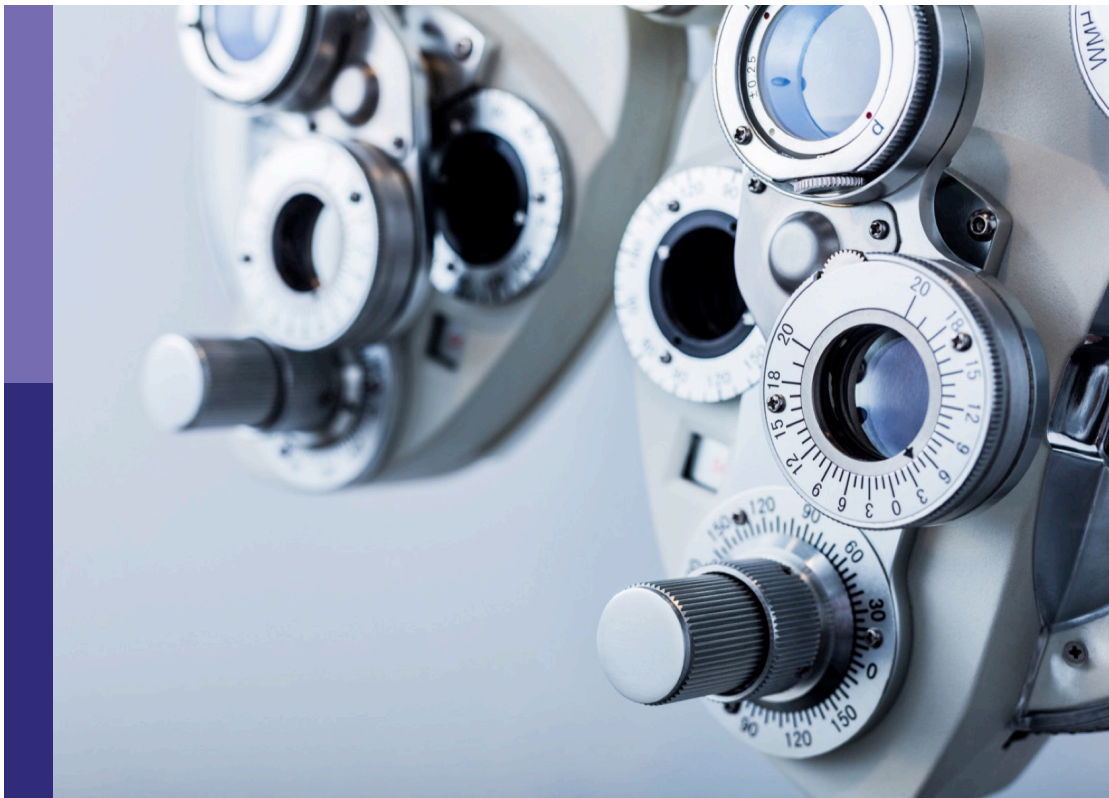

ISSN 1664-8714
ISBN 978-2-8325-6376-2
DOI 10.3389/978-2-8325-6376-2

About Frontiers

Frontiers is more than just an open access publisher of scholarly articles: it is a pioneering approach to the world of academia, radically improving the way scholarly research is managed. The grand vision of Frontiers is a world where all people have an equal opportunity to seek, share and generate knowledge. Frontiers provides immediate and permanent online open access to all its publications, but this alone is not enough to realize our grand goals.

Frontiers journal series

The Frontiers journal series is a multi-tier and interdisciplinary set of open-access, online journals, promising a paradigm shift from the current review, selection and dissemination processes in academic publishing. All Frontiers journals are driven by researchers for researchers; therefore, they constitute a service to the scholarly community. At the same time, the *Frontiers journal series* operates on a revolutionary invention, the tiered publishing system, initially addressing specific communities of scholars, and gradually climbing up to broader public understanding, thus serving the interests of the lay society, too.

Dedication to quality

Each Frontiers article is a landmark of the highest quality, thanks to genuinely collaborative interactions between authors and review editors, who include some of the world's best academicians. Research must be certified by peers before entering a stream of knowledge that may eventually reach the public - and shape society; therefore, Frontiers only applies the most rigorous and unbiased reviews. Frontiers revolutionizes research publishing by freely delivering the most outstanding research, evaluated with no bias from both the academic and social point of view. By applying the most advanced information technologies, Frontiers is catapulting scholarly publishing into a new generation.

What are Frontiers Research Topics?

Frontiers Research Topics are very popular trademarks of the *Frontiers journals series*: they are collections of at least ten articles, all centered on a particular subject. With their unique mix of varied contributions from Original Research to Review Articles, Frontiers Research Topics unify the most influential researchers, the latest key findings and historical advances in a hot research area.

Find out more on how to host your own Frontiers Research Topic or contribute to one as an author by contacting the Frontiers editorial office: frontiersin.org/about/contact

Women in lens and cataract

Topic editors
Catherine Cheng — Indiana University, United States
Barbara Pierscionek — Anglia Ruskin University, United Kingdom

Citation
Cheng, C., Pierscionek, B., eds. (2025). *Women in lens and cataract*. Lausanne: Frontiers Media SA. doi: 10.3389/978-2-8325-6376-2

Table of contents

frontiers | Frontiers in Ophthalmology

TYPE Editorial
PUBLISHED 09 May 2025
DOI 10.3389/fopht.2025.1616466

OPEN ACCESS

EDITED AND REVIEWED BY
Michael Wormstone,
The University of Nottingham Ningbo (China), China

*CORRESPONDENCE
Catherine Cheng
ckcheng@iu.edu
Barbara Pierscionek
barbara.pierscionek@aru.ac.uk

RECEIVED 22 April 2025
ACCEPTED 25 April 2025
PUBLISHED 09 May 2025

CITATION
Cheng C and Pierscionek B (2025) Editorial: Women in lens and cataract. *Front. Ophthalmol.* 5:1616466. doi: 10.3389/fopht.2025.1616466

Editorial: Women in lens and cataract

Catherine Cheng[1]* and Barbara Pierscionek[2]*

[1]School of Optometry and Vision Science Program, Indiana University, Bloomington, IN, United States, [2]Faculty of Health Medicine and Social Care, Medical Technology Research Centre, Anglia Ruskin University, Chelmsford, United Kingdom

KEYWORDS

lens, cataract, biomechanics, oxidation, microcirculation, signalling, glutathione, connexin

Editorial on the Research Topic
Women in lens and cataract

The ocular lens is a highly organized and complex tissue that is an ideal model for understanding the challenges of aging and long-term cellular and molecular homeostasis. This transparent and ellipsoid tissue in the anterior chamber of the eye changes shape to fine-tune the focusing of light onto the retina to form a clear image. The lens is suspended behind the iris by a ring of thin zonules that are connected to the ciliary muscles. The tension exerted by the zonules on the lens changes during muscle contractions that allow for the lens shape changes to focus on near objects through the process of accommodation.

At first glance, the lens is deceptively simple because it is devoid of blood vessels and nerves, and the entire tissue is made up of just two cell types, a monolayer of epithelial cells covering the anterior hemisphere and a bulk mass of fiber cells that differentiate from epithelial cells. Yet, the seeming lack of complexity in structure and function is enigmatic; the structure/function relationship between lens proteins and its optical and biomechanical properties, how the lens proteins change with age, and what mechanisms lead to age-related pathologies remain unanswered. The lens poses extraordinary challenges for cellular homeostasis because all the lens cells ever made in the lens are retained in the tissue. The lens never loses or sheds any cells, and it continues to grow by accruing new layers of cells overlaid onto existing generations of lens fiber cells, akin to the growth mode that creates rings in a tree. The oldest lens cells, which are also some of the oldest cells in the body, are at the center of tissue through which the optic axis passes. As an avascular tissue, the lens generates its own microcirculation current to transport of nutrients, antioxidants, and other small molecules to maintain life-long growth and homeostasis.

The elegance of this clear and light-focusing tissue is only revealed at close examination of the cell-cell interactions and 3D architecture. The review by Greiling et al. undertakes an investigation of the lens structure/function relationship from a different perspective: that of the lamellar formation of the lens that is a consequence of its mode of growth and how this may be linked to its microcirculation and hence maintenance of transparency. Work by Crews et al. considers the biomechanical aspects and how changes in lens shape and tension may impact on transport of nutrients. Variability of diffusion patterns between anterior and posterior lens poles was noted for three of the dyes, and one dye suggested an active transport mechanism may be present. The lens microcirculation pathway requires large gap

junction plaques made from connexin proteins, and the importance of gap junction communication in lens and eye growth and homeostasis are revealed in two articles. Painter et al. used optical coherence tomography to reveal that loss of connexin 50 in mouse lenses led to changes in anterior chamber depth, suggesting that normal lens size and growth are a prerequisite for normal eye size and development. Sellitto and White show that connexin 50, hosphoinositide 3-kinase (PI3K), and phosphatase and tensin homolog (PTEN) all play roles in lens size and growth.

The prevention or minimization of protein oxidation is another factor for maintaining lens homeostasis. A fascinating study on circadian rhythms in the lens presents a number of avenues for further study on regulation of a major antioxidant, namely glutathione (Li et al.). The implications of these results are that glutathione and enzymes responsible for its homeostasis may be dependent on circadian rhythms and that oxidative stress in the lens could be regulated by manipulating the circadian clock. This offers a novel and exciting means of controlling the health of the lens and potentially maintaining transparency.

Cataracts, defined as any opacity in the lens, remain the leading cause of blindness in the world. We continue to explore the genes, signaling pathways, age-related protein changes, and external factors that can lead to cataractogenesis. Choquet et al. reveal novel genetic markers for age-related cataract development, suggesting markers for genetic susceptibility to cataracts may exist outside the lens tissue. Dysfunction of the Eph/ephrin bidirectional signaling pathway has been linked to congenital and age-related cataracts in human patients. Huynh and Cheng conducted a thorough investigation of the expression levels of the Eph/ephrin genes in the lens that change with age or due to disruption of the signaling pathway. A detailed mass spectrometry study by Paredes et al. describes the irreversible crosslinking of proteins through the formation of reactive intermediates, dehydroalanine (DHA) and dehydrobutyrine (DHB). Increased levels of DHA and DHB are found in cataractous lenses, suggesting that protein crosslinking is linked to age-related opacities. The role of light, and in particular UV light, on the biochemical properties of the lens is reviewed by MacFarlane et al. Whether UV exposure leads to cataract or expediates the process of cataract formation has been debated for decades. MacFarlane et al. considered several different animal models of UV light exposure to gain a deeper comprehension of the effects of UV light on lens structure and function. Collectively, these studies reveal the potential causes for cataracts from genetic variation to protein aggregation to exposure to UV rays. It is likely that a combination of these factors contributes to the development of cataracts. Recent focus on elucidating the mechanisms for cataractogenesis, especially age-related opacities, will lead to novel non-surgical methods to prevent or delay cataracts.

We were delighted to curate this special topic with 7 original articles and 2 reviews to highlight the contribution of women to vision science and lens research. While there has been an increase in women in STEM, we welcome further opportunities to foster scientific curiosity in girls and encourage new generations of women to pursue careers in engineering, math, and science.

Author contributions

CC: Writing – review & editing, Writing – original draft. BP: Writing – original draft, Writing – review & editing.

Funding

The author(s) declare that no financial support was received for the research and/or publication of this article.

Conflict of interest

The authors declare that the research was conducted in the absence of any commercial or financial relationships that could be construed as a potential conflict of interest.

The author(s) declared that they were an editorial board member of Frontiers, at the time of submission. This had no impact on the peer review process and the final decision.

Generative AI statement

The author(s) declare that no Generative AI was used in the creation of this manuscript.

Publisher's note

frontiers | Frontiers in Ophthalmology

TYPE Original Research
PUBLISHED 26 October 2023
DOI 10.3389/fopht.2023.1241001

OPEN ACCESS

EDITED BY
Jeff Gross,
The University of Texas at Austin,
United States

REVIEWED BY
Mason Posner,
Ashland University, United States
Juliet Moncaster,
Boston University, United States

*CORRESPONDENCE
Kevin L. Schey
kevin.schey@vanderbilt.edu

RECEIVED 15 June 2023
ACCEPTED 02 October 2023
PUBLISHED 26 October 2023

CITATION
Paredes J, Wang Z, Patel P, Rose KL and Schey KL (2023) Dehydroalanine and dehydrobutyrine in aging and cataractous lenses reveal site-specific consequences of spontaneous protein degradation. *Front. Ophthalmol.* 3:1241001. doi: 10.3389/fopht.2023.1241001

Dehydroalanine and dehydrobutyrine in aging and cataractous lenses reveal site-specific consequences of spontaneous protein degradation

Jessica Paredes[1], Zhen Wang[2], Purvi Patel[3], Kristie L. Rose[2,3] and Kevin L. Schey[1,2,3]*

[1]Department of Chemistry, Vanderbilt University, Nashville, TN, United States, [2]Department of Biochemistry, Vanderbilt University, Nashville, TN, United States, [3]Mass Spectrometry Research Center, Vanderbilt University, Nashville, TN, United States

Introduction: Protein post-translational modifications (PTMs) have been associated with aging and age-related diseases. PTMs are particularly impactful in long-lived proteins, such as those found in the ocular lens, because they accumulate with age. Two PTMs that lead to protein-protein crosslinks in aged and cataractous lenses are dehydroalanine (DHA) and dehydrobutyrine (DHB); formed from cysteine/serine and threonine residues, respectively. The purpose of this study was to quantitate DHA and DHB in human lens proteins as a function of age and cataract status.

Methods: Human lenses of various ages were divided into five donor groups: transparent lenses (18–22-year-old, 48–64-year-old, and 70–93-year-old) and cataractous human lenses of two age groups (48–64-year-old lenses, and 70–93-year-old lenses) and were subjected to proteomic analysis. Relative DHA and DHB peptide levels were quantified and compared to their non-modified peptide counterparts.

Results: For most lens proteins containing DHA or DHB, higher amounts of DHA- and DHB-modified peptides were detected in aged and cataractous lenses. DHA-containing peptides were classified into three groups based on abundance changes with age and cataract: those that (1) increased only in age-related nuclear cataract (ARNC), (2) increased in aged and cataractous lenses, and (3) decreased in aged lenses and ARNC. There was no indication that DHA or DHB levels were dependent on lens region. In most donor groups, proteins with DHA and DHB were more likely to be found among urea-insoluble proteins rather than among water- or urea-soluble proteins.

Discussion: DHA and DHB formation may induce structural effects that make proteins less soluble in water that leads to age-related protein insolubility and possibly aggregation and light scattering.

KEYWORDS

post-translational modifications, proteomics, lens, cataracts, aging

1 Introduction

The function of the ocular lens depends on the stability of long-lived proteins due to the almost non-existent protein turnover in mature lens fiber cells (1–4). However, the vulnerability of long-lived proteins to spontaneous degradation has been implicated in the formation of high-molecular weight crosslinks and protein aggregation in the lens (4–7). Highly studied age-related post-translational modifications (PTMs) such as deamidation (8, 9), oxidation (10–13), and crosslinking (14–16) have been identified in lens proteins and linked to age-related diseases in other tissues (15, 17). Proteins in the lens are exposed to reactive oxygen species during aging and some oxidized products, such as protein disulfides, can be reversed by protective mechanisms (18–20). Oxidative stress repair biomolecules in the lens, such as glutathione (GSH), and small heat-shock proteins, such as α-crystallins, are subject to age-related decline or modification (21–24). Increased oxidation with age can result in irreversible oxidation products that limit the ability of protective biomolecules to maintain lens transparency (25, 26). Over time, oxidative damage accumulates in the lens, which leads to age-related nuclear cataracts (ARNC) (16, 27). Opacification of the nucleus of the lens in ARNC has been associated with an increase of high-molecular weight crosslinks, protein-protein aggregation, and a reduction of protein-solubility (28).

Irreversible PTMs can result in protein-protein crosslinking and aggregation. Reactive intermediates that lead to irreversible crosslinking are dehydroalanine (DHA) and dehydrobutyrine (DHB) (29). The formation of DHA and DHB residues in proteins is caused by a β-elimination reaction occurring on cysteine, serine, phosphoserine residues for DHA and on phosphothreonine, or threonine residues for DHB. A scheme for DHA formation is shown in Figure 1. DHA has been identified in long-lived proteins in lens tissue (30) and has been hypothesized to form via both nonenzymatic and enzymatic mechanisms (31, 32). After DHA or DHB form, these intermediates can react with nucleophilic residues in proteins such as cysteine to form lanthionine, histidine to form histodinoalanine, and lysine to form lysinoalanine (33). These reaction products have been identified in significantly higher levels in cataractous lenses compared to age-matched transparent lenses (33, 34). DHA can also react with cysteine on GSH, and DHA-GSH crosslinks on essential proteins for lens transparency have been associated with aging and cataracts (25). Although DHA-mediated crosslinks have been identified, the stability, abundance, and effects of DHA and DHB modifications have not been examined. In this study, we quantified the abundances of DHA and DHB in five groups of transparent and cataractous human lenses across the age ranges 18-22-years-old, 48-64-years-old, 48-64-years-old with cataracts, 70-93-years-old, and 70-93-years-old with cataracts. Our results suggest that DHA and DHB formation can lead to insolubilization of multiple lens proteins and is often elevated in cataract lenses.

Abbreviations: PTM, Post-translational Modification; GSH, Glutathione; ARNC, Age-related Nuclear Cataracts; DHA, Dehydroalanine; DHB, Dehydrobutyrine; C, Cortex; ON, Outer Nucleus; IN, Inner Nucleus; WSF, Water-Soluble Fraction; USF, Urea-Soluble Fraction; UIF, Urea-Insoluble Fraction; BCA, Bicinchoninic Acid Assay; LC-MS/MS, Liquid chromatography tandem mass spectrometry; CAN, Acenonitrile; STAGE, Stop and Go Extraction; FDR, False Discovery Rate; FAMD, Factor Analysis of Mixed Data; ANOVA, Analysis of Variance; BFSP2, Phakinin; BFSP1, Filensin; CRYAA, αA-crystallin.

2 Materials and methods

The methods of preparing, measuring, and analyzing data were conducted as outlined in Wang and Schey in 2018 (25).

2.1 Lens samples

Senior donors with and without advanced stages of ARNC were received as a gift from Dr. Donita Garland. Lenses older than 70 years old were selected for proteomic analysis and data collected were added to the dataset from Wang and Schey (25). An image of each lens in this older group, before dissection, can be found in Supplementary Figure 1. Meta data for each lens can be found in Table 1. Lenses analyzed by Wang and Schey (25) were from donors in the following groups: ages 18-22-years-old with no cataract history, ages 48-64-years-old with no cataract history, and ages 48-64-years-old with cataract (25). These lenses were obtained from NDRI (Philadelphia, PA). Each group had 4 lenses except for 70-93-years-old lenses, which was composed of three lenses. Lenses were excluded if lenses were deformed or were badly dissected. Two lenses with ARNC, aged 70 and 75, had both nuclear cataracts and posterior subcortical cataracts.

2.2 Lens dissection

Anterior and posterior regions of the lens were removed by sectioning equatorially at 30 μm thickness using a Lecia CM3050 S Research Cryostat (Leica Biosystems, Buffalo Grove, IL, USA) and about 1 mm from the anterior pole and 1.5 mm from the posterior pole were removed. Lens cortex (C), outer nucleus (ON), and inner nucleus (IN) regions were dissected from the remaining uncut lens based on radial distance from the lens center using surgical trephines. The IN was defined as the lens region from the lens center to a radial distance of 4.5 mm. The ON was defined as the region between a radial distance of 4.5 to 6 mm. Lens tissue greater than a radial distance of 6 mm was defined as the cortex.

2.3 Lens homogenization and fractionation

Lens tissue was manually homogenized in homogenization buffer comprised of 25 mM Tris, 150 mM NaCl, and 5 mM EDTA and centrifuged at 20,000 g for 30 minutes. The supernatant was isolated and defined as the water-soluble fraction (WSF). The pellet was solubilized in 8M urea, 25 mM Tris, 150 mM

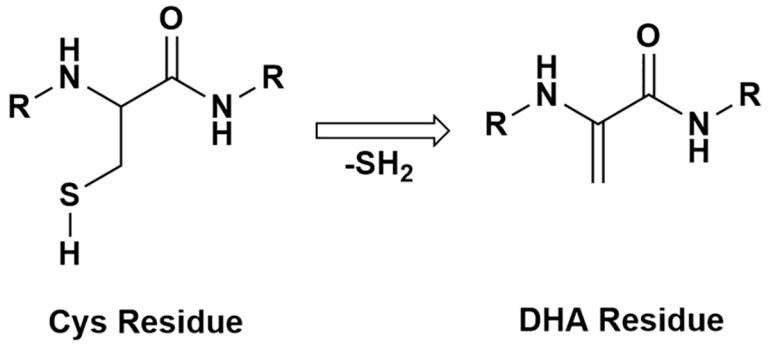

FIGURE 1
A schematic of a protein with a cysteine residue undergoing β-elimination and forming DHA.

NaCl, and 5 mM EDTA and centrifuged at 20,000 g for 30 minutes. The supernatant was isolated, and this fraction was defined as the urea-soluble fraction (USF). The remaining pellet was suspended in water and proteins from this fraction were defined as the urea-insoluble fraction (UIF).

2.4 Sample preparation for liquid chromatography and tandem mass spectrometry

Proteins from each region and fraction (WSF-IN, WSF-ON, WSF-C, USF-IN, USF-ON, USF-C, UIF-IN, UIF-ON, and UIF-C) were quantified via a bicinchoninic acid (BCA) assay. 50 µg from each region and fraction were aliquoted for proteomic analysis. Sample proteins were reduced via incubation in 10 mM DTT at 56° C for one hour. Proteins were alkylated with iodoacetamide, added to a final concentration of 55 mM, and incubated in the dark at room temperature for 45 mins. WSF and USF fractions were precipitated by methanol-chloroform as described by Wessel et al. (35). UIF fractions in water were spun down at 20,000 g for 20 minutes in 4°C and the supernatant was removed. Precipitated WSF, USF, and pelleted UIF fractions of each region were suspended in 10 µL acetonitrile and diluted with 90 µL of 50 mM Tris. Proteins were digested by the addition of trypsin at a 1:50 trypsin to protein ratio. Samples were dried via SpeedVac and re-solubilized in 0.1% formic acid. Samples were cleaned with stop and go extraction (STAGE) tips and analyzed with liquid chromatography tandem mass spectrometry (LC-MS/MS).

2.5 Liquid chromatography and tandem mass spectrometry

Tryptic peptides corresponding to 0.5 µg of total protein were separated on a one-dimensional fused silica capillary column (100 µm x 20 cm). This column was packed with C_{18} Phenomenex Jupiter resin (3 µm mean particle size, 300 Å pore size) and coupled with an Dionex Ultimate 3000 nanoLC (Thermo Scientific, San Jose, CA). A 90-minute gradient was performed, consisting of: 1-68 minutes at 2-38% acetonitrile (ACN) in 0.1% formic acid, 68-74 minutes at 38-95% ACN in 0.1% formic acid, 74-75 minutes at 95% ACN in 0.1% formic acid, 76-76 minutes at 95-2% ACN in 0.1% formic acid and 76-85 at 2% ACN in 0.1% formic acid. The mobile phase was balanced with 0.1% formic acid. The eluate was directly infused into a Q Exactive Plus instrument (Thermo Scientific, San Jose, CA) equipped with a nanoelectrospray ionization source. The data-dependent acquisition method consisted of MS1 acquisition (R=70,000) using an MS AGC target value of 3e6, followed by up to 15 MS/MS scans (R=17,500) of the most abundant ions detected in the preceding MS scan. The MS2 AGC target value was set to 1e5, with a maximum ion time of 100 milliseconds, and intensity threshold of 3e4. HCD collision energy was set to 27 NCE, and dynamic exclusion was set to 10 seconds, and peptide match and isotope exclusion were enabled.

2.6 MaxQuant search

For identification of DHA and DHB modification sites, the raw data were processed and searched against a concatenated forward and reversed (decoy) human Swissprot (Oct 2022) database. The data were searched with MaxQuant version 2.1.4.0. The false discovery date (FDR) was set to 1%. Differential modifications included carbamidomethylation of cysteine, oxidation of methionine, Gln conversion to pyro Glu, DHA modifications on cysteine (-33.9877 Da) and serine (-18.0106 Da), and DHB modification on threonine (-18.0106 Da). All modified peptides sequences were manually verified by inspection of peptide tandem mass spectra with 5 ppm mass accuracy for parent masses and 10 ppm for product ions.

2.7 Data analysis

Selected ion chromatograms of modified and non-modified peptides were extracted using the Qual Browser tool in Xcalibur software (Thermo Scientific) using a 10 ppm mass tolerance. Peak areas of DHA modified peptides and non-modified peptides were calculated for all charge states and the most intense three isotopes were summed. The relative level of modification was defined as the

10.3389/fopht.2023.1241001

TABLE 1 Age, cataract status, and sex of lenses analyzed.

Age	Grouping	Cataract Status	Sex
18	18-22	None	Female
19	18-22	None	Male
21	18-22	None	Male
22	18-22	None	Female
48	48-64	None	Male
53	48-64	None	Male
53	48-64	None	Male
56	48-64	None	Male
50	48-64 & cat	Nuclear Cataract	Male
57	48-64 & cat	Nuclear Cataract	Male
58	48-64 & cat	Nuclear Cataract	Male
64	48-64 & cat	Nuclear Cataract	Male
78	70-93	None	*
82	70-93	None	*
93	70-93	None	*
70	70-93 & cat	Nuclear Cataract	*
72	70-93 & cat	Nuclear Cataract; Posterior Subcortical Cataract	Male
75	70-93 & cat	Nuclear Cataract; Posterior Subcortical Cataract	Male
80	70-93 & cat	Nuclear Cataract	Male

*Sex information unavailable.

ratio of the peak area of modified peptide to the peak area of the non-modified summed with the modified peptide and multiplied by 100. The results are presented as mean +/- standard deviation of each modified peptide abundance in each solubility fraction and each region of four different lenses in each group. The data were analyzed in R 4.2.2. A factor analysis of mixed data (FAMD) was done with FactoMineR. Samples without peak areas for modified peptides were not used in further statistical analysis (36). Quantile normalization was done to account for biological variability (37). To determine relationships between age groups within lenses of the same solubility fraction and region, an analysis of variance (ANOVA) was used followed by a *post-hoc* Tukey test. Results were considered statistically significant when $p < 0.05$.

3 Results

3.1 Aging and cataracts influence the lens proteome

Global changes in the lens proteome were analyzed using a data dimensionality reduction method, factor analysis of mixed data (FAMD), to assess the variables that most contributed to variance in the data. The results of the FAMD analysis are shown in Figure 2. The six variables compared in the FAMD included: solubility, region, protein presence, protein sequence coverage, age, and age range and cataract status of each peptide identified by MaxQuant. Age and protein sequence coverage were continuous data while the others were categorical data. The variables that contributed to

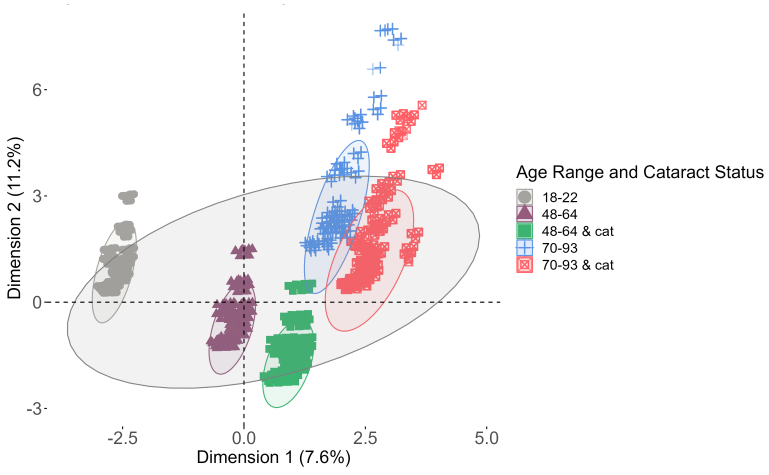

FIGURE 2
Factor analysis of mixed data (FAMD) analysis. Each ellipse represents a 95% confidence level among each group of data (lenses 18-22, 48-64, 46-64 with cataracts, 70-93, and 70-93 with cataracts). The largest ellipse is a confidence level among the entire data set.

10.3389/fopht.2023.1241001

Dimension 1 were age and age range and cataract status whereas Dimension 2 was most affected by the protein identified and its corresponding sequence coverage. Data for each lens group as well as the complete data were grouped by an ellipse representing a 95% confidence interval.

Each group of data has the same orientation against both axes, which suggests that the data have similar distributions. The datasets clearly segregate by age. Healthy lenses compared to cataractous lenses have large overlaps, suggesting that proteins were more likely to be affected by age than by cataract status. The overlap among middle-aged and senior lenses suggests that these data have more in common with one another than with younger lenses, which has no overlap with any other group. The total variance extracted from both dimensions of the data was 18.8%, suggesting that the data is well-represented by both dimensions. Overall, most of the data in each group is within a 95% confidence interval of the mean of the entire data set, which indicates that previously acquired data can be compared to recently acquired data.

3.2 DHA and DHB abundances

Previous identification of DHA in lens proteins has been limited to Ser59 on αA-crystallin (30), which was not detected in the current study. To the best of our knowledge, the 24 sites of DHA and DHB identified in our study are novel. Manual inspection of DHA containing peptide MS/MS spectra revealed that DHA formation was more commonly observed at cysteine residues compared to DHA or DHB formation at serine or threonine residues. DHA and DHB formed from water loss were often the result of artifactual in-source decay during analysis, i.e. water loss from glutamic and aspartic acid misidentified as DHA or DHB, or a potential loss of phosphoric acid from phosphoserine or phosphothreonine residues. To avoid analysis of artifactual DHA or DHB formation, only peptides that displayed a shift in retention time between modified and non-modified sequences were selected for quantitation. Among the entire dataset, 20 sites were found with cysteine-based DHA, 2 sites showed DHB from water loss, and 1 DHA site from water loss (Table 2). An example of a DHA-modified peptide tandem mass spectrum is shown in Figure 3. The masses of y_7 and y_8 ions define the site of DHA as occurring on residues Cys65 in phakinin (BFSP2). Among the detected peptides, the relative levels of modification on 13 unique peptides were abundant enough in most samples to be quantified.

3.3 DHA-modified peptides associated with only ARNC

DHA levels among each solubility fraction and lens region for BFSP2 Cys326 (Figure 4A), βA4-crystallin Cys5 (Figure 4B), and βA3-crystallin Cys170 (Figure 4C) were compared. DHA levels that were significantly different between different age groups and cataract status were denoted with color coded boxes above the bars being compared. Outlined boxes represent comparisons where one age group has cataracts. DHA levels were highest in the UIF for most age groups independent of region or cataract status for all three modified proteins. The relatively high abundance of DHA modified peptides in all UIF samples is noteworthy because non-modified crystallins are water soluble and non-modified BFSP2,

TABLE 2 Identified sites of DHA and DHB on lens proteins.

Protein: Peptide Residues	Modified Residue	Peptide with Modification
αA-crystallin: 118-145	C131, C142	YRLPSNVDQSALS**C(ALK)**SLSADG**M(OX)**LTF**C(DHA)**GPK
αB-crystallin: 22-56	S35	LFDQFFGEHLLE**S(DHA)**DLFPTSTSLSPFYLRPPSFLR
αB-crystallin: 164-175	T170	EEKPAV**T(DHB)**AAPK
βA3-crystallin: 46-58	C52	**M(OX)**EFTSS**C(DHA)**PNVSERSFDNVR
βA3-crystallin: 65-95	C82	SLKVESGAWIGYEHTSF**C(DHA)**GQQFILERGEYPR
βA3-crystallin: 126-137	T127	**M(OX)T(DHB)**IFEKENFIGR
βA3-crystallin: 163-177	C170	IQSGAWV**C(DHA)**YQYPGYR
βA4-crystallin: 2-7	C5	**T(ACE)**LQ**C(DHA)**TK
βA4-crystallin: 26-45	C33	RHEFTAE**C(DHA)**PSVLELGFETVR
βA4-crystallin: 159-177	C166	GFQYVLE**C(DHA)**DHHSGDYK
βB1-crystallin: 73-92	C79	RAEFSGE**C(DHA)**SNLADRGFDRVR
βB2-crystallin: 49-81	C67	AGSVLVQAGPWVGYEQAN**C(DHA)**KGEQFVFEKGEYPR
γB-crystallin: 16-32	C19, C23	SYE**C(DHA)**TTD**C(ALK)**PNLQPYFSR
γC-crystallin: 16-32	C23	SLHVLEG**C(DHA)**WVLYELPNYR
γD-crystallin: 16-38	C19	HYE**C(DHA)**SSDHPNLQPYLSR
γD-crystallin: 102-117	C109, C111	EDYRGQMIEFTED**C(DHA)**S**C(ALK)**LQDRFR
γS-crystallin: 20-36	C23, C25, C27	YD**C(ALK)**D**C(ALK)**D**C(DHA)**ADFHTYLSR
BFSP1: 255-276	C259	SAHE**C(DHA)**YDDEIQLYNEQIETLRK
BFSP2: 53-72	C65	APGVYVGTAPSG**C(DHA)**IGGLGAR
BFSP2: 90-121	C114	SSGLATVPAPGLERDHGAVEDLGG**C(DHA)**LVEYMAK
BFSP2: 157-173	C161	ASWASS**C(DHA)**QQVGEAVLENAR

(Continued)

10.3389/fopht.2023.1241001

TABLE 2 Continued

Protein: Peptide Residues	Modified Residue	Peptide with Modification
BFSP2: 251-276	C255	QLAG**C(DHA)** ELEQMDAPIGTGLDDILETIR
BFSP2: 318-339	C326	VELHNTS**C(DHA)**QVQSLQAETESLR
CBR1: 119-134	C122	DV**C(DHA)**TELLPLIKPQGR

*ALK refers to alkylated and a mass shift of 57.0215. OX refers to oxidized and a mass shift of 15.9949. ACE refers to acetylated and a mass shift of 42.0106. C(DHA) refers to a mass shift of -33.9877. S(DHA) and T(DHB) refer to a mass shift of -18.0106. BFSP1 and BFSP2 refer to filensin and phakinin, respectively.

being a cytoskeletal protein, is more likely to be identified in the USF.

In Figure 4, DHA abundance of BFSP2 Cys326, βA4-crystallin Cys5, and βA3-crystallin Cys170 were highest among senior donors with cataracts (pink bars) in all regions of the UIF. Transparent senior lenses (blue bars) displayed lower DHA levels when detected. Although not all DHA abundance differences between age groups in the UIF were statistically significant due to high variability among donors and a small sample size, a similar trend was observed for these three different proteins.

DHA levels on BFSP2 Cys326 and βA4-crystallin Cys5 in the UIF significantly increased from the C region to the IN region in lenses within each group: 18–22-year-old in BFSP2 Cys326 (Figure 4A), and 48–64-year-old with and without cataracts in βA4-crystallin Cys5 (Figure 4B). These results suggest a regional trend toward higher DHA content in older fiber cells in the UIF, which are the regions of the lens most impacted by ARNC. However, no trend could be identified when comparing younger, middle-aged, and senior lenses within each region in the UIF. The abundance of DHA-containing peptides did not show a strong association with aging even though a slight regional trend was detected.

βA3-crystallin Cys170 (Figure 4C) showed relatively high levels of DHA in senior cataractous lenses in the WSF-IN but not in the WSF-ON, where high levels of DHA were seen in transparent senior lenses. DHA-modified peptides of βB1-crystallin Cys79 in Supplementary Figure 2 displayed similar trends where high levels of DHA were observed in senior lenses with cataracts in the WSF-IN and senior lenses without cataracts were highest in ON and C regions of the WSF. The highest levels of DHA on βB1-crystallin Cys79 were seen in the UIF. Surprisingly, relatively high levels of DHA were observed in the UIF compared to the WSF from young lenses suggesting a shift from a highly water-soluble protein to an insoluble protein upon DHA formation.

3.4 DHA-modified peptides associated with aging and ARNC

Four DHA sites whose abundances were strongly associated with lens age are BFSP2 Cys255 (Figure 5A), BFSP2 Cys65 (Figure 5B), βA3-crystallin Cys82 (Figure 5C), and βA4-crystallin Cys33 (Figure 5D). All four sites showed a high abundance of DHA in the UIF in all three regions of the lens. In each region of the UIF, DHA levels increased from younger to middle-aged to senior lenses. The other solubility fractions did not show any discernable trend. In the UIF, transparent senior lenses and senior lenses with cataracts (blue and pink bars respectively) showed greater differences in the C region than in the ON and IN regions.

In all four peptides, the range of levels of DHA between transparent and cataractous lenses in the IN and ON overlap. There is not a significant difference among these senior lenses. However, in BFSP2 Cys 255 in Figure 5A, a significant difference of DHA levels between transparent and cataractous senior lenses

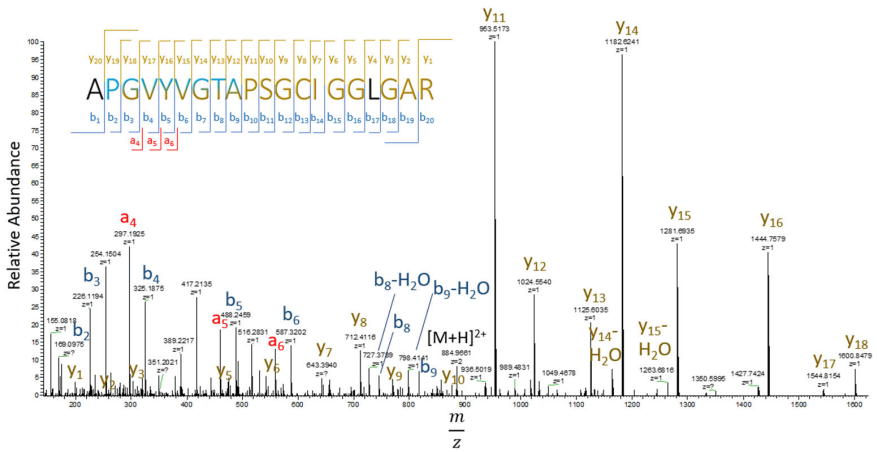

FIGURE 3
Tandem mass spectrum of residues 53-72 (APGVYVGTAPSGCIGGLGAR) of BFSP2 (phakinin). DHA is formed from hydrogen sulfide loss from cysteine with a mass shift of -33.9877 Da. b-ions are labeled in blue, y-ions yellow, and a-ions are red. Letters in black refer to residues not identified by b, y, and a ions.

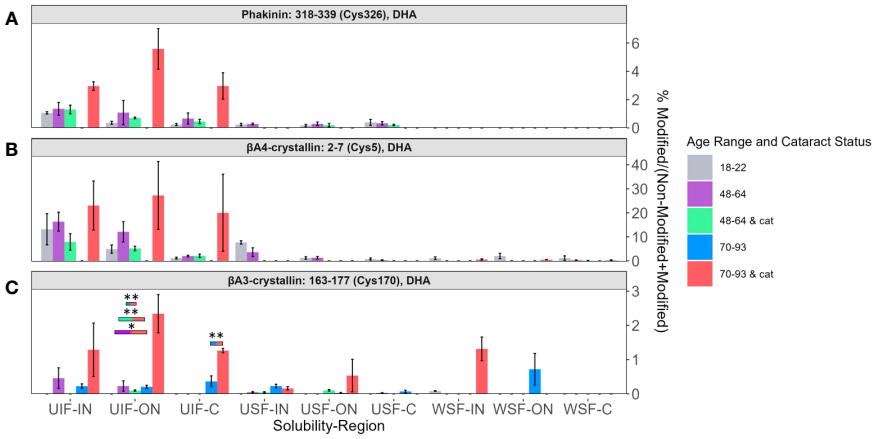

FIGURE 4
DHA containing peptides abundant in age-related nuclear cataract. Relative levels of DHA are shown for **(A)** BFSP2 (Phakinin) Cys326, **(B)** βA4-crystallin Cys5, and **(C)** βA3-crystallin Cys170 among each fractionated region, solubility group, and donor group. WSF-IN, WSF-ON, and WSF-C refers to the water-soluble inner nucleus, outer nucleus, and cortex. USF-IN, USF-ON, and USF-C refer to the urea-soluble inner nucleus, outer nucleus, and cortex. UIF-IN, UIF-ON, and UIF-C refer to the urea-insoluble inner nucleus, outer nucleus, and cortex. Boxes above each result are colored to show which groups are statistically significantly ($p<0.05$) different. The boxes are colored according to the legend to indicate which bars are compared and show significant abundance differences. Boxes outlined in black represent comparisons where at least one lens group has cataracts; boxes without outlines represent comparisons where neither lens groups have cataracts. An asterisk (*) represents a p-value less than 0.05; ** represents a p-value less than 0.01.

was seen (pink and blue bars, respectively). Similarly, significant regional differences between the IN region and C region in senior transparent lenses (blue bars) and regional differences in middle aged transparent and cataractous lenses between the ON region and C region (purple and green bars respectively) were seen in DHA levels in BFSP2 Cys65 in Figure 5B.

3.5 DHA-modified peptides not associated with aging or ARNC

Relative abundances of two peptides: βA3-crystallin T127 containing DHB (Figure 6A) and γC-crystallin Cys23 containing DHA (Figure 6B) showed, again, that the highest levels of

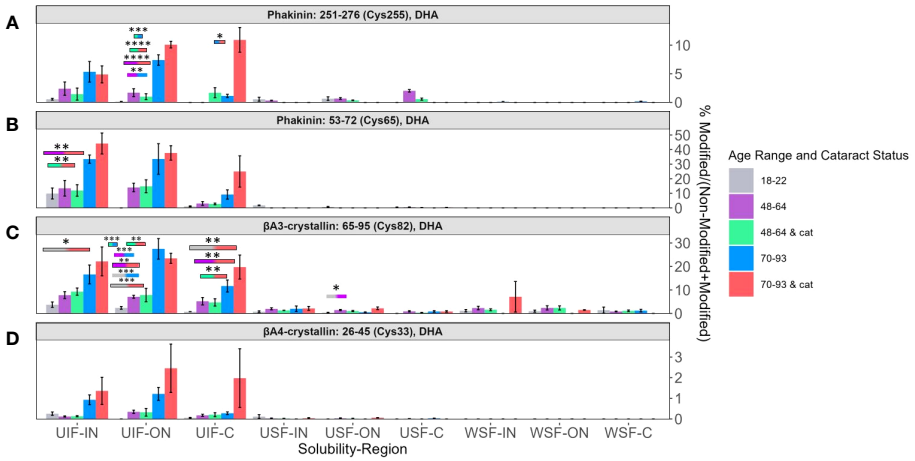

FIGURE 5
Relative abundance of DHA containing peptides associated with aging. Relative levels of DHA are shown for **(A)** BFSP2 (Phakinin) Cys255, **(B)** BFSP2 Cys65, **(C)** βA3-crystallin Cys82, and **(D)** βA4-crystallin Cys33. Boxes above each result are colored to show which groups are statistically significantly ($p<0.05$) different. Boxes outlined in black represent comparisons where at least one lens group has cataracts; boxes without outlines represent comparisons where neither lens groups have cataracts. An asterisk (*) represents a p-value less than 0.05; ** represents a p-value less than 0.01; *** represents a p-value less than 0.001; and **** represents a p-value less than 0.0001.

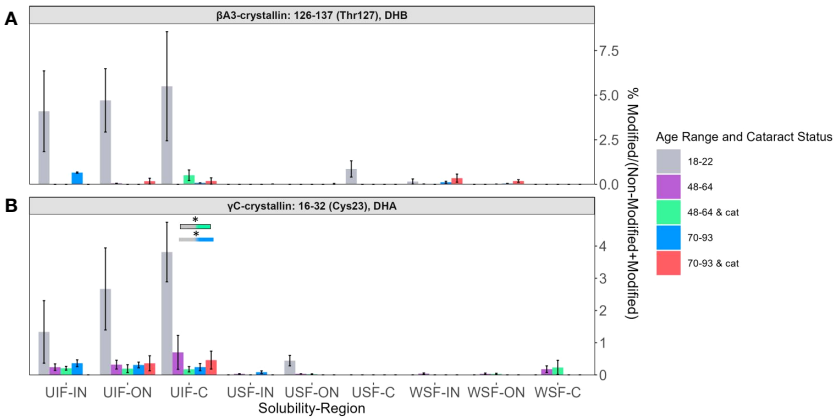

FIGURE 6
DHB and DHA containing peptides abundant in young lenses. Relative levels of DHB are shown for **(A)** βA3-crystallin Thr127 and of DHA for **(B)** γC-crystallin Cys23. Boxes above each result are colored to show which groups are statistically significantly ($p<0.05$) different. Boxes outlined in black represent comparisons where at least one lens group has cataracts; boxes without outlines represent comparisons where neither lens groups have cataracts. An asterisk (*) represents a p-value less than 0.05.

modification were detected among the UIF samples. In contrast, to the peptides discuss above, DHA and DHB were more likely to be detected in 18-22-year-old lenses for these two peptides. The relative lack of these modifications in lenses from older subjects suggests that DHA and DHB at these sites may reacting with lens nucleophiles over time.

DHA in filensin (BFSP1) Cys259 was more likely to be present in younger lenses (Supplementary Figure 3) like the trends seen in Figure 6. In fact, DHA was not detected in senior lenses with or without cataracts in most regions and fractions. DHA in BFSP1 Cys259 also exhibited a solubility shift from the expected presence in the USF to predominant present in the UIF. Interestingly, transparent 48-64-year-old lenses showed relative high abundance in the WSF-C compared to all other age groups. Although it is unclear as to why such changes in hydrophobicity would occur, these results provide additional evidence that that DHA may be involved in structural changes that affect the overall protein solubility. In fact, DHA was not detected in senior lenses with or without cataracts in most regions and fractions. The results from this site also suggest that DHA and DHB may be participating in other reactions.

Although most detected DHA modified peptides were abundant in the UIF, there were notable exceptions. The DHA site that displayed unique changes in solubility was αA-crystallin, residues Cys131 and Cys142, which is typically a water-soluble protein. DHA in αA-crystallin Cys131 and Cys142 (Supplementary Figure 4) showed an age-related trend in the ON and C regions of the UIF but not in the IN region of UIF, which is the region most impacted by aging and cataracts. Additionally, DHA levels among senior cataractous lenses were only high among the UIF whereas age-related trends could be seen in the USF except for senior cataractous lenses. Interestingly, DHB in αB-crystallin T170 did not exhibit a solubility shift (Supplementary Figure 5), unlike most of the other sites discussed above, and no discernable trends were identified.

4 Discussion

Twenty-four new sites of DHA and DHB were identified on thirteen human lens proteins. Of these sites, thirteen were quantified as a function of age, solubility, and lens region. For most proteins, the presence of DHA or DHB resulted in a shift of the protein to the insoluble fraction. In addition, three general trends were observed in aged and cataractous lenses: (1) DHA/DHB abundance increased with ARNC but not age, (2) DHA/DHB abundance increased with both age and ARNC, and (3) DHA/DHB abundance had no relationship with aging and ARNC.

DHA and DHB modifications were identified in many of the same protein residues and tertiary structures as previously reported to contain DHA or DHB-mediated crosslinks (25) and cysteine oxidation (13, 17). The correlation of DHA to these previously published sites reaffirms that there may be residues, such as cysteine, that may be 'hotspots' for spontaneous degradation (38). The presence of DHA and DHB in long-lived lens proteins suggests a stability not previously considered. Although subjects of nucleophilic attack by lysine, cysteine, and histidine residues, our results demonstrate that DHA and DHB can be relatively stable, and their reactivity may depend on surface exposure and/or proximity to nucleophilic residues.

Loss of free thiol groups on cysteine residues is a form of protein oxidation associated with aging and cataractogenesis. Hains and Truscott measured the relative abundance of oxidized and disulfide bonded cysteine in human lenses; however, DHA was not measured in that study (17). Similar to Hains and Truscott and Fan et al. (13) and as stated above, our data displayed three trends: (1) DHA/DHB abundance increased with ARNC but not age, (2) DHA/DHB abundance increased with both age and ARNC, and (3) DHA/DHB abundance had no relationship with aging and ARNC (17). Specifically, DHA levels in BFSP2 Cys326 (Figure 4A) and βA3-crystallin Cys170 (Figure 4C) were highest in ARNC lenses but no association with lens age was observed. A similar result for βA3-

crystallin Cys170 cysteine oxidation was reported by Hains and Truscott (17). Another DHA site that displayed similar trends as those seen in previous work was βA3-crystallin Cys82 (Figure 5C). Hains and Truscott found that cysteine oxidation on βA3-crystallin Cys82 was highly related to aging and ARNC our results found DHA levels increased strongly with age (17) in senior ARNC donors but these results were less pronounced compared to the age-related trends observed. αA-crystallin Cys131 and Cys142 (Supplementary Figure 3) displayed age and ARNC related changes when measuring cysteine oxidation or DHA levels (17). These results suggest that DHA formation is correlated to cysteine oxidation. This finding is consistent with our previous study that disulfide bonded cysteine residues readily form DHA (39).

To understand the reactivity of cysteine oxidation during low GSH levels, Fan et al. (13) identified changes in disulfide bond levels. Proteins and residues associated with cysteine oxidation levels that increased with age and ARNC were βA3-crystallin Cys170 (Figure 4C), and βA4-crystallin Cys33 (Figure 5D) (13), which were also found to have increased DHA levels with age or ARNC. These results provide more evidence that DHA is correlated to cysteine oxidation. Fan et al. showed that cysteine oxidation was correlated to intermolecular disulfide crosslinks during the aging process and cataractogenesis as opposed to intramolecular disulfide crosslinks in younger lenses (13). We posit that DHA formation would similarly cause structural changes as the loss of intramolecular disulfide crosslinks. βB1-crystallin Cys79 (Supplementary Figure 2), and γC-crystallin Cys23 (Figure 6B) did not show increased levels with aging and ARNC with DHA abundance but did with oxidized cysteine levels (13), which may be due to the other nucleophiles in the lens. Interestingly, several sites that did not show cysteine oxidation levels change with age or ARNC did show a relationship with DHA levels and age or ARNC (13), such as αA-crystallin Cys131 and Cys142 (Supplementary Figure 3), βA3-crystallin Cys82 (Figure 5C), and βA4-crystallin Cys5 (Figure 4B). These results suggest that DHA abundance may be influenced by more than GSH levels and that DHA may be another barometer of cysteine oxidation.

DHA- and DHB-modified proteins were more likely to be found in the UIF fraction, as observed in 10 of the 13 quantified sites, regardless of the specific protein, native protein solubility, region of the protein, or trend identified. This was unexpected because non-modified protein and peptide counterparts were more likely to be in WSFs or USFs. This is exemplified by the shift in solubility of αA-crystallin from a typically water-soluble protein to a urea-soluble and urea-insoluble protein when DHA is present on residues Cys131 and Cys142 (Supplementary Figure 4). These data suggest that DHA and DHB may induce structural changes that cause protein insolubilization. A critique of this hypothesis arises from the fact that DHA can also be found in the other solubility fractions, albeit in much lower abundances. Furthermore, the likelihood of other protein modifications occurring increases with age, and these may also change the solubility of proteins. For example, previous research by Grey and Schey found that intact αA-crystallin could be found in younger lenses in all regions of the lens (40). However, intact αA-crystallin could not be found in the nucleus of older lenses and, instead, multiple subspecies of truncated αA-crystallin were found (40). Another hypothesis that may explain the low levels of soluble DHA containing proteins is that proteins with DHA/DHB could be targeted for degradation when soluble; however, once insoluble, they may escape proteostatic mechanisms.

Whether DHA and DHB formation is causing insolubilization and aggregation remains to be established. It is very likely that other modifications, known to accumulate with age, may be influencing protein structure in combination with DHA and the combined effects on protein structure will be difficult to determine. Alternatively, if DHA can induce the solubility changes seen in this study, it is possible that protein precipitation or aggregation occurs when DHA or DHB forms on multiple sites of the same protein (41). Further testing is necessary to determine what effect DHA or DHB has on protein structures. Some of the factors that may influence the impact of DHA/DHB formation at each identified site are accessibility of the site, the role of the site in protein-protein interactions or protein structure and flexibility, and the charge states and reactivity of nearby residues. Our data suggest that DHA formation affects protein solubility and may have some impact on protein rigidity. For example, DHA on BFSP2 residue Cys326 (Figure 4A) showed no age-related trend but an ARNC trend whereas BFSP2 Cys255 (Figure 5A) and Cys65 (Figure 5B) showed progressive increases with age. This difference suggests that regions within the same protein can have different effects on protein structure and solubility. If, as our data suggest, structural changes induced by DHA/DHB formation lead to solubility changes, then it is possible for some buried sites to be exposed only after significant protein modification. Thus, some modifications will accumulate with age while others appear only at advanced stages of denaturation. Evidence that may support this notion is that BFSP2 Cys326 is present in the coiled region of the protein whereas BFSP2 Cys65 and Cys255 are in the head and rod domains respectively. Cys326 is present in a region responsible for the overall shape of the dimer and flexibility of BFSP2 (42, 43). This buried residue is not as exposed as other regions and may only be accessible when BFSP2 is unfolded, which is more likely during the denaturing conditions of advanced age or cataractogenesis. In contrast, BFSP2 Cys65 and Cys255 are involved in the assembly of beaded filaments. An age-related trend may be more likely to occur for these more exposed residues.

Like BFSP2, βA4-crystallin containing DHA on Cys5 showed a strong relationship with ARNC (Figure 4B) while DHA-modified βA4-crystallin Cys33 showed a strong relationship with aging and ARNC (Figure 5D). βA4-crystallin Cys5 and Cys33 are located on subdomains within the protein that have distinct structural differences. Cys33 is buried within a Greek key motif; a secondary structure that allow regions within a protein to be highly compact and less vulnerable to stress (44). Previous studies found that when a mutation arises within a single Greek key motif the protein will then self-aggregate and precipitate (44). This information combined with the change in solubility (Figure 5D) suggests that DHA on Cys33 may cause structural deficits associated with function loss. When a mutation occurred in a region not associated with the Greek key motif, the protein remained more stable than its counterpart even if those changes could induce structural and functional deficits (44). That

DHA on Cys33 increases with age suggests that, over time, misfolding or aggregation occurs, which is consistent with previous research (5). βA4-crystallin Cys5 (Figure 4B) is on the N-terminal arm of the protein, which is hypothesized to stabilize protein-protein interactions among complexes (45). Cys5 is a highly exposed residue, which shows high levels of DHA in ARNC similar to BFSP2 Cys326. When comparing the abundance of DHA on βA4-crystallin Cys5 to DHA-GSH crosslinks identified by Wang and Schey (25), high levels of DHA were found among senior cataractous lenses in this current study whereas DHA-GSH crosslinks where more likely to be identified among transparent senior lenses. DHA-GSH crosslinks were found in much higher abundances, which suggests that DHA formation and reaction with GSH may be one cause of age-related decline of GSH (46) and reaffirms the potential for DHA to impair lens transparency.

In contrast to the age and cataract specific trends described above, DHA levels at γC-crystallin residue Cys23 and βA3-crystallin T127 (seen in Figure 6) showed high abundance among younger lenses compared to senior or cataractous lenses. γC-crystallin Cys23 was not found to have a relationship between cysteine oxidation and aging or age-related diseases (17). We speculate that these residues are exposed on the protein surface, and upon, DHA/DHB formation, readily react with lens nucleophiles.

In summary, our results show that there is a relationship between DHA and DHB levels and age and ARNC. Many fewer sites with DHB were identified compared to DHA, which suggests that DHB containing peptides may need further enrichment for detection and quantification. Although DHA and DHB are known to contribute to high molecular weight crosslinks correlated to cataracts (33), it is unclear to what extent or how DHA or DHB may be involved in cataractogenesis since this modification is present throughout the aging process. However, our data suggest that for most of the proteins examined, DHA modifications shifted the protein solubility to the insoluble fraction, even for soluble crystallins. Further work is needed to determine the specific role of DHA on protein insolubilization, and our results suggest that this phenomenon may be protein and/or site-specific.

Data availability statement

The data presented in the study are deposited in the ProteomeXchange Consortium via the PRIDE (47) partner repository, accession number PXD045734. The data can be accessed via URL: http://www.ebi.ac.uk/pride/archive/projects/PXD045734.

Ethics statement

The studies involving humans were approved by Institutional Review Board, Vanderbilt University. The studies were conducted in accordance with the local legislation and institutional requirements. The human samples used in this study were acquired from another group as a gift and de-identified and others were obtained as de-identified samples from deceased donors. Written informed consent for participation was not required from the participants or the participants' legal guardians/next of kin in accordance with the national legislation and institutional requirements.

Author contributions

JP, ZW, PP, and KR performed experiments. JP and ZW analyzed data. JP, ZW, KR and KS designed experiments. JP and KS wrote manuscript. All authors contributed to the article and approved the submitted version.

Funding

We acknowledge support from the NIH grants EY-024258 and EY008126 to KS and an NSF graduate research fellowship (GRFP) to JP.

Acknowledgments

We thank Dr. Donna Garland and Dr. Nathan Congdon for the generous gift of aged and cataractous human lenses.

Conflict of interest

The authors declare that the research was conducted in the absence of any commercial or financial relationships that could be construed as a potential conflict of interest.

The author(s) KS and ZW declared that they were an editorial board member of Frontiers, at the time of submission. This had no impact on the peer review process and the final decision.

Publisher's note

Supplementary material

The Supplementary Material for this article can be found online at: https://www.frontiersin.org/articles/10.3389/fopht.2023.1241001/full#supplementary-material

References

1. Monnier V, Cerami A. Nonenzymatic browning *in vivo*: possible process for aging of long-lived proteins. *Science* (1981) 211(4481):491–3. doi: 10.1126/science.6779377

2. Lynnerup N, Kjeldsen H, Heegaard S, Jacobsen C, Heinemeier J. Radiocarbon dating of the human eye lens crystallins reveal proteins without carbon turnover throughout life. *PloS One* (2008) 3(1):e1529. doi: 10.1371/journal.pone.0001529

3. Thayer NH, Leverich CK, Fitzgibbon MP, Nelson ZW, Henderson KA, Gafken PR, et al. Identification of long-lived proteins retained in cells undergoing repeated asymmetric divisions. *Proc Natl Acad Sci* (2014) 111(39):14019–26. doi: 10.1073/pnas.1416079111

4. Grosas AB, Carver JA. Eye lens crystallins: remarkable long-lived proteins. *Long-lived Proteins Hum Aging Dis* (2021) 16:55–96. doi: 10.1002/9783527826759.ch3

5. Moreau KL, King JA. Protein misfolding and aggregation in cataract disease and prospects for prevention. *Trends Mol Med* (2012) 18(5):273–82. doi: 10.1016/j.molmed.2012.03.005

6. Truscott R. Age-related nuclear cataract – oxidation is the key. *Exp Eye Res* (2005) 80:709–25. doi: 10.1016/j.exer.2004.12.007

7. Takemoto L, Sorensen CM. Protein–protein interactions and lens transparency. *Exp eye Res* (2008) 87(6):496–501. doi: 10.1016/j.exer.2008.08.018

8. Lampi KJ, Wilmarth PA, Murray MRM, David LL. Lens β-crystallins: The role of deamidation and related modifications in aging and cataract. *Prog Biophysics Mol Biol* (2014) 115(1):21–31. doi: 10.1016/j.pbiomolbio.2014.02.004

9. Takata T, Oxford JT, Demeler BD, Lampi KJ. Deamidation destabilizes and triggers aggregation of a lens protein, βA3-crystallin. *Protein Sci* (2008) 17(9):1565–75. doi: 10.1110/ps.035410.108

10. Garland D, Russell P, Zigler JS. The oxidative modification of lens proteins. In: Simic MG TKA, Ward JF, von Sonntag C, editors. *Oxygen Radicals in Biology and Medicine. Basic Life Sciences*. Boston: Springer (1988). p. 347–52.

11. Stadtman E. Protein oxidation in aging and age-related diseases. *Ann N Y Acad Sci* (2001) 928:22–38. doi: 10.1111/j.1749-6632.2001.tb05632.x

12. Ahmad A, Ahsan H. Biomarkers of inflammation and oxidative stress in ophthalmic disorders. *J Immunoassay Immunochemistry* (2020) 41(3):257–71. doi: 10.1080/15321819.2020.1726774

13. Fan X, Zhou S, Wang B, Guo M, Li B, Yang J, et al. Evidence of highly conserved β-crystallin disulfidome that can be mimicked by *in vitro* oxidation in age-related human cataract and glutathione depleted mouse lens*. *Mol Cell Proteomics* (2015) 14 (12):3211–23. doi: 10.1074/mcp.M115.050948

14. Nagaraj R, Sell D, Prabhakaram M, Ortwerth B, Monnier V. High correlation between pentosidine protein crosslinks and pigmentation implicates ascorbate oxidation in human lens senescence and cataractogenesis. *Proc Natl Acad Sci USA* (1991) 88:10257–61. doi: 10.1073/pnas.88.22.10257

15. Truscott RJW, Schey KL, Friedrich MG. Old proteins in man: a field in its infancy. *Trends Biochem Sci* (2016) 41:654–64. doi: 10.1016/j.tibs.2016.06.004

16. Nandi SK, Rankenberg J, Glomb MA, Nagaraj RH. Transient elevation of temperature promotes cross-linking of α-crystallin-client proteins through formation of advanced glycation endproducts: A potential role in presbyopia and cataracts. *Biochem Biophys Res Commun* (2020) 533(4):1352–8. doi: 10.1016/j.bbrc.2020.10.018

17. Hains PG, Truscott RJW. Proteomic analysis of the oxidation of cysteine residues in human age-related nuclear cataract lenses. *Biochim Biophys Acta (BBA) - Proteins Proteomics* (2008) 1784(24):1959–64. doi: 10.1016/j.bbapap.2008.07.016

18. Ho MC, Peng YJ CSJ, Chiou SH. Senile cataracts and oxidative stress. *J Clin gerontology geriatrics* (2010) 1(1):17–21. doi: 10.1016/j.jcgg.2010.10.006

19. Leichert LI, Jakob U. Protein thiol modifications visualized *in vivo*. *PloS Biol* (2004) 2:e333. doi: 10.1371/journal.pbio.0020333

20. Gallogly MM, Mieyal JJ. Mechanisms of reversible protein glutathionylation in redox signaling and oxidative stress. *Curr Opin Pharmacol* (2007) 7:381–91. doi: 10.1016/j.coph.2007.06.003

21. Horwitz J, Emmons T, Takemoto L. The ability of lens alpha crystallin to protect against heat-induced aggregation is age-dependent. *Curr eye Res* (1992) 11(8):817–22. doi: 10.3109/02713689209000754

22. Derham BK, Harding JJ. α-Crystallin as a molecular chaperone. *Prog Retinal Eye Res* (1999) 18(4):463–509. doi: 10.1016/S1350-9462(98)00030-5

23. Hong Y, Harding JJ, Xing K, Lou MF. Revival of glutathione reductase in human cataractous and clear lens extracts by thioredoxin and thioredoxin reductase, in conjunction with alpha-crystallin or thioltransferase. *Curr Eye Res* (2007) 32(5):455–63. doi: 10.1080/02713680701257837

24. Giblin FJ. Glutathione: A vital lens antioxidant. *J Ocular Pharmacol Ther* (2009) 16(2):121–35. doi: 10.1089/jop.2000.16.121

25. Wang Z, Schey K. Quantification of thioether-linked glutathione modifications in human lens proteins. *Exp Eye Res* (2018), 175:83–9. doi: 10.1016/j.exer.2018.06.002

26. Brennan LA, McGreal RS, Kantorow M. Oxidative stress defense and repair systems of the ocular lens. *Front Bioscience-Elite* (2012) 4(1):141–55. doi: 10.2741/e365

27. Giblin FJ, Padgaonkar VA, Leverenz VR, Lin LR, Lou MF, Unakar NJ, et al. Nuclear light scattering, disulfide formation and membrane damage in lenses of older Guinea pigs treated with hyperbaric oxygen. *Exp eye Res* (1995) 60(3):219–35. doi: 10.1016/S0014-4835(05)80105-8

28. Pirie A. Color and solubility of the proteins of human cataracts. *Invest Opthalmol* (1968) 7:634–50.

29. Wang Z, Lyons B, Truscott RJ, Schey KL. Human protein aging: modification and crosslinking through dehydroalanine and dehydrobutyrine intermediates. *Aging Cell* (2014) 13:226–34. doi: 10.1111/acel.12164

30. Srivastava O, Kirk M, Srivastava K. Characterization of covalent multimers of crystallins in aging human lenses. *J Biol Chem* (2004) 279:10901–9. doi: 10.1074/jbc.M308884200

31. Brennan DF, Barford D. Eliminylation: a post-translational modification catalyzed by phosphothreonine lyases. *Trends Biochem Sci* (2009) 34:108–14. doi: 10.1016/j.tibs.2008.11.005

32. Townsend D, Lushchak VICA. A comparison of reversible versus irreversible protein glutathionylation. *Adv Cancer Res* (2014) 122:177–98. doi: 10.1016/B978-0-12-420117-0.00005-0

33. Linetsky M, Hill J, LeGrand R, Hu F. Dehydroalanine crosslinks in human lens. *Exp Eye Res* (2004) 79:499–512. doi: 10.1016/j.exer.2004.06.026

34. Kanayama T, Miyanaga Y, Horiuchi K, Fujimoto D. Detection of the cross-linking amino acid, histidinoalanine, in human brown cataractous lens protein. *Exp Eye Res* (1987) 44:165–9. doi: 10.1016/S0014-4835(87)80001-5

35. Wessel K, Kaever V, Resch K. Measurement of prostaglandins from biological samples in the subnanogram range by fluorescence labelling and HPLC separation. *J liquid Chromatogr* (1988) 11(6):1273–92. doi: 10.1080/01483918808067172

36. Chen C, Hou J, Tanner JJ, Cheng J. Bioinformatics methods for mass spectrometry-based proteomics data analysis. *Int J Mol Sci* (2020) 21(8):2873. doi: 10.3390/ijms21082873

37. Callister SJ, Barry RC, Adkins JN, Johnson ET, Wj Q, Webb-Robertson BJM, et al. Normalization approaches for removing systematic biases associated with mass spectrometry and label-free proteomics. *J Proteome Res* (2006) 5(2):277–86. doi: 10.1021/pr050300l

38. Friedrich MG, Wang Z, Oakley K, Schey KL, Truscott RJW. Hotspots of age-related protein degradation: the importance of neighboring residues for the formation of non-disulfide crosslinks derived from cysteine. *Biochem J* (2017) 474(14):2475–87. doi: 10.1042/BCJ20170268

39. Friedrich MG, Wang Z, Schey K, Truscott RJW. DehydroalanylGly, a new post translational modification resulting from the breakdown of glutathione. (2018) *Biochim Biophys Acta Gen Subj*. 1862(4):907–13. doi: 10.1016/j.bbagen.2018.01.003

40. Grey AC, Schey KL. Age-related changes in the spatial distribution of human lens α-crystallin products by MALDI imaging mass spectrometry. *Invest Ophthalmol Visual Sci* (2009) 50(9):4319–29. doi: 10.1167/iovs.09-3522

41. Hejtmancik JF, Shiels A. Chapter nine - overview of the lens. In: Hejtmancik JF, Shiels A, Nickerson JM, editors. *Progress in Molecular Biology and Translational Science*. Waltham: Acadmic Press (2015). p. 119–27.

42. Herrmann H, Aebi U. Intermediate filaments: structure and assembly. *Cold Spring Harb Perspect Biol* (2016) 8(11):1–22. doi: 10.1101/cshperspect.a018242

43. Herrmann H, Häner M, Brettel M, Müller SA, Goldie KN, Fedtke B, et al. Structure and assembly properties of the intermediate filament protein vimentin: the role of its head, rod and tail domains. *J Mol Biol* (1996) 264(5):933–53. doi: 10.1006/jmbi.1996.0688

44. Vendra V, Rao P, Agarwal G, Chandani S, Talla V, Srinivasan N, et al. Structural integrity of the greek key motif in βγ-crystallins is vital for central eye lens transparency. *PloS One* (2013) 8(8):e70336. doi: 10.1371/journal.pone.0070336

45. Basha E, Friedrich KL, Valerian E. The N-terminal arm of small heat shock proteins is important for both chaperone activity and substrate specificity. *J Biol Chem* (2006) 281(52):39943–52. doi: 10.1074/jbc.M607677200

46. Kamei A. Glutathione levels of the human crystalline lens in aging and its antioxidant effect against the oxidation of lens proteins. *Biol Pharm Bull* (1993) 16 (9):870–5. doi: 10.1248/bpb.16.870

47. Perez-Riverol Y, Bai J, Bandla C, Hewapathirana S, García-Seisdedos D, Kamatchinathan S, et al. (2022). The PRIDE database resources in 2022: A Hub for mass spectrometry-based proteomics evidences. *Nucleic Acids Res* 50(D1):D543–52. doi: 10.1093/nar/gkab1038

frontiers | Frontiers in Ophthalmology

TYPE Original Research
PUBLISHED 16 April 2024
DOI 10.3389/fopht.2024.1362350

OPEN ACCESS

EDITED BY
Barbara Pierscionek,
Anglia Ruskin University, United Kingdom

REVIEWED BY
Akihiro Ikeda,
University of Wisconsin-Madison, United States
Nazarul Hasan,
University of Louisville, United States

*CORRESPONDENCE
Hélène Choquet
Helene.Choquet@kp.org

RECEIVED 28 December 2023
ACCEPTED 01 April 2024
PUBLISHED 16 April 2024

CITATION
Choquet H, Duot M, Herrera VA, Shrestha SK, Meyers TJ, Hoffmann TJ, Sangani PK and Lachke SA (2024) Multi-tissue transcriptome-wide association study identifies novel candidate susceptibility genes for cataract. *Front. Ophthalmol.* 4:1362350. doi: 10.3389/fopht.2024.1362350

Multi-tissue transcriptome-wide association study identifies novel candidate susceptibility genes for cataract

Hélène Choquet[1]*, Matthieu Duot[2,3], Victor A. Herrera[1], Sanjaya K. Shrestha[2], Travis J. Meyers[1], Thomas J. Hoffmann[4,5], Poorab K. Sangani[6] and Salil A. Lachke[2,7]

[1]Kaiser Permanente Northern California (KPNC), Division of Research, Oakland, CA, United States, [2]Department of Biological Sciences, University of Delaware, Newark, DE, United States, [3]The National Centre for Scientific Research (CNRS), IGDR (Institut de Génétique et Développement de Rennes) - Joint Research Units (UMR), Univ Rennes, Rennes, France, [4]Institute for Human Genetics, University of California San Francisco (UCSF), San Francisco, CA, United States, [5]Department of Epidemiology and Biostatistics, UCSF, San Francisco, CA, United States, [6]Department of Ophthalmology, KPNC, South San Francisco, CA, United States, [7]Center for Bioinformatics and Computational Biology, University of Delaware, Newark, DE, United States

Introduction: Cataract is the leading cause of blindness among the elderly worldwide. Twin and family studies support an important role for genetic factors in cataract susceptibility with heritability estimates up to 58%. To date, 55 loci for cataract have been identified by genome-wide association studies (GWAS), however, much work remains to identify the causal genes. Here, we conducted a transcriptome-wide association study (TWAS) of cataract to prioritize causal genes and identify novel ones, and examine the impact of their expression.

Methods: We performed tissue-specific and multi-tissue TWAS analyses to assess associations between imputed gene expression from 54 tissues (including 49 from the Genotype Tissue Expression (GTEx) Project v8) with cataract using FUSION software. Meta-analyzed GWAS summary statistics from 59,944 cataract cases and 478,571 controls, all of European ancestry and from two cohorts (GERA and UK Biobank) were used. We then examined the expression of the novel genes in the lens tissue using the iSyTE database.

Results: Across tissue-specific and multi-tissue analyses, we identified 99 genes for which genetically predicted gene expression was associated with cataract after correcting for multiple testing. Of these 99 genes, 20 (*AC007773.1*, *ANKH*, *ASIP*, *ATP13A2*, *CAPZB*, *CEP95*, *COQ6*, *CREB1*, *CROCC*, *DDX5*, *EFEMP1*, *EIF2S2*, *ESRRB*, *GOSR2*, *HERC4*, *INSRR*, *NIPSNAP2*, *PICALM*, *SENP3*, and *SH3YL1*) did not overlap with previously reported cataract-associated loci. Tissue-specific analysis identified 202 significant gene-tissue associations for cataract, of which 166 (82.2%), representing 9 unique genes, were attributed to the previously reported 11q13.3 locus. Tissue-enrichment analysis revealed that gastrointestinal tissues represented one of the highest proportions of the Bonferroni-significant gene-tissue associations (21.3%). Moreover, this gastrointestinal tissue type was the only anatomical category significantly enriched in our results, after correcting for the number of tissue donors and

imputable genes for each reference panel. Finally, most of the novel cataract genes (e.g., *Capzb*) were robustly expressed in iSyTE lens data.

Discussion: Our results provide evidence of the utility of imputation-based TWAS approaches to characterize known GWAS risk loci and identify novel candidate genes that may increase our understanding of cataract etiology. Our findings also highlight the fact that expression of genes associated with cataract susceptibility is not necessarily restricted to lens tissue.

KEYWORDS

genetics, TWAS - transcriptome-wide association study, gene expression, lens tissue, cataract, multi-tissue analysis

Introduction

Cataract is the leading cause of blindness among older people worldwide and is a leading cause of vision loss in the United States (U.S.), affecting 22% of Americans aged 40 years and older (1). Cataracts are characterized by the opacification of the crystalline lens, leading to progressive loss of vision. Risk factors for cataract include type 2 diabetes, high blood pressure, high body mass index, myopic refractive error, cigarette smoking, and alcohol consumption (2). However, in a recent Mendelian randomization study, we demonstrated that only genetically determined myopic refractive error and primary open-angle glaucoma were significantly associated with cataract risk (3). In addition, women have a higher cataract burden than men of the same age (4), however it is not clear why this sex difference exists.

Twin and family studies strongly support an important role for genetic factors in cataract risk with heritability estimates up to 58% (5–10). Over the past few years, genome-wide association studies (GWASs) have identified more than 50 genetic susceptibility loci for cataracts in adults (11–13). Although those GWASs revealed many genetic loci associated with cataract susceptibility, the causal genes underlying those associations remain poorly understood. Moreover, the role of potential causal genes in the lens and other tissues and cataract is unknown.

We have previously conducted a multiethnic GWAS meta-analysis of cataract (11), using the Kaiser Permanente Northern California (KPNC) Genetic Epidemiology Research on Adult Health and Aging (GERA) cohort, the UK Biobank, and data from the 23andMe research cohort, and identified 55 genetic loci associated at a genome-wide level of significance ($P < 5 \times 10^{-8}$) with cataract (11). Interestingly, one of these loci (*CASP7*) was specific to women (11). However, the number of risk factors associated with cataract specifically in women that may explain the sex difference in disease burden remain limited.

Recently, transcriptome-wide association study (TWAS) approaches have been developed to characterize established GWAS risk loci and uncover additional gene–disease associations (14–19). These TWAS approaches leverage data from GWAS and expression quantitative trait loci (eQTL) to impute differential expression and test for gene expression associated with the GWAS disease of interest. TWASs have been fruitful in detecting functioning genes regulated by disease-associated variants, thus providing important insight into mechanisms of diseases (19).

In addition to GWAS findings, our previous GWAS meta-analysis of cataract (11) also reported positive genetic correlations between cataract with disorders other than eye disorders, including chronic pulmonary and gastrointestinal diseases. For this reason, we hypothesized that tissues in other anatomical parts of the body than the eye could be relevant to investigate, to better understand the mechanisms underlying cataract.

In this study, we conducted a TWAS of cataract to identify novel associated genes and interpret the transcriptional and disease risk mechanisms for cataract susceptibility genes. We imputed gene expression into GWAS data (59,944 cataract cases and 478,571 controls of European ancestry from GERA and UK Biobank cohorts) from our previous GWAS (11) using eQTL datasets (20) from multiple tissues (54 tissue reference panels). We conducted tissue-specific and multi-tissue TWAS analyses, as well as tissue type-enrichment analysis. Finally, we subsequently fine-mapped those associations and examined the expression of the novel genes identified in the current TWAS in lens tissues using the iSyTE database (21–24). The data sources used for the current TWAS study and TWAS analyses and results are summarized in a flowchart (Supplementary Figure S1).

Methods

Cataract GWAS data

We used summary statistics from our recent GWAS meta-analysis (11). Briefly, we conducted a meta-analysis, including 538,515 individuals of European ancestry (59,944 cataract cases and 478,571 controls) from the GERA (25) and UK Biobank (26,

27) cohorts. The meta-analysis was performed using the R package "meta" (28) and fixed-effects summary estimates were calculated for an additive model. In total, 9,056,148 single nucleotide variations (SNVs) passing quality control were used for the TWAS analyses.

For the GERA cohort, all study procedures were approved by the Institutional Review Board of the Kaiser Permanente Northern California, and written informed consent was obtained from all participants. For the UK Biobank, this research has been conducted using the UK Biobank Resource project #14105.

FUSION eQTL data

Local (*cis*) eQTL datasets for 54 tissue types were downloaded from the FUSION website. These reference data were sourced from the Genotype Tissue Expression (GTEx) Project v8 (N=49 tissue reference panels) (20), the CommonMind Consortium (CMC) (N=2 tissue reference panels) (29), the Metabolic Syndrome in Men Study (METSIM) (N=1 tissue reference panel) (30), the Netherlands Twin Registry (NTR) (N=1 tissue reference panel) (31), and the Cardiovascular Risk in Young Finns Study (YFS) (N=1 tissue reference panel) (32). Supplementary Table S1 reports the datasets sources, number of individuals, and number of imputable genes for each tissue reference panel.

Tissue-specific TWAS analyses

We conducted a TWAS of cataract using FUSION (18), which computes predictive models for eQTLs from reference data, and tests the association between predicted gene expression with a trait from GWAS summary statistics. As previously done (33), we performed tissue-specific TWAS analyses using FUSION default settings and the three following data inputs: 1) the above-mentioned GWAS summary statistics for cataract; 2) FUSION gene expression predictive models for 54 reference tissues; and 3) 1000 Genomes (European ancestry) Phase 3 data from the 1000 Genomes Project (34) as a reference panel for linkage disequilibrium (LD). Model weights for tissue-specific gene expression regressed on SNVs were computed from best linear unbiased predictor (BLUP), Bayesian sparse linear mixed model (BSLMM), least absolute shrinkage and selection operator (LASSO), and elastic net regression, as well as from the model with the top associated SNV.

A total of 325,513 gene-tissue-pairs (representing 37,920 unique genes across 54 tissue reference panels) were tested for associations between imputed gene expression with cataract susceptibility. Associations with a Bonferroni significance p-value less than 1.54×10^{-7} (=0.05/325,513) were considered significant. Novel TWAS genes were defined as those located over 1 Mb apart from any previously reported cataract GWAS loci (i.e., no prior GWAS SNVs within 1 Mb from the start or end of the gene).

Colocalization analyses

To assess whether GWAS SNVs colocalized with eQTLs, we conducted a Bayesian colocalization analysis using the COLOCv3.2.1 software, which is implemented in FUSION using marginal expression weights, for Bonferroni-significant TWAS associations (35). Thus, we tested the hypothesis that a single variant in each TWAS-significant model was associated with both cataract (from the GWAS) and imputed gene expression. Bayesian posterior probability greater than 0.9 was considered supporting evidence for colocalization.

Conditional and joint analyses

To determine if the TWAS associations were conditionally independent of the GWAS hits, we conducted conditional analyses by adjusting transcriptome-wide associations for SNV-level effects from GWAS. Specifically, we used the COJO software program to adjust the GWAS summary statistics (the meta-analyzed results from the GERA and UK Biobank European samples) by the most statistically significant risk variants within 1 Mb of each TWAS gene (36). Using the marginal TWAS associations from the single-tissue analysis, we performed a FUSION joint analysis for cataract-associated genes located on the same chromosome region within each reference panel.

Tissue enrichment analyses

To identify tissues potentially relevant to cataract, we assigned the 54 tissue reference panels to 12 anatomical categories as per Strunz et al. (2020) (37): adipose (n = 3 reference panels), brain (n = 15), cardiovascular (n = 9), female reproductive (n = 3), gastrointestinal (n = 7), gland (n = 11), lung (n = 1), skeletal muscle (n = 1), skin (n = 2), tibial nerve (n = 1), and transformed fibroblasts (n = 1). Supplementary Table S1 lists the tissue reference panels and their corresponding anatomical categories used for this analysis. We assessed the frequency of Bonferroni-significant TWAS genes in each anatomical category. Because more Bonferroni-significant TWAS genes are expected from eQTL reference panels with more tissue donors and more imputable genes, we used the hypergeometric test to estimate the probability of observing at least as many TWAS-significant genes from all the gene-tissue pairs that we tested in each anatomical category.

Sex-specific TWAS analyses

We also conducted sex-specific TWAS analyses using sex-specific GWAS summary statistics (i.e., women and men analyzed separately) and tissue reference panels (i.e., ovary, uterus, and vagina eQTLs for women; and prostate and testis eQTLs for men).

Multi-tissue TWAS analysis

We conducted an omnibus test in FUSION for associations with cataract across multiple tissues. Specifically, TWAS associations from all 54 tissue reference panels were jointly analyzed accounting for correlation between expression weights across tissues. Two filters were applied to the omnibus test results to consider a

multi-tissue gene expression test significant: 1) using a Bonferroni correction, we divided the α of 0.05 by the effective number of genes tested (n = 13,328), and retained genes with omnibus test p-values less than this value ($P < 3.75x10^{-6}$); and 2) genes with a minimum tissue-specific p-value suggestive of a significant association ($P < 1x10^{-5}$) were retained as described by Barbeira et al (17).

Expression of novel cataract-associated genes in lens tissues

The iSyTE 2.0 database, which contains meta-analyzed mouse lens gene expression data across different stages, was used to examine the expression of the novel genes identified in the current study in the lens tissue (21–23). Mouse orthologs of the human candidate genes for the novel cataract genes identified in the current TWAS analyses were examined in iSyTE, which contains meta-analyzed lens transcriptome data generated on microarrays or RNA-sequencing (RNA-seq) (21, 23). Mouse whole lens tissue gene expression datasets at embryonic day (E) stages E10.5, E11.5, E12.5, E16.5, E17.5, E19.5, and postnatal (P) day stages P0, P2, and P56, in addition to isolated lens epithelium at P28 were available on the Affymetrix 430 2.0 platform (GeneChip Mouse Genome 430 2.0 Array and/or 430A 2.0 Array) and were used in this analysis. Further, mouse whole lens tissue gene expression datasets at stages P4, P8, P12, P20, P30, P42, P52, and P60 were available on the Illumina platform (BeadChip MouseWG-6 v2.0 Expression arrays), and were used in this analysis. We also examined RNA-seq data generated on mouse whole lens tissue at E10.5, E12.5, E14.5 and E16.5. Additionally, because lens-enriched expression of a candidate gene has proven to be an effective predictor of its role in the lens (21, 22), the lens-enrichment of these candidate genes was also investigated at these stages. "Lens-enriched expression" is a measure of expression of a candidate gene in the lens compared to that in mouse whole embryonic body (WB) as described (21–23, 38, 39). Microarray expression data is publicly available on several gene-specific perturbation mouse models that exhibit lens defects or cataract, as described (21). We analyzed these datasets to examine potential changes in expression of the novel cataract candidate genes, as done before (11). Additionally, to gain insights into expression of candidate genes specifically in lens epithelial or fiber cells, we examined previously described RNA-seq data from isolated epithelium and fiber cells (40, 41). Gene expression analysis was performed as previously described (11, 23, 42). The University of Delaware Institutional Animal Care and Use Committee (IACUC) reviewed and approved the animal protocol.

Results

Tissue-specific TWAS analysis identified 202 gene-tissue pairs associated with cataract

We found that 202 gene-tissue pairs reached the Bonferroni significance threshold for their associations between imputed gene expression with cataract susceptibility (Supplementary Table S2). While increased predicted expression was associated with cataract risk for 79 of the Bonferroni-significant gene-tissue pairs (e.g., *IGHMBP2*-colon sigmoid, z = 8.25), decreased predicted expression was associated with cataract for 123 Bonferroni-significant gene-tissue pairs (e.g., *MRPL21* - whole blood, z = -7.64) (Figures 1, 2).

These 202 gene-tissue pairs were represented by 27 unique genes across 54 tissue reference panels (Figures 1, 2). Importantly, 2 of the 27 unique genes did not overlap previously identified cataract GWAS loci: *INSRR* on chromosome 1, and *CEP95* on chromosome 17 (Table 1). Furthermore, out of the 27 genes, we found that 9 (33.3%) were located in the 11q13.3 genomic region which was previously identified in our GWAS (11). These include: *TESMIN*, *AP000808.1*, *MRPL21*, *IGHMBP2*, *MRGPRD*, *MRGPRF*, *AP003071.4*, *MRGPRF-AS1*, and *TPCN2* (Figure 1).

Interestingly, 12 genes were Bonferroni-significant in only one tissue reference panel; these included 10 genes within previously reported cataract-associated loci: *ARL4D* (thyroid); *CDC42BPA* (heart atrial appendage); *CDKN2A* (brain cortex); *GSTM2* (whole blood); *OCA2* (brain); *PKD2L1* (lung); *SEMA4D* (spleen); *ST6GALNAC4* (blood); *TESMIN* (adipose subcutaneous); and *TPCN2* (brain cerebellar hemisphere); and 2 genes newly identified in the current study: *CEP95* (skin sun exposed lower leg), and *INSRR* (brain nucleus accumbens basal ganglia) Supplementary Table S2.

To assess whether common genetic variants underly eQTL and GWAS associations with cataract, we conducted a colocalization analysis for the 202 Bonferroni-significant gene-tissue pairs. We found that 128 (63.4%) of the Bonferroni-significant gene-tissue pairs had a colocalized variant associated with both cataract risk (from GWAS) and predicted gene expression based on our TWAS results (column COLOC.PP4 in Supplementary Table S2).

Conditional analyses provide additional support for cataract TWAS associations

To identify TWAS signals for cataract independent of GWAS genome-wide significant risk variants, we repeated the FUSION analysis with GWAS summary statistics conditioned on the top GWAS SNV in each of the 202 Bonferroni-significant gene-tissue pairs. We found that all gene-tissue pairs reached nominal significance ($P < 0.05$) (Supplementary Table S2). Furthermore, we assessed joint TWAS associations in tissue reference panels with more than one Bonferroni-significant gene on the same chromosome region (Supplementary Table S3). Of the four pairwise joint models including six unique genes, all the associations were attenuated but retained marginal significance ($P<0.05$). All six of these genes (*IGHMBP2*, *TPCN2*, *MRPL21*, *MRGPRF-AS1*, *AP000808.1*, and *MRGPRD*) are located within the 11q13.3 chromosome region, which has been previously identified as a GWAS susceptibility locus for cataract (11, 12).

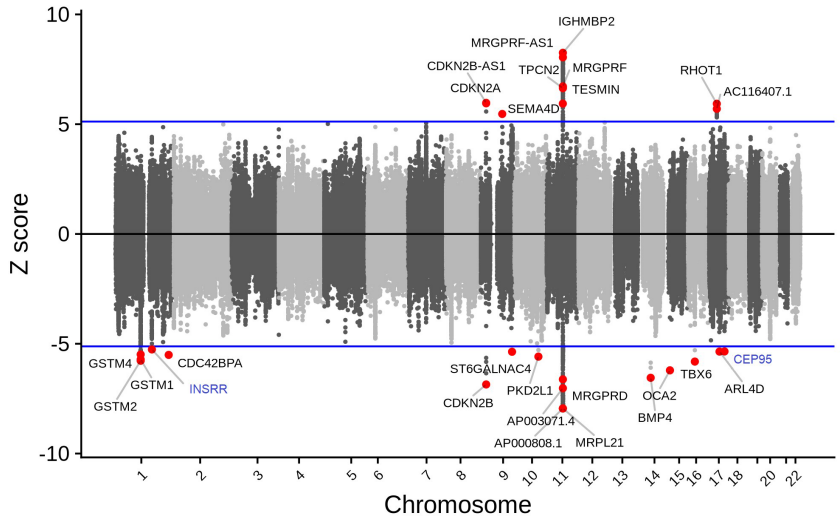

FIGURE 1
Tissue-specific TWAS analysis identified 27 unique genes associated with cataract. While increased predicted expression was associated with cataract risk for 10 genes (i.e., genes with z > 5.0; which corresponds to the results presented on the upper panel), decreased predicted expression was associated with cataract risk for 17 genes (i.e., genes with z < -5.0; which corresponds to the results presented on the lower panel). Genes in blue are novel (i.e., no prior reported GWAS SNV within 1 Mb).

Sex-specific TWAS analyses revealed 9 genes associated with cataract

Because cataracts are more common in women (4) and genetic susceptibility loci specific to women have been previously identified (11), we evaluated sex-specific TWAS associations. We used sex-specific GWAS summary statistics and tissue reference panels, i.e., GWAS summary statistics from women for TWAS of ovary, uterus, and vagina eQTLs; and GWAS summary statistics from men for TWAS of prostate and testis eQTLs. We found that 22 of the sex-

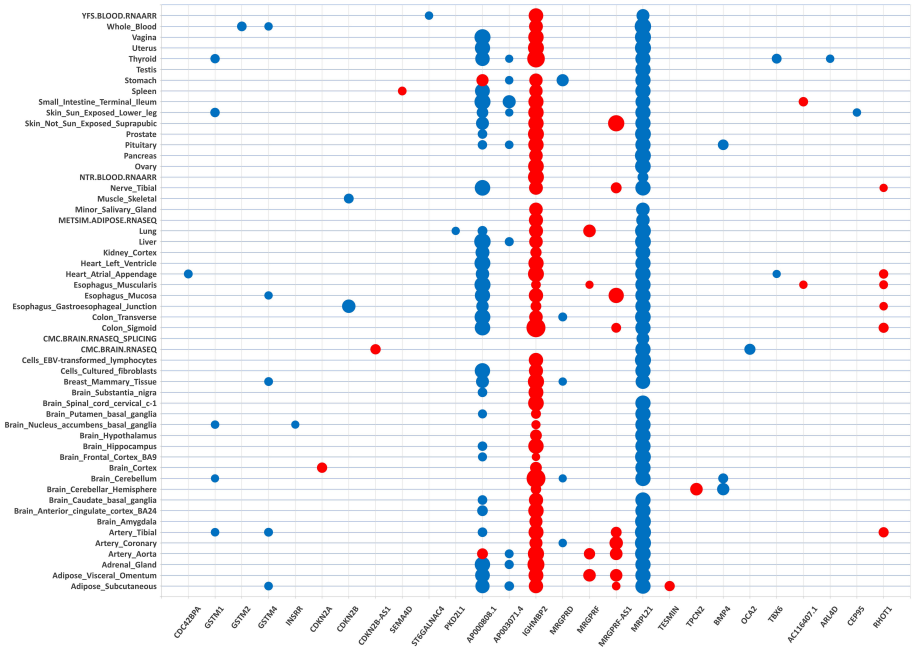

FIGURE 2
Transcriptome-wide association matrix of cataract significant gene-tissue associations. Tissue-specific TWAS analysis identified 202 gene-tissue pairs represented by 27 unique genes (on the x-axis) across 54 tissue reference panels (on the y-axis). The 27 unique genes are listed by chromosome position order (chr 1 on the left side of the matrix; chr 22 on the right side of the matrix). The tissue reference panels are listed by alphabetic order. The size of the dot for each gene-tissue association is proportional -$\log_{10}$ (TWAS.P). Color corresponds to the predicted direction of expression changes: red and blue for increased and decreased expression changes, respectively.

TABLE 1 TWAS analyses of cataract identified 99 unique genes.

GENE	Chr:position (GRCh37/hg19)	TWAS Type analyses	Novel gene (compared to known GWAS loci that reached GW level of significance)
CROCC	**chr1:17248426-17299459**	Multi-tissue TWAS	**novel**
ATP13A2	**chr1:17312453-17338423**	Multi-tissue TWAS	**novel**
CAPZB	**chr1:19665269-19810789**	Multi-tissue TWAS	**novel**
GSTM4	chr1:110198721-110204322	Tissue-specific TWAS	*GSTM2* - PMID: 34127677
GSTM2	chr1:110210679-110217908	Tissue-specific TWAS	
GSTM1	chr1:110230439-110236367	Tissue-specific TWAS	
ADAM15	chr1:155023792-155031159	Multi-tissue TWAS	*DPM3-KRTCAP2* - PMID: 34127677
EFNA1	chr1:155100352-155107375	Multi-tissue TWAS	
INSRR	**chr1:156809855-156828909**	Tissue-specific TWAS	**novel**
ADCK3	chr1:227127938-227175246	Multi-tissue TWAS	*ADCK3* - PMID: 34127677
CDC42BPA	chr1:227177559-227506193	both	
SH3YL1	**chr2:218136-261130**	Multi-tissue TWAS	**novel**
TRIB2	chr2:12857062-12882860	Multi-tissue TWAS	near *TRIB2* - PMID: 34127677
TRMT61B	chr2:29072687-29093175	Multi-tissue TWAS	*PLB1* - PMID: 34127677
EFEMP1	**chr2:56093102-56150917**	Multi-tissue TWAS	**novel**
CREB1	chr2:208394616-208470284	Multi-tissue TWAS	**novel**
DIRC3	chr2:218148746-218621316	Multi-tissue TWAS	*DIRC3* - PMID: 34127677
CXCR2	chr2:218990736-219001976	Multi-tissue TWAS	
PPM1M	chr3: 52279808-52284615	Multi-tissue TWAS	*NT5DC2* - PMID: 34127677
GLYCTK	chr3:52321844-52329273	Multi-tissue TWAS	
WDR82	chr3:52288438-52312659	Multi-tissue TWAS	
SEMA3G	chr3:52467268-52479043	Multi-tissue TWAS	
NT5DC2	chr3:52558403-52567873	Multi-tissue TWAS	
PBRM1	chr3:52579383-52719615	Multi-tissue TWAS	
GNL3	chr3:52719936-52728513	Multi-tissue TWAS	
SPCS1	chr3:52739857-52742197	Multi-tissue TWAS	
NEK4	chr3:52742460-52804956	Multi-tissue TWAS	
ITIH1	chr3:52811615-52826078	Multi-tissue TWAS	
PRKCD	chr3:53195225-53226733	Multi-tissue TWAS	
THOC7	chr3:63819546-63849481	Multi-tissue TWAS	*ATXN7* - PMID: 34127677
ATXN7	chr3:63884075-63989136	Multi-tissue TWAS	
ANKH	chr5:14704909-14871887	Multi-tissue TWAS	**novel**
HLA-DQB1	chr6:32627244-32634434	Multi-tissue TWAS	*3' HLA-DQB1* - PMID: 31816047
QKI	chr6:163835675-163999628	Multi-tissue TWAS	*QKI* - PMID: 34127677
IGFBP3	chr7:45951844-45960871	Multi-tissue TWAS	*IGFBP3-TNS3* - PMID: 34127677
NIPSNAP2	**chr7:56032278-56067872**	Multi-tissue TWAS	**novel**
C8orf58	chr8:22457112-22461655	Multi-tissue TWAS	*BIN3-EGR3* - PMID: 34127677

(Continued)

10.3389/fopht.2024.1362350

TABLE 1 Continued

GENE	Chr:position (GRCh37/hg19)	TWAS Type analyses	Novel gene (compared to known GWAS loci that reached GW level of significance)
BIN3	chr8:22477931-22526634	Multi-tissue TWAS	
CCAR2	chr8:22462270-22477984	Multi-tissue TWAS	
CDKN2B-AS1	chr9:21994790-22077889	Tissue-specific TWAS	*CDKN2B-DMRTA1* - PMID: 34127677
CDKN2A	chr9:21967751-21974856	Tissue-specific TWAS	
CDKN2B	chr9:22002902-22009304	Tissue-specific TWAS	
DMRTA1	chr9:22446823-22455739	Multi-tissue TWAS	
SEMA4D	chr9:91975702-92094805	both	*SEMA4D* - PMID: 34127677
FKTN	chr9:108320411-108403399	Multi-tissue TWAS	*FKTN-TAL2* - PMID: 34127677
ST6GALNAC4	chr9:130670165-130679320	Tissue-specific TWAS	*ST6GALNAC4-PIP5KL1* - PMID: 34127677
HERC4	chr10:69681656-69835103	Multi-tissue TWAS	**novel**
PLCE1	chr10:95753688-96092580	Multi-tissue TWAS	*PLCE1* - PMID: 34127677
NOC3L	chr10:96092988-96122683	Multi-tissue TWAS	
ABCC2	chr10:101542397-101612351	Multi-tissue TWAS	*DNMBP* - PMID: 34127677
PKD2L1	chr10:102047906-102089985	both	
ENTPD7	chr10:101419266-101470998	Multi-tissue TWAS	
CUTC	chr10:101491991-101515891	Multi-tissue TWAS	
DNMBP	chr10:101635328-101673849	Multi-tissue TWAS	
MRPL21	chr11:68658746-68671300	both	11q13.3 - PMID: 34127677
IGHMBP2	chr11:68671359-68708069	both	
TESMIN	chr11:68474908-68518988	both	
AP000808.1	chr11:68708971-68710320	Tissue-specific TWAS	
MRGPRD	chr11:68747490-68748455	Tissue-specific TWAS	
AP003071.4	chr11:68768233-68769516	Tissue-specific TWAS	
MRGPRF-AS1	chr11:68779822-68785915	Tissue-specific TWAS	
MRGPRF	chr11:68771866-68780714	both	
TPCN2	chr11:68816400-68858065	both	
PICALM	**chr11:85668218-85780126**	Multi-tissue TWAS	**novel**
CAPRIN2	chr12:30862487-30907885	Multi-tissue TWAS	*CAPRIN2* - PMID: 34127677
UBE3B	chr12:109915439-109928527	Multi-tissue TWAS	*MVK-FAM222A* - PMID: 34127677
BMP4	chr14:54416454-54420113	both	*BMP4* - PMID: 34127677
COQ6	**chr14:74416629-74430373**	Multi-tissue TWAS	**novel**
ESRRB	**chr14:76837614-76968180**	Multi-tissue TWAS	**novel**
OCA2	chr15:28000021-28344461	both	*OCA2* - PMID: 34127677
MVP	chr16:29831715-29859360	Multi-tissue TWAS	*ALDOA* - PMID: 34127677
TBX6	chr16:30097114-30103245	Tissue-specific TWAS	
NFAT5	chr16:69599869-69738569	Multi-tissue TWAS	*WWP2* - PMID: 34127677

(Continued)

TABLE 1 Continued

GENE	Chr:position (GRCh37/hg19)	TWAS Type analyses	Novel gene (compared to known GWAS loci that reached GW level of significance)
NOB1	chr16:69775757-69788871	Multi-tissue TWAS	
WWP2	chr16:69796186-69975644	Multi-tissue TWAS	
CLEC18A	chr16:69984805-69997889	Multi-tissue TWAS	
NPIPB14P	chr16:70010291-70030091	Multi-tissue TWAS	
NQO1	chr16:69743304-69760463	Multi-tissue TWAS	
PDXDC2P	chr16:70,010,201-70,099,851	Multi-tissue TWAS	
PDPR	chr16:70147529-70196440	Multi-tissue TWAS	
DDX19A	chr16:70380806-70407286	Multi-tissue TWAS	
COG4	chr16:70514470-70557457	Multi-tissue TWAS	
SENP3	**chr17:7465236-7475287**	Multi-tissue TWAS	**novel**
UTP6	chr17:30187923-30228727	Multi-tissue TWAS	*RHOT1-RHBDL3* - PMID: 34127677
RHBDL3	chr17:30592851-30651678	Multi-tissue TWAS	
RHOT1	chr17:30469521-30552746	both	
AC116407.1	chr17:30462748-30462833	Tissue-specific TWAS	
CNTNAP1	chr17:40834549-40852011	Multi-tissue TWAS	near *MIR2117HG* - PMID: 34127677
ARL4D	chr17:41476361-41478505	Tissue-specific TWAS	
GOSR2	**chr17:45000526-45014188**	Multi-tissue TWAS	**novel**
DDX5	**chr17:62494374-62502484**	Multi-tissue TWAS	**novel**
CEP95	**chr17:62503095-62534064**	Tissue-specific TWAS	**novel**
AC007773.1	**chr19:32868188-32868273**	Multi-tissue TWAS	**novel**
NECTIN2	chr19:45349554-45382195	Multi-tissue TWAS	near *EXOC3L2* - PMID: 34127677
JAG1	chr20:10618332-10654694	Multi-tissue TWAS	*JAG1* - PMID: 34127677
SLC24A3	chr20:19193286-19703570	Multi-tissue TWAS	*SLC24A3* - PMID: 34127677
EIF2S2	chr20:32676115-32700085	Multi-tissue TWAS	**novel**
ASIP	chr20:32848171-32857148	Multi-tissue TWAS	
MTMR3	chr22:30279163-30426857	Multi-tissue TWAS	*HORMAD2* - PMID: 34127677

Genes in bold are novel (i.e., no prior reported GWAS SNV within 1 Mb).

specific tests reached the Bonferroni significance level that we applied to the main analysis ($P<1.54x10^{-7}$), including 3, 5, and 4 genes for ovary, uterus, and vagina, respectively, and 7 and 3 genes for prostate and testis, respectively (Supplementary Table S4). Of those 22 sex-specific associations, 9 unique genes were identified, all of these genes (*ITPKB, AC104162.1, AP000808.1, MRPL21, IGHMBP2, CAPRIN2, CLEC18A, LINC01229* and *AC003681.1*) were located nearby previously identified GWAS loci for cataract (11, 12). For instance, while differential gene expression of *MRPL21* at 11q13.3 was associated with cataract in the 5 sex-specific tissue reference panels (i.e., ovary, uterus, vagina, prostate, and testis), differential gene expression of *ITPKB* was associated with cataract in vagina only.

Importance of gastrointestinal tissues in cataract susceptibility

Across the 54 tissue reference panels, the greatest number of Bonferroni-significant gene-tissue pairs was observed for the GTEx adipose subcutaneous, artery tibial, and thyroid datasets (seven gene-tissue pairs for each dataset), followed by the GTEx artery aorta, heart atrial appendage, esophagus muscularis, and skin sun exposed datasets (six gene-tissue pairs for each dataset) (Supplementary Table S1). To identify tissues potentially relevant to cataract, we assigned tissue reference panels to anatomical categories as described above in the Methods (Supplementary Table S1). In the tissue-specific TWAS results, gastrointestinal

tissues represented one of the highest proportion of the 202 Bonferroni-significant genes (43 genes; 21.3%) (Supplementary Figure S2). Interestingly, this gastrointestinal tissue type was the only anatomical category significantly enriched in our results, after accounting for the number of gene-tissue pairs tested per anatomical category (p-value from the hypergeometric test = 0.0055) (Supplementary Table S5).

Multi-tissue TWAS revealed additional novel candidate genes for cataract susceptibility

The multi-tissue TWAS using the omnibus test in FUSION revealed 86 genes for which imputed expression was associated with cataract susceptibility (Bonferroni p-value <0.05/13,328 effective gene tests ≈ $3.75x10^{-6}$ and minimum tissue-specific p-value < $1 x 10^{-5}$) (Supplementary Table S6). Interestingly, 14 of the 86 multi-tissue associated genes were also associated with cataract in tissue-specific models, including *INSRR* (chr1), *CDC42BPA* (chr1), *CDKN2A* (chr9), *CDKN2B* (chr9), *SEMA4D* (chr9), *ST6GALNAC4* (chr9), *PKD2L1* (chr10), *TESMIN* (chr11), *IGHMBP2* (chr11), *BMP4* (chr14), *OCA2* (chr15), *TBX6* (chr16), *RHOT1* (chr17) and*ARL4D* (chr17). In addition, 18 of the 86 multi-tissue associated genes were located outside of previously described risk loci (Table 1). These included: *CROCC* (chr1), *ATP13A2* (chr1), *CAPZB* (chr1), *SH3YL1* (chr2), *EFEMP1* (chr2), *CREB1* (chr2), *ANKH* (chr5), *NIPSNAP2* (chr7), *HERC4* (chr10), *PICALM* (chr11), *COQ6* (chr14), *ESRRB* (chr14), *SENP3* (chr17), *GOSR2* (chr17), *DDX5* (chr17), *AC007773.1* (chr19), *EIF2S2* (chr20), and *ASIP* (chr20).

Gene expression in the lens tissue

We identified the mouse orthologs for 19 of the 20 novel genes as follows. For *NIPSNAP2*, in the Affy and Illumina microarray data, the gene alias for mouse *Gbas* was used. For AC007773.1, *ZNF507* (mouse ortholog, *Zfp507*) and *DPY19L3* (mouse ortholog, *Dpy19l3*) were considered as candidate genes. We first examined the expression of these genes in the lens tissue across various stages using the iSyTE microarray database (21, 22). While majority of the genes were found to be expressed, several exhibited robust expression (Figure 3A). For example, *Atp13a2*, *Capzb*, *Crocc*, *Efemp1*, *Gbas*, *Gosr2*, *Picalm*, *Senp3* and *Zfp507* had high expression in Affymetrix datasets. When examined for "enriched expression" in the lens, several candidates (*e.g.*, *Atp13a2*, *Capzb*, *Cep95*, *Crocc*, *Dpy19l3*, *Efemp1*, *Esrrb*, *Gbas*, *Gosr2*, *Insrr*, *Picalm*, and *Senp3*) were identified (Figure 3B). Moreover, RNA-seq data from whole lens tissue confirmed 10 of the mouse orthologs to have expression or enriched expression in the lens (Supplementary Figures S3, 4). Further, expression data from isolated lens epithelium and fiber cells at different time-points, spanning embryonic (E14.5 through newborn) through aging stages (3 months through age 2 years) showed that all the novel cataract candidate genes with mouse orthologs exhibit robust expression in the epithelium and/or fiber cells (Supplementary Figure S5). Interestingly, this cell-specific data also shows that three candidate genes are specifically enriched in the postnatal epithelium (*e.g.*, *Efemp1*, *Esrrb*, *Insrr*) and a subset of these exhibit progressively high expression with aging in the epithelium (*e.g.*, *Efemp1*, *Insrr*). Finally, all novel candidate genes exhibited differential expression in at least one gene-perturbation mouse models of lens defects/cataract (Supplementary Figure S6).

Discussion

By leveraging data from GWAS and eQTL, we identified 99 genes associated with cataract susceptibility (16 from the tissue-specific analysis alone, 69 from the multi-tissue analysis alone, and 14 from both analyses). Of these 99 genes, 20 were novel to the extent they did not overlap known cataract risk loci from GWAS (2 of these, *INSRR and CEP95*, were from tissue-specific models, and 18 from the multi-tissue analysis). Mouse orthologs of the vast majority of the human candidate genes were found to be robustly expressed in the lens. We also highlighted the contribution of the 11q13.3 genomic region in cataract susceptibility. Our results implicated a role for gastrointestinal tissues and confirmed the importance of the lens in cataract etiology.

Our tissue-specific TWAS analysis identified *INSRR* (1q23.1) and *CEP95* (17q23.3) as novel cataract-associated genes. *INSRR* encodes the insulin receptor related receptor which is involved in the transmembrane receptor protein tyrosine kinase activity, actin cytoskeleton reorganization, and the protein autophosphorylation, and has an important role in the alkaline pH-dependent activation mechanism (43). *CEP95* encodes the centrosomal protein 95 and belongs to the family of proteins containing coiled-coil domains (CCDCs), which are involved in several functions in cell growth and development, such as regulation of gene expression (44). To date, no mutations in either *INSRR* or *CEP95* have been linked to eye diseases, and further studies are needed to confirm the role of these genes in cataract etiology and determine their precise role in cataract susceptibility.

Our multi-tissue TWAS analysis identified *ATP13A2* (1p36.13), *CAPZB* (1p36.13), *EFEMP1* (2p16.1), and *SENP3* (17p13.1) associated with cataract, all were not previously reported as significant in GWA studies of cataract. *ATP13A2* encodes a member of the P5 subfamily of ATPases which transports inorganic cations as well as other substrates. The *ATP13A2* locus has been previously reported to be associated with age-related cataract in a GWAS conducted in a Chinese cohort (45); however, this association did not reach a genome-wide level of significance (lead SNV rs2871776, P=$4.18x10^{-5}$), possibly due to limited sample size (total of 191 cataract cases and 208 controls) (45). *CAPZB* encodes the beta subunit of the barbed-end actin binding protein, which belongs to the F-actin capping protein family. Interestingly, *CAPZB* is located within the 1p36 chromosome region that was previously linked to congenital cataract in three genetic linkage studies (46–48). However, no segregating mutations that contribute to congenital cataract were identified in this *CAPZB* gene in a six-generation Australian family displaying linkage to chromosome 1p36 (49). *EFEMP1* encodes a

10.3389/fopht.2024.1362350

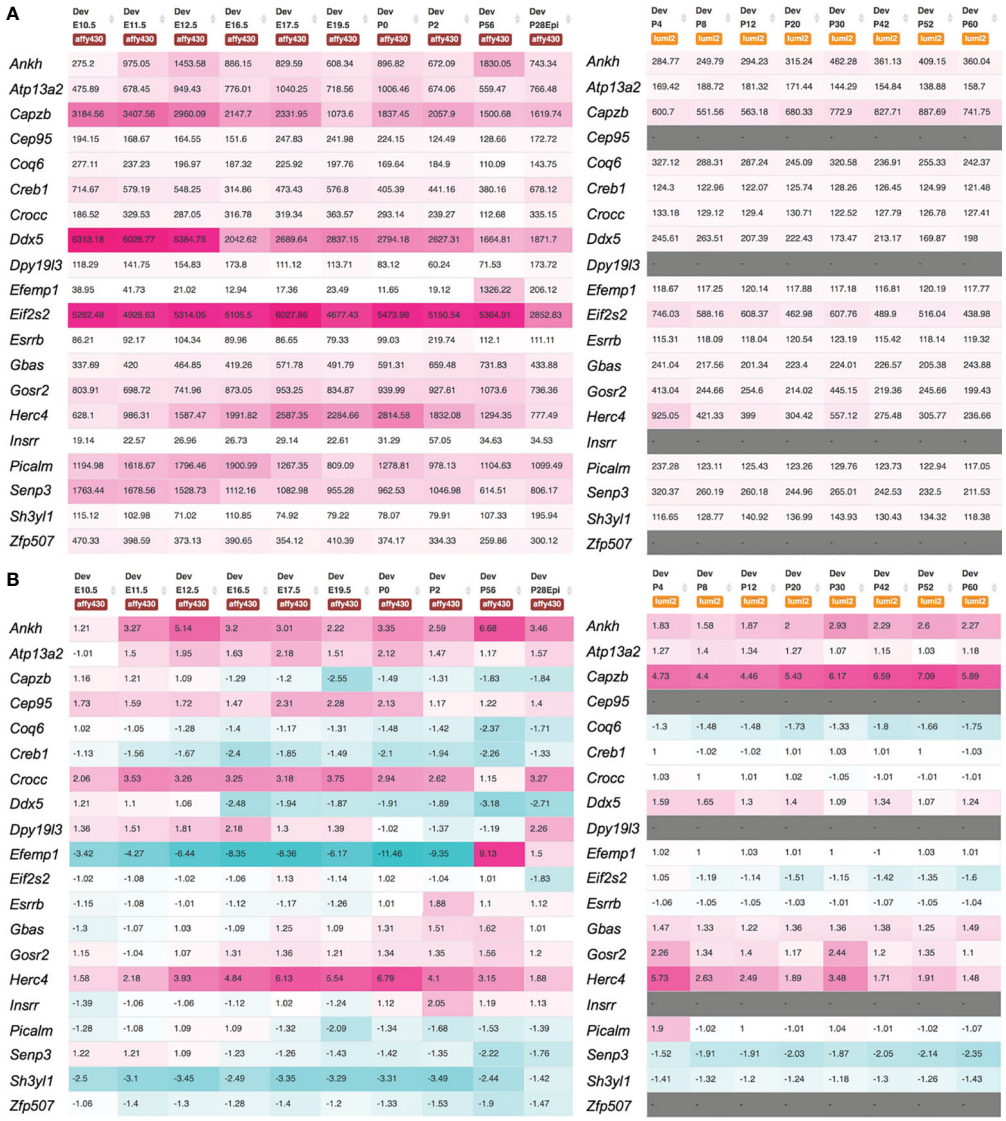

FIGURE 3
Expression of novel candidate genes for cataract in the mouse lens. Mouse orthologs of the human candidate genes were examined for their lens expression in the iSyTE microarray datasets. **(A)** Analysis of whole lens tissue data on the Affymetrix and Illumina microarray platforms at different embryonic (E) and postnatal (P) stages indicates that majority of the candidates are expressed in the lens. The heat-map denotes the range of expression on either the Affymetrix or Illumina platform, while the number represents the mean fluorescence intensity for individual genes. **(B)** Mouse orthologs of the human candidate genes were examined for their "lens enriched" expression in the iSyTE microarray data. "Enriched expression" in the lens is estimated by analyzing the fold-change enrichment of candidate gene expression in the lens compared to that in whole embryonic body as indicated by the number and heatmap. Please note that WEB in the Affymetrix data represents expression in whole embryonic body in **(A)** and P28Epi in the Affymetrix data represents expression data on isolated lens epithelium in **(A, B)**.

member of the fibulin family of extracellular matrix glycoproteins, and mutations in this gene have been shown to cause Doyne honeycomb retinal dystrophy and familial juvenile-onset open-angle glaucoma (50, 51). Recently, *EFEMP1* has been demonstrated to be a potential biomarker for choroidal neovascularization in age-related macular degeneration, and for choroidal thickness change in myopia (52, 53). Interestingly, a transcriptome analysis of neural progenitor cells derived from patients with Lowe syndrome, a multisystem disorder characterized notably by anomalies affecting the eye, including congenital cataracts, identified *EFEMP1* as a candidate gene (54). Future studies will clarify how *EFEMP1* contributes to cataract susceptibility. Our study also identified *SENP3* as a cataract-associated gene. *SENP3* encodes the SUMO specific peptidase 3 which is a de-sumoylation enzyme (SENP) that plays an important role in regulating eye development and is highly expressed in vertebrate ocular cell lines, including human, mouse, and rabbit lens epithelial cells lines (55, 56). Previous works have demonstrated that sumoylation function plays indispensable roles during lens differentiation (57, 58). Recently, glucose oxidase and UVA irradiation seem to affect the expression patterns of the *SENP*s, including *SENP3*, in the *in vitro* cataract models, providing evidence to link sumoylation function to stress-induced cataractogenesis (59). Moreover, the changing patterns in some *SENP*s levels seem

to act as molecular markers for both senile and complicated cataracts (60). Additional studies investigating the sumoylation functions and the related mechanisms in cataract development and progression will help to understand the role of *SENP3* in cataract susceptibility.

Among the 9 unique genes identified in the tissue-sex specific analyses of cataract, we identified *ITPKB* (1q42.12), which was differentially expressed in the vagina. *ITPKB* encodes the inositol-trisphosphate 3-kinase B that plays an important role in the regulation of the levels of a large number of inositol polyphosphates (61). A *de novo* 5.8-Mb deletion encompassing the chromosome 1q42.12q42.2 region (and *ITPKB*, among other genes) was reported in a 4-year-old child who presented hypoplastic corpus callosum and bilateral cataracts, in addition to other clinical features such as epilepsy (62). Future investigations may determine the implication of *ITPKB* in cataract etiology.

Our study should be interpreted within the context of its limitations. Although GTEx data for the 49 tissues represent the most comprehensive eQTL dataset of human tissues, it does not include ocular tissues and consequently we may have failed to identify the real causal genes in the unsampled ocular tissue. However, we have confirmed using the iSyTE database that novel cataract genes identified in the current study are robustly expressed in lens tissue, which is a cataract relevant eye tissue. Moreover, although cataract is primarily a lens disorder, it has been demonstrated that most complex diseases, including vision disorders such as age-related macular degeneration, might manifest in several tissues across the body (63). Despite the great success in prioritizing gene-trait associations in complex diseases and traits, TWAS may present multiple hits per locus, owing to co-regulation, which remain problematic (14, 19). Thus, future models could consider more complex genetic architecture containing different regulatory effects, and our TWAS results could benefit from subsequent functional assays to indicate the potential targets underlying the identified associations, notably at 11q13.3. Despite these limitations, our TWAS study is based on results from a large GWAS meta-analysis on almost 60,000 cataract cases, enabling the prioritization and the discovery of potential causal genes for cataract. Finally, in the current study, we performed a multi-tissue TWAS analysis which enables increased statistical precision compared to single-tissue approaches (17, 64, 65).

Our study also highlighted the important contribution of gastrointestinal tissues in cataract susceptibility consistent with previous work showing associations between cataracts and gastrointestinal disorders (66, 67). For instance, patients diagnosed with early-onset cataracts have been shown to be at increased risk of peptic ulcer (66). Furthermore, rare syndromic disorders for which patients present early-onset congenital cataracts can present gastrointestinal disorders as additional features (68–71). For instance, patients with Lowe Syndrome (oculocerebrorenal syndrome) can present both dense congenital cataracts and gastroesophageal reflux (68). Similarly, patients with inherited spastic paraplegia can present with bilateral cataracts and gastroesophageal reflux with persistent vomiting (69). A splice site mutation in *CYP27A1* has been reported to lead to cerebrotendinous xanthomatosis which can be characterized by pulverulent cataracts and gastrointestinal problems such as diarrhea (71). Recently, pathogenic variants in the *WFS1/RP1/NOD2* genes have been shown to cause congenital cataract, retinitis pigmentosa, and Crohn's disease in a five generation British family (70). A comprehensive evaluation of systemic disorders associated with age-related cataract – as previously done for dry eye disease (72)- would help to identify which gastrointestinal disorders are risk factors for cataract. Altogether, expression of genes associated with cataract seems not to be restricted to lens tissue, as could be expected for this lens disorder, and the processes underlying cataract pathology seem to be systemic as observed for other vision disorders, such as age-related macular degeneration and exfoliation syndrome (37, 73).

In conclusion, we identified 99 genes associated with cataract susceptibility, of which 20 did not overlap with known cataract risk loci. Our results provide evidence of the utility of imputation-based TWAS approaches to characterize known GWAS risk loci and identify novel candidate genes that may increase our understanding of cataract etiology.

Data availability statement

The original contributions presented in the study are publicly available. FUSION models trained on the GTEx version 8 data are available here: http://gusevlab.org/projects/fusion/. Gene expression and eQTL data are freely available at https://gtexportal.org/home/datasets. Expression or lens-enriched expression heat-map for candidate genes can be accessed through the iSyTE web-tool (https://research.bioinformatics.udel.edu/iSyTE). The RNA-seq data can be found here: Gene Expression Omnibus (GEO; GSE113887, GSE166619, GSE119596). The microarray data can be found here: Gene Expression Omnibus (GEO; GSE100136, GSE32334, GSE65500, GSE47694, GSE16533, GSE31643, GSE9711, GSE13402, GSE25775, GSE25776, GSE22322, GSE22362, GSE9711). To protect individual's privacy, complete GERA data are available upon approved applications to the KP Research Bank Portal (https://researchbank.kaiserpermanente.org/). A subset of the GERA cohort consented for public use can be found at NIH/dbGaP: phs000674.v3.p3.

Ethics statement

The studies involving humans were approved by The Institutional Review Board of the Kaiser Permanente Northern California. The studies were conducted in accordance with the local legislation and institutional requirements. The participants provided their written informed consent to participate in this study. The animal study was approved by The University of Delaware Institutional Animal Care and Use Committee (IACUC). The study was conducted in accordance with the local legislation and institutional requirements.

Author contributions

HC: Conceptualization, Funding acquisition, Resources, Supervision, Visualization, Writing – original draft, Writing – review & editing. MD: Formal analysis, Visualization, Writing – review & editing. VH: Formal analysis, Visualization, Writing – review & editing. SS: Formal analysis, Visualization, Writing – review & editing. TM: Conceptualization, Methodology, Writing – review & editing. TH: Methodology, Resources, Writing – review & editing. PS: Conceptualization, Writing – review & editing. SL: Conceptualization, Funding acquisition, Resources, Supervision, Visualization, Writing – original draft, Writing – review & editing.

Funding

The author(s) declare financial support was received for the research, authorship, and/or publication of this article. Support for participant enrollment, survey completion, and biospecimen collection for the Kaiser Permanente Research Program on Genes, Environment, and Health was provided by the Robert Wood Johnson Foundation, the Wayne and Gladys Valley Foundation, the Ellison Medical Foundation, and Kaiser Permanente Community Benefit Programs. Genotyping of the GERA cohort was funded by a grant from the National Institute on Aging, National Institute of Mental Health, and National Institute of Health Common Fund (RC2 AG036607). HC and SL are supported by the National Eye Institute (NEI) grant R01 EY033010.

Acknowledgments

We are grateful to the Kaiser Permanente Northern California members who have generously agreed to participate in the Kaiser Permanente Research Program on Genes, Environment, and Health.

Conflict of interest

The authors declare that the research was conducted in the absence of any commercial or financial relationships that could be construed as a potential conflict of interest.

Publisher's note

Supplementary material

The Supplementary Material for this article can be found online at: https://www.frontiersin.org/articles/10.3389/fopht.2024.1362350/full#supplementary-material

References

1. Congdon N, Vingerling JR, Klein BE, West S, Friedman DS, Kempen J, et al. Prevalence of cataract and pseudophakia/aphakia among adults in the United States. *Arch Ophthalmol*. (2004) 122:487–94. doi: 10.1001/archopht.122.4.487

2. Liu YC, Wilkins M, Kim T, Malyugin B, Mehta JS. Cataracts. *Lancet*. (2017) 390:600–12. doi: 10.1016/S0140-6736(17)30544-5

3. Jiang C, Melles RB, Sangani P, Hoffmann TJ, Hysi PG, Glymour MM, et al. Association of behavioral and clinical risk factors with cataract: A two-sample mendelian randomization study. *Invest Ophthalmol Vis Sci*. (2023) 64:19. doi: 10.1167/iovs.64.10.19

4. Lou L, Ye X, Xu P, Wang J, Xu Y, Jin K, et al. Association of sex with the global burden of cataract. *JAMA Ophthalmol*. (2018) 136:116–21. doi: 10.1001/jamaophthalmol.2017.5668

5. Heiba IM, Elston RC, Klein BE, Klein R. Genetic etiology of nuclear cataract: evidence for a major gene. *Am J Med Genet*. (1993) 47:1208–14. doi: 10.1002/ajmg.1320470816

6. Hammond CJ, Snieder H, Spector TD, Gilbert CE. Genetic and environmental factors in age-related nuclear cataracts in monozygotic and dizygotic twins. *N Engl J Med*. (2000) 342:1786–90. doi: 10.1056/NEJM200006153422404

7. Hammond CJ, Duncan DD, Snieder H, de Lange M, West SK, Spector TD, et al. The heritability of age-related cortical cataract: the twin eye study. *Invest Ophthalmol Vis Sci*. (2001) 42:601–5.

8. Congdon N, Broman KW, Lai H, Munoz B, Bowie H, Gilber D, et al. Nuclear cataract shows significant familial aggregation in an older population after adjustment for possible shared environmental factors. *Invest Ophthalmol Vis Sci*. (2004) 45:2182–6. doi: 10.1167/iovs.03-1163

9. Sanfilippo PG, Hewitt AW, Hammond CJ, Mackey DA. The heritability of ocular traits. *Surv Ophthalmol*. (2010) 55:561–83. doi: 10.1016/j.survophthal.2010.07.003

10. Yonova-Doing E, Forkin ZA, Hysi PG, Williams KM, Spector TD, Gilbert CE, et al. Genetic and dietary factors influencing the progression of nuclear cataract. *Ophthalmology*. (2016) 123:1237–44. doi: 10.1016/j.ophtha.2016.01.036

11. Choquet H, Melles RB, Anand D, Yin J, Cuellar-Partida G, Wang W, et al. A large multiethnic GWAS meta-analysis of cataract identifies new risk loci and sex-specific effects. *Nat Commun*. (2021) 12:3595. doi: 10.1038/s41467-021-23873-8

12. Boutin TS, Charteris DG, Chandra A, Campbell S, Hayward C, Campbell A, et al. Insights into the genetic basis of retinal detachment. *Hum Mol Genet*. (2020) 29:689–702. doi: 10.1093/hmg/ddz294

13. Yonova-Doing E, Zhao W, Igo RP Jr., Wang C, Sundaresan P, Lee KE, et al. Common variants in SOX-2 and congenital cataract genes contribute to age-related nuclear cataract. *Commun Biol*. (2020) 3:755. doi: 10.1038/s42003-020-01421-2

14. Wainberg M, Sinnott-Armstrong N, Mancuso N, Barbeira AN, Knowles DA, Golan D, et al. Opportunities and challenges for transcriptome-wide association studies. *Nat Genet*. (2019) 51:592–9. doi: 10.1038/s41588-019-0385-z

15. Nica AC, Montgomery SB, Dimas AS, Stranger BE, Beazley C, Barroso I, et al. Candidate causal regulatory effects by integration of expression QTLs with complex trait genetic associations. *PloS Genet*. (2010) 6:e1000895. doi: 10.1371/journal.pgen.1000895

16. Mancuso N, Gayther S, Gusev A, Zheng W, Penney KL, Kote-Jarai Z, et al. Large-scale transcriptome-wide association study identifies new prostate cancer risk regions. *Nat Commun*. (2018) 9:4079. doi: 10.1038/s41467-018-06302-1

17. Barbeira AN, Pividori M, Zheng J, Wheeler HE, Nicolae DL, Im HK. Integrating predicted transcriptome from multiple tissues improves association detection. *PloS Genet*. (2019) 15:e1007889. doi: 10.1371/journal.pgen.1007889

18. Gusev A, Ko A, Shi H, Bhatia G, Chung W, Penninx BW, et al. Integrative approaches for large-scale transcriptome-wide association studies. *Nat Genet*. (2016) 48:245–52. doi: 10.1038/ng.3506

19. Mai J, Lu M, Gao Q, Zeng J, Xiao J. Transcriptome-wide association studies: recent advances in methods, applications and available databases. *Commun Biol*. (2023) 6:899. doi: 10.1038/s42003-023-05279-y

20. GTEx project maps wide range of normal human genetic variation: A unique catalog and follow-up effort associate variation with gene expression across dozens of body tissues. *Am J Med Genet A*. (2018) 176:263–4. doi: 10.1002/ajmg.a.38426

21. Kakrana A, Yang A, Anand D, Djordjevic D, Ramachandruni D, Singh A, et al. iSyTE 2.0: a database for expression-based gene discovery in the eye. *Nucleic Acids Res*. (2018) 46:D875–85. doi: 10.1093/nar/gkx837

22. Lachke SA, Ho JW, Kryukov GV, O'Connell DJ, Aboukhalil A, Bulyk ML, et al. iSyTE: integrated Systems Tool for Eye gene discovery. *Invest Ophthalmol Vis Sci*. (2012) 53:1617–27. doi: 10.1167/iovs.11-8839

23. Anand D, Kakrana A, Siddam AD, Huang H, Saadi I, Lachke SA. RNA sequencing-based transcriptomic profiles of embryonic lens development for cataract gene discovery. *Hum Genet*. (2018) 137:941–54. doi: 10.1007/s00439-018-1958-0

24. Aryal S, Anand D, Hernandez FG, Weatherbee BAT, Huang H, Reddy AP, et al. MS/MS in silico subtraction-based proteomic profiling as an approach to facilitate disease gene discovery: application to lens development and cataract. *Hum Genet*. (2020) 139:151–84. doi: 10.1007/s00439-019-02095-5

25. Banda Y, Kvale MN, Hoffmann TJ, Hesselson SE, Ranatunga D, Tang H, et al. Characterizing race/ethnicity and genetic ancestry for 100,000 subjects in the genetic epidemiology research on adult health and aging (GERA) cohort. *Genetics*. (2015) 200:1285–95. doi: 10.1534/genetics.115.178616

26. Bycroft C, Freeman C, Petkova D, Band G, Elliott LT, Sharp K, et al. The UK Biobank resource with deep phenotyping and genomic data. *Nature*. (2018) 562:203–9. doi: 10.1038/s41586-018-0579-z

27. Sudlow C, Gallacher J, Allen N, Beral V, Burton P, Danesh J, et al. UK biobank: an open access resource for identifying the causes of a wide range of complex diseases of middle and old age. *PloS Med*. (2015) 12:e1001779. doi: 10.1371/journal.pmed.1001779

28. Balduzzi S, Rucker G, Schwarzer G. How to perform a meta-analysis with R: a practical tutorial. *Evid Based Ment Health*. (2019) 22:153–60. doi: 10.1136/ebmental-2019-300117

29. Hoffman GE, Bendl J, Voloudakis G, Montgomery KS, Sloofman L, Wang YC, et al. CommonMind Consortium provides transcriptomic and epigenomic data for Schizophrenia and Bipolar Disorder. *Sci Data*. (2019) 6:180. doi: 10.1038/s41597-019-0183-6

30. Laakso M, Kuusisto J, Stancakova A, Kuulasmaa T, Pajukanta P, Lusis AJ, et al. The Metabolic Syndrome in Men study: a resource for studies of metabolic and cardiovascular diseases. *J Lipid Res*. (2017) 58:481–93. doi: 10.1194/jlr.O072629

31. Ligthart L, van Beijsterveldt CEM, Kevenaar ST, de Zeeuw E, van Bergen E, Bruins S, et al. The Netherlands twin register: longitudinal research based on twin and twin-family designs. *Twin Res Hum Genet*. (2019) 22:623–36. doi: 10.1017/thg.2019.93

32. Akerblom HK, Uhari M, Pesonen E, Dahl M, Kaprio EA, Nuutinen EM, et al. Cardiovascular risk in young Finns. *Ann Med*. (1991) 23:35–9. doi: 10.3109/07853899109147928

33. Meyers TJ, Yin J, Herrera VA, Pressman AR, Hoffmann TJ, Schaefer C, et al. Transcriptome-wide association study identifies novel candidate susceptibility genes for migraine. *HGG Adv*. (2023) 4:100211. doi: 10.1016/j.xhgg.2023.100211

34. Genomes Project, C, Auton A, Brooks LD, Durbin RM, Garrison EP, Kang HM, et al. A global reference for human genetic variation. *Nature*. (2015) 526:68–74. doi: 10.1038/nature15393

35. Giambartolomei C, Vukcevic D, SChadt EE, Franke L, Hingorani AD, Wallace C, et al. Bayesian test for colocalisation between pairs of genetic association studies using summary statistics. *PloS Genet*. (2014) 10:e1004383. doi: 10.1371/journal.pgen.1004383

36. Yang J, Ferreira T, Morris AP, Medland SEGenetic Investigation of, A.T.C. and Replication, D.I.G., Meta-analysis, C., et al. Conditional and joint multiple-SNP analysis of GWAS summary statistics identifies additional variants influencing complex traits. *Nat Genet*. (2012) 44:369–375, S361–363. doi: 10.1038/ng.2213

37. Strunz T, Lauwen S, Kiel CInternational, A.M.D.G.C., , Hollander AD, Weber BHF. A transcriptome-wide association study based on 27 tissues identifies 106 genes potentially relevant for disease pathology in age-related macular degeneration. *Sci Rep*. (2020) 10:1584. doi: 10.1038/s41598-020-58510-9

38. Anand D, Agrawal S, Siddam A, Motohashi H, Yamamoto M, Lachke SA. An integrative approach to analyze microarray datasets for prioritization of genes relevant to lens biology and disease. *Genom Data*. (2015) 5:223–7. doi: 10.1016/j.gdata.2015.06.017

39. Anand D, Lachke SA. Systems biology of lens development: A paradigm for disease gene discovery in the eye. *Exp Eye Res*. (2017) 156:22–33. doi: 10.1016/j.exer.2016.03.010

40. Zhao Y, Zheng D, Cvekl A. A comprehensive spatial-temporal transcriptomic analysis of differentiating nascent mouse lens epithelial and fiber cells. *Exp Eye Res*. (2018) 175:56–72. doi: 10.1016/j.exer.2018.06.004

41. Faranda AP, Shihan MH, Wang Y, Duncan MK. The aging mouse lens transcriptome. *Exp Eye Res*. (2021) 209:108663. doi: 10.1016/j.exer.2021.108663

42. Siddam AD, Duot M, Coomson SY, Anand D, Aryal S, Weatherbee BAT, et al. High-throughput transcriptomics of celf1 conditional knockout lens identifies downstream networks linked to cataract pathology. *Cells*. (2023) 12(7):1070. doi: 10.3390/cells12071070

43. Wang L, Hall C, Li J, Choi E, Bai XC. Structural basis of the alkaline pH-dependent activation of insulin receptor-related receptor. *Nat Struct Mol Biol*. (2023) 30:661–9. doi: 10.1038/s41594-023-00974-0

44. Liu S, Jia L, Quan B, Rong G, Li M, Xie R, et al. Coiled-coil domain-containing protein 45 is a potential prognostic biomarker and is associated with immune cell enrichment of hepatocellular carcinoma. *Dis Markers*. (2022) 2022:7745315. doi: 10.1155/2022/7745315

45. Li JK, Li LL, Li W, Wang ZW, Gao FJ, Hu FY, et al. Panel-based targeted exome sequencing reveals novel candidate susceptibility loci for age-related cataracts in Chinese Cohort. *Mol Genet Genomic Med*. (2020) 8:e1218. doi: 10.1002/mgg3.1218

46. Eiberg H, Lund AM, Warburg M, Rosenberg T. Assignment of congenital cataract Volkmann type (CCV) to chromosome 1p36. *Hum Genet*. (1995) 96:33–8. doi: 10.1007/BF00214183

47. Ionides AC, Berry V, Mackay DS, Moore AT, Bhattacharya SS, Shiels A. A locus for autosomal dominant posterior polar cataract on chromosome 1p. *Hum Mol Genet*. (1997) 6:47–51. doi: 10.1093/hmg/6.1.47

48. McKay JD, Patterson B, Craig JE, Russell-Eggitt IM, Wirth MG, Burdon KP, et al. The telomere of human chromosome 1p contains at least two independent autosomal dominant congenital cataract genes. *Br J Ophthalmol*. (2005) 89:831–4. doi: 10.1136/bjo.2004.058495

49. Burdon KP, Hattersley K, Lachke SA, Laurie KJ, Maas RL, Mackey DA, et al. Investigation of eight candidate genes on chromosome 1p36 for autosomal dominant total congenital cataract. *Mol Vis*. (2008) 14:1799–804.

50. Collantes ERA, Delfin MS, Fan B, Torregosa JMR, Siguan-Bell C, Florcruz NVG, et al. EFEMP1 rare variants cause familial juvenile-onset open-angle glaucoma. *Hum Mutat*. (2022) 43:240–52. doi: 10.1002/humu.24320

51. Stone EM, Lotery AJ, Munier FL, Heon E, Piguet B, Guymer RH, et al. A single EFEMP1 mutation associated with both Malattia Leventinese and Doyne honeycomb retinal dystrophy. *Nat Genet*. (1999) 22:199–202. doi: 10.1038/9722

52. Cheng L, Chen C, Guo W, Liu K, Zhao Q, Lu P, et al. EFEMP1 overexpression contributes to neovascularization in age-related macular degeneration. *Front Pharmacol*. (2020) 11:547436. doi: 10.3389/fphar.2020.547436

53. Shi WQ, Wan T, Li B, Li T, Zhou XD. EFEMP1 is a potential biomarker of choroid thickness change in myopia. *Front Neurosci*. (2023) 17:1144421. doi: 10.3389/fnins.2023.1144421

54. Liu H, Barnes J, Pedrosa E, Herman NS, Salas F, Wang P, et al. Transcriptome analysis of neural progenitor cells derived from Lowe syndrome induced pluripotent stem cells: identification of candidate genes for the neurodevelopmental and eye manifestations. *J Neurodev Disord*. (2020) 12:14. doi: 10.1186/s11689-020-09317-2

55. Liu Y, Zhang L, Tang X, Liu F, Fu JL, Gong XD, et al. Determination of expression patterns of seven de-sumoylation enzymes in major ocular cell lines. *Curr Mol Med*. (2018) 18:584–93. doi: 10.2174/1566524019666190107153440

56. Liu Y, Liu F, Wang L, Fu JL, Luo ZW, Nie Q, et al. Localization analysis of seven de-sumoylation enzymes (SENPs) in ocular cell lines. *Curr Mol Med*. (2018) 18:523–32. doi: 10.2174/1566524019666190112142025

57. Yan Q, Gong L, Deng M, Zhang L, Sun S, Liu J, et al. Sumoylation activates the transcriptional activity of Pax-6, an important transcription factor for eye and brain development. *Proc Natl Acad Sci U.S.A*. (2010) 107:21034–9. doi: 10.1073/pnas.1007866107

58. Gong L, Ji WK, Hu XH, Hu WF, Tang XC, Huang ZX, et al. Sumoylation differentially regulates Sp1 to control cell differentiation. *Proc Natl Acad Sci U.S.A*. (2014) 111:5574–9. doi: 10.1073/pnas.1315034111

59. Xiang JW, Xiao Y, Gan Y, Chen H, Liu Y, Wang L, et al. Glucose oxidase- and UVA-induced changes in the expression patterns of seven de-sumoylation enzymes (SENPs) are associated with cataract development. *Curr Mol Med*. (2019) 19:48–53. doi: 10.2174/1566524019666190311094313

60. Liu FY, Fu JL, Wang L, Nie Q, Luo Z, Hou M, et al. Molecular signature for senile and complicated cataracts derived from analysis of sumoylation enzymes and their substrates in human cataract lenses. *Aging Cell*. (2020) 19:e13222. doi: 10.1111/acel.13222

61. Erneux C, Ghosh S, Koenig S. Inositol(1,4,5)P3 3-kinase isoenzymes: Catalytic properties and importance of targeting to F-actin to understand function. *Adv Biol Regul*. (2016) 60:135–43. doi: 10.1016/j.jbior.2015.09.004

62. Radha Rama Devi A, Ganapathy A, Mannan AU, Sabharanjak S, Naushad SM. 1q42.12q42.2 deletion in a child with midline defects and hypoplasia of the corpus callosum. *Mol Syndromol*. (2019) 10:161–6. doi: 10.1159/000496079

63. Ongen H, Brown AA, Delaneau O, Panousis NI, Nica ACConsortium, G.T., et al. Estimating the causal tissues for complex traits and diseases. *Nat Genet*. (2017) 49:1676–83. doi: 10.1038/ng.3981

64. Grinberg NF, Wallace C. Multi-tissue transcriptome-wide association studies. *Genet Epidemiol*. (2021) 45:324–37. doi: 10.1002/gepi.22374

65. Hu Y, Li M, Lu Q, Weng H, Wang J, Zekavat SM, et al. A statistical framework for cross-tissue transcriptome-wide association analysis. *Nat Genet*. (2019) 51:568–76. doi: 10.1038/s41588-019-0345-7

66. Hsia NY, Tsai YY, Lin CL, Chiang CC. Increased risk of peptic ulcer in patients with early-onset cataracts: A nationwide population-based study. *PloS One*. (2018) 13:e0207193. doi: 10.1371/journal.pone.0207193

67. Trumler AA. Evaluation of pediatric cataracts and systemic disorders. *Curr Opin Ophthalmol*. (2011) 22:365–79. doi: 10.1097/ICU.0b013e32834994dc

68. Lewis RA, Nussbaum RL, Brewer ED. Lowe Syndrome. In: Adam MP, Feldman J, Mirzaa GM, Pagon RA, Wallace SE, Bean LJH, . Gripp KW, Amemiya A, editors. *GeneReviews((R))* (1993). Seattle (WA): University of Washington, Seattle.

69. Lo Nigro C, Cusano R, Gigli GL, Forabosco P, Valente M, Ravazzolo R, et al. Genetic heterogeneity in inherited spastic paraplegia associated with epilepsy. *Am J Med Genet A*. (2003) 117A:116–21. doi: 10.1002/ajmg.a.10141

70. Berry V, Ionides A, Georgiou M, Quinlan RA, Michaelides M. Multimorbidity due to novel pathogenic variants in the WFS1/RP1/NOD2 genes: autosomal dominant congenital lamellar cataract, retinitis pigmentosa and Crohn's disease in a British family. *BMJ Open Ophthalmol*. (2023) 8(1):e001252. doi: 10.1136/bmjophth-2023-001252

71. Bourkiza R, Joyce S, Patel H, Chan M, Meyer E, Maher ER, et al. Cerebrotendinous xanthomatosis (CTX): an association of pulverulent cataracts and pseudo-dominant developmental delay in a family with a splice site mutation in CYP27A1–a case report. *Ophthalmic Genet*. (2010) 31:73–6. doi: 10.3109/13816810903584963

72. Vehof J, Snieder H, Jansonius N, Hammond CJ. Prevalence and risk factors of dry eye in 79,866 participants of the population-based Lifelines cohort study in the Netherlands. *Ocul Surf*. (2021) 19:83–93. doi: 10.1016/j.jtos.2020.04.005

73. Hirbo JB, Pasutto F, Gamazon ER, Evans P, Pawar P, Berner D, et al. Analysis of genetically determined gene expression suggests role of inflammatory processes in exfoliation syndrome. *BMC Genomics*. (2023) 24:75. doi: 10.1186/s12864-023-09179-7

frontiers | Frontiers in Ophthalmology

TYPE Original Research
PUBLISHED 03 May 2024
DOI 10.3389/fopht.2024.1387961

OPEN ACCESS

EDITED BY
Barbara Pierscionek,
Anglia Ruskin University, United Kingdom

REVIEWED BY
Eric C. Beyer,
The University of Chicago, United States
Paul James Donaldson,
The University of Auckland, New Zealand

*CORRESPONDENCE
Chun-hong Xia
chxia@berkeley.edu

RECEIVED 19 February 2024
ACCEPTED 15 April 2024
PUBLISHED 03 May 2024

CITATION
Painter T, Ou C, Gong X and Xia C-h (2024) Longitudinal study of microphthalmia in connexin 50 knockout mice using spectral-domain optical coherence tomography. *Front. Ophthalmol.* 4:1387961. doi: 10.3389/fopht.2024.1387961

Longitudinal study of microphthalmia in connexin 50 knockout mice using spectral-domain optical coherence tomography

Taishi Painter, Chenxi Ou, Xiaohua Gong and Chun-hong Xia*

Herbert Wertheim School of Optometry and Vision Science Program, University of California, Berkeley, Berkeley, CA, United States

Connexin 50 (Cx50) mediated signaling is essential for controlling the lens growth and size. Cx50 mutations cause microphthalmia, smaller lenses, and cataracts in humans and animals. These ocular defects have never been investigated in live Cx50 mutant mice by using non-invasive imaging techniques. Here, we report a longitudinal study of the ocular defects in Cx50 knockout (Cx50KO) mice from the ages of 3 weeks to 12 months by using spectral-domain optical coherence tomography (SD-OCT). The anterior chamber depth (ACD), lens thickness (LT), vitreous chamber depth (VCD), and axial length (AL) were measured along the visual axis and adjusted with corresponding refractive indices. The SD-OCT image data confirm age-related reductions of LT and AL in live Cx50KO mice compared to age-matched wild-type (WT) controls, and the reduction values are comparable to the *in vitro* measurements of Cx50KO eyeballs and lenses reported previously. Moreover, reductions of ACD were observed in Cx50KO mice at all ages studied while VCD changes are statistically insignificant in comparison to the WT controls. Therefore, Cx50KO's microphthalmia with small lens is selectively associated with delayed ACD development but not the vitreous formation. This work supports the notion that lens size and/or growth is important for anterior chamber development.

KEYWORDS

optical coherence tomography, lens growth, cataract, connexin 50, knockout

Introduction

The ocular lens growth, transparency, and homeostasis rely on distinct functions of gap junction channels formed by connexins including connexin 46 (Cx46) or Gja3 and Cx50 or Gja8 (1–6). Cx50 knockout mice display smaller lenses with mild nuclear cataracts (7, 8), indicating connexin 50 is essential for lens growth control. Previous studies on mouse lens

growth have relied on the *in vitro* measurements of the size and weight of enucleated eyeballs and lenses from euthanized mice (6–14). The advance of non-invasive spectral-domain optical coherence tomography (SD-OCT) allows for the acquisition of a single image that reaches a maximum imaging depth sufficient to capture the entire axial length of the mouse eye, thus providing a valuable tool for longitudinally monitoring the eye/lens growth and cataract formation in live mice.

Optical coherence tomography is one of the standard tools to image and measure the retinal thickness (15) and the anterior chamber for angle closure (16) for the diagnosis and management of some eye diseases in ophthalmologic clinics. OCT has also been used in animal models to measure biometric properties of the eye longitudinally (17–19), it provides an effective tool to determine anterior segment features, the lens, and the retina in different mouse eye models *in vivo* (20–23). Here, we have used OCT to carry out a longitudinal study of the eye and lens growth in live Cx50KO mice.

Cx50 is restrictively utilized in the lens but not in the other parts of the eye (7, 24, 25). Cx50KO and mutant mice develop small lenses containing nuclear cataracts and microphthalmia (7–9, 25–28). The loss of Cx50 function suppresses the proliferation and differentiation of lens epithelial cells to lead to a smaller lens. Small sized lenses seem to directly cause microphthalmia in Cx50KO mice. Human Cx50 mutations cause cataracts, microphthalmia, microcornea, and anomalies of iris in patients (29–37). Therefore, Cx50KO mice provide a valuable model for investigating different ocular structures such as measuring anterior chamber depth (ACD), lens thickness (LT), vitreous chamber depth (VCD), and visual axial length (AL) along the optical axis in the eyes of live mice by SD-OCT. The precise measurement of anatomic structures in the eye can be determined in the optical axis and adjusted with corresponding refractive indices (20). We have characterized the longitudinal changes of ACD, LT, VCD, and AL in both wildtype (WT) and Cx50KO mice from the ages of three weeks to 12 months.

Materials and methods

Animals

Wild-type (WT) mice and Cx50 knockout ($Gja8^{tm1}$) mice (7) at the C57BL/6J background were used for the study. Mice were housed under a 12-hour light cycle with normal food and water. All experimental procedures were approved by the Animal Care and Use Committee (ACUC) at the University of California, Berkeley (Berkeley, CA, USA), and were conducted in accordance with the ARVO Statement for the Use of Animals in Ophthalmic and Vision Research.

Optical coherence tomography

The Leica Envisu R4310 spectral domain OCT system (Bioptigen, Leica Microsystems Inc.) with a center wavelength of 840nm and a telecentric 10mm lens was used to image the eyes of live mice *in vivo*. Mice were anesthetized during the OCT imaging with an intraperitoneal injection of ketamine (80mg/kg) and xylazine (12mg/kg) diluted in 1x PBS (Phosphate buffer saline); mouse corneas were continuously hydrated using lubricating eye drops during and after imaging until the mice would wake up to prevent drying and maintain transparency. Three types of scans were acquired: rectangular 600 A-scans x 600 B-scans at 3.5mm by 3.5mm, rectangular 600 A-scans x 600 B-scans at 3mm by 3mm, and a radial 600 A-scans x 600 B-scans at a radius of 3mm. For each mouse eye, all three scans were taken for measurements. It took approximately 15 minutes to image both eyes of each mouse; the mouse was placed on a heated mat to stay warm until awake afterward.

Published images were processed using ImageJ/FIJI (NIH, Bethesda, MD, USA). Images were averaged over 10 frames to reduce noise. All OCT images shown (Figures 1, 2) are from 3x3mm rectangular scans.

Biometry and image processing

Measurements, mainly from the radial scans, were manually taken with calipers along the Purkinje line near the center of the pupil for each eye using the InVivoVue 2.4 OCT Management Software. The following measurements were obtained: corneal thickness (CT), anterior chamber depth (ACD), lens thickness (LT), vitreous chamber depth (VCD), retinal thickness (RT), and axial length (AL). Measurements were converted into geometric distances using corresponding refractive indices based on previous publications (11, 20): 1.4015 for the cornea, 1.3336 for the anterior chamber, 1.45 for the lens thickness, 1.3329 for the vitreous chamber, and 1.38 for the retina. The geometric distance for axial length was calculated by summing CT, AC, LT, VC, and RT.

Statistical analysis

The Two-sided Wilcoxon Rank Sum test was performed to determine if there is a significant difference between the two different genotypes across all age groups, while a One-sided Wilcoxon Rank Sum test was performed to compare the change of biometric measurements for one genotype over time.

Results

The non-invasive SD-OCT imaging system can capture the entire axial length of a mouse eye. The SD-OCT image of a 3-week-old WT eye shows the cornea, the anterior chamber, the lens, the vitreous chamber, and the retina (Figure 1A); and the CT, ACD, LT, VCD, and RT are indicated with colored lines in Figure 1A. The SD-OCT image of a 3-week-old Cx50KO eye also displays dark areas in the lens core (Figure 1B), which correspond to the mild nuclear cataract (7, 8).

To compare the lens and eye growth between the WT and Cx50KO mice during postnatal development, SD-OCT images were acquired from mice at the ages of 3 weeks, 1 month, 2 months, 6

10.3389/fopht.2024.1387961

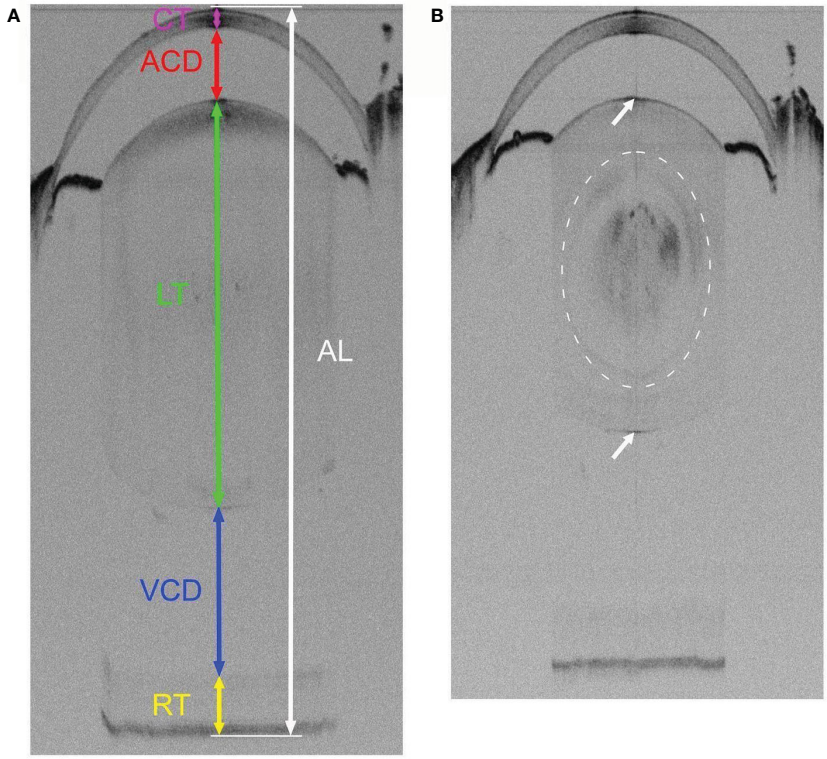

FIGURE 1
Representative SD-OCT whole eye images of 3-week-old WT **(A)** and Cx50KO **(B)** mice. OCT scan captures the entire visual axial length from the surface of the anterior cornea to the back of the posterior retina of the mouse eyeball. **(A)** The colored lines represent the measurements of different parts of ocular structures along the visual axis using the Bioptigen Envisu Software: corneal thickness (CT, magenta), anterior chamber depth (ACD, red), lens thickness (LT, green), vitreous chamber depth (VCD, blue), retinal thickness (RT, yellow), and visual axial length (AL, white). **(B)** A mild nuclear cataract, indicated by a dashed cycle, can be seen as noticeable diffused black areas in the Cx50KO lens core. Both anterior and posterior surfaces of the lens are indicated by arrows.

months, and 12 months (Figure 2). Table 1 presents all measurements (mean ± SD, n = number of imagined eyes) for lens thickness (LT), axial length (AL), anterior chamber depth (ACD), and vitreous chamber depth (VCD). The growth rates of the lens and the eye are reflected by the increases in the lens thickness and the axis length in the SD-OCT images, respectively, as mice aging (Figure 3A). In the WT mice, the steep increase of lens thickness is observed between 3 weeks to 1 month, the LT continues to increase until reaching the age of 2 months, from which the LT growth rate tapers off. The Cx50KO mice exhibit a similar growth rate compared to the WT, except for the period between 3 weeks and 1 month, when the growth curve is much flatter than the WT, suggesting a much slower growth of Cx50KO lens during this period. The AL growth curves (Figure 3B) also indicate a slower growth rate in Cx50KO between 3 weeks to 1 month. Overall, the Cx50KO mice show significant reductions of both LT and AL at all ages examined compared to the WT controls (Figure 3; Table 2). Moreover, the AL growth rate in Cx50KO mice obviously lags that of WT mice between 3 weeks to 1 month old (Figure 3B; Table 2). Table 2 lists percentage change values for all measurements between Cx50KO and WT. In summary, the data reveal an obvious reduction in the sizes of the lens and the eye in Cx50KO mice at all ages.

The SD-OCT data show significantly reduced anterior chamber depth in Cx50KO eyes compared to WT controls at all ages ($P < 0.01$, Two-sided Wilcoxon test, n = 5-13 eyes per data point) (Figure 4A). Moreover, the ACD differences between Cx50KO and WT increase from ~15% at 3 weeks old to ~22% at 12 months old. In the Cx50KO eyes, the ACD values reach a plateau after the age of 2 months, as the values remain almost the same from 2 months until 12 months. Thus, SD-OCT image data indicate a specific suppression of ACD expansion in Cx50KO mice after 2 months. In both Cx50KO and WT mice, the VCD reduces as the mice age (Figure 4B) and displays a reduction of about 27% from 1 month to 12 months (One-sided Wilcoxon test, $P < 0.01$, n = 5-8 eyes). There are no significant VCD differences between WT and Cx50KO mice at all ages examined (Two-sided Wilcoxon test, $P > 0.05$, n = 4-12 eyes per data point), except at 1 month when the Cx50KO mice display ~6% reduction of VCD (Two-sided Wilcoxon test, $P < 0.01$; Table 2). From 3 weeks to 1 month, a reduction of VCD occurs in Cx50KO mice while the value stays similar in WT mice (Figure 4B); this probably leads to the significant difference in VCD between Cx50KO and WT at 1 month old. To address whether the lens size determines the anterior chamber depth, we have selectively examined the eyes of 6-month-old Cx50KO mice and 2-month-old WT mice that have

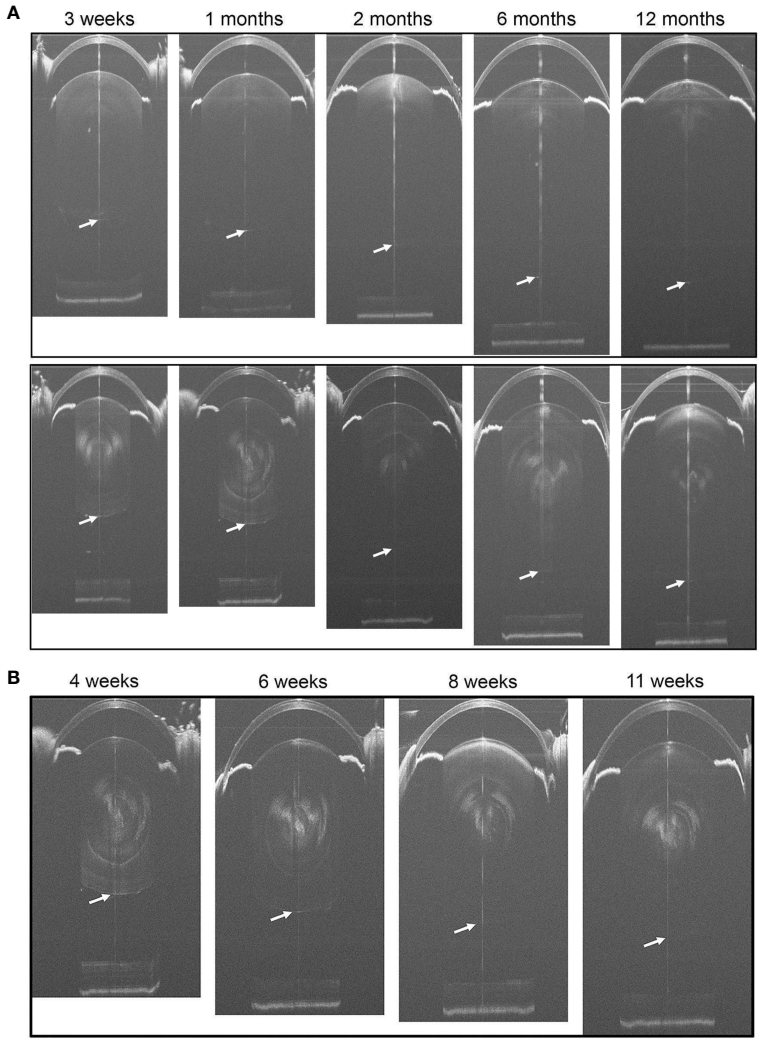

FIGURE 2
(A) Representative SD-OCT whole-eye images of WT (the upper panels) and Cx50KO (the lower panels) mice at different ages from 3 weeks to 12 months. Cataracts in the lens core of Cx50KO mice are clearly visible as opaque white areas. The lens posterior poles are indicated by the arrows. **(B)** Longitudinal SD-OCT eye images of the same eye of a KO mouse from 4 weeks to 11 weeks old. The posterior surfaces of lenses are indicated by white arrows.

the same lens thickness (Figure 4C). The bar graphs show that the LT values are about the same between 6-month-old Cx50KO and 2-month-old WT (Two-sided Wilcoxon test, $P = 0.49$), but the ACD of Cx50KO mice is about 5% reduced than that of WT controls (Two-sided Wilcoxon test, $P < 0.01$).

Discussion

The SD-OCT imaging data precisely reveal the longitudinal growth changes of anterior chamber depth, lens thickness, vitreous chamber depth, and visual axial length between WT and Cx50KO eyes from the ages of 3 weeks to 12 months *in vivo*. We applied an average 1.45 refractive index for mouse lenses at all ages according to the previous OCT study of mouse lenses (20), assuming the lens is a sphere and the gradient of refractive index (GRIN) of the lens is parabolic; we did not consider minor GRIN differences among wild-type lenses at different ages or cataract formation in Cx50KO lenses. A previous study reports that the lens max refractive indexes are 1.43 to 1.54 from 2-week-old to 2-year-old lenses, and the 6-week-old lens has the max refractive index of 1.5 with an average refractive index of about 1.45 (38). Thus, the application of the 1.45 average refractive index over an age-dependent GRIN causes minor differences, about 2-4%, in 3-week-old or 1-year-old lenses. Such minor differences are neglectable in this study comparing the significant differences between age-matched wild-type and Cx50KO lenses. The reduction of the lens thickness and axial length in Cx50KO eyes *in vivo* is consistent with previous studies of lens weight and eye size *in vitro* (6–8, 10). Similar growth trajectory of the lens and the eye between Cx50KO and WT mice at the ages of 3 weeks to 12 months further indicates that disruption of Cx50 mostly impacts early development before 3 weeks, which is supported by the fact that Cx50 deletion inhibits lens epithelial cell proliferation within the first postnatal week when the maximum mouse lens

10.3389/fopht.2024.1387961

TABLE 1 Measured values for lens thickness (LT), axial length (AL), anterior chamber depth (ACD), and vitreous chamber depth (VCD).

WT	Age	LT (mm)	AL (mm)	ACD (mm)	VCD (mm)
	3 weeks	1.667±0.024 (n=5)	3.046±0.033 (n=5)	0.311±0.020 (n=6)	0.729±0.018 (n=5)
	1 month	1.76±0.010 (n=4)	3.173±0.047 (n=4)	0.337±0.016 (n=5)	0.729±0.028 (n=5)
	2 months	1.916±0.017 (n=8)	3.245±0.020 (n=8)	0.361±0.010 (n=8)	0.650±0.025 (n=8)
	6 months	2.221±0.010 (n=8)	3.536±0.023 (n=8)	0.425±0.013 (n=8)	0.563±0.026 (n=8)
	12 months	2.328±0.033 (n=5)	3.678±0.047 (n=5)	0.452±0.021 (n=5)	0.533±0.036 (n=5)
Cx50KO	**Age**	**LT (mm)**	**AL (mm)**	**ACD (mm)**	**VCD (mm)**
	3 weeks	1.366±0.032 (n=10)	2.706±0.019 (n=6)	0.265±0.018 (n=13)	0.743±0.040 (n=6)
	1 month	1.409±0.011 (n=12)	2.720±0.033 (n=12)	0.283±0.014 (n=12)	0.688±0.022 (n=12)
	2 months	1.659±0.011 (n=6)	2.966±0.0493 (n=4)	0.325±0.011 (n=6)	0.609±0.030 (n=4)
	6 months	1.923±0.015 (n=8)	3.140±0.026 (n=8)	0.342±0.010 (n=8)	0.547±0.019 (n=8)
	12 months	2.010±0.012 (n=8)	3.212±0.029 (n=8)	0.351±0.014 (n=8)	0.507±0.013 (n=8)

The data are shown as mean ± standard deviation (n = number of individual eyes measured).

growth occurs (6, 8, 39). However, it is difficult to perform the OCT imaging in the small eyes of Cx50KO mice before 3 weeks and SD-OCT measurement is not applicable until the mouse opens its eyelid around postnatal day 14. Therefore, this work evaluates only the eye and lens growth after the age of 3 weeks *in vivo*.

For lens growth, our SD-OCT data show that the steepest increase of lens thickness occurs between 3 weeks to 1 month, and the LT growth rate of Cx50KO is lower than the WT control during this period. The LT growth gradually slows down after 1 month, and the LT growth rate is comparable between Cx50KO and WT after 2 months old. Based on the lens thickness curve, the Cx50KO eyes exhibit a similar growth rate compared to the WT, except for the period between 3 weeks and 1 month, when the growth curve is much flatter than the WT, suggesting a much slower growth of Cx50KO lens compared to the WT control during this period.

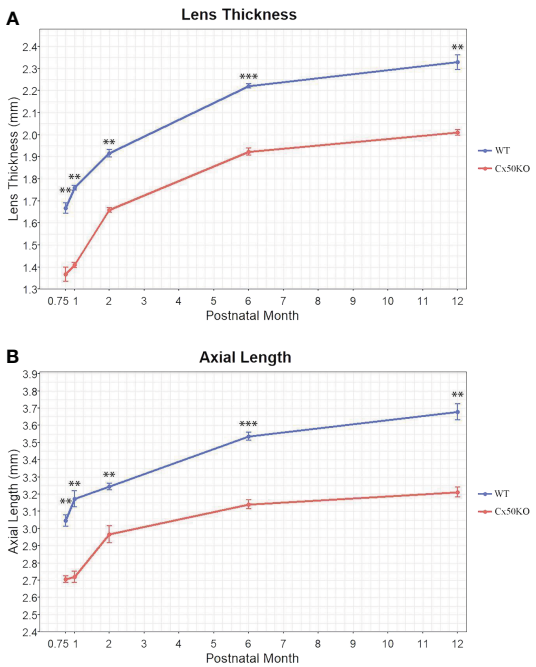

FIGURE 3
Comparisons of lens thickness **(A)** and visual axial length **(B)** of WT and Cx50KO mice at the ages of 3 weeks, 1 month, 2 months, 6 months, and 12 months old. Data points represent the mean ± SD (n = 4-12 per data point). Two-sided Wilcoxon test was performed for statistical analysis, ** $P < 0.01$, *** $P < 0.001$.

If we use the lens thickness as the spherical diameter to calculate the lens volume, the Cx50KO lenses are approximately 40% smaller than the WT lenses at the age of 3 weeks; this reduction value is very similar to our previous data using dissected lens measurement *in vitro* (9).

The axial length growth rate of Cx50KO is drastically lower than WT control from 3 weeks to 1 month; an obviously faster AL growth rate was observed in Cx50KO compared to the WT control from 1 month to 2 months; then the AL growth rate of Cx50KO becomes slower than the WT after the age of 2 months. Therefore, SD-OCT data detects a unique difference in the AL growth rate between WT and Cx50KO. AL growth burst occurs before the age of 1 month in WT while Cx50 AL growth burst occurs at the ages between 1-2 months. The cause for such a unique difference in AL growth is probably related to the growth difference of anterior chamber depth between WT and Cx50KO. The ACD curves (Figure 4A) indicate that the ACD growth of Cx50KO reaches almost a plateau at 2 months old while the ACD of WT gradually increases at all ages. The ACD growth of WT mice starts to decrease after the age of 1 month, then maintains at a similar level between the ages of 1 month to 6 months and reduces slightly between 6 months to 12 months. In contrast, the ACD growth of Cx50KO shows a steady increase between 3 weeks and 2 months, then the growth becomes drastically slower after 2 months to 12 months. The ACD differences between Cx50KO and WT increase after the ages of 2 months until 12 months. Cx50 is restrictively expressed in the lens and Cx50KO directly affects postnatal lens size/growth. Therefore, anterior chamber growth defect in Cx50KO is the

10.3389/fopht.2024.1387961

TABLE 2 Percentage change of LT, AL, ACD, and VCD in Cx50KO mice compared to WT controls.

Age	Δ LT (%)	Δ AL (%)	Δ ACD (%)	Δ VCD (%)
3 weeks	-18.05±2.27% **	-11.14±1.15% **	-14.85±7.99% ***	1.88±6.07%
1 month	-19.93±0.79% **	-14.29±1.64% **	-16.13±5.77% **	-5.56±4.72% **
2 months	-13.41±0.96% **	-8.58±1.62% **	-9.85±3.85% **	-6.28±5.90%
6 months	-13.40±0.78% ***	-11.21±0.95% ***	-19.63±3.49% ***	-2.94±5.60%
12 months	-13.68±1.33% **	-12.68±1.35% **	-22.35±4.84% **	-4.72±6.94%

Negative values are percentage reduction, positive values are percentage increase. The data are shown as mean ± standard deviation. Two-sided Wilcoxon test was performed for statistical analysis, *P < 0.05, **P < 0.01, ***P < 0.001.

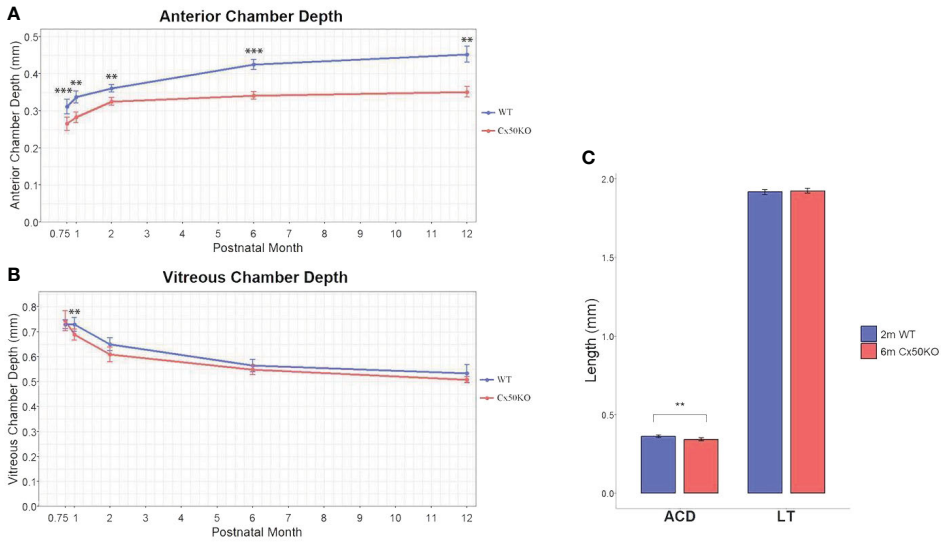

FIGURE 4
(A) Comparison of anterior chamber depth in WT and Cx50KO mice from 3 weeks to 12 months old. Data points represent mean ± SD (n = 5-13 per data point)). Two-sided Wilcoxon test was performed for statistical analysis, $^{**}P < 0.01$, $^{***}P < 0.001$. **(B)** Comparison of vitreous chamber depth in the WT and Cx50KO mice from 3 weeks to 12 months old. Data points represent mean ± SD (n = 4-12 per data point). Two-sided Wilcoxon test was performed for statistical analysis. There are no significant VCD changes between WT and Cx50KO mice, except at 1 month old, $^{**}P < 0.01$. **(C)** Bar graphs showing the comparisons of anterior chamber depth (ACD) and lens thickness (LT) between 6-month-old Cx50KO and 2-month-old WT mice. Data are mean ± SD (n = 8), Two-sided Wilcoxon test was performed for statistical analysis, $^{**}P < 0.01$ for ACD. No significant difference for LT.

secondary effect of Cx50KO postnatal lens defects. Altered ACD in Cx50KO mice indicates that the growth rate of postnatal lens size affects ACD development in the anterior segment.

Our SD-OCT data precisely reveal the growth defects of LT, AL, and ACD in Cx50KO eyes *in vivo* at different ages. More importantly, this *in vivo* study reveals that postnatal lens growth is one of the key factors to regulate the development of anterior chamber formation. The comparison between 2-month-old WT and 6-month-old Cx50KO mice further reveals that even when the Cx50KO lens eventually reaches the same LT as the WT lens, the ACD of Cx50KO lens is still significantly reduced than that of WT (Figure 4C). This further supports a conclusion that the postnatal growth rate of the lens size is critical for the development of the anterior chamber. This conclusion is also supported by studies in teleost that show the lens is necessary for the development of the overall eye in the early stages of growth (40) and can explain disrupted anterior segments in both mice and humans with mutated Cx50 (26, 29–32, 34, 37). The mechanism underlying the coordinated growth regulation among LT, AL, and ACD is not well studied. Cx50KO mice may provide an invaluable model for investigating the regulatory mechanism of anterior chamber development. Future investigation will be needed to address how the lens size can promote or inhibit the formation of the anterior segment.

The vitreous chamber depth decreases from three weeks to 12 months in both WT and Cx50KO mice. Although human studies have reported VCD increases as aging (41–43), VCD reduction as mice age has been reported in previous studies (20, 23). The age-related VCD differences between humans and mice likely rely on the fact that the human lens is about 3% of the eyeball size while the mouse lens accounts for one-third of the eyeball size. Age-related VCD reduction is likely due to the increase in lens size in mice. Statistical analysis indicates that the VCD differences between Cx50KO and WT mice are insignificant. Overall, our data suggest

that the vitreous is well formed in mice before the age of three weeks, Cx50 deletion seems to cause little impact on the vitreous development.

In summary, SD-OCT is a powerful system to precisely measure the biometric properties of WT and Cx50KO eyes in live mice at postnatal ages. This *in vivo* imaging study reveals unique and intricate growth defects in ACD and AL in Cx50KO mice, that cannot be characterized by *in vitro* approaches. Cx50KO mice may be a valuable model for understanding how the growth of the postnatal lens size regulates the anterior chamber formation and for further investigating the regulatory mechanism underlying anterior segment development and visual axis length development during aging.

Data availability statement

The raw data supporting the conclusions of this article will be made available by the authors, without undue reservation.

Ethics statement

The animal study was approved by the Animal Care and Use Committee (ACUC) at University of California, Berkeley. The study was conducted in accordance with the local legislation and institutional requirements.

Author contributions

TP: Data curation, Formal analysis, Investigation, Methodology, Software, Validation, Visualization, Writing – original draft, Writing – review & editing. CO: Data curation, Formal analysis, Investigation, Methodology, Software, Validation, Visualization, Writing – review & editing. XG: Conceptualization, Funding acquisition, Resources, Writing – review & editing, Writing – original draft. C-hX: Conceptualization, Funding acquisition, Investigation, Project administration, Supervision, Validation, Writing – original draft, Writing – review & editing.

Funding

The author(s) declare financial support was received for the research, authorship, and/or publication of this article. We acknowledge the support by the NIH grant EY031253 (XG) and a donation fund from Dr. Weylin Eng and Rose Eng.

Conflict of interest

The authors declare that the research was conducted in the absence of any commercial or financial relationships that could be construed as a potential conflict of interest.

Publisher's note

References

1. Mathias RT, Rae JL. The lens: local transport and global transparency. *Exp Eye Res.* (2004) 78:689–98. doi: 10.1016/j.exer.2003.07.001

2. Mathias RT, White TW, Gong X. Lens gap junctions in growth, differentiation, and homeostasis. *Physiol Rev.* (2010) 90:179–206. doi: 10.1152/physrev.00034.2009

3. Gong X, Cheng C, Xia CH. Connexins in lens development and cataractogenesis. *J Membr Biol.* (2007) 218:9–12. doi: 10.1007/s00232-007-9033-0

4. Gong X, Li E, Klier G, Huang Q, Wu Y, Lei H, et al. Disruption of alpha3 connexin gene leads to proteolysis and cataractogenesis in mice. *Cell.* (1997) 91:833–43. doi: 10.1016/s0092-8674(00)80471-7

5. White TW, Gao Y, Li L, Sellitto C, Srinivas M. Optimal lens epithelial cell proliferation is dependent on the connexin isoform providing gap junctional coupling. *Invest Ophthalmol Vis Sci.* (2007) 48:5630–7. doi: 10.1167/iovs.06-1540

6. Sellitto C, Li L, White TW. Connexin50 is essential for normal postnatal lens cell proliferation. *Invest Ophthalmol Vis Sci.* (2004) 45:3196–202. doi: 10.1167/iovs.04-0194

7. Rong P, Wang X, Niesman I, Wu Y, Benedetti LE, Dunia I, et al. Disruption of Gja8 (alpha8 connexin) in mice leads to microphthalmia associated with retardation of lens growth and lens fiber maturation. *Development.* (2002) 129:167–74. doi: 10.1242/dev.129.1.167

8. White TW, Goodenough DA, Paul DL. Targeted ablation of connexin50 in mice results in microphthalmia and zonular pulverulent cataracts. *J Cell Biol.* (1998) 143:815–25. doi: 10.1083/jcb.143.3.815

9. Tjahjono N, Xia CH, Li R, Chu S, Wang J, Gong X. Connexin 50-R205G mutation perturbs lens epithelial cell proliferation and differentiation. *Invest Ophthalmol Vis Sci.* (2020) 61:25. doi: 10.1167/iovs.61.3.25

10. Gerido DA, Sellitto C, Li L, White TW. Genetic background influences cataractogenesis, but not lens growth deficiency, in Cx50-knockout mice. *Invest Ophthalmol Vis Sci.* (2003) 44:2669–74. doi: 10.1167/iovs.02-1311

11. Remtulla S, Hallett PE. A schematic eye for the mouse, and comparisons with the rat. *Vision Res.* (1985) 25:21–31. doi: 10.1016/0042-6989(85)90076-8

12. Schachar RA. Growth patterns of fresh human crystalline lenses measured by in *vitro* photographic biometry. *J Anat.* (2005) 206:575–80. doi: 10.1111/j.1469-7580.2005.00422.x

13. Rosen AM, Denham DB, Fernandez V, Borja D, Ho A, Manns F, et al. *In vitro* dimensions and curvatures of human lenses. *Vision Res.* (2006) 46:1002–9. doi: 10.1016/j.visres.2005.10.019

14. Uhlhorn SR, Borja D, Manns F, Parel JM. Refractive index measurement of the isolated crystalline lens using optical coherence tomography. *Vision Res.* (2008) 48:2732–8. doi: 10.1016/j.visres.2008.09.010

15. Izatt JA, Boppart S, Bouma B, de Boer J, Drexler W, Li X, et al. Introduction to the feature issue on the 25 year anniversary of optical coherence tomography. *BioMed Opt Express.* (2017) 8:3289–91. doi: 10.1364/BOE.8.003289

16. Nolan WP, See JL, Chew PT, Friedman DS, Smith SD, Radhakrishnan S, et al. Detection of primary angle closure using anterior segment optical coherence tomography in Asian eyes. *Ophthalmology.* (2007) 114:33–9. doi: 10.1016/j.ophtha.2006.05.073

17. Zhou X, Xie J, Shen M, Wang J, Jiang L, Qu J, et al. Biometric measurement of the mouse eye using optical coherence tomography with focal plane advancement. *Vision Res.* (2008) 48:1137–43. doi: 10.1016/j.visres.2008.01.030

18. Wang L, Povazay B, Chen YP, Hofer B, Drexler W, Guggenheim JA. Heritability of ocular component dimensions in mice phenotyped using depth-enhanced swept source optical coherence tomography. *Exp Eye Res*. (2011) 93:482–90. doi: 10.1016/j.exer.2011.06.008

19. Park H, Qazi Y, Tan C, Jabbar SB, Cao Y, Schmid G, et al. Assessment of axial length measurements in mouse eyes. *Optom Vis Sci*. (2012) 89:296–303. doi: 10.1097/OPX.0b013e31824529e5

20. Chou TH, Kocaoglu OP, Borja D, Ruggeri M, Uhlhorn SR, Manns F, et al. Postnatal elongation of eye size in DBA/2J mice compared with C57BL/6J mice: in *vivo* analysis with whole-eye OCT. *Invest Ophthalmol Vis Sci*. (2011) 52:3604–12. doi: 10.1167/iovs.10-6340

21. Chakraborty R, Lacy KD, Tan CC, Park HN, Pardue MT. Refractive index measurement of the mouse crystalline lens using optical coherence tomography. *Exp Eye Res*. (2014) 125:62–70. doi: 10.1016/j.exer.2014.05.015

22. Pawliczek D, Dalke C, Fuchs H, Gailus-Durner V, Hrabe de Angelis M, Graw J, et al. Spectral domain - Optical coherence tomography (SD-OCT) as a monitoring tool for alterations in mouse lenses. *Exp Eye Res*. (2020) 190:107871. doi: 10.1016/j.exer.2019.107871

23. Jiang M, Wu PC, Fini ME, Tsai CL, Itakura T, Zhang X, et al. Single-shot dimension measurements of the mouse eye using SD-OCT. *Ophthalmic Surg Lasers Imaging*. (2012) 43:252–6. doi: 10.3928/15428877-20120308-04

24. Gong X, Baldo GJ, Kumar NM, Gilula NB, Mathias RT. Gap junctional coupling in lenses lacking alpha3 connexin. *Proc Natl Acad Sci U.S.A*. (1998) 95:15303–8. doi: 10.1073/pnas.95.26.15303

25. Chang B, Wang X, Hawes NL, Ojakian R, Davisson MT, Lo WK, et al. A Gja8 (Cx50) point mutation causes an alteration of alpha 3 connexin (Cx46) in semi-dominant cataracts of Lop10 mice. *Hum Mol Genet*. (2002) 11:507–13. doi: 10.1093/hmg/11.5.507

26. Xia CH, Chang B, Derosa AM, Cheng C, White TW, Gong X. Cataracts and microphthalmia caused by a Gja8 mutation in extracellular loop 2. *PloS One*. (2012) 7:e52894. doi: 10.1371/journal.pone.0052894

27. Xia CH, Liu H, Cheung D, Cheng C, Wang E, Du X, et al. Diverse gap junctions modulate distinct mechanisms for fiber cell formation during lens development and cataractogenesis. *Development*. (2006) 133:2033–40. doi: 10.1242/dev.02361

28. Berthoud VM, Gao J, Minogue PJ, Jara O, Mathias RT, Beyer EC. The connexin50D47A mutant causes cataracts by calcium precipitation. *Invest Ophthalmol Vis Sci*. (2019) 60:2336–46. doi: 10.1167/iovs.18-26459

29. Devi RR, Vijayalakshmi P. Novel mutations in GJA8 associated with autosomal dominant congenital cataract and microcornea. *Mol Vis*. (2006) 12:190–5.

30. Hu S, Wang B, Zhou Z, Zhou G, Wang J, Ma X, et al. A novel mutation in GJA8 causing congenital cataract-microcornea syndrome in a Chinese pedigree. *Mol Vis*. (2010) 16:1585–92.

31. Dong S, Zou T, Zhen F, Wang T, Zhou Y, Wu J, et al. Association of variants in GJA8 with familial acorea-microphthalmia-cataract syndrome. *Eur J Hum Genet*. (2023) 32:413–20. doi: 10.1038/s41431-023-01503-9

32. Yu Y, Wu M, Chen X, Zhu Y, Gong X, Yao K. Identification and functional analysis of two novel connexin 50 mutations associated with autosome dominant congenital cataracts. *Sci Rep*. (2016) 6:26551. doi: 10.1038/srep26551

33. Zhu Y, Yu H, Wang W, Gong X, Yao K. A novel GJA8 mutation (p.V44A) causing autosomal dominant congenital cataract. *PloS One*. (2014) 9:e115406. doi: 10.1371/journal.pone.0115406

34. Zhang H, Chen Z, He K, Chang P, Zhao Y, Huang X, et al. Unique presentation of congenital cataract concurrent with microcornea, microphthalmia plus posterior capsule defect in monozygotic twins caused by a novel GJA8 mutation. *Eye*. (2019) 33:686–9. doi: 10.1038/s41433-018-0277-y

35. Ceroni F, Aguilera-Garcia D, Chassaing N, Bax DA, Blanco-Kelly F, Ramos P, et al. New GJA8 variants and phenotypes highlight its critical role in a broad spectrum of eye anomalies. *Hum Genet*. (2019) 138:1027–42. doi: 10.1007/s00439-018-1875-2

36. Kuo DS, Sokol JT, Minogue PJ, Berthoud VM, Slavotinek AM, Beyer EC, et al. Characterization of a variant of gap junction protein alpha8 identified in a family with hereditary cataract. *PloS One*. (2017) 12:e0183438. doi: 10.1371/journal.pone.0183438

37. Ma AS, Grigg JR, Prokudin I, Flaherty M, Bennetts B, Jamieson RV. New mutations in GJA8 expand the phenotype to include total sclerocornea. *Clin Genet*. (2018) 93:155–9. doi: 10.1111/cge.13045

38. Cheng C, Parreno J, Nowak RB, Biswas SK, Wang K, Hoshino M, et al. Age-related changes in eye lens biomechanics, morphology, refractive index and transparency. *Aging*. (2019) 11:12497–531. doi: 10.18632/aging.102584

39. White TW, Sellitto C, Paul DL, Goodenough DA. Prenatal lens development in connexin43 and connexin50 double knockout mice. *Invest Ophthalmol Vis Sci*. (2001) 42:2916–23.

40. Yamamoto Y, Jeffery WR. Central role for the lens in cave fish eye degeneration. *Science*. (2000) 289:631–3. doi: 10.1126/science.289.5479.631

41. Jiang BC, Woessner WM. Vitreous chamber elongation is responsible for myopia development in a young adult. *Optom Vis Sci*. (1996) 73:231–4. doi: 10.1097/00006324-199604000-00003

42. Hyman L, Gwiazda J, Hussein M, Norton TT, Wang Y, Marsh-Tootle W, et al. Relationship of age, sex, and ethnicity with myopia progression and axial elongation in the correction of myopia evaluation trial. *Arch Ophthalmol*. (2005) 123:977–87. doi: 10.1001/archopht.123.7.977

43. Mutti DO, Sinnott LT, Zadnik KGroup BS, the CSG. Compensation for vitreous chamber elongation in infancy and childhood. *Optom Vis Sci*. (2023) 100:43–51. doi: 10.1097/OPX.0000000000001970

frontiers | Frontiers in Ophthalmology

TYPE Original Research
PUBLISHED 04 June 2024
DOI 10.3389/fopht.2024.1410860

OPEN ACCESS

EDITED BY
Jeff Gross,
The University of Texas at Austin,
United States

REVIEWED BY
Mason Posner,
Ashland University, United States
Irene Vorontsova,
The University of Auckland, New Zealand
Salil A. Lachke,
University of Delaware, United States

*CORRESPONDENCE
Catherine Cheng
ckcheng@iu.edu

RECEIVED 01 April 2024
ACCEPTED 06 May 2024
PUBLISHED 04 June 2024

CITATION
Huynh PN and Cheng C (2024) Spatial-temporal comparison of Eph/Ephrin gene expression in ocular lenses from aging and knockout mice.
Front. Ophthalmol. 4:1410860.
doi: 10.3389/fopht.2024.1410860

Spatial-temporal comparison of Eph/Ephrin gene expression in ocular lenses from aging and knockout mice

Peter N. Huynh and Catherine Cheng*

School of Optometry and Vision Science Program, Indiana University, Bloomington, IN, United States

Cataracts, defined as any opacity in the transparent ocular lens, remain the leading cause of blindness and visual impairment in the world; however, the etiology of this pathology is not fully understood. Studies in mice and humans have found that the EphA2 receptor and the ephrin-A5 ligand play important roles in maintaining lens homeostasis and transparency. However, due to the diversity of the family of Eph receptors and ephrin ligands and their promiscuous binding, identifying functional interacting partners remains a challenge. Previously, 12 of the 14 Ephs and 8 of 8 ephrins in mice were characterized to be expressed in the mouse lens. To further narrow down possible genes of interest in life-long lens homeostasis, we collected and separated the lens epithelium from the fiber cell mass and isolated RNA from each compartment in samples from young adult and middle-aged mice that were either wild-type, *EphA2*$^{-/-}$ (knockout), or ephrin-A5$^{-/-}$. Reverse transcription quantitative polymerase chain reaction (RT-qPCR) was implemented to compare transcript levels of 33 Eph and ephrin gene variants in each tissue compartment. Our results show that, of the Eph and ephrin variants screened, 5 of 33 showed age-related changes, and 2 of 33 showed genotype-related changes in lens epithelium. In the isolated fibers, more dynamic gene expression changes were observed, in which 12 of 33 variants showed age-related changes, and 6 of 33 showed genotype-related changes. These data allow for a more informed decision in determining mechanistic leads in Eph-ephrin-mediated signaling in the lens.

KEYWORDS

EphA2, Ephrin-A5, RT-qPCR, epithelium, lens fibers

1 Introduction

The ocular lens is a transparent and avascular structure in the anterior chamber of the eye that facilitates the fine focusing of light onto the retina. Cataracts, describing any opacification of the lens, remain the leading cause of blindness in the world (1). While cataract surgery is a common medical treatment, access to adequately equipped medical

professionals and facilities remains difficult for many people (1). To better treat and prevent these afflictions, a deeper understanding of how the lens maintains its homeostasis, transparency, and accommodative ability is required.

Recent studies have highlighted the importance of the Eph-ephrin signaling pathway in lens transparency (2–7). Erythropoietin-producing hepatocellular (Eph) receptors make up the largest family of receptor tyrosine kinases and facilitate diverse signaling with their endogenous ligands, the ephrins. Ephs are divided into two families, EphAs and EphBs, and likewise ephrins are divided into ephrin-As and ephrin-Bs. Generally, ephrin-As bind to EphA receptors, and ephrin-Bs bind to EphBs (8, 9). However, cases of ephrin-As binding to EphBs and ephrin-Bs binding to EphAs have been observed as instances of inter-family crosstalk (10, 11). EphA and EphB receptors are encoded by *Epha* and *Ephb* genes, while ephrin-A and ephrin-B ligands are encoded by *Efna* and *Efnb* genes, respectively. Ephs and ephrins facilitate a wide assortment of cellular and developmental processes, including cell morphology, migration, adhesion, and differentiation, resulting in diverse phenotypes when these pathways are dysregulated (12, 13).

Currently, 16 Ephs and 9 ephrins have been identified in total, with 14 Ephs and 8 ephrins present in mice and humans. Two members of these families, the receptor EphA2 and the ligand ephrin-A5, have been targets of interest in lens research due to known mutations linked to both congenital and age-related cataracts in human patients (6, 14–18). The phenotypes manifested from mutations of *EPHA2* and *EFNA5* in human patients are diverse, and the cellular mechanisms involved remain unclear. While EphA2 and ephrin-A5 are known binding partners in other tissues, this receptor and ligand pair are not exclusive binding partners and are spatially segregated in the ocular lens, suggesting their primary binding partners are other ephrins and Ephs (5, 19). In the endeavor to identify relevant binding partners to EphA2 and ephrin-A5, the number of permutations between Ephs and ephrins, and their uncharacterized lens distribution present a challenge in prioritizing targets to investigate.

The lens is composed of two cell types, a monolayer of epithelial cells covering the anterior hemisphere and a bulk mass of fiber cells. Our previous work revealed that loss of EphA2 or ephrin-A5 in mouse lenses lead to either mild nuclear cataracts at the center of the lens or anterior cataracts, respectively. At a cellular level, *Epha2* knockout ($^{-/-}$; KO) lenses display misaligned equatorial epithelial cells, a disrupted fulcrum, and disorganized fiber cells (3, 5, 19–22). Additionally, it was observed that *Epha2*$^{-/-}$ also results in smaller, more spherical lenses with reduced refractive power and degraded optical quality and decreased proliferation of lens epithelial cells (23, 24). Ephrin-A5 (*Efna5*) knockout lenses develop anterior polar cataracts due to disruption of cell-cell adhesion via E-cadherin and β-catenin mislocalization leading to epithelial-to-mesenchymal transition (EMT) in anterior epithelial cells (3, 5).

While prominent cataract phenotypes and epithelial cell changes are observed in these *Epha2* and *Efna5* knockout mice, the specific downstream signaling and binding partners of these targets have not yet been elucidated in the lens. Due to the promiscuous nature of Eph-ephrin binding, the number of permutations of receptor-ligand combinations presents a formidable barrier to identify binding partners of interest (10, 25, 26). In the endeavor to narrow targets, a concerted effort to identify the Ephs and ephrins that are present in the mouse lens found that 12 of 14 known Ephs and 8 of 8 known ephrins were expressed (27). Here, the next step of this search is presented, in which these previously observed Ephs and ephrins are investigated in a quantitative manner. mRNA transcripts of each target were measured in isolated lens epithelium or fibers to identify targets that significantly change with age or disruption of *Epha2* or *Efna5* as potential targets of interest from a functional and geographical standpoint.

2 Materials and methods

2.1 Animals

Mice were maintained in accordance with an approved Institutional Animal Care and Use Committee (IACUC) protocols (#21-010 and #24-002) and the Guide for the Care and Use of Laboratory Animals by the National Institutes of Health (NIH). Generation of *Epha2*$^{-/-}$ and *Efna5*$^{-/-}$ mice was previously described (28, 29). All mice were maintained in C57BL/6J backgrounds with wild-type beaded filament structural protein 2 (*Bfsp2*; CP49) genotypes, as *Bfsp2*$^{-/-}$ mice exhibit disruptions in the lens fiber cytoskeleton, gap junctions, and ionic homeostasis (3, 30). *Bfsp2* mutations occur spontaneously across various inbred strains, including 129/SvJ, 129/OLa, and FVB/N mice, and have been linked to cataracts in both humans and mice (31–34). Therefore, the wild-type *Bfsp2* gene was validated in these mice prior to investigating cataract mechanisms. Male and female mice ranging from 6-9 weeks (young adult; Y) and 7 months (middle-aged; M) were used for these studies. Littermates were used for comparison between wild-type and KO samples.

2.2 RNA isolation

RNA was isolated from epithelium and fiber cell mass fractions using our previous protocol (35). Briefly, samples were collected from at least three different mice of each genotype and each age for RNA isolation. For *Efna5*$^{-/-}$ mice, the lenses can present with obvious anterior cataracts. *Efna5*$^{-/-}$ mice were excluded if the lenses had obvious cellular defects to prevent detection of gene expression changes that are downstream of EMT in the KO lens epithelial cells (3, 5). Briefly, lenses were carefully dissected from freshly enucleated eyes. To isolate lens epithelium, the collagenous basement membrane around the lens, the capsule, was gently peeled from the lens posterior. The epithelial cells are well-adhered to the lens capsule (3, 35, 36). The remaining fiber mass was not further separated as the organelle-free nuclear fibers are presumed to contain little to no mRNA. Autologous pairs of capsules with attached epithelial cells or fiber cell bulk masses were pooled and homogenized into 400 µL of cold TRIzol (Invitrogen; Waltham, MA, USA; Cat # 15596026). Samples were incubated for 30 minutes at room temperature. For phase separation, 200 µL of chloroform

(Alfa Aesar; Ward Hill, MA, USA; Cat # 22920) was added and the samples were shaken vigorously for 15 seconds by hand. Samples were incubated at room temperature for 15 minutes and centrifuged at 14,000*g* for 15 minutes at 4°C. The aqueous phase was transferred to RNase-free tubes (USA Scientific; Ocala, FL; Cat # 1615-5500), and 1 equivalent volume of 200 proof ethanol (Fisher Scientific; Waltham, MA, USA; Cat # BP2818500) was added. Samples were transferred to 'RNA Clean and Concentrator-5' kit columns (Zymo Research; Tustin, CA, USA; Cat # ZR1013), and RNA was isolated using manufacturer instructions, with the omission of RNA Binding Buffer. RNA concentrations were measured using a NanoDrop One™ (Thermo Scientific; Waltham, MA, USA; Cat # ND-ONE-W).

2.3 Reverse transcription polymerase chain reaction

RNA samples were reverse transcribed to cDNA using a SuperScript™ IV VILO™ polymerase (Invitrogen; Cat # 11756010), according to manufacturer instructions. RNA transcripts were reverse transcribed using the commercial kit primers containing a mix of random and oligo(dT) primers (37). Briefly, 2000 ng of RNA was added to 4 µL of 5X VILO™ reaction mix and brought to a total of 20 µL with molecular grade water (Fisher Scientific; Cat # BP2819-1). The samples were thermocycled for 1 step of annealing at 25°C for 10 minutes, 1 step of reverse transcription at 50°C for 10 minutes, followed by 1 step of enzyme inactivation at 85°C for 5 minutes. These experiments were performed using a MiniAmp Thermal Cycler (Applied Biosystems; Waltham, MA, USA; Cat # A37834). cDNA content was assumed to be a 1:1 conversion from starting RNA. cDNA samples were divided into lots so that no sample would exceed 5 freeze-thaw cycles. cDNA lots were stored at -80°C until use.

2.4 Quantitative polymerase chain reaction

For each reaction, 5 ng of cDNA was amplified using standard TaqMan probe conditions. Briefly, forward and reverse primers (900 nM each), a TaqMan probe (250 nM), and TaqMan Fast Advanced Master Mix (ThermoFisher Scientific; Cat # 4444557) were mixed to a final reaction volume of 10 µL. TaqMan primers and probes details are listed in Supplementary Table S1. Plates were sealed using MicroAmp™ optical adhesive film (Applied Biosystems; Cat # 4360954). PCR samples were thermocycled for 1 step of uracil-N-glycosylase (UNG) inactivation at 50°C for 2 minutes, 1 step of denaturation at 95°C for 2 minutes, followed by 45 cycles of denaturation at 95°C for 1 second and annealing at 60°C for 20 seconds. Samples were cycled using a QuantStudio 3 Real-Time PCR System (96-well, 0.1 mL format; Applied Biosystems; Cat # A28567). Custom TaqMan probes and primers were designed using Primer Express 3.0.1 (Applied Biosystems; Cat # 4363991), spanning exon-exon junctions where possible. Quantification cycle (C_q) values were compared to the reference gene, peptidylprolyl isomerase a (*Ppia*). *Ppia* was chosen from a screen of 32 potential reference genes supplied in a TaqMan Array Mouse Endogenous Control Plate (Applied Biosystems; Cat # 4426696).

2.5 *Epha7* primer design

Epha7 has 6 variants, none of which have any regions unique to a given variant within the coding sequence. Therefore, a combinatorial approach was taken to selectively amplify each variant (Supplementary Figure S1). Exons 8 and 9 are conserved across all 6 variants, so a single probe was designed to target a region within exon 8 (Variant 1; 1868–1882; NM_010141). A 15-nucleotide sequence at the 5' end of exon 7 is present in variants 1-3, but not in 4-6 (Variant 1; 1838-1852). Exon-spanning forward primers (referred to as forward A and B) were targeted towards this site to differentiate variants into two sets. Reverse primers were designed at the exon 9-10 junction, as exon 10 had variations that clustered the 6 variants into 3 pairs (reverse primers 1-3). Using the 6 permutations of forward primers A and B with reverse primers 1-3, each of the 6 variants could be specifically targeted (Supplementary Table S1). Custom primers were validated on mouse brain samples (data not shown). Further validation was performed only on EphA7 due to every sample yielding signal indistinguishable from noise. Other custom probes were presumed effective based on effective amplification, PrimerExpress 3.0.1 (Applied Biosystems) scoring, and Primer BLAST comparison.

2.6 Qualitative polymerase chain reaction and sequencing

For each reaction, 20 ng of cDNA was amplified using Quick-Load Taq 2X Master Mix (New England Biolabs; Ipswich, MA, USA; Cat # M0271) and 200 nM of each primer, following the manufacturer's protocol (25). Primers and amplicon information are listed in Supplementary Table S1. Reactions were performed using the manufacturer-recommended mix composition at a final reaction volume of 25 µL. PCR samples were thermocycled for 1 step of initial denaturation at 95°C for 30 seconds, followed by 45 cycles of denaturation at 95°C for 30 seconds, annealing at 53°C or 54°C for 30 seconds, and elongation at 68°C for 60 seconds per kilobase. A final extension step at 68°C for 5 minutes followed. Samples were separated using a 1% agarose gel supplemented with GelGreen Nucleic Acid Gel Stain (Biotium; Fremont, CA, USA; Cat # 41005). Bands were cut and isolated using the Qiaquick Gel Extraction Kit (Qiagen; Hilden, Germany; Cat # 28704) following manufacturer instructions. The isolated amplified products were sent to Quintara Biosciences (Cambridge, MA, USA) for Sangar sequencing following Quintara sample preparation guidelines.

2.7 qPCR data analysis

QuantStudio 3 readings were interpreted using QuantStudio Design & Analysis Software 2.6.0 (Thermo Fisher Scientific). A signal threshold of 0.3 was used to determine quantification cycle

(C_q) values (31, 32). ΔC_q values were determined using a custom R script and analyzed using GraphPad Prism version 9.0.0 (121) (GraphPad Software, LLC; Boston, MA, USA). Two-way ANOVA followed by multiple comparison correction by controlling for false discovery rate was implemented. A two-stage linear step-up procedure of Benjamini, Krieger, and Yekutieli was used with a Q value (false discovery rate) of 0.05. A noise threshold of $\Delta C_q = 11.9$ was determined using *Epha2* TaqMan probe readings from *Epha2*$^{-/-}$ mice, taking the lowest (strictest) ΔC_q value obtained from this data set. Data sets with more than 2 biological test groups exhibiting a mean above this threshold were considered non-specific amplification and were not included in statistical analysis. *Epha2* and *Efna5* readings in their respective knockouts were tested using multiple unpaired t-tests followed by a two-stage step-up method of Benjamini, Krieger, and Yekutieli with a Q value of 0.05.

3 Results

Using traditional, qualitative PCR, 12 of 14 Ephs and 8 of 8 ephrins were previously detected in the lenses of young adult wild-type, *EphA2*$^{-/-}$, and *Efna5*$^{-/-}$ mice (27). Unfortunately, the large number of genes expressed did not sufficiently narrow down targets of interest to pursue. Thus, a reverse transcription quantitative polymerase chain reaction (RT-qPCR) method was implemented to determine whether any Eph or ephrin genes are changed by age and/or genotype with considerable magnitude. While qPCR results are commonly presented as $2^{-\Delta\Delta Cq}$, this relies on normalizing readings to a reference group. In this experimental design, there are multiple comparisons that utilize more than a single reference group. Moreover, using ΔC_q values allows us to compare relative expression levels between genes rather than normalizing to a control group per gene. Therefore, the majority of data presented are shown as ΔC_q values, and it should be noted that lower ΔC_q values indicate higher transcript levels.

3.1 Establishing an appropriate endogenous control

To appropriately control for well-to-well variation, an internal reference gene was used for each sample. Thirty-two potential reference genes were screened and assessed based on quantification cycle (C_q) and standard deviation (Supplementary Figure S2). Probes and primers for the target genes were pre-aliquoted into a pre-configured 96-well plate containing 16 commonly used reference genes and 16 mouse orthologs of human genes shown to be constitutively expressed in mice (Applied Biosystems; Cat # 4226694). As this screen was in search of endogenous controls, these samples did not include an internal reference gene and were quality controlled based on the passive reference dye, ROX. Therefore, results are shown and analyzed as C_q values rather than ΔC_q.

Of the targets screened, the 18s ribosomal RNA was the highest expressing (lowest C_q) reference gene with a mean C_q (M_{Cq}) = 10.4 (SD = 0.79). However, 18s was not chosen as the internal control to avoid depletion of reaction reagents due to its rapid amplification. The next cluster of moderately-expressed targets amplified with C_q values between 19.0-22.0. This group consisted of ß-actin (*Actb*), mitochondrially encoded ATP synthase 6 (*ATP6*), glyceraldehyde-3-phosphate dehydrogenase (*Gapdh*), and peptidylprolyl isomerase A (*Ppia*). Previous studies showed that disruption of EphA2 can dysregulate actin distribution and alter cytoskeletal morphology (20). Thus, *Actb* was eliminated as a candidate control despite being a commonly used control. Between *ATP6* (M_{Cq} = 21.5, SD = 1.07), *Gapdh* (M_{Cq} = 20.0, SD = 0.61), and *Ppia* (M_{Cq} = 20.5, SD = 0.39), *Ppia* exhibited the smallest standard deviation. The ribosomal protein L37a (*Rpl37a;* M_{Cq}= 25.8, SD = 0.40) also had a comparable standard deviation but crossed the detection threshold at a later amplification cycle. Ultimately, *Ppia* was chosen as the endogenous control due to its earlier amplification and tighter standard deviation. The distribution of *Ppia* across all tested samples are compiled in Supplementary Figure S3.

3.2 Preliminary qPCR validation with knockout samples

The nature of the *Epha2* and *Efna5* knockout mice results in successfully disrupted protein products; however, portions of the gene remain in the mRNA transcripts. The *Epha2* gene is disrupted with the insertion of a neomycin resistance (*neo*) cassette at a HindIII restriction site located in exon 5 at positions 1410–1415 (NM_010139.3), previously reported at position 1372 (NM_010139), and a downstream XbaI site. This is predicted to produce a non-functional protein truncated after Arg426, between the two extracellular fibronectin domains (28). The *Efna5* knockout uses a similar *neo* insertion technique, targeting a BamHI site at positions 249-254 in exon 1 and an EcoRI restriction site at positions 691-696 in exon 2 (NM_207654.3), replacing amino acids 1–128 (29).

Custom *Epha2* probes were designed to amplify a 65-base-pair (bp) amplicon from positions 1405–1469 (NM_010139.3). The forward primer bound at positions 1405–1422 (Supplementary Table S1), spanning the HindIII restriction site. This *Epha2* primer set should not amplify the template if the *neo* cassette is present, and the TaqMan probe was designed to bind 3' of the restriction site in a presumably deleted portion. However, the custom *Epha2* probe yielded a positive signal in 2 of the 12 *Epha2*$^{-/-}$ samples. These readings were used to determine a noise threshold of $\Delta C_q = 11.9$, denoting any higher quantification cycles as non-specific signal.

Custom *Efna5* probes and primers were designed to amplify a 70 bp amplicon from positions 831-900 (NM_207654.3). This TaqMan probe spanned exons 4 and 5, binding from positions 860-876. Although this portion of the gene was 3' of the *neo* insertion, this position was targeted to differentiate *Efna5* variant 2 from variants 1 and 3, which are identical within the coding sequence and only differ in the 5' untranslated region (UTR). Surprisingly, this probe produced a positive signal from all *Efna5*$^{-/-}$ samples, so the knockout was further investigated using Sangar sequencing.

Sequencing results from *Efna5*$^{-/-}$ isolated lens fiber samples revealed that exon 2 of the *Efna5* gene was excised, resulting in an out-of-frame deletion from bases 432–724 (amino acids 43–139) (data not shown). This was not expected based on the information available from the original paper describing the construction of the knockout (29). Importantly, exon 2 contains almost the entirety of the receptor binding ectodomain (amino acids 30-159) that is conserved through ephrin-A ligands (Conserved Domain Database: cd10425) (38). While the protein products are non-functional, amplifiable transcripts are still produced and thus, can be detected using RT-qPCR. These knockout readings were not included in our analyses.

3.3 Biological groups, target selection, and expression parameters

To investigate gene expression differences related to age and *Epha2* or *Efna5* knockouts, 4 sample groups were used per strain: young-adult wild-type (Y-WT), middle-aged wild-type (M-WT), young-adult knockouts (Y-KO), and middle-aged knockouts (Y-KO). Age-related changes were determined by Y-WT vs. M-WT and Y-KO vs. M-KO comparisons. Genotype-related changes were determined by Y-WT vs. Y-KO and M-WT vs. M-KO. Transcript measures were not compared between tissue compartments nor between strains. Y-WT vs M-KO and M-WT vs Y-KO were not considered useful comparisons due to the confounding effects of both age and genotype. Eph and ephrin targets were chosen based on previous qualitative PCR results (27). Targets and variants that were absent from the lens from the initial screen were not quantitated in this current study.

Expression levels were further divided into three categories of high, moderate, and low expression based on their ΔC_q values. While the noise threshold was determined via the *Epha2* knockout, the lowest ΔC_q value in the dataset was used to determine a maximum expression value. This lowest ΔC_q value also belonged to an *Epha2* reading from *Efna5*$^{-/-}$ fibers, at $\Delta C_q = 2.9$. Using a ΔC_q range of 2.9 – 11.9, the readings were binned into approximate categories using a step size of 3. Using *Epha2* in the fibers ($M_{\Delta Cq} = 3.9$) and *Efna5*$^{V1/3}$ in the epithelium ($M_{\Delta Cq} = 4.4$) as high-expression landmarks, samples were categorized into high expression ($M_{\Delta Cq} < 6.0$), moderate expression ($6.0 \leq M_{\Delta Cq} < 9.0$), low expression ($9.0 \leq M_{\Delta Cq} < 11.9$), and noise ($M_{\Delta Cq} \geq 11.9$) categories. These thresholds were based on previous observations that EphA2 is predominantly expressed in the fibers while ephrin-A5 is predominantly expressed in epithelial cells (3).

3.4 Eph expression changes in the aging lens epithelium

Within the lens epithelium, *Epha1*, *Epha5*^{V3}, and *Epha5*^{V12} changed significantly with age regardless of genotype (Figures 1A, C). *Epha1* increased with age regardless of genotype in both strains (*Epha2* and *Efna5*; Y-WT vs. M-WT; Y-KO vs. M-KO). A genotype-dependent change was seen in *Epha5*^{V3}, where expression levels increase with age only in the *Efna5*$^{-/-}$ samples (*Efna5;* Y-KO vs. M-KO). In contrast, a strain difference is observed with *Epha5*^{V12} as expression decreased with age in both wild-type and *Efna5*$^{-/-}$lens epithelium (*Efna5;* Y-WT vs M-WT; Y-KO vs. M-KO), but not between the matched samples in the *Epha2* strain. *Epha2* did not show appreciable change in either strain (Table 1). *Epha3*, *Epha4*, *Epha5*^{V9}, *Epha5*^{V14}, *Epha6*, *Epha7*$^{V1-6}$, and *Epha8* were all either in the noise range or did not produce readable signal due to low transcript levels.

While no changes were observed in any of the quantitated *Ephb* genes in the lens epithelium (Figures 1B, D), *Ephb2*, *Ephb3*, and *Ephb4*^{V1} were moderately expressed, while *Ephb4*^{V2} and *Ephb6* were highly expressed (Table 2). Although both mouse strains are backcrossed to the C57BL/6J background, the two strains are maintained separately and not intermixed. Due to the separate maintenance of these inbred colonies, some genetic drift, and therefore some endogenous strain-related changes are expected. This highlights the necessity of using littermate controls for experiments. Overall, the strains are similar, but strain-dependent differences are evident and discussed below. Of the 14 characterized Ephs in the mouse, only 3 showed notable changes in the epithelium.

3.5 Ephrin expression changes in the aging lens epithelium

Ephrin-A and ephrin-B ligands are encoded by *Efna* and *Efnb* genes, respectively. Within the lens epithelium, only three ephrin ligands showed significant changes in transcript levels. *Efna2*, *Efna3*$^{IsoA/C}$ (isoforms A and C), and *Efna5*$^{V1/3}$ changed significantly with expression levels in the valid range (Figures 2A, C, Table 1). *Efna2* exhibits an age-dependent decrease in both *Epha2*$^{-/-}$ and *Efna5*$^{-/-}$ epithelium (*Epha2* and *Efna5*; Y-KO vs M-KO). This age-related decrease is also seen in *Efna5*$^{+/+}$ samples (*Efna5;* Y-WT vs. M-WT) but was not significant in *Epha2*$^{+/+}$ mice (Figure 2A).

Efna3 has 7 variants characterized to date that produce 4 unique protein isoforms. Variant 1 codes for isoform A, the longest of all the isoforms, which has an additional 81-amino-acid extension on the N-terminus compared to isoforms C and D. Variant 2 encodes for isoform B and also has the 81 amino acid extension; however, it lacks exon 4 (bases 591-668 in variant 1, NM_010108.1; bases 242-319 in variants 3 (NM_001377116.1), 4 (NM_001377117.1), and 5 (NM_001377118.1). Variants 3–5 encode for isoform C and only differ in the 5' untranslated region (UTR), sharing an identical coding region. Isoform C lacks the 81 N-terminal residues but retains exon 4. Isoform D is encoded by *Efna3* variants 6 and 7, which also only differ in the 5' UTR. Isoform D lacks the 81 amino acid N-terminal extension like isoform C and also lacks exon 4, making this the shortest isoform. An age-matched genotype difference is observed where *Efna3*$^{IsoA/C}$ expression increases between young-adult *Epha2*$^{+/+}$ and *Epha2*$^{-/-}$ mice (*Epha2*; Y-WT vs. Y-KO), but not in middle-aged mice. However, it should be noted that *Efna3*$^{IsoA/C}$ was very low expressing with a mean ΔC_q of 11.84, compared to the noise threshold of $\Delta C_q = 11.9$.

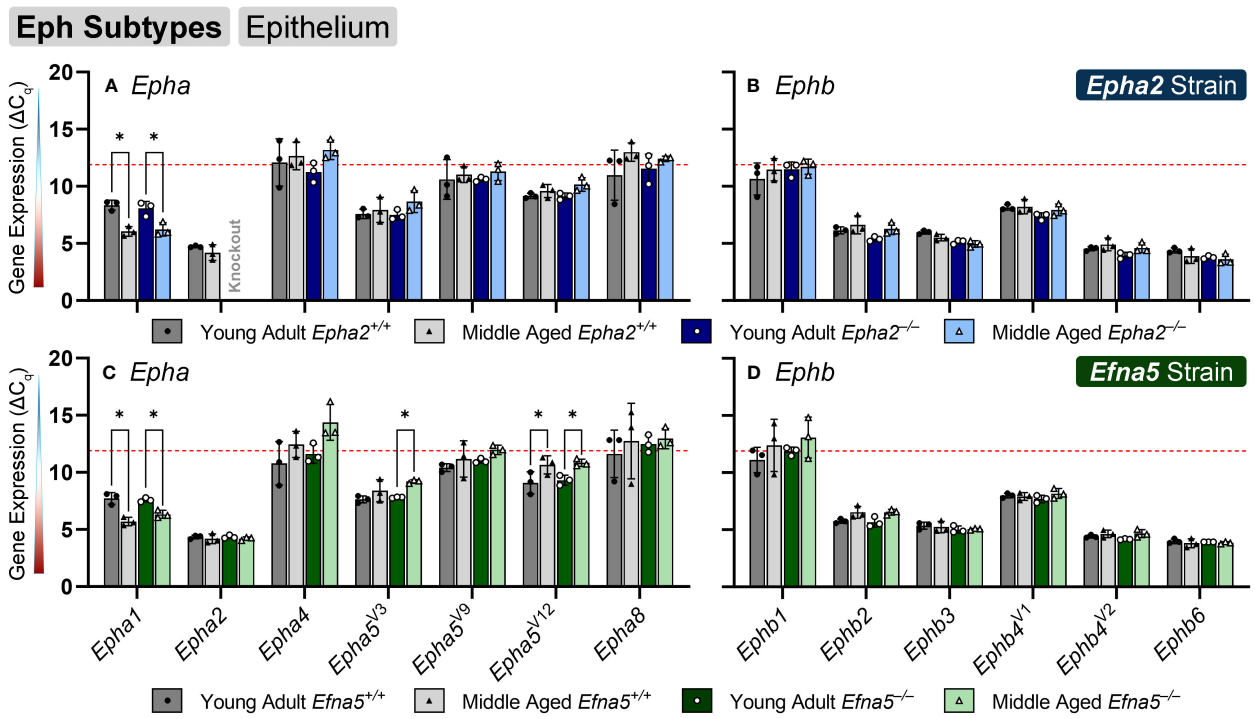

FIGURE 1
Eph subtypes in lens epithelium. *Epha* and *Ephb* transcripts from lens epithelial cells displayed as ΔC_q values. Lower ΔC_q values indicate higher expression. *Epha* and *Ephb* gene expression from the *Epha2* strain (panels **A**, **B**; top row; blue palette) and *Efna5* strain (panels **C**, **D**; bottom row; green palette) are displayed separately. Wild-type animals are indicated by filled symbols and grayscale bars, while knockout animals are indicated by hollow symbols and colored bars. Young-adult mice are represented by darker-shaded bars while middle-aged mice are shaded lighter. Significant changes were observed in *Epha1*, *Epha5*^{V3}, and *Epha5*^{V12} with age. Statistically significant changes with ΔC_q values in the noise range ($\Delta C_q \geq 11.9$), as indicated by the red dotted line, were not considered meaningful hits. Two-way ANOVA or multiple unpaired t-tests were used followed by multiple comparison correction. Benjamini-Krieger-Yekutieli-adjusted p-values (q) < 0.05 are considered discoveries and are indicated by asterisks (*).

Although ephrin-A5 is not an exclusive binding partner of EphA2, the knockout of *Epha2* resulted in an increased expression of *Efna5* variants 1 and 3 compared to wild-type in young adult mice (*Epha2*; Y-WT vs Y-KO). This elevated expression diminishes with age (*Epha2*; Y-KO vs. M-KO), becoming indistinguishable from wild-type at middle-age (*Epha2*; M-WT vs. M-KO, ns). *Efna1*^{V2} and *Efna3*$^{IsoB/D}$ were both in the noise range ($\Delta C_q \geq 11.9$) and thus were not considered meaningful readings. None of the *Efnb* genes showed significant changes between test groups (Figures 2B, D). Although the following genes did not change with age or genotype, *Efna4*, *Efna5*^{V2}, *Efnb2*, and *Efnb3* were moderately expressed, and *Efna1*^{V1}, *Efna5*$^{V1\&3}$, and *Efnb1* were highly expressed (Table 2). Overall, 3 out of 8 ephrins showed significantly altered transcript levels in the lens epithelium (Table 1).

3.6 Eph expression changes in aging lens fibers

In isolated lens fibers, *Epha2*, *Epha5*^{V3}, and all the *Ephb* subtypes (*Ephb1-4*, *Ephb6*) showed altered gene expression either with age or genotype (Figure 3, Table 3). *Epha2* levels increased with age in *Epha2*$^{+/+}$ fibers (*Epha2*; Y-WT vs. M-WT) but showed no changes in *Efna5* mice (Figure 3C). *Epha5*^{V3} showed both age- and genotype-dependent increases in expression. *Epha5*^{V3} transcript levels increased in aging mice regardless of genotype (*Epha2*; Y-WT vs. M-WT; Y-KO vs. M-KO). Moreover, genotype differences were observed where *Epha5*^{V3} transcript levels were increased in *Epha2*$^{-/-}$ lens fibers compared to wild-type mice at both age groups (*Epha2*; Y-WT vs. Y-KO; M-WT vs. M-KO). In contrast, a strain difference is observed where *Epha5*^{V3} only increased in *Efna5*$^{-/-}$ fibers with aging (*Efna5*; Y-KO vs. M-KO) but not in aging *Efna5*$^{+/+}$ mice (*Efna5*; Y-WT vs. M-WT, ns) or in response to *Efna5* knockout (*Efna5*; Y-WT vs. Y-KO, ns; M-WT vs. M-KO, ns).

All the tested *Ephb* genes exhibited a significant change in the lens fibers (Figures 3B, D); however strain-dependent changes are evident here. *Ephb1* expression did not change in *Epha2*$^{+/+}$ WT lens fibers (*Epha2;* Y-WT vs. M-WT, ns), but showed a marked increase with age in *Epha2*$^{-/-}$ fibers (*Epha2;* Y-KO vs. M-KO). *Ephb1* undergoes a strain-dependent increase in aging wild-type lenses (*Efna5;* Y-WT vs. M-WT) of *Efna5*$^{+/+}$ mice, unlike the *Epha2* strain. A further genotype difference is seen where *Ephb1* increases with the knockout of *Efna5* in young-adult mice (*Efna5;* Y-WT vs. Y-KO). In the *Epha2* strain, *Ephb2* transcript levels decrease between young-adult and middle-aged wild-type mice (*Epha2*; Y-WT vs. M-WT) but remains steady in middle-aged *Epha2*$^{-/-}$ mice (*Epha2*; Y-KO vs. M-KO). The level of *Ephb2* expression is significantly higher in middle-aged *Epha2*$^{-/-}$ fibers compared to middle-aged wild-type

TABLE 1 Lens epithelium dynamics summary.

Expression Change Summary	*Epha2* Lens Epithelium				*Efna5* Lens Epithelium			
	Y WT vs M WT	Y KO vs M KO	Y WT vs Y KO	M WT vs M KO	Y WT vs M WT	Y KO vs M KO	Y WT vs Y KO	M WT vs M KO
Epha1	▲	▲			▲	▲		
Epha2								
Epha5^{V3}						▼		
Epha5^{V12}					▼	▼		
Ephb1								
Ephb2								
Ephb3								
Ephb4^{V1}								
Ephb4^{V2}								
Ephb6								
Efna1								
Efna2		▼			▼	▼		
Efna3$^{IsoA/C}$			▲					
Efna5$^{V1\&3}$		▼	▲					
Efna5^{V2}								
Efnb1								
Efnb2								

A summary table of significant gene expression hits in epithelial cells across *Epha2* and *Efna5* strains. Young-adult (Y) vs. middle-aged (M) comparisons (columns 1 and 2 in each set) indicate age-related changes, while wild-type (WT) vs knockout (KO) comparisons in columns 3 and 4 indicate a genotype-related change. Gene upregulation (▲) is indicated in black, while downregulation (▼) is shown in red. Genes that did not change across any of the characterized groups are not included in the table.

samples (*Epha2*; M-WT vs. M-KO). *Ephb2* is the only instance of decreased expression with age observed within lens fibers in this screen. *Ephb3* only showed an age-related increase in *Epha2*$^{-/-}$ fibers (*Epha2*; Y-KO vs. M-KO).

Ephb4^{V1} increased with age in both strains (*Epha2* and *Efna5*; Y-WT vs. M-WT; Y-KO vs. M-KO), but also showed an increased expression in middle-aged *Epha2*$^{-/-}$ samples (*Epha2*; M-WT vs. M-KO). In contrast, *Ephb4*^{V2} increased with age only in the *Efna5* strain (*Efna5*; Y-WT vs. M-WT; Y-KO vs. M-KO). *Ephb6* showed a significant increase in the middle-aged *Epha2*$^{-/-}$ fibers compared to its wild-type counterpart (*Epha2*; M-WT vs. M-KO) and its young-adult knockout control (*Epha2*; Y-KO vs. M-KO).

Of all the Eph changes in aging lens fibers, *Ephb1* was the only target that changed concomitantly with the knockout of *Efna5* (Figure 3D). *Epha5*^{V3}, *Ephb2*, Ephb4^{V1}, and *Ephb6* all showed increases in expression in *Epha2*$^{-/-}$ samples compared to their age-matched *Epha2*$^{+/+}$ control (Table 3). *Epha3*, *Epha4*, *Epha*^{V9}, *Epha5*^{V14}, *Epha6*, and all *Epha7* variants (1–6) were in the noise range or did not produce readable signal due to low transcript levels. *Epha8* was above the threshold in the *Efna5* strain and was low expressing in the *Epha2* strain. *Epha5*^{V12}, *Epha8*, *Ephb1*, and *Ephb4*^{V1} were all low expressing, and *Epha1*, *Epha5*^{V3}, *Ephb2*, *Ephb3*, *Ephb4*^{V2}, and *Ephb6* were all moderately expressing (Table 4). Out of all the Eph receptor genes in the fibers, *Epha2* was the only highly expressed target with a mean ΔC_q of 3.9. Overall, changes in *Eph* gene expression are more numerous in the lens fibers compared to the epithelium, with 7 of 14 characterized Ephs exhibiting a significant change.

3.7 Ephrin expression changes in aging lens fibers

In the isolated lens fibers, *Efna1*^{V1}, *Efna5*^{V2}, *Efnb1*, and *Efnb2* showed significant changes with age or genotype (Figure 4, Table 4). *Efna1*^{V1} increased with age across both strains in wild-type and knockout lens fibers (*Epha2* and *Efna5*; Y-WT vs. M-WT; Y-KO vs. M-KO). A genotype difference is observed as young adult *Epha2*$^{-/-}$ fibers showed significantly higher expression of *Efna1*^{V1} than the wild-type controls (*Epha2*; Y-KO vs. M-KO). *Efna5*^{V2} increased with age in wild-type *Efna5* mice (*Efna5*; Y-WT vs. M-WT), but not in the *Epha2* strain (Figures 4A, C). In contrast, *Efna5*$^{V1/3}$ did not change in the fibers. Targets in the noise range included *Efna1*^{V2}, *Efna2*, *Efna3*$^{IsoA/C}$, *Efna3*$^{IsoB/D}$, and *Efnb3*. These targets either returned low transcript levels indistinguishable from noise or failed to produce readable signals. *Efnb1* and *Efnb2* increased with age regardless of genotype across both strains (*Epha2* and *Efna5*; Y-WT vs. M-WT; Y-KO vs. M-KO). However, *Efnb1* also

TABLE 2 Lens epithelium expression table.

Mean ΔC_q Summary	*Epha2* Lens Epithelium								*Efna5* Lens Epithelium							
	Y WT		M WT		Y KO		M KO		Y WT		M WT		Y KO		M KO	
	Mean	St.Dev.	Mean	St.Dev.	Mean	St.Dev.	Mean	St.Dev.	Mean	St.Dev.	Mean	St.Dev.	Mean	St.Dev.	Mean	St.Dev.
Epha1	**8.34**	0.428	**6.05**	0.427	**8.06**	0.619	**6.22**	0.585	**7.73**	0.505	**5.69**	0.374	**7.58**	0.182	**6.33**	0.346
Epha2	**4.73**	0.087	**4.19**	0.681	In Noise Range		In Noise Range		**4.35**	0.163	**4.19**	0.423	**4.36**	0.151	**4.20**	0.152
Epha3	**11.04**	1.764	In Noise Range		**11.39**	0.365	In Noise Range		In Noise Range		In Noise Range		In Noise Range		In Noise Range	
Epha4	In Noise Range		In Noise Range		**11.25**	0.851	In Noise Range		**10.79**	1.912	In Noise Range		**11.63**	0.838	In Noise Range	
Epha5^{V3}	**7.58**	0.413	**7.93**	1.103	**7.48**	0.435	**8.65**	0.949	**7.64**	0.300	**8.39**	0.956	**7.81**	0.057	**9.20**	0.156
Epha5^{V9}	**10.61**	1.734	**11.02**	0.696	**10.61**	0.196	**11.30**	0.793	**10.42**	0.339	**11.18**	1.582	**11.01**	0.206	In Noise Range	
Epha5^{V12}	**9.16**	0.234	**9.59**	0.570	**9.13**	0.286	**10.16**	0.592	**9.09**	0.973	**10.65**	0.793	**9.31**	0.436	**10.83**	0.321
Epha5^{V14}	In Noise Range		In Noise Range		In Noise Range		In Noise Range		In Noise Range		In Noise Range		In Noise Range		In Noise Range	
Epha6	In Noise Range		In Noise Range		In Noise Range		In Noise Range		In Noise Range		In Noise Range		In Noise Range		In Noise Range	
Epha7^{V1-6}																
Epha8	**10.97**	2.194	In Noise Range		**11.56**	1.252	In Noise Range		**11.62**	2.084	In Noise Range		In Noise Range		In Noise Range	
Ephb1	**10.64**	1.395	**11.45**	0.970	**11.49**	0.645	**11.71**	0.668	**11.10**	1.116	In Noise Range		**11.87**	0.368	In Noise Range	
Ephb2	**6.14**	0.300	**6.62**	0.791	**5.40**	0.196	**6.28**	0.505	**5.76**	0.190	**6.53**	0.518	**5.67**	0.427	**6.55**	0.253
Ephb3	**5.99**	0.167	**5.51**	0.279	**5.14**	0.179	**4.95**	0.282	**5.36**	0.304	**5.24**	0.501	**5.02**	0.308	**5.05**	0.069
Ephb4^{V1}	**8.15**	0.249	**8.22**	0.629	**7.37**	0.307	**7.93**	0.510	**7.99**	0.203	**7.92**	0.336	**7.69**	0.325	**8.17**	0.434
Ephb4^{V2}	**4.54**	0.178	**4.91**	0.562	**3.96**	0.270	**4.62**	0.426	**4.41**	0.144	**4.63**	0.329	**4.17**	0.053	**4.66**	0.341
Ephb6	**4.38**	0.219	**3.89**	0.626	**3.79**	0.138	**3.60**	0.457	**3.99**	0.201	**3.82**	0.394	**3.93**	0.004	**3.86**	0.097
Efna1^{V1}	**4.59**	0.135	**4.59**	0.317	**4.09**	0.199	**4.28**	0.327	**4.49**	0.033	**4.18**	0.220	**4.14**	0.264	**4.35**	0.282
Efna1^{V2}	In Noise Range		In Noise Range		In Noise Range		In Noise Range		In Noise Range		In Noise Range		In Noise Range			
Efna2	**10.12**	0.754	**11.00**	0.853	**9.29**	0.532	**10.60**	0.197	**10.28**	0.562	**10.99**	1.150	**9.89**	0.665	**11.54**	0.560
Efna3$^{IsoA/C}$	**11.84**	0.469	In Noise Range		**10.28**	0.668	In Noise Range		**11.30**	1.049	**11.58**	0.351	**11.27**	0.583	In Noise Range	
Efna3$^{IsoB/D}$	In Noise Range		In Noise Range		In Noise Range		In Noise Range		In Noise Range		In Noise Range		In Noise Range		In Noise Range	
Efna4	**7.07**	0.407	**7.06**	0.525	**6.25**	0.105	**6.77**	0.442	**6.90**	0.178	**6.85**	0.088	**6.46**	0.013	**6.66**	0.157
Efna5$^{V1\&3}$	**4.42**	0.336	**4.79**	0.780	**3.51**	0.179	**4.85**	0.529	**4.26**	0.327	**4.67**	0.333	**4.90**	0.070	**5.18**	0.170
Efna5^{V2}	**6.24**	0.234	**6.39**	0.670	**5.52**	0.211	**6.38**	0.468	**5.98**	0.175	**6.28**	0.366	**6.13**	0.083	**6.16**	0.129
Efnb1	**4.42**	0.237	**4.15**	0.662	**3.87**	0.199	**4.13**	0.423	**3.95**	0.139	**3.82**	0.634	**3.83**	0.172	**4.07**	0.226
Efnb2	**6.49**	0.256	**6.85**	0.938	**5.92**	0.438	**6.91**	0.582	**6.04**	0.267	**6.75**	0.316	**6.04**	0.029	**6.59**	0.244
Efnb3	**8.38**	0.099	**9.38**	0.379	**8.03**	0.321	**8.57**	0.702	**8.56**	0.138	**9.36**	0.513	**8.55**	0.585	**9.52**	1.739

A summary of mean ΔC_q and standard deviation from epithelial cell readings. Expression levels are color coded in 5 categories: 3-color gradients ranging from dark to light shading indicate high to low expression, respectively; gray boxes with faded text indicate readings in the noise range ($\Delta C_q \geq 11.9$); Stippled boxes indicate undetermined or non-detected readings. Data sets with fewer than 3 replicates and/or a mean in the noise range were removed.

10.3389/fopht.2024.1410860

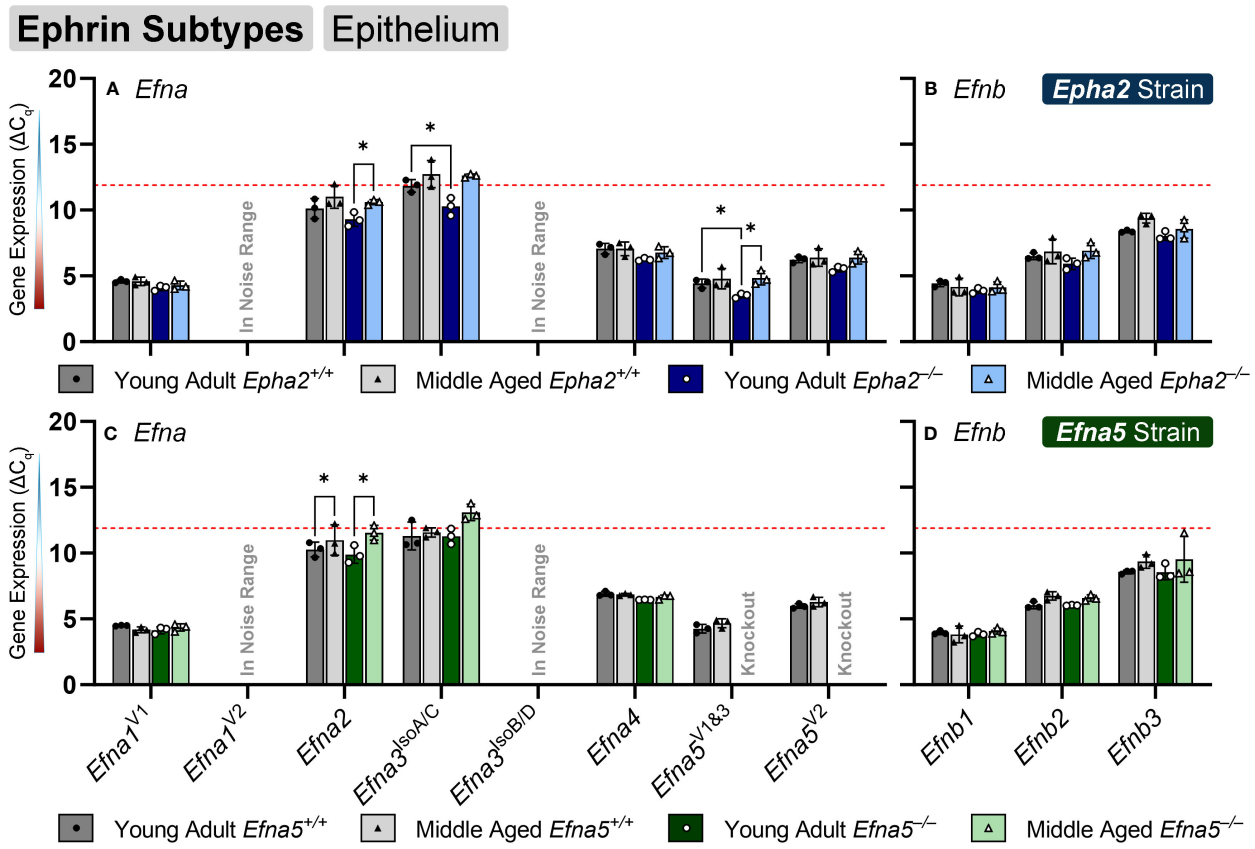

FIGURE 2
Ephrin subtypes in lens epithelium. *Efna* and *Efnb* transcripts from lens epithelial cells displayed as ΔC_q values. Lower ΔC_q values indicates higher expression. *Efna* and *Efnb* gene expression from the *Epha2* strain (panels **A**, **B**; top row; blue palette) and *Efna5* strain (panels **C**, **D**; bottom row; green palette) are displayed separately. Wild-type animals are indicated by filled symbols and grayscale bars, while knockout animals are indicated by hollow symbols and colored bars. Young-adult mice are represented by darker-shaded bars while middle-aged mice are shaded lighter. Statistically significant changes were observed in *Efna2*, and $Efna5^{V1\&3}$ with age, and *Efna2*, $Efna3^{IsoA/C}$ and $Efna5^{V1\&3}$ with genotype. Statistically significant changes with ΔC_q values in the noise range ($\Delta C_q \geq 11.9$), as indicated by the red dotted line, were not considered meaningful hits. Two-way ANOVA or multiple unpaired t-tests were used followed by multiple comparison correction. Benjamini-Krieger-Yekutieli-adjusted p-values (q) < 0.05 are considered discoveries and are indicated by asterisks (*).

increased in *Epha2* knockouts compared to their wild-type counterparts (*Epha2*; Y-WT vs. Y-KO; M-WT vs. M-KO). In the lens fibers, *Efna1* and *Efna4* were lowly expressed while $Efna5^{V1\&3}$, $Efna5^{V2}$, *Efnb1*, and *Efnb2* were moderately expressed. There were no ephrins considered highly expressed in the lens fibers (Table 3).

In summary, within the lens epithelium, *Epha1*, $Epha5^{V3}$, $Epha5^{V12}$, *Efna2*, $Efna3^{IsoA/C}$, and $Efna5^{V1\&3}$, showed significant changes with age. $Efna3^{IsoA/C}$, *and Efna5* were the only targets that changed with genotype, increasing in middle-aged $Efna5^{-/-}$ and young adult $Epha2^{-/-}$ epithelium, respectively, compared to their age-matched wild-type samples. In the lens fibers, *Epha2*, $Epha5^{V3}$, all the *Ephb* genes (*Ephb1-Ephb6*), $Efna1^{V1}$, $Efna5^{V2}$, *Efnb1*, and *Efnb2* demonstrated age-related changes, some of which were strain-dependent. $Epha5^{V3}$, *Ephb2*, $Ephb4^{V1}$, *Ephb6*, and *Efna4* exhibited expression changes concomitant with genotype, notably all in $Epha2^{-/-}$ samples. *Ephb1* was the only target that increased in *Efna5* knockout fibers compared to the wild-type control (Figure 4D). Moreover, *Ephb2* was the only target that decreased with age in the lens fibers.

4 Discussion

Our data show a constellation of gene expression changes between young-adult and middle-aged lenses, as well as changes concomitant with the disruption of *Epha2* or *Efna5* in both cell types of the ocular lens. While transcript-level changes were observed in both the epithelium and isolated fibers, the majority of altered gene expression was observed in the lens fiber cells. Of the genes and variants screened, 6 out of 33 genes and variants screened in the lens epithelium were considered hits, as opposed to 12 out of 33 in the fiber cells. Collapsing these metrics to gene families, 3 of 14 Ephs and 3 of 8 ephrins were considered hits in the epithelium, while 7 of 14 Ephs and 4 of 8 ephrins were regarded as hits in the lens fibers. Our previous work found that 12 of 14 Ephs and 8 of 8 ephrins were present in the ocular mouse lens (27). This work has characterized that, of these previous hits, *Epha3*, $Epha5^{V14}$, $Epha7^{V1-6}$, $Efna1^{V2}$, and $Efna3^{IsoB/D}$ are very low expressing (in the noise range or not detected) and confirmed the non-detection of *Epha6* in both the epithelium and isolated fibers (Tables 2, 4).

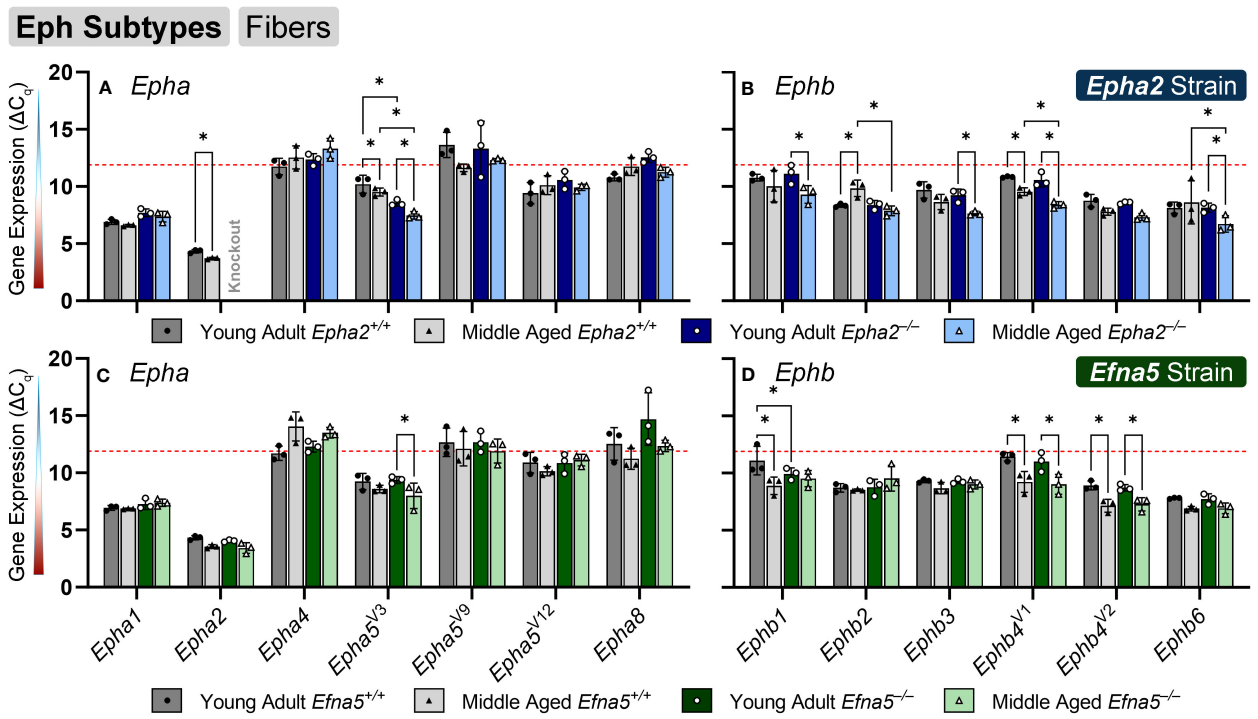

FIGURE 3
Eph subtypes in lens fibers. *Epha* and *Ephb* transcripts from lens fiber cells displayed as ΔC_q values. Lower ΔC_q values indicates higher expression. *Epha* and *Ephb* gene expression from the *Epha2* strain (panels **A**, **B**; top row; blue palette) and *Efna5* strain (panels **C**, **D**; bottom row; green palette) are displayed separately. Wild-type animals are indicated by filled symbols and grayscale bars, while knockout animals are indicated by hollow symbols and colored bars. Young-adult mice are represented by darker-shaded bars while middle-aged mice are shaded lighter. Significant changes were observed in $Epha5^{V3}$, *Ephb1*, *Ephb2*, *Ephb3*, *Ephb4*, *Ephb5*, and *Ephb6* with age and genotype. Statistically significant changes with ΔC_q values in the noise range ($\Delta C_q \geq 11.9$), as indicated by the red dotted line, were not considered meaningful hits. Two-way ANOVA or multiple unpaired t-tests were used followed by multiple comparison correction. Benjamini-Krieger-Yekutieli-adjusted p-values (q) < 0.05 are considered discoveries and are indicated by asterisks (*).

Moreover, these data are generally consistent with the previously reported Affymetrix 430 2.0 data from P28 epithelium and P56 whole lenses obtained from the iSyTE 2.0 database (27). Here, we can prioritize targets based on changes with age, genotype, or expression level, allowing the finer focusing of future studies.

In order to properly control for variation from tissues and genetic knockouts, we screened for a reference gene that is consistent across all of our determined test conditions. While ß-actin is commonly used as an endogenous control, *Epha2* knockout mice exhibited dysregulation of actin and actin-binding proteins (20). Therefore, a non-cytoskeletal control had to be used in this study. This is an important step if the reference gene has not already been characterized in each disease or transgenic model.

In determining meaningful hits from this set of experiments, several different criteria were considered. Data sets with a mean $\Delta C_q \geq 11.9$ were regarded as noise based on the threshold obtained from the *Epha2* in $Epha2^{-/-}$ samples. Although low-expressing targets can play important biological roles, these were considered low priority due to additional steps required to differentiate this signal from noise. Moreover, samples with wild-type controls that did not match across the *Epha2* and *Efna5* strains were considered lower priority due to potential strain differences. In determining statistical significance, a false discovery rate (FDR) approach was chosen over a family-wise error rate (FWER), allowing for more leniency towards type I errors (false positives) (39–41). This was considered more useful than a stricter FWER approach in this context as the goal of these experiments was to establish meaningful leads rather than a mechanistic or diagnostic investigation.

In the traditional PCR screening of Ephs and ephrins in the lens, $Epha7^{V1}$, was identified to be present in wild-type mice, but not in $Epha2^{-/-}$ or $Efna5^{-/-}$ samples, identifying this target as a potential lead (27). In the current study, $Epha7^{V1}$ was not detected in any of the samples, indicating the expression levels may be too low to easily pursue. Previously, $Efna1^{V2}$ was shown to be present in lens epithelium but not isolated fibers. Here, $Efna1^{V2}$ resulted in 12/24 non-detects in epithelial samples, and the remaining 12/24 were in the noise range. In the lens fibers, only 1/24 samples yielded a detectable signal, and that reading was in the noise range, consistent with the qualitative PCR data (27). *Efnb3* was also previously detected in the epithelium but not fibers. Here, *Efnb3* was consistently detected in the lens epithelium with 24/24 valid readings, but not in the isolated lens fibers where 6/24 readings were detected, of which 4 were in the noise range.

Previous work successfully narrowed down the 14 variants of *Epha5* to variants 3, 9, 12, and 14 that were present in the lens. This current work further narrowed down these variants, finding that $Epha5^{V14}$ produced a signal indistinguishable from noise. The remaining variants 3, 9, and 12 were present in both lens

TABLE 3 Lens fiber dynamics summary.

Expression Change Summary	*Epha2* Lens Fiber				*Efna5* Lens Fiber			
	Y WT vs M WT	Y KO vs M KO	Y WT vs Y KO	M WT vs M KO	Y WT vs M WT	Y KO vs M KO	Y WT vs Y KO	M WT vs M KO
Epha1								
Epha2	▲							
Epha5^{V3}	▲	▲	▲	▲		▲		
Epha5^{V12}								
Ephb1		▲			▲		▲	
Ephb2	▼			▲				
Ephb3		▲						
Ephb4^{V1}	▲	▲		▲	▲	▲		
Ephb4^{V2}					▲	▲		
Ephb6		▲		▲				
Efna1	▲	▲			▲	▲		
Efna2								
Efna3$^{IsoA/C}$								
Efna5$^{V1\&3}$								
Efna5^{V2}					▲			
Efnb1	▲	▲	▲	▲	▲	▲		
Efnb2	▲	▲			▲	▲		

A summary table of significant gene expression hits in fiber cells across *Epha2* and *Efna5* strains. Young-adult (Y) vs. middle-aged (M) comparisons (columns 1 and 2 in each set) indicate age-related changes, while wild-type (WT) vs knockout (KO) comparisons in columns 3 and 4 indicate a genotype-related change. Gene upregulation (▲) is indicated in black, while downregulation (▼) is shown in red. Genes that did not change across any of the characterized groups are not included in the table.

epithelium and fibers. *Epha5^{V9}* was low expressing and did not show appreciable change across any of the test conditions in this screen. However, *Epha5^{V3}* expression showed opposite trends between tissue compartments, decreasing with age in the epithelium (*Efna5*; Y-KO vs. M-KO) and increasing with age in the isolated lens fibers (*Efna5*; Y-KO vs. M-KO). The opposing trends between tissues and the increase of expression in the *Epha2* fibers may indicate a compensatory or related physiological role linked to the knockout of *Epha2* or *Efna5*. Meanwhile, *Epha5^{V12}* decreased with age only in the epithelium of both wild-type and *Efna5$^{-/-}$* mice, but not in the *Epha2* strain. *Epha5* was previously observed to be highly expressed in the lenses of embryonic mice, second only to *Epha2* based on iSyTE analysis, and the EphA5 receptor is known to bind to ephrin-A5. Moreover, *Epha5* expression was decreased in *Mafg$^{-/-}$;Mafk$^{-/-}$* double knockout mice, a model that exhibits cataracts after 4 months of age (42). These findings highlight potential roles of *Epha5^{V3}* and *Epha5^{V12}* that differ between the epithelium and isolated fibers, and also between closely related variants. Further study into the roles of *Epha5* variants in the epithelium vs. bulk fiber mass may be a promising avenue into revealing the mechanisms of cataractogenesis.

Finding the binding partners of EphA2 and ephrin-A5, even with a putatively narrowed list of hits, can be a time- and resource-intensive process. Given that EphAs typically bind to ephrin-As, and EphBs typically bind to ephrin-Bs, targets can be tentatively filtered in this way; however, there are several exceptions to this paradigm that must be considered. Although the roles of other Ephs and ephrins in the lens remain unclear, interactions between EphA2, ephrin-A5, and other binding partners have been reported in other tissues. Several studies have been conducted investigating the interactions between EphA2 and ephrin-A1, showing roles in processes ranging from angiogenesis, proliferation, cell migration, and adhesion via an assortment of secondary messengers (43–52). In this study, *Efna1* is a high-expressing ligand in the lens epithelium and a moderately-expressing target in the isolated fibers. When *Epha2* is knocked out, the expression level of *Efna1* increases significantly in both the epithelium and fibers, suggesting a possible compensatory mechanism. The previously observed interactions between EphA2 and ephrin-A1 make this a promising interaction to further investigate at the protein level.

Beyond binding with several ephrin ligands, EphA2 has also been shown to interact with other Eph receptors as well. In the PC3 human prostate cancer cell line, EphA2 coimmunoprecipitated with EphB2 via the ligand binding domain, showing a co-clustering of these receptors that may differentially affect the Eph-ephrin signaling landscape based on the present heteromers (53). Here, a marked increase in *Ephb2* expression is observed in middle-aged *Epha2$^{-/-}$* fibers compared to its middle-aged wild-type counterpart, and this change is not seen in *Efna5$^{-/-}$* samples.

TABLE 4 Lens fiber expression table.

Mean ΔC_q Summary	*Epha2* Lens Fiber								*Efna5* Lens Fiber							
	Y WT		M WT		Y KO		M KO		Y WT		M WT		Y KO		M KO	
	Mean	St.Dev.	Mean	St.Dev.	Mean	St.Dev.	Mean	St.Dev.	Mean	St.Dev.	Mean	St.Dev.	Mean	St.Dev.	Mean	St.Dev.
Epha1	**6.91**	0.223	**6.61**	0.088	**7.71**	0.334	**7.36**	0.473	**6.93**	0.211	**6.87**	0.042	**7.26**	0.463	**7.39**	0.313
Epha2	**4.34**	0.146	**3.72**	0.089					**4.32**	0.177	**3.55**	0.162	**4.05**	0.096	**3.42**	0.459
Epha3	In Noise Range				In Noise Range											
Epha4	**11.75**	0.720	In Noise Range		In Noise Range		In Noise Range		**11.72**	0.618	In Noise Range		In Noise Range		In Noise Range	
Epha5^{V3}	**10.20**	0.776	**9.52**	0.350	**8.56**	0.270	**7.48**	0.327	**9.24**	0.708	**8.58**	0.328	**9.38**	0.298	**7.99**	1.122
Epha5^{V9}	In Noise Range		**11.63**	0.327	In Noise Range		In Noise Range		In Noise Range		In Noise Range		In Noise Range		**11.90**	1.050
Epha5^{V12}	**9.41**	0.930	**10.12**	0.832	**10.57**	0.775	**9.92**	0.272	**10.90**	0.902	**10.14**	0.406	**10.86**	0.858	**11.12**	0.507
Epha5^{V14}	In Noise Range		In Noise Range		In Noise Range		In Noise Range				In Noise Range		In Noise Range			
Epha6																
Epha7^{V1-6}																
Epha8	**10.79**	0.298	**11.74**	0.788	In Noise Range		**11.25**	0.440	In Noise Range		**11.23**	0.925	In Noise Range		In Noise Range	
Ephb1	**10.77**	0.305	**10.03**	1.375	**11.11**	0.837	**9.30**	0.779	**11.09**	1.245	**8.90**	0.763	**9.93**	0.512	**9.52**	0.712
Ephb2	**8.34**	0.144	**9.84**	0.720	**8.38**	0.391	**7.86**	0.424	**8.71**	0.369	**8.52**	0.088	**8.76**	0.702	**9.55**	1.124
Ephb3	**9.70**	0.725	**8.64**	0.662	**9.23**	0.551	**7.64**	0.196	**9.31**	0.149	**8.69**	0.494	**9.27**	0.201	**9.01**	0.393
Ephb4^{V1}	**10.83**	0.062	**9.55**	0.343	**10.57**	0.613	**8.39**	0.292	**11.42**	0.363	**9.22**	0.912	**11.00**	0.846	**9.01**	0.866
Ephb4^{V2}	**8.77**	0.553	**7.79**	0.313	**8.58**	0.098	**7.33**	0.317	**8.91**	0.391	**7.14**	0.566	**8.71**	0.289	**7.27**	0.576
Ephb6	**8.13**	0.500	**8.61**	1.884	**8.14**	0.404	**6.73**	0.713	**7.81**	0.055	**6.89**	0.207	**7.73**	0.465	**6.92**	0.475
Efna1^{V1}	**11.27**	0.580	**9.01**	0.199	**9.98**	0.450	**8.04**	0.070	**10.40**	0.631	**8.46**	0.376	**10.95**	0.196	**8.89**	0.496
Efna1^{V2}	In Noise Range															
Efna2	In Noise Range				In Noise Range		In Noise Range		In Noise Range				In Noise Range			
Efna3$^{IsoA/C}$					In Noise Range						In Noise Range				In Noise Range	
Efna3$^{IsoB/D}$					In Noise Range											
Efna4	In Noise Range		**10.81**	2.062	In Noise Range		**9.58**	1.525	In Noise Range		**10.42**	0.540	In Noise Range		**10.22**	0.450
Efna5$^{V1\&3}$	**7.45**	0.154	**6.32**	0.720	**7.05**	0.395	**6.22**	0.069	**7.29**	0.339	**6.39**	0.395	**7.73**	0.470	**6.79**	0.291
Efna5^{V2}	**9.43**	0.338	**8.19**	0.334	**8.68**	0.669	**8.36**	0.296	**8.97**	0.241	**8.36**	0.106	**8.82**	0.206	**8.14**	0.195
Efnb1	**8.17**	0.193	**5.89**	0.104	**7.30**	0.126	**5.43**	0.206	**7.92**	0.853	**5.42**	0.089	**7.63**	0.080	**5.71**	0.483
Efnb2	**8.77**	0.202	**7.29**	0.294	**8.59**	0.155	**7.09**	0.340	**8.69**	0.317	**6.91**	0.144	**8.85**	0.365	**7.16**	0.219
Efnb3	In Noise Range		In Noise Range		In Noise Range		In Noise Range		In Noise Range							

A summary of mean ΔC_q and standard deviation from fiber cell readings. Expression levels are color coded in 5 categories: 3-color gradients ranging from dark to light shading indicate high to low expression, respectively; gray boxes with faded text indicate readings in the noise range ($\Delta C_q \geq 11.9$); Stippled boxes indicate undetermined or non-detected readings. Data sets with fewer than 3 replicates and/or a mean in the noise range were removed

10.3389/fopht.2024.1410860

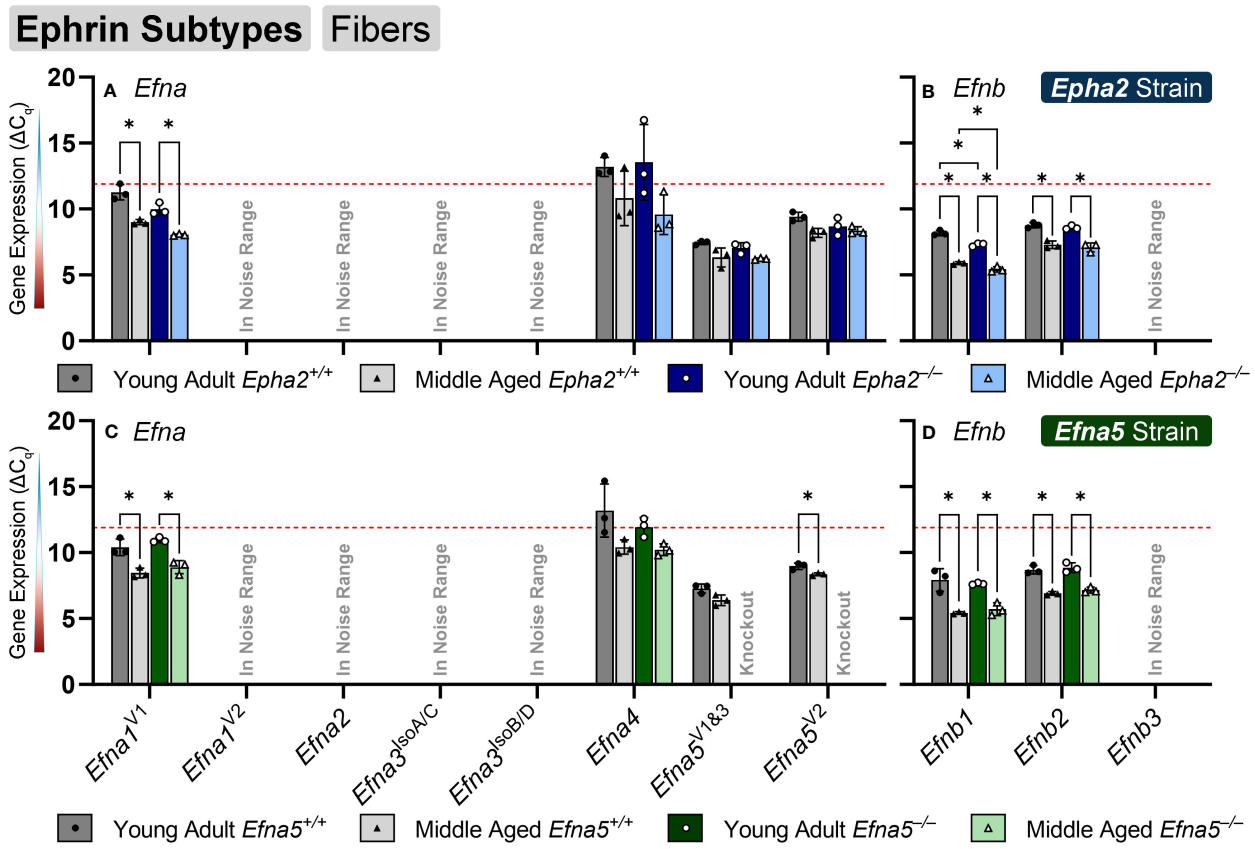

FIGURE 4
Ephrin subtypes in lens fibers. *Efna* and *Efnb* transcripts from lens fiber cells displayed as ΔC_q values. Lower ΔC_q values indicates higher expression. *Efna* and *Efnb* gene expression from the *Epha2* strain (panels **A**, **B**; top row; blue palette) and *Efna5* strain (panels **C**, **D**; bottom row; green palette) are displayed separately. Wild-type animals are indicated by filled symbols and grayscale bars, while knockout animals are indicated by hollow symbols and colored bars. Young-adult mice are represented by darker-shaded bars while middle-aged mice are shaded lighter. Significant changes were observed in $Efna1^{V1}$, *Efna4*, *Efnb1*, and *Efnb2* with age and genotype. $Efna1^{V1}$, *Efnb1*, and *Efnb2* all increased with age, however $Efna1^{V1}$ also showed an increased expression in $Epha2^{-/-}$ fiber cells compared to the age-matched $Epha2^{+/+}$ samples. A genotype difference was also observed with increased Efna4 expression in middle-aged $Epha2^{-/-}$ and $Epha2^{+/+}$ mice. Statistically significant changes with ΔC_q values in the noise range ($\Delta C_q \geq 11.9$), as indicated by the red dotted line, were not considered meaningful hits. Two-way ANOVA or multiple unpaired t-tests were used followed by multiple comparison correction. Benjamini-Krieger-Yekutieli-adjusted p-values (q) < 0.05 are considered discoveries and are indicated by asterisks (*).

Like EphA2, ephrin-A5 has also been shown to interact with several other Eph receptors. Ephrin-A5 interaction with *EphA5* has been shown to promote synaptogenesis through activation of voltage-gated calcium channels, promoting downstream signaling through protein kinase A (54). While calcium is a broad secondary messenger, calcium-dependent or calcium-modulated targets play important roles in the lens and cataract formation, including cadherins, calcium-activated proteases (calpain), aquaporin-0, and connexins (4, 55–58). These calcium-dependent targets have been observed to be dysregulated in cataractous lenses, suggesting that disruption of ephrin-A5 and EphA5 interactions could play a role in these mechanisms of cataractogenesis. Moreover, ephrin-A5 and *EphB2* have been shown to interact with high affinity, and here, *Ephb2* is observed at moderate to high expression levels in the lens epithelium and moderate levels in the fibers (10). Between activating protein kinase A and increasing calcium influxes, the downstream effectors of ephrin-A5 are vast. Considering interactions with EphA5 and EphB2, identifying other Ephs and ephrins as interacting partners of ephrin-A5 may provide leads for a more targeted search for calcium- and phosphorylation-dependent mechanisms of cataractogenesis.

As the roles of Ephs and ephrins are characterized in other tissues, these data can be used to help direct the focus of future studies in the lens. Several transgenic models are available for Ephs and ephrins, however, little phenotypic data of the lens has been reported to date in these models. Reporting these phenotypes can also help identify Ephs and ephrins of interest and rapidly expand the compendium of relevant targets. In the context of previous studies investigating EphA2 and ephrin-A5, the spatial and temporal expression data presented here may help inform the choice of targets of interest of lens homeostasis and cataractogenesis in the lens,

Although mRNA transcripts are well understood in the central dogma of molecular biology to encode the translation of protein, the correlation between transcript and protein levels is weak (59–62). This is observed here, where the data presented in this study indicates an increase in *Epha2* transcripts, however, western blot

data shows a decrease in EphA2 protein between 2 weeks and 5 months of age in mice (6). In order to pursue meaningful hits, quantification of the relevant proteins should be performed to ensure that the target is present in a given strain before undergoing an in-depth physiological assessment. Moreover, in our endeavor to identify binding partners of EphA2 and ephrin-A5, characterizing the localization of the target of interest will be a necessary step. This is due to the observation that EphA2 sequesters mostly in the fiber cells and while ephrin-A5 is mostly present in the epithelial cells, resulting in a spatial barrier of interaction (5). Additionally, the loss of nuclei and other organelles in the nuclear fiber cells presumably limits transcriptomics data to the peripheral fiber cells. Therefore, characterization of these targets at the protein level will be an important step in informing their role in the lens, particularly in the lens nucleus.

Currently, the primary interacting partners of EphA2 and ephrin-A5 in the lens are not known. Here, we present the characterization of a dynamic gene network, changing concomitantly within two transgenic models. These data provide an informed prioritization of targets to pursue in upcoming mechanistic studies to determine how EphA2 and ephrin-A5 maintain lens homeostasis and lens transparency. This perspective on gene network changes in these transgenic cataract models has helped focus the Eph-ephrin search to fewer, manageable targets to pursue in future studies.

Data availability statement

The original contributions presented in the study are included in the Supplementary Material, further inquiries can be directed to the corresponding author.

Ethics statement

The animal study was approved by The Bloomington Institutional Animal Care and Use Committee. The study was conducted in accordance with the local legislation and institutional requirements.

Author contributions

PH: Conceptualization, Data curation, Formal analysis, Investigation, Methodology, Project administration, Software, Validation, Visualization, Writing – original draft, Writing – review & editing. CC: Conceptualization, Funding acquisition, Investigation, Methodology, Project administration, Resources, Supervision, Visualization, Writing – review & editing.

Funding

The author(s) declare financial support was received for the research, authorship, and/or publication of this article. This research was funded by grant R01 EY032056 from the National Eye Institute (to CC).

Acknowledgments

We thank Michael Vu, Dr. Alex Corrion, and Dr. Jonathan Timmons for their helpful discussion and Isaiah Innis for his assistance in maintaining the animal colony.

Conflict of interest

The authors declare that the research was conducted in the absence of any commercial or financial relationships that could be construed as a potential conflict of interest.

The author(s) declared that they were an editorial board member of Frontiers, at the time of submission. This had no impact on the peer review process and the final decision.

Publisher's note

Supplementary material

The Supplementary Material for this article can be found online at: https://www.frontiersin.org/articles/10.3389/fopht.2024.1410860/full#supplementary-material

SUPPLEMENTARY FIGURE 1
Epha7 probe design strategy. Probe permutations used to target *Epha7* variants 1–6. Each bar represents the sequence ranging from the end of exon 7 to beginning of exon 10. The primer permutations and expected amplicon sizes are listed in the bottom panel.

SUPPLEMENTARY FIGURE 2
Endogenous gene panel. Quantification cycle (C_q) values of endogenous reference genes from the ocular lenses of young-adult (6-week-old) mice. The chosen reference gene, peptidylprolyl isomerase A (*Ppia*) is indicated by a red box. Each of the 8 test groups denoted were tested in triplicate (n=3 per group).

SUPPLEMENTARY FIGURE 3
Peptidylprolyl isomerase A distribution. Quantification cycle (C_q) values of the endogenous internal control gene, peptidylprolyl isomerase a (*Ppia*) across biological groups. These are aggregates of all the readings taken from 48 biological samples across all the reported assays (n=1584).

SUPPLEMENTARY TABLE 1
Primer and probe library. The primers and probes used in this study with sequences of custom probes and assay IDs of commercial probes are provided. For custom probes, the exon-spanning oligonucleotide is indicated as the forward primer (F), reverse primer (R), or TaqMan probe (P). The sequencing primers used for Efna5−/− validation are included as the last entry in the table. Alternative exons are designated as 'a-d' using variant 1 as

reference (except for Epha5, for which variant 3 was used as reference). Greyed out exons indicate untranslated regions (UTRs).

SUPPLEMENTARY TABLE 2
Lens epithelium statistics. A compiled table of two-way ANVOAs and multiple t-tests with two-stage linear step-up procedure of Benjamini, Krieger, and Yekutieli multiple comparison correction. Significant hits are indicated as discoveries.

SUPPLEMENTARY TABLE 3
Lens fiber statistics. A compiled table of two-way ANVOAs and multiple t-tests with two-stage linear step-up procedure of Benjamini, Krieger, and Yekutieli multiple comparison correction. Significant hits are indicated as discoveries.

SUPPLEMENTARY TABLE 4
Assay data. Sorted assay data containing Cq and ΔCq values for each gene of interest.

References

1. World Health Organization. *World report on vision*. Geneva. (2019).

2. Murugan S, Cheng C. Roles of eph-ephrin signaling in the eye lens cataractogenesis, biomechanics, and homeostasis. *Front Cell Dev Biol*. (2022) 10:852236. doi: 10.3389/fcell.2022.852236

3. Cheng C, Gong X. Diverse roles of eph/ephrin signaling in the mouse lens. *PloS One*. (2011) 6:e28147. doi: 10.1371/journal.pone.0028147

4. Bassnett S, Shi Y, Vrensen GF. Biological glass: structural determinants of eye lens transparency. *Philos Trans R Soc Lond B Biol Sci*. (2011) 366:1250–64. doi: 10.1098/rstb.2010.0302

5. Cheng C, Fowler VM, Gong X. EphA2 and ephrin-A5 are not a receptor-ligand pair in the ocular lens. *Exp Eye Res*. (2017) 162:9–17. doi: 10.1016/j.exer.2017.06.016

6. Jun G, Guo H, Klein BE, Klein R, Wang JJ, Mitchell P, et al. EPHA2 is associated with age-related cortical cataract in mice and humans. *PloS Genet*. (2009) 5:e1000584. doi: 10.1371/journal.pgen.1000584

7. Cooper MA, Son AI, Komlos D, Sun Y, Kleiman NJ, Zhou R. Loss of ephrin-A5 function disrupts lens fiber cell packing and leads to cataract. *Proc Natl Acad Sci U.S.A*. (2008) 105:16620–5. doi: 10.1073/pnas.0808987105

8. Gale NW, Holland SJ, Valenzuela DM, Flenniken A, Pan L, Ryan TE, et al. Eph receptors and ligands comprise two major specificity subclasses and are reciprocally compartmentalized during embryogenesis. *Neuron*. (1996) 17:9–19. doi: 10.1016/s0896-6273(00)80276-7

9. Kullander K, Klein R. Mechanisms and functions of eph and ephrin signalling. *Nat Rev Mol Cell Biol*. (2002) 3:475–86. doi: 10.1038/nrm856

10. Himanen JP, Chumley MJ, Lackmann M, Li C, Barton WA, Jeffrey PD, et al. Repelling class discrimination: ephrin-A5 binds to and activates ephB2 receptor signaling. *Nat Neurosci*. (2004) 7:501–9. doi: 10.1038/nn1237

11. Takemoto M, Fukuda T, Sonoda R, Murakami F, Tanaka H, Yamamoto N. Ephrin-B3-ephA4 interactions regulate the growth of specific thalamocortical axon populations *in vitro*. *Eur J Neurosci*. (2002) 16:1168–72. doi: 10.1046/j.1460-9568.2002.02166.x

12. Arvanitis D, Davy A. Eph/ephrin signaling: networks. *Genes Dev*. (2008) 22:416–29. doi: 10.1101/gad.1630408

13. Pasquale EB. Eph-ephrin bidirectional signaling in physiology and disease. *Cell*. (2008) 133:38–52. doi: 10.1016/j.cell.2008.03.011

14. Zhai Y, Zhu S, Li J, Yao K. A novel human congenital cataract mutation in EPHA2 kinase domain (p.G668D) alters receptor stability and function. *Invest Ophthalmol Vis Sci*. (2019) 60:4717–26. doi: 10.1167/iovs.19-27370

15. Shiels A, Bennett TM, Knopf HLS, Maraini G, Li A, Jiao X, et al. The EPHA2 gene is associated with cataracts linked to chromosome 1p. *Mol Vision*. (2008) 14:2042–55.

16. Kaul H, Riazuddin SA, Shahid M, Kousar S, Butt NH, Zafar AU, et al. Autosomal recessive congenital cataract linked to EPHA2 in a consanguineous Pakistani family. *Mol Vis*. (2010) 16:511–7.

17. Lin Q, Zhou N, Zhang N, Qi Y. Mutational screening of EFNA5 in chinese age-related cataract patients. *Ophthalmic Res*. (2014) 52:124–9. doi: 10.1159/000363139

18. Masoodi TA, Shammari SA, Al-Muammar MN, Almubrad TM, Alhamdan AA. Screening and structural evaluation of deleterious non-synonymous SNPs of epha2 gene involved in susceptibility to cataract formation. *Bioinformation*. (2012) 8:562–7. doi: 10.6026/97320630008562

19. Cheng C. EphA2 and ephrin-A5 guide eye lens suture alignment and influence whole lens resilience. *Invest Ophthalmol Vis Sci*. (2021) 62:3. doi: 10.1167/iovs.62.15.3

20. Cheng C, Ansari MM, Cooper JA, Gong X. EphA2 and src regulate equatorial cell morphogenesis during lens development. *Development*. (2013) 140:4237–45. doi: 10.1242/dev.100727

21. Cheng C, Gao J, Sun X, Mathias RT. Eph-ephrin signaling affects eye lens fiber cell intracellular voltage and membrane conductance. *Front Physiol*. (2021) 12:772276. doi: 10.3389/fphys.2021.772276

22. Cheng C, Wang K, Hoshino M, Uesugi K, Yagi N, Pierscionek B. EphA2 affects development of the eye lens nucleus and the gradient of refractive index. *Invest Ophthalmol Vis Sci*. (2022) 63:2. doi: 10.1167/iovs.63.1.2

23. Shi Y, De Maria A, Bennett T, Shiels A, Bassnett S. A role for epha2 in cell migration and refractive organization of the ocular lens. *Invest Ophthalmol Vis Sci*. (2012) 53:551–9. doi: 10.1167/iovs.11-8568

24. Zhou Y, Shiels A. Epha2 and efna5 participate in lens cell pattern-formation. *Differentiation*. (2018) 102:1–9. doi: 10.1016/j.diff.2018.05.002

25. Himanen JP. Ectodomain structures of eph receptors. *Semin Cell Dev Biol*. (2012) 23:35–42. doi: 10.1016/j.semcdb.2011.10.025

26. Singla N, Goldgur Y, Xu K, Paavilainen S, Nikolov DB, Himanen JP. Crystal structure of the ligand-binding domain of the promiscuous ephA4 receptor reveals two distinct conformations. *Biochem Biophys Res Commun*. (2010) 399:555–9. doi: 10.1016/j.bbrc.2010.07.109

27. Vu MP, Cheng C. Mapping the universe of eph receptor and ephrin ligand transcripts in epithelial and fiber cells of the eye lens. *Cells*. (2022) 11. doi: 10.3390/cells11203291

28. Brantley-Sieders DM, Caughron J, Hicks D, Pozzi A, Ruiz JC, Chen J. EphA2 receptor tyrosine kinase regulates endothelial cell migration and vascular assembly through phosphoinositide 3-kinase-mediated rac1 GTPase activation. *J Cell Sci*. (2004) 117:2037–49. doi: 10.1242/jcs.01061

29. Frisen J, Yates PA, McLaughlin T, Friedman GC, O'Leary DD, Barbacid M. Ephrin-A5 (AL-1/RAGS) is essential for proper retinal axon guidance and topographic mapping in the mammalian visual system. *Neuron*. (1998) 20:235–43. doi: 10.1016/s0896-6273(00)80452-3

30. Cheng C, Nowak RB, Gao J, Sun X, Biswas SK, Lo WK, et al. Lens ion homeostasis relies on the assembly and/or stability of large connexin 46 gap junction plaques on the broad sides of differentiating fiber cells. *Am J Physiol Cell Physiol*. (2015) 308:C835–47. doi: 10.1152/ajpcell.00372.2014

31. Alizadeh A, Clark J, Seeberger T, Hess J, Blankenship T, FitzGerald PG. Characterization of a mutation in the lens-specific CP49 in the 129 strain of mouse. *Invest Ophthalmol Vis Sci*. (2004) 45:884–91. doi: 10.1167/iovs.03-0677

32. Gokhin DS, Nowak RB, Kim NE, Arnett EE, Chen AC, Sah RL, et al. Tmod1 and CP49 synergize to control the fiber cell geometry, transparency, and mechanical stiffness of the mouse lens. *PloS One*. (2012) 7:e48734. doi: 10.1371/journal.pone.0048734

33. Sandilands A, Wang X, Hutcheson AM, James J, Prescott AR, Wegener A, et al. Bfsp2 mutation found in mouse 129 strains causes the loss of CP49' And induces vimentin-dependent changes in the lens fibre cell cytoskeleton. *Exp Eye Res*. (2004) 78:875–89. doi: 10.1016/j.exer.2003.09.028

34. Simirskii VN, Lee RS, Wawrousek EF, Duncan MK. Inbred FVB/N mice are mutant at the CP49/bfsp2 locus and lack beaded filament proteins in the lens. *Invest Ophthalmol Vis Sci*. (2006) 47:4931–4. doi: 10.1167/iovs.06-0423

35. Parreno J, Emin G, Vu MP, Clark JT, Aryal S, Patel SD, et al. Methodologies to unlock the molecular expression and cellular structure of ocular lens epithelial cells. *Front Cell Dev Biol*. (2022) 10:983178. doi: 10.3389/fcell.2022.983178

36. Wang K, Cheng C, Li L, Liu H, Huang Q, Xia CH, et al. GammaD-crystallin associated protein aggregation and lens fiber cell denucleation. *Invest Ophthalmol Vis Sci*. (2007) 48:3719–28. doi: 10.1167/iovs.06-1487

37. Invitrogen. *SuperScript IV VILO master mix for optimal RT-qPCR*. (2016), COL31250 0716. Waltham, MA, USA. doi: 10.1101/pdb.rec091082

38. Himanen JP, Yermekbayeva L, Janes PW, Walker JR, Xu K, Atapattu L, et al. Architecture of eph receptor clusters. *Proc Natl Acad Sci U.S.A*. (2010) 107:10860–5. doi: 10.1073/pnas.1004148107

39. Benjamini Y, Hochberg Y. Controlling the false discovery rate - A practical and powerful approach to multiple testing. *J R Stat Soc B*. (1995) 57:289–300. doi: 10.1111/j.2517-6161.1995.tb02031.x

40. Benjamini Y, Krieger AM, Yekutieli D. Adaptive linear step-up procedures that control the false discovery rate. *Biometrika*. (2006) 93:491–507. doi: 10.1093/biomet/93.3.491

41. Benjamini Y, Yekutieli D. Quantitative trait loci analysis using the false discovery rate. *Genetics*. (2005) 171:783–90. doi: 10.1534/genetics.104.036699

42. Patel SD, Anand D, Motohashi H, Katsuoka F, Yamamoto M, Lachke SA. Deficiency of the bZIP transcription factors mafg and mafk causes misexpression of

genes in distinct pathways and results in lens embryonic developmental defects. *Front Cell Dev Biol*. (2022) 10:981893. doi: 10.3389/fcell.2022.981893

43. Miao H, Burnett E, Kinch M, Simon E, Wang B. Activation of ephA2 kinase suppresses integrin function and causes focal-adhesion-kinase dephosphorylation. *Nat Cell Biol*. (2000) 2:62–9. doi: 10.1038/35000008

44. Miao H, Wei BR, Peehl DM, Li Q, Alexandrou T, Schelling JR, et al. Activation of ephA receptor tyrosine kinase inhibits the ras/MAPK pathway. *Nat Cell Biol*. (2001) 3:527–30. doi: 10.1038/35074604

45. Zantek ND, Azimi M, Fedor-Chaiken M, Wang B, Brackenbury R, Kinch MS. E-cadherin regulates the function of the epha2 receptor tyrosine kinase. *Cell Growth Differ*. (1999) 10:629–38.

46. Hess AR, Seftor EA, Gruman LM, Kinch MS, Seftor RE, Hendrix MJ. VE-cadherin regulates ephA2 in aggressive melanoma cells through a novel signaling pathway: implications for vasculogenic mimicry. *Cancer Biol Ther*. (2006) 5:228–33. doi: 10.4161/cbt.5.2.2510

47. Ojima T, Takagi H, Suzuma K, Oh H, Suzuma I, Ohashi H, et al. EphrinA1 inhibits vascular endothelial growth factor-induced intracellular signaling and suppresses retinal neovascularization and blood-retinal barrier breakdown. *Am J Pathol*. (2006) 168:331–9. doi: 10.2353/ajpath.2006.050435

48. Rodriguez S, Rudloff S, Koenig KF, Karthik S, Hoogewijs D, Huynh-Do U. Bidirectional signalling between ephA2 and ephrinA1 increases tubular cell attachment, laminin secretion and modulates erythropoietin expression after renal hypoxic injury. *Pflugers Arch*. (2016) 468:1433–48. doi: 10.1007/s00424-016-1838-1

49. Sabet O, Stockert R, Xouri G, Bruggemann Y, Stanoev A, Bastiaens PIH. Ubiquitination switches ephA2 vesicular traffic from A continuous safeguard to A finite signalling mode. *Nat Commun*. (2015) 6:8047. doi: 10.1038/ncomms9047

50. Wykosky J, Debinski W. The ephA2 receptor and ephrinA1 ligand in solid tumors: function and therapeutic targeting. *Mol Cancer Res*. (2008) 6:1795–806. doi: 10.1158/1541-7786.MCR-08-0244

51. Yeddula N, Xia Y, Ke E, Beumer J, Verma IM. Screening for tumor suppressors: loss of ephrin receptor A2 cooperates with oncogenic KRas in promoting lung adenocarcinoma. *Proc Natl Acad Sci U.S.A*. (2015) 112:E6476–85. doi: 10.1073/pnas.1520110112

52. Youngblood VM, Kim LC, Edwards DN, Hwang Y, Santapuram PR, Stirdivant SM, et al. The ephrin-A1/EPHA2 signaling axis regulates glutamine metabolism in HER2-positive breast cancer. *Cancer Res*. (2016) 76:1825–36. doi: 10.1158/0008-5472.CAN-15-0847

53. Janes PW, Griesshaber B, Atapattu L, Nievergall E, Hii LL, Mensinga A, et al. Eph receptor function is modulated by heterooligomerization of A and B type eph receptors. *J Cell Biol*. (2011) 195:1033–45. doi: 10.1083/jcb.201104037

54. Akaneya Y, Sohya K, Kitamura A, Kimura F, Washburn C, Zhou R, et al. Ephrin-A5 and ephA5 interaction induces synaptogenesis during early hippocampal development. *PloS One*. (2010) 5:e12486. doi: 10.1371/journal.pone.0012486

55. Shearer TR, David LL, Anderson RS, Azuma M. Review of selenite cataract. *Curr Eye Res*. (1992) 11:357–69. doi: 10.3109/02713689209001789

56. Vrensen GF, de Wolf A. Calcium distribution in the human eye lens. *Ophthalmic Res*. (1996) 28 Suppl 2:78–85. doi: 10.1159/000267960

57. Gao J, Sun X, Martinez-Wittinghan FJ, Gong X, White TW, Mathias RT. Connections between connexins, calcium, and cataracts in the lens. *J Gen Physiol*. (2004) 124:289–300. doi: 10.1085/jgp.200409121

58. Maddala R, Nagendran T, de Ridder GG, Schey KL, Rao PV. L-type calcium channels play a critical role in maintaining lens transparency by regulating phosphorylation of aquaporin-0 and myosin light chain and expression of connexins. *PloS One*. (2013) 8:e64676. doi: 10.1371/journal.pone.0064676

59. Edfors F, Danielsson F, Hallstrom BM, Kall L, Lundberg E, Ponten F, et al. Gene-specific correlation of RNA and protein levels in human cells and tissues. *Mol Syst Biol*. (2016) 12:883. doi: 10.15252/msb.20167144

60. Silva GM, Vogel C. Quantifying gene expression: the importance of being subtle. *Mol Syst Biol*. (2016) 12:885. doi: 10.15252/msb.20167325

61. Gygi SP, Rochon Y, Franza BR, Aebersold R. Correlation between protein and mRNA abundance in yeast. *Mol Cell Biol*. (1999) 19:1720–30. doi: 10.1128/MCB.19.3.1720

62. Maier T, Guell M, Serrano L. Correlation of mRNA and protein in complex biological samples. *FEBS Lett*. (2009) 583:3966–73. doi: 10.1016/j.febslet.2009.10.036

frontiers | Frontiers in Ophthalmology

TYPE Review
PUBLISHED 19 July 2024
DOI 10.3389/fopht.2024.1434327

OPEN ACCESS

EDITED BY
Barbara Pierscionek,
Anglia Ruskin University, United Kingdom

REVIEWED BY
Eric C. Beyer,
The University of Chicago, United States
Yanzhong Hu,
Henan University, China

*CORRESPONDENCE
John I. Clark
clarkji@uw.edu

RECEIVED 17 May 2024
ACCEPTED 27 June 2024
PUBLISHED 19 July 2024

CITATION
Greiling TM, Clark JM and Clark JI (2024) The significance of growth shells in development of symmetry, transparency, and refraction of the human lens.
Front. Ophthalmol. 4:1434327.
doi: 10.3389/fopht.2024.1434327

The significance of growth shells in development of symmetry, transparency, and refraction of the human lens

Teri M. Greiling[1], Judy M. Clark[2] and John I. Clark[2,3]*

[1]Department of Dermatology, School of Medicine, Oregon Health & Science University, Portland, OR, United States, [2]Department of Biological Structure, University of Washington, Seattle, WA, United States, [3]Department of Biological Structure & Ophthalmology, School of Medicine, University of Washington, Seattle, WA, United States

Human visual function depends on the biological lens, a biconvex optical element formed by coordinated, synchronous generation of growth shells produced from ordered cells at the lens equator, the distal edge of the epithelium. Growth shells are comprised of straight (St) and S-shaped (SSh) lens fibers organized in highly symmetric, sinusoidal pattern which optimizes both the refractile, transparent structure and the unique microcirculation that regulates hydration and nutrition over the lifetime of an individual. The fiber cells are characterized by diversity in composition and age. All fiber cells remain interconnected in their growth shells throughout the life of the adult lens. As an optical element, cellular differentiation is constrained by the physical properties of light and its special development accounts for its characteristic symmetry, gradient of refractive index (GRIN), short range transparent order (SRO), and functional longevity. The complex sinusoidal structure is the basis for the lens microcirculation required for the establishment and maintenance of image formation.

KEYWORDS

lens development, growth shells, symmetry, transparency, refraction, microcirculation

Introduction

Symmetry, refraction and transparency are optical properties of the biological lens required for image formation in the human eye. Studies of lens growth and development across species report that exponential growth is continuous throughout life without loss or replacement of cells. A typical model for exponential growth is: $W = Wm\ e^{-k/A}$ (where "W" is dry weight, "Wm" = maximum weight, "k" is rate of growth, and "A" is postnatal age) (1, 2). Lens dimensions increase synchronously and continuously through the addition of symmetric growth shells. These growth shells form a complex sinusoidal structure that

forms the basis for the lens microcirculation and the formation and maintenance of transparency.

Brief summary of lens embryology

Lens placode

At ~3 weeks of gestation in humans, a small number of cells (50 to 100) swell, thicken, and form a lens placode at the edge of the neural plate (neuroectoderm). This lens placode is the origin of the cells that generate the refractile, symmetric, transparent lens (Figure 1). The cells in cranial placodes resemble neural progenitors that differentiate into sensory neurons characterized by cytoskeleton-enriched processes, forming dendrites and axons, extending from a cell body containing a nucleus and plentiful organelles to support cell-to-cell connectivity (3–7). In contrast to cells in the sensory placodes, cells in the lens placode swell, thicken and invaginate to form a fluid-filled lens vesicle superficial to the developing optic cup (future retina) (Figure 2) (3, 8–11).

Lens vesicle becomes the lens nucleus

Elongation of the posterior cells in the lens vesicle closest to the optic cup results in a solid cellular mass with the apical surfaces facing inward and the basal surfaces outward. The intercellular space is compressed, and these cells become the "primary" fibers of the "embryonic nucleus", supplied temporarily by the hyaloid artery, a branch of the ophthalmic artery to the optic cup (2, 3, 11, 12). The anterior cells of the lens vesicle distal to the optic cup are not induced to elongate and remain an epithelial monolayer covering the anterior surface of the embryonic nucleus, and the germinative center for future growth shells (Figure 2). (NOTE ABOUT TERMINOLOGY: Early studies suggested the lens was a single giant cell, with a pale yellow nucleus at the core, surrounded by a clear albuminoid cortex, like an egg. When the lens was confirmed to be a cellular tissue, use of the terminology "cortex" and "nucleus" continued to describe cells in the lens periphery and lens center, respectively (13, 14).

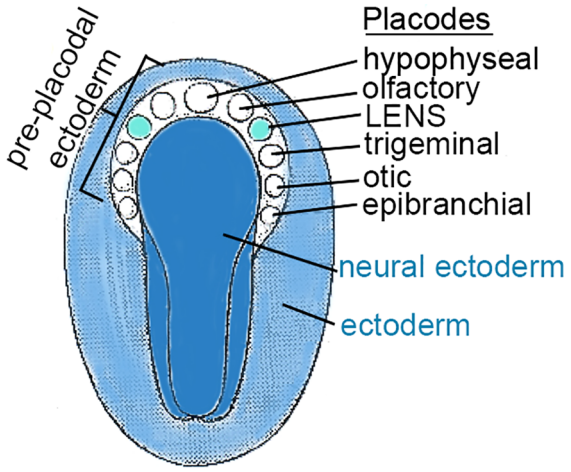

FIGURE 1
CRANIAL PLACODES in the TRILAMINAR EMBRYO. This figure represents a dorsal view of the ectodermal surface of a trilaminar embryo, prior to neural tube formation (K. Altdorfer, https://slideplayer.com/slide/12872844/). As the neural plate forms, a horseshoe shaped region peripheral to the cranial end of the neural ectoderm, called pre-placodal ectoderm (PPE), forms localized thickenings, "cranial placodes", for specialized structures including the lens. A number of cranial placodes are indicated by circles and labeled. The lens placode responds to signaling pathways involving FGF, BMP, Notch, Wnt, betacatenin, and others described elsewhere in the text.

First growth shells

The cells in the anterior epithelial layer can proliferate and migrate toward the equator of the developing lens, where they organize into ordered meridional rows. Synchronized elongation of the meridional cells, posteriorly and anteriorly, initiates the formation of a coordinated band of arc-shaped secondary cells, parallel to the optic axis. This band will become a growth shell at the peripheral lens cortex (Figure 3) (2, 9, 11, 15, 16). As the temporary vessels of the hyaloid vasculature regress, each growth shell becomes the developmental mechanism for adding symmetric layers of new "secondary" fibers that increase the size of the lens during formation of the visual system (Figure 2). New growth shells contain malleable, refractile, organelle-free secondary fibers that subsume previous shells surrounding the lens nucleus (17–20). New growth shells can adjust to the optical needs of a growing eye (16, 21).

It is important to emphasize that the coordinated addition of symmetric growth shells of secondary fibers expands the size of the lens and creates a biconvex, biological spheroid that functions as an optical element in the human eye (Figure 4) (11, 19, 22–24). The spheroid is defined by an equator separating the anterior from the posterior hemisphere. The radius of curvature of the surface anterior to the lens equator is ~10mm and the radius of curvature of the surface posterior to the equator is ~6mm (see Figure 2) (25, 26). With the growth of the visual system, the optical curvatures vary slightly as they adjust the focal length of the lens to the dimensions of the changing eye (16, 27). Throughout development of visual function, the optics of the growing lens are carefully synchronized with the establishment and maintenance of optical quality during the life of an individual (16, 22, 28). As a mechanism for the development of optics, growth shells are an unprecedented success.

Cellular specialization

In the absence of blood vessels, each growth shell develops symmetric layers of cellular fibers, containing condensed cytoplasmic proteins, largely crystallins and cytoskeleton, to increase the refractive index, and establish transparent short-range order necessary for focusing images on the retina (3, 22, 29). Growth shells can do more. Without blood vessels, structural specializations in the fibers of growth shells contribute to a symmetric circulatory system for fluid flow that regulates hydration, ionic homeostasis, and uniform distribution of nutrients, in support of dynamic growth to

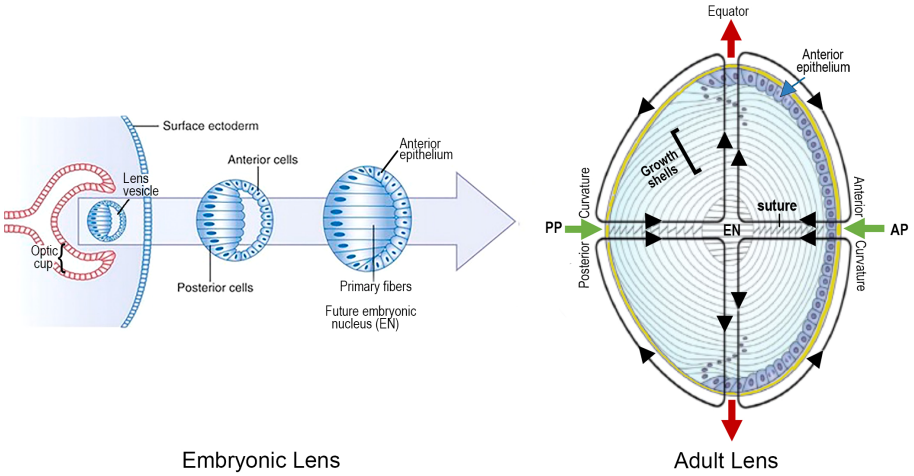

FIGURE 2
LENS DEVELOPMENT is a MULTISTEP PROCESS BEGINNING at ~3 to 4 WEEKS of EMBRYONIC AGE in the HUMAN: An optic cup extends toward the surface ectoderm from the neural tube, deep to the lens placode. The optic cup induces invagination of the lens placode, followed by its separation from the surface as the lens vesicle. Hyaloid vessels (not shown) supply the developing lens briefly, before regressing. Maturation of the lens vesicle is accompanied by lengthening of the posterior lens cells, adjacent to the optic cup, to form "primary lens fibers". These cells lose their nuclei and close the vesicle to create a solid cellular mass. In contrast, the anterior cells become an anterior epithelium that maintains its proliferative ability. Synchronous proliferation, migration and elongation of waves of epithelial cells generate "secondary" lens fibers that form growth shells. The growth shells surround the primary fibers of the "embryonic nucleus" (EN), to expand the size of the lens as the optics adjust to the growing eye. The entire lens mass develops within a thick basement membrane capsule (thick yellow line). An adult lens is refractile, transparent and biconvex, consisting of concentric layers of lens fiber growth shells. The functional viability and plasticity of an adult lens is prolonged through a unique microcirculation that nourishes, hydrates and maintains normal electrophysiological homeostasis as the lens grows and adjusts to the optical needs of the growing retina. The image on the right summarizes the microcirculation: Green arrows indicate the inflow of fluid at the anterior (AP) and posterior (PP) poles at the center of the anterior and posterior curvatures. Red arrows represent the fluid outflow at the equator. A number of growth factor pathways are essential for regulation during both embryogenesis and growth shell formation.

optimize the optics for the growing, changing visual system (Figure 2) (3, 7, 12, 30, 31). Without a functioning microcirculation, the lens cannot develop the symmetric gradient of refractive index (GRIN) and transparency required for image formation in the growing visual system (32–35). In fact, the lens might as well be a piece of glass or plastic. Instead, nature created a growth shell mechanism for the biological lens, that is unique in all of developmental biology (36, 37).

Growth shells

Structure: straight and S-shaped fibers

Each growth shell is comprised of two types of secondary fibers: straight (St) and S-shaped (SSh) fibers (Figure 4) (22, 36). St fibers are crescent-shaped, parallel to the visual axis, and attached to either the posterior or anterior pole (Figures 4A, B), where they become growth centers for the anterior or posterior hemispheres of the growth shell. Posterior to the lens equator, St fibers radiate away from the posterior pole, separated by 120 degrees (Figure 4B) and anterior to the lens equator, St fibers radiate away from the anterior pole separated by 120 degrees (Figure 4B). Notice that the tips of the elongating St fibers stop short of the opposite poles, ending at the tips of the Y suture (Figure 4B) (15, 22, 38).

The second type of lens fibers, the SSh fibers, fill in the growth shell (Figure 4A). SSh fibers are oriented along, and adjacent to, the St fibers (Figures 4A, B). SSh fibers have three parts: a straight middle segment, parallel to the St fiber, and two tips, curving away from the St fiber, to meet curved tips from other SSh fibers forming a pair of SSh fibers (Figure 4, red fibers). Anterior to the equator, where the curved tips meet, the anterior suture forms, and posterior to the equator, where the curved tips meet, the posterior suture forms. The sutures are formed where pairs of SSh fibers meet, anteriorly or posteriorly (Figure 4, red fibers). Because the tips curve to meet other SSh fibers, they appear as symmetric, sigmoid-shaped fiber cells when projected in 2-D (Figure 4D). The trigonometric function describing the SSh fiber is $f(x) = \arctan(x)$, which is the basis for the symmetry of a growth shell and accounts for the symmetric index of refraction, transparency, and the anterior and posterior curvatures of the lens.

Structure: sinusoidal networks form Y sutures

Where the curved tips meet anteriorly, the sutures are positioned in a "Y-shape" and posteriorly, the sutures form an "inverted Y-shape" (22). The anterior and posterior sutures are not aligned and are offset by 60 degrees. This is because of the sigmoid shape of SSh fibers (Figure 4D). Because the SSh tips curve in opposite directions away from their middle (Figure 4C), they are no longer in the same anterior/posterior plane (22, 37–39). Still, symmetry is maintained in normal development. The result is a continuous, interconnected sinusoidal network of fibers throughout the entire growth shell. Throughout the growth shell, SSh fibers in the posterior hemisphere connect directly with the fibers in the

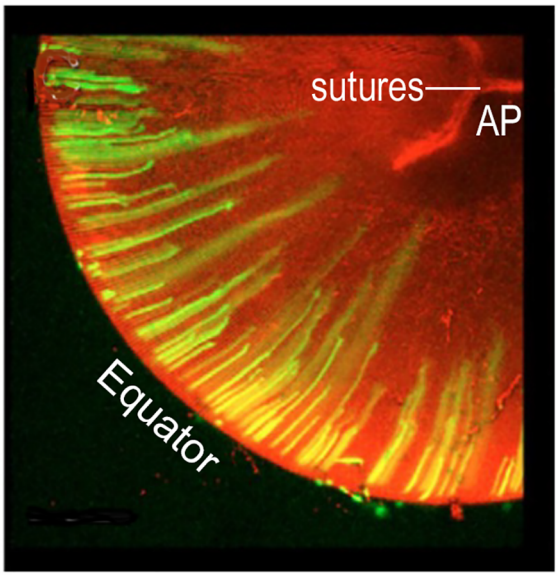

FIGURE 3
GROWTH SHELL FORMATION BEGINS WITH COORDINATED, PERIODIC ELONGATION of EPITHELIAL CELLS at the EQUATOR. Initially, anterior and posterior elongation of lens epithelial cells produces straight segments that form a discontinuous band around the lens periphery. In this image, green fluorescent protein, GFP, labels the cells elongating away from the equator. With continued elongation, a small number of these fibers will attach at the anterior (AP) or posterior (PP) poles separated radially by ~120 deg, (2.09 radians) (not shown). These are the straight (St) fibers that orient all other cells to fill in the growth shell. The optic axis (not shown) connects the AP with the PP. Elongation is synchronous and coordinated. In the figure, the longer fibers are believed to be forming one growth shell and the shorter fibers are beginning to elongate to form the next growth shell. Growth shells form concentric layers observed in intact lenses. (modified from Shi et al. (2009) J. Cell Sci. 122:1607-15).

anterior hemisphere. It is easy to understand how reactive oxygen species, advanced glycation end products, inflammatory agents, osmolytes, or other systemic stresses can disrupt the coordinated, symmetric elongation of fibers and alter the suture patterns.

Careful analysis of electron micrographs of developing lenses confirms that sutures in a growth shell are formed by the connections between differentiating SSh fibers (22, 36, 38–40). In contrast, the embryonic lens nucleus at the center of the adult lens has no sutures and consists of the primary fibers that elongated to obliterate the lens vesicle and establish the original cell mass (Figure 2). Subsequently the embryonic nucleus is overlain by secondary fibers (22, 38). As lens development continues, secondary fibers organize into isomorphic interconnected growth shells in a coordinated, synchronized process. The amount of curvature in the individual tips of the SSh fibers varies relative to position relative to where the pairs meet and establish a suture (Figure 4) (39). An unexpected result is the normal variability in the lengths of the SSh fibers connecting along the suture lines. The lengths oscillate with a regular, sinusoidal pattern, another indication of coordinated, synchronization of growth shell formation (Figure 5). It should be noted that the ends of secondary fibers expand and overlap at the sutures (39, 40). The overlap is part of the 3-D interconnected suture planes, extending from the surface into the embryonic nucleus. The suture can act as a channel carrying fluid containing ions, nutrients, soluble factors, and antioxidants that regulate and maintain symmetric structure (7, 22, 41, 42). When normal fiber differentiation is disrupted, the sutures appear abnormal (22).

Structure modeling

When first observed, the unusual organization of St and SSh fibers is a bit confusing and difficult to understand. To visualize the details and the overall structure of a growth shell during development, growth, and aging, Kuszak chose 2-D projections (22, 36–38, 40). Using computer aided drawings, he applied geometric methods known since Babylonian times for navigation of the earth (a spheroid) to study fiber patterns in growth shells of the biological lens (also a spheroid) (Figure 6) (22, 38). Combining computer aided drawing with thorough, careful scanning electron microscopy, Kuszak revealed new information about the assembly of symmetric growth shells in the lens. His results represent the synchronous differentiation that is the structural basis for both the lens optics and the symmetric microcirculation of fluid throughout the lens, in the absence of vasculature. When differentiating fibers in the growth shells are exposed to fluid influx through posterior and anterior sutures, they can respond to the fluid contents like ions, nutrients, and soluble factors controlling lens growth. The extensive connectivity between SSh fibers in the growth shells, specifically posterior and anterior to the equator, accounts for the symmetry of the posterior and anterior curvatures of the developing lens. The importance of two organizing centers at the posterior and anterior poles is very clear. While growth shells were recognized previously in lens research, the 3-D computer aided drawing provides much greater detail about their symmetric structure and, potentially, their functional significance. The collective interactions between component St and SSh fibers account for the connectivity and symmetry in the growth shells (22, 36, 37).

Function in microcirculation

Growth shell formation is not simply a space-filling exercise. It is the basis for a highly connected, complex cellular network, organized to provide maximal image quality to millions of photoreceptors in the visual system. Lens growth is carefully regulated to form a symmetric, refractive optical element that transmits light waves for the formation of accurate visual images (7, 31). It is often unappreciated that a lens consists of diverse populations of fibers constituted from various protein and membrane specializations completed at very different ages across the life of the organism. The process of growth shell formation is the foundation for the symmetry necessary to optimize optical quality, including the gradient of refractive index, GRIN, and transparency in a growing eye.

Many biologists accept the correlation between structure and function (11, 37, 40, 43, 44). As explained in the legend of Figure 6,

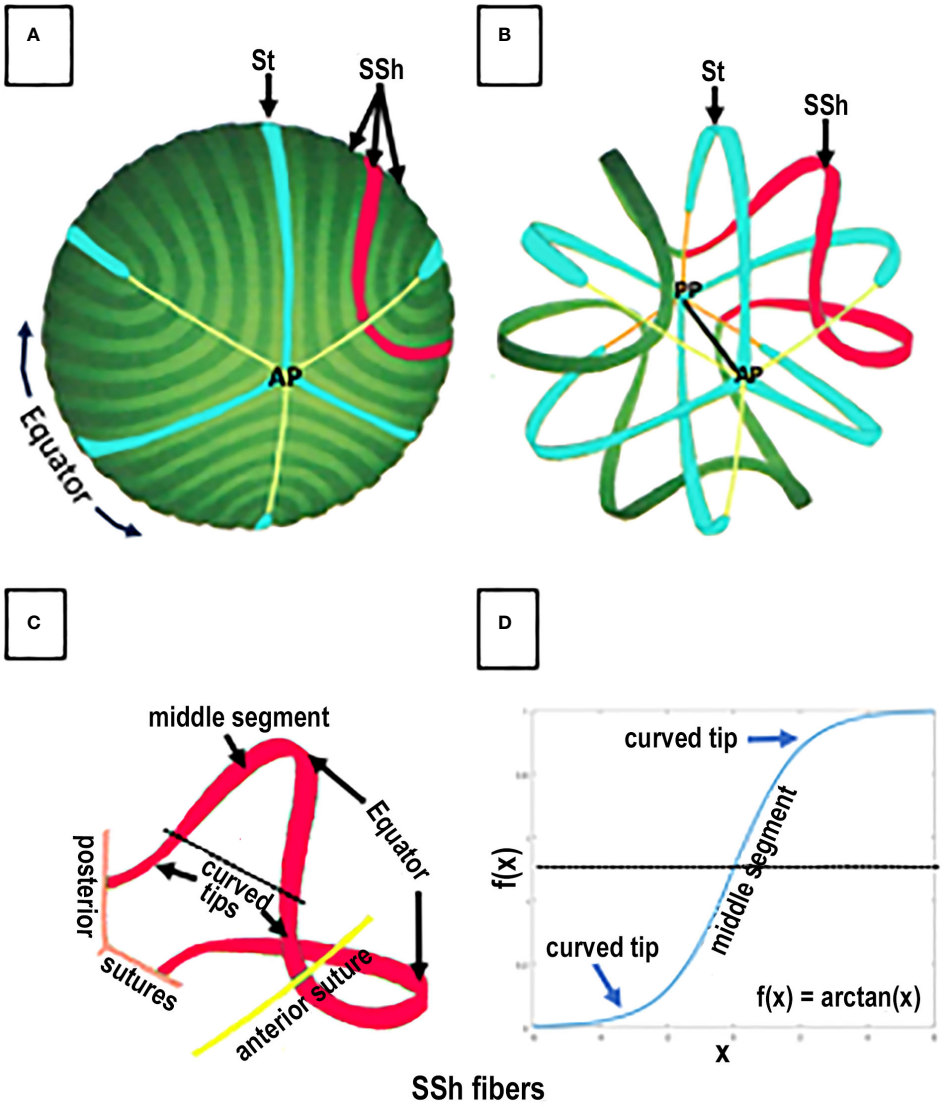

FIGURE 4
SPACE FILLING and FIBER ORGANIZATION in a GROWTH SHELL. An anterior view of the lens fibers in a typical GROWTH SHELL is shown in **(A)**. The dark and light green bands, each representing 20 individual fibers, are modeled from scanning electron micrographs of the growth shell surface. A few straight (St) fibers (turquoise) attaching at the anterior pole **(B)** are organizing centers for the many S-shaped (SSh) fibers (example highlighted in red) that fill-in the developing growth shell forming the anterior and posterior curvatures of each hemisphere in the biconvex lens **(A, B)**. Three sutures originating at the anterior (AP) poles are shown as thin yellow lines. Removing a number of fibers (in the figure) allows both the anterior (AP) and posterior (PP) poles to be seen **(B)** where three attachments for St fibers and three sutures (orange line) are shown. The optic axis (black line) connects the anterior and posterior poles. Space filling is a complex process of fiber assembly. During the start of fiber elongation, the middle segment of each SSh fiber is parallel to the optic axis (as in Figure 3). While one tip of an St fiber (blue) attaches at either the anterior (AP) or posterior (PP) pole, the other tip is the origin of the sutures **(A, B)** and the St fibers remain parallel to the optic axis. In contrast, the tips of elongating SSh fibers (red) do NOT attach at either pole. Instead, the elongating tips of SSh fibers curve away from the poles, toward the plane of the orienting St fibers, where they join the curved tips from a corresponding SSh fiber, to form a pair and create a suture (**B** red). For example, **(C)** represents a pair of red SSh fibers. An anterior tip curves to meet the curved tip of an SSh fiber (red) elongating from the opposite side of the St fiber and form anterior (yellow) suture. Note that the SSh fibers are not attached at a pole and each new connection between the SSh fibers lengthens the suture. Similarly, the posterior tip of the same red SSh fiber curves to meet the tip of a corresponding SSh fiber (not shown) to form and lengthen the posterior suture **(C)**. Both sutures are shown in the figure, but the suture is only formed when the tips of each SSh pair connect. In this way pairs of elongating SSh fibers fill in a GROWTH SHELL as they establish the sutures. (NOTE about TERMINOLOGY: The SSh fibers are described as having "opposite end curvature" by Kuszak because they curve away from the St fibers and the poles. In a 2-D projection of an SSh fiber **(D)**, each SSh fiber can be described as having a distinctive symmetric, sigmoid shape with the two curved tips extending away from a straight middle segment **(D)**. The sigmoid function is defined as f(x) = arctan(x). It is well established, but not widely appreciated, that when SSh fibers meet other SSh fibers, the pairs of SSh fibers fill in and form the posterior and the anterior surface of a GROWTH SHELL. When SSh pairs connect, the sutures are formed. Altered sutures are an indication of abnormal lens fiber differentiation and function.

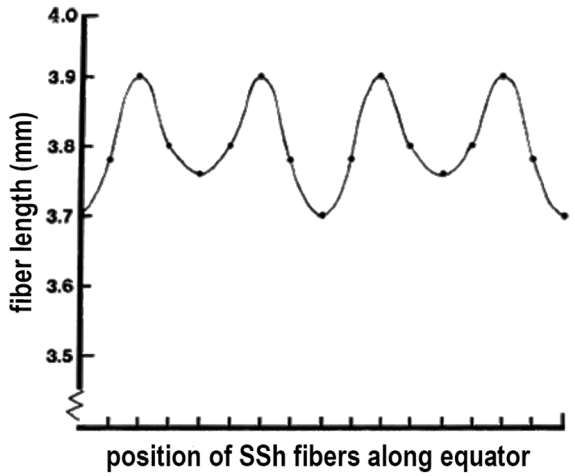

FIGURE 5
VARIATIONS in FIBER LENGTH in a GROWTH SHELL. Because the pairs of elongating SSh fibers intersect the equator, the length from the equator to fiber tip is expected to be unequal. When actually measured and plotted, an unexpected finding is that the variations in length are regular and periodic. Periodic oscillations in lens fiber lengths represent a sinusoidal pattern, reflecting the careful synchronization in growth shell formation.

the 2-D map of the growth shell introduces distortion at the anterior and posterior poles enlarging the dimension of the St fibers (Figure 6). Regardless of the distortion in a 2-D map, the regular, symmetric pattern of oscillating fibers posterior and anterior to the lens equator is expected to be critical for the growth shell mechanism of lens development (Figure 6) (22). The vertical clefts labeled "St" are the straight (St) fibers. Together with the sutures, St fibers are positioned every 60 degrees (1.05 radians) forming regular orienting centers for "waves" of SSh fibers (wavelength 120 degrees or 2.1 radians) above and below the equator (Figure 6). The periodic oscillations are oriented to the positions of the St fibers and sutures anteriorly and posteriorly. In the absence of vasculature, a simple hypothesis is that these sinusoidal oscillations are the structural basis for uniform symmetric fluid flow, known as microcirculation. If St fibers are spatial organizing centers for symmetric SSh fiber elongation, then the microcirculation can facilitate uniform fluid flow into the growth shells, anteriorly and posteriorly, to carry nutrients, growth factors, and protective molecules deep into the lens to organize and maintain function (Figure 2) (7, 42, 45). Recent studies report the importance of uniform, symmetric fluid flow in the control of hydration, ion homeostasis, refraction, and transparency in the biological lens (31, 32, 42, 45–47).

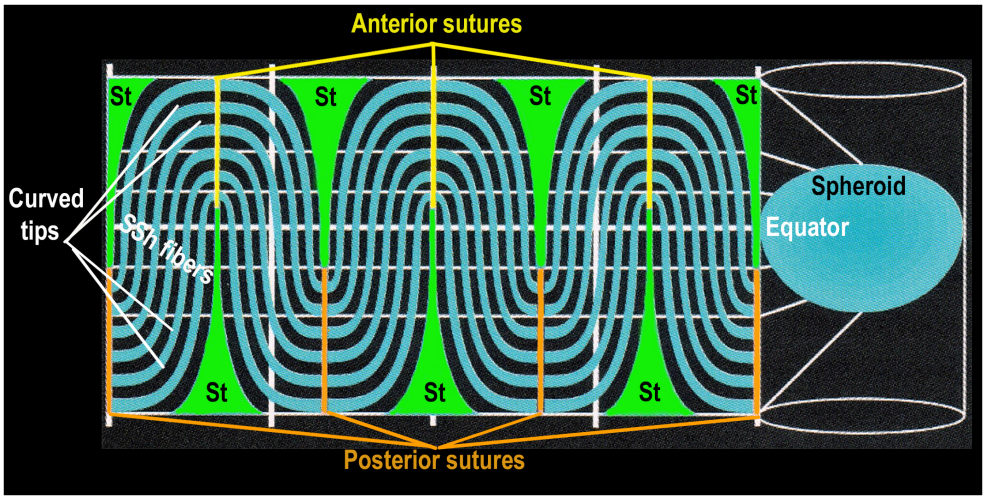

FIGURE 6
SYMMETRY is DETERMINED by TWO TYPES of DIFFERENTIATED FIBER CELLS. This is a 2-dimensional projection of a GROWTH SHELL. The computer aided drawing software generates a 2-D map by projecting the 3-D lens spheroid (growth shell) onto a 2-D cylindrical surface (Figure 6 right side). It is known as a projection because it simulates a bright light placed inside the spheroid so that any point (x,y,z) on the surface of the 3-D spheroid is projected to a point (x,y) on the surface of a cylindrical screen, surrounding the spheroid (Figure 6, right side). The lens equator is represented as a horizontal white line on the cylinder, between the anterior and posterior poles, represented as the open ends of the cylinder. When the computer "unfolds" the cylinder, the most obvious structural features of the 2-D projection of a typical growth shell are the symmetric oscillations of the SSh fibers (black and turquoise) above and below the equator (dashed white line), centered on the St fibers (green), positioned ~60 deg (1.05 radians) apart. The St fibers appear "cone shaped" with a wide base near the pole and a narrow tip at the beginning of each suture, near the equator. This distortion of St fiber dimensions is the result of an increase in scale near top and bottom of the cylinder, making the St fibers appear disproportionately large at the poles. (The St fibers are represented accurately in Figures 4A, B where their relative size is the same size as that observed *in situ* in electron micrographs of actual lenses.) In the 2-D map, the anterior sutures are represented by yellow vertical lines at the top of the 2-D map and the posterior sutures are orange vertical lines at the bottom of the 2-D map. Even though distorted, the St fibers extend from a pole to a tip of each suture near the equator (white line). The curved S-shaped (SSh) fibers form the oscillating pattern filling the growth shell. One curved tip of the SSh fibers connects to a posterior suture and the other curved tip connects to an anterior suture. The extensive fiber interconnections throughout the growth shell form a symmetric sinusoidal pattern essential for the organization of a symmetric microcirculation. This fiber symmetry is the basis for establishment and maintenance of refraction and transparency in an effective optical element in the human lens.

Few examples of symmetry in a biological tissue are more impressive than the experimental measurement of the loops of current flow in a biological lens (Figure 2) (46, 48–53). At the time it was reported, the significance of the symmetric current inflow and outflow in lens fiber symmetry and function was unrecognized (48, 53). Now, penetration of nutrients, metabolites, ions, and soluble factors is thought to occur through influx of fluid into the anterior and posterior suture planes, established by the alignment of sutures during the synchronized formation of growth shells (Figure 6). Fluid efflux occurs at the equator through an intercellular outflow pathway thought to be mediated by gap junctions. Hydrostatic pressure as high as 335 mm Hg centrally, falls to 0 mm Hg at the periphery, creating a pressure gradient for driving flow. The activity and localization of channels in the fiber membranes regulate flow and are critical for the optics of the visual system (7, 11, 31, 42, 45, 47, 50, 54).

There is much to learn from the lens about biological symmetry. The growth shell mechanism is a rare example of a developmental process for continuous formation and maintenance, year after year, of a highly symmetric refractile, transparent tissue, and the establishment of corresponding microcirculation. No other cellular tissue in the human compares with the transparent lens for studies of complex molecular and cellular function over a lifetime. Lens structure and function for image formation is intimately linked to symmetry, the gradient of refractive index (GRIN), and transparent short range order. In the eye, the dynamics of collective, often complex, interactions, at the molecular and cellular levels are accessible to modern, non-invasive methods of research in living individuals.

The current hypothesis that the microcirculation is a primary factor in the formation of the biconvex, human lens, places an emphasis directly on the significance of fiber membranes (45, 55–58). The 1000-fold elongation of the SSh secondary lens fibers is achieved through a dramatic expansion of the membrane surface area (22, 38, 59–63) accompanied by an elaborate reorganization of the lens fiber cytoskeleton (11, 60, 61, 64–69). It is well established that lens fiber membranes are specialized to facilitate fluid flow throughout the decreased intercellular spaces. During the formation of a growth shell the cytoskeleton condenses at the periphery of the hexagonal fibers, as a dramatic increase in the proportion of membrane cholesterol accompanies the increase in fiber membranes, and the intercellular spaces are narrowed (11, 70–75). Intuitively, a decrease in the extracellular space might be expected to increase resistance to fluid flow through the lens microcirculation. Studies of microfluidity suggest the opposite effect (76–79). High cholesterol can stabilize membranes, increase hydrophobicity to decrease surface tension, and help move fluids through the microcirculation of the lens (80). The complexity and heterogeneity of fiber membranes and their microenvironment make the study of microcirculation a challenge. While discussion of the origins of the microcirculation in the growth shell mechanism is beyond the scope of this article, growth shells are incredibly important as a foundation for development of the lens as an optical element in the human eye (58).

When the space between cell membranes decreases, the resistance to turbulent flow can decrease to favor laminar flow, increasing microfluidity (77, 79). The microfluidity between membranes can be enhanced further by an increase in the area of hydrophobic surface, reducing interactions between aqueous fluid and charged membrane phospholipids (80). Increased membrane cholesterol resists oxygen permeability favoring elimination of intracellular organelles (81, 82) and stabilizes the elongated fiber shape, the condensation of the cytoskeleton at the cell periphery, the establishment of transparent short range order, phospholipid surface projections, and a decrease the intercellular spaces (83–85). A dynamic cytoskeleton compresses and stabilizes the cell membrane and positions membrane channels, cell adhesion molecules, and connexins along the cell surface. The constructive effects of high cholesterol levels in fiber membrane can contribute to lens microcirculation and improve symmetry, transparency, and GRIN in the lens as new symmetric growth shells are added (82, 84–86).

When growth shells are added at the lens periphery, they seem most responsive to constituents of the microcirculation. There appears to be a narrow band of growth shells forming a supranuclear region between the lens nucleus and cortex, where plasticity permits fiber reorganization (17, 87–90). Both electrophysiology and light scattering results indicate a subtle change several layers deep to the surface, consistent with an electrophysiological syncytium, and/or a network of interacting proteins and membranes (16, 17, 27, 90–92). Apparently, supranuclear fibers in new shells share plasticity to remodel the surface curvatures and adjust the biconvex lens to changes in optical requirements as the eye grows. The plasticity that accounts for variations in light scattering appears be sensitive to intracellular modifications associated with clinical conditions specific to light scattering phenotypes, including myotonic dystrophy, genetic mutations, Down Syndrome and Alzheimer's Disease (89, 93–95).

Plasticity of growth shells

Plasticity of the lens growth shells allows for subtle improvements in the optical properties as eyes grow from youth to adult (16, 96, 97). Developmentally, dramatic plasticity is demonstrated in lens inversion experiments (98, 99). After removal from the optic cup, a developing lens can be rotated 180 degrees, and then replaced in the eye so that the epithelium now faces the vitreous (posteriorly) instead of the aqueous (anteriorly). After replacement, repolarization occurs so that the (now) posterior epithelium elongates to fill-in the lens vesicle and a "cap" of new epithelium forms anteriorly facing the cornea. The results represent an extraordinary malleability that allows the newest growth shells to respond to factors carried through the microcirculation from the anterior aqueous and/or posterior vitreous. In a separate example of plasticity, a second lens mass develops in a mutant zebrafish, apparently because of two growth centers (100). One of the most extreme examples of lens plasticity during normal development is the lens of the "four-eyed" fish, Anablebs anablebs (101–103). The two growth centers in the growth shells account for the formation of a pyriform-shaped lens that focuses light waves simultaneously, from two separate environments: air and water, onto separate regions of the same retina. In a 2-D map of a growth shell, individual SSh fibers are exposed to both the posterior and anterior environments by an influx of fluid carried through their posterior or anterior sutures (Figure 6). Lens fiber plasticity permits the posterior

and/or anterior curvatures to adjust refraction in response to either environment (posterior or anterior).

Each growth shell generates symmetric posterior and anterior convexities, with different radii of curvature, to adjust lens optics for precise focusing of images on a growing, expanding retina with minimal spherical aberration. Generation of two biconvex surfaces in the biological lens is achieved when posterior and anterior growth centers are established by the St fibers. Orientation of the SSh fibers, connecting at the sutures posteriorly and anteriorly, forms two biconvex surfaces that optimize the optics of the visual system. The number and orientation of lens fibers need to adjust the size of each new growth shell with age, to conform to the principles of image formation in the changing human eye (19, 22, 104).

Regulation of growth shell formation

Growth shell development is regulated largely by growth factor and signaling pathways involving FGF, BMP, IGF, TGFbeta, Notch, wnt, PDGF, and others (2, 3, 10, 23, 57, 105–112). Numerous studies support the hypothesis that concentration gradients of FGF and BMP are central to the regulation of elongation and maturation of lens fibers (14, 113). These are reviewed in detail elsewhere (10, 14). Both the levels of the growth factors in aqueous and vitreous and the locations of their receptors in the lens regulate formation of the symmetric growth shells (108, 111, 114, 115). The impact of these regulatory pathways on lens growth and differentiation is so important that there is systematic redundancy, so that IGF, EGF, TGFbeta, and other soluble factors contribute to formation of a growth shell. Redundancy benefits and protects the effectiveness of the growth shell mechanism in the formation of symmetric, concentric spherical layers. Given the complexities of the relationships between growth factors, signaling pathways and, gene regulatory networks on fiber differentiation, the importance of the synchronization of growth shell formation is sometimes overlooked. Bursts of transcription are a direct measure of the synchronized fiber differentiation in the coordinated development of the growth shells, and are necessary for generation of symmetry (10, 32, 116–118). The pulsatile activity of PDGF and the discovery of PDGF receptor in distal regions of lens epithelium where synchronicity is initiated, altered our understanding of the regulation of periodic symmetry in the biological lens (106, 119–123). Correlation of the cellular distributions of growth factors and receptors will clarify the link between growth factor activity and coordination of the remarkable geometric patterns (Figure 6) accounting for symmetry, GRIN, and transparent short range order in the biological lens.

Research continues to demonstrate the importance of synchronization of growth factors in regulating development and maintenance of symmetry, GRIN, and transparency in the biological lens (2, 10, 105, 106, 109–113, 119–122, 124–126). Differentiation of symmetric, concentric layers of elongated, denucleated, transparent, refractile fiber cells in the lens spheroid is complex and represents unprecedented spatio-temporal regulation in biology (11, 22, 37, 38, 121). Although the lens is ordered at all scales of structure, from molecules to the whole tissue, the "crystalline" biological lens is not crystalline. It is formed by concentric shells of symmetric lens fibers (Figures 2, 4, 6). Complex, synergistic, and cooperative, often overlapping, signaling pathways promote structural and functional longevity of lens function (11, 24) Current research needs to consider interactions within networks of growth factors in the regular and coordinated assembly of new growth shells in the mechanism of lens development.

Discussion

It is important to realize that the radius of curvature of a growth shell is symmetric both anteriorly and posteriorly. The precise dimensions are carefully regulated to maximize the optical function of the biconvex, biological lens. The St fibers attached at the posterior and anterior poles form two spatial organizing centers, separated by the equator, in each growth shell (Figures 4, 6). Posterior to the lens equator, the St fibers orient the SSh fibers to form a posterior convexity, and anterior to the equator the St fibers orient SSh fibers to form an anterior convexity. The focal point of a biconvex lens depends on the symmetric gradient in the index of refraction, and the curvature of both the anterior and posterior surfaces. While formed by secondary fibers in the peripheral cortex, each GROWTH SHELL is dynamic and plastic. The surface curvatures of the posterior and anterior hemispheres can adjust to the changing optical requirements of image formation during development and growth of the eye (97, 127, 128). As the lens grows, the newest growth shells (Figures 3, 4) are added between the elongating cortical fibers and the deeper established growth shells. Between the deep cortex and the superficial nucleus, new growth shells form a thin layer that can respond and continuously modify the optics of the growing eye. In contrast, fibers in older, deeper growth shells become highly interconnected and stabilized in the nucleus, in what is known as an electrophysiological "syncytium" (17).

It should be emphasized that not all light scattering is the same. Light scattering depends on wavelength, intensity and scattering angle, the index of refraction, the size, shape and concentration of scatterers, their interactions, symmetry, order, and other biophysical parameters including pressure, temperature, and concentration (129–133). The diversity of differentiating cells and fibers generated in growth shells can be evaluated *in vivo* as variations in fiber structure optimize image formation in the human visual system (130, 134–136). The diversity of fibers and the plasticity of growth shells seem to account for the variability observed in the zones of discontinuity (Figure 7) (11, 137, 138). Plasticity can account for sensitivity of differentiating fibers to environmental factors including glucose levels, toxic substances, or osmolytes penetrating the lens through the microcirculation to reach the differentiating lens fibers.

When the layered structure of the lens was first observed *in vivo* by Gullstrand, the inventor of the slit lamp, variations in scattered

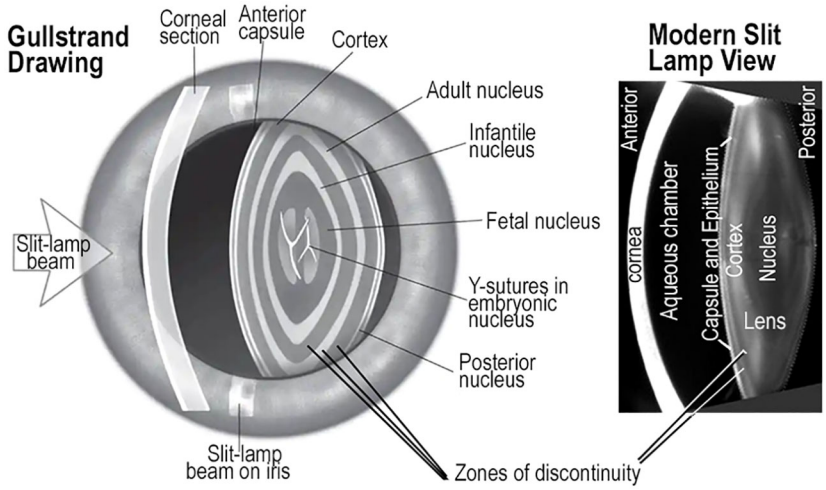

FIGURE 7
ZONES of DISCONTINUITY and GROWTH SHELLS. Drawings made by Gullstrand of the human eye resemble a photograph from a modern slit lamp. Both show oscillations in light scattering known as zones of discontinuity. In both images, the variations in light scattering appear as concentric, symmetric layers in the lens, and are consistent with the growth shell mechanism of lens development and aging. The Gullstrand drawing appears to have much more prominent scattering from the zones of discontinuity than the modern photo image. The main point is that zones of discontinuity in the refractile, transparent lens of living patients are concentric and symmetric, consistent with growth shell structure. These images confirm the value of direct analysis of lens structure and function in living individuals across a broad range of ages using modern optical technology.

light established the basis for understanding the concentric growth shells. Their symmetry, refraction, and transparency could be observed directly in the human lens (Figure 7) (139). Small fluctuations in refractive index gradient and non-random scattering are associated with normal growth and development resulting from modified apoptosis, mitophagy, or autophagocytosis (136, 140–142). These mechanisms are commonly associated with cell death and cell replacement, not prolongation of molecular and cellular longevity, typical of the biological lens (143, 144). In a healthy eye, small fluctuations in the refractive index that produce light scattering from zones of discontinuity, do not impair vision (145) (Figure 7). Detailed computer aided drawings of differentiating lens fibers in normal growth shells can explain images commonly recorded in slit lamp examinations (22, 36–38, 41, 65). In a growth shell, decreasing oxidative metabolism results in the loss of organelles and the reduction in reactive oxygen species to improve transparency during growth of the lens. In fact, all primary and secondary fibers formed in a lens are retained for a lifetime. Lens fiber differentiation involves unique protective mechanisms including antioxidants, microcirculation, cytoskeletal stability, post-translational modification (PTM), and high levels of small heat shock proteins (sHSP) to enhance optical function (symmetry, GRIN, and transparency) of a lens (11). Failure to preserve the viability of any fiber is presumed to lead to pathology. Typical lens fiber differentiation, occurring during lens growth, seeks to decrease the dimensions of irregularities in the refractive index, "n", well below micron sizes. The subtle light scattering from tiny, often temporal, spatial fluctuations in "n", is known as Rayleigh scattering. These tiny fluctuations in "n" are not readily observed histologically, even in electron micrographs (130, 133, 146, 147). While changes in Rayleigh scattering can be a measure of differentiation of normal transparent subcellular structure in living animals, it can also be predictive of the progressive loss of transparency under unfavorable conditions of molecular and cellular aging (11, 91, 92, 130–132, 148, 149).

Conclusion

The human lens is not glass, but could be, if nature chose a developmental mechanism different than growth shells. Other ectodermal derivatives in the integument are dehydrated, including hair, nails, feathers, and claws. Dehydration of the fibers of the developed lens is all that is needed to produce a solid, glass-like lens, similar to a camera lens. For example, when a lens is removed from an eye (rodent, cat, dog, zebrafish, other) and allowed to dehydrate slowly, in a controlled laboratory environment, a biological lens can transition into a transparent, refractile solid. Instead, nature chose to (bio)engineer a highly symmetric and interconnected growth shell system of lens fibers, supported by an unusual microcirculation that limits oxidative metabolism and conserves hydration, physiological homeostasis, and uniform nourishment in a cellular lens. In a biological lens, optical function is prolonged in the visual system over a lifetime (7, 30, 31, 47, 56). A relevant comparison can be made between hydration in a lens and the tardigrade, an extremotolerant organism known to be able to maintain its cellular structure under conditions of complete dehydration (anhydrobiosis) (150). Similarly, the fiber structure of a lens must be maintained under conditions of severe dehydration. While there are advantages to conducting research on biological lenses from a materials science perspective, human vision demands more than a piece of glass or plastic. The symmetry of the growth shells not only prolongs the functional life of a lens, it supports dynamic modifications that optimize the optics of the visual system. The growth shell microcirculation is a major physiological innovation. The vascular system in non-lens tissue

consists of lymphatics and blood vessels that supply oxygen and nutrients to cells. The vasculature modulates cell and tissue fluid homeostasis. In a lens, oxygen is toxic and lymphatics carry immune cells that can recognize modified, aging cells, like the lens fibers, as abnormal and destroy them. In growth shells, the microcirculation is a natural alternative to the typical systemic vasculature. The growth shell microcirculation regulates hydration and provides nutrition in a protective environment of antioxidants and stress response proteins, to optimize cellular, molecular, and functional longevity of refractile, transparent lens fibers.

Coordinated, synchronous differentiation of lens fibers in growth shells is necessary for the optics of the human eye to adjust as the visual system grows and ages. Even though multiple levels of protection (including post-translation modifications, anti-oxidants, and small heat shock proteins) prolong the biological lens for an unusually long functional life, tiny failures at the molecular level and multifactorial, submicroscopic events can slowly and progressively accumulate and disrupt symmetry and order until a "tipping" point is reached (11, 151–154). The greatest risk factor for loss of transparency is aging of molecular and cellular constituents (11, 24). Membrane specializations (projections, protrusions and connections) between fiber cells change with normal lens development and are associated with formation of the symmetric growth shells. Specific surface features characterizing the boundary of the organelle free zone (OFZ), are not well defined in a normal lens. In abnormal lenses, where fiber differentiation is disrupted, the symmetric relationship(s) between straight and S-shaped fibers in growth shells is distorted, and result in an asymmetric pattern of sutures. (22,37,38). Advances in imaging and analytical sciences suggest that novel integrated research on lens symmetry, GRIN, and transparency in growth shells, will improve our knowledge of natural protection for the optics of individuals at risk for lens opacification that accounts for more than 50% of vision impairment globally (58, 130, 133, 155–157).

Author contributions

TG: Conceptualization, Data curation, Formal analysis, Validation, Visualization, Writing – review & editing. JC: Conceptualization, Formal analysis, Validation, Visualization, Writing – review & editing, Software, Supervision, Writing – original draft. JC: Conceptualization, Formal analysis, Software, Supervision, Validation, Visualization, Writing – original draft, Writing – review & editing, Data curation, Funding acquisition, Investigation, Methodology, Project administration, Resources.

Funding

The author(s) declare that no financial support was received for the research, authorship, and/or publication of this article.

Acknowledgments

This article is dedicated to M. Delaye, PhD and B. Brewitt, PhD, two scientists who made significant contributions to lens research prior to their death early in their careers. Dr. Delaye published on the interpretation of dynamic light scattering from the lens which is still relevant today. Dr. Brewitt discovered pulses of PDGF enhanced lens transparency in cultured lenses. At the time, PDGF was thought to be tissue specific for vasculature (mesodermal derivatives) and her results were published in SCIENCE.

Conflict of interest

The authors declare that the research was conducted in the absence of any commercial or financial relationships that could be construed as a potential conflict of interest.

Publisher's note

References

1. Augusteyn RC. Growth of the eye lens: I. Weight accumulation in multiple species. *Mol Vis*. (2014) 20:410–26.

2. Bassnett S, Sikic H. The lens growth process. *Prog Retin Eye Res*. (2017) 60:181–200. doi: 10.1016/j.preteyeres.2017.04.001

3. Cvekl A, Ashery-Padan R. The cellular and molecular mechanisms of vertebrate lens development. *Development*. (2014) 141:4432–47. doi: 10.1242/dev.107953

4. Sjodal M, Edlund T, Gunhaga L. Time of exposure to BMP signals plays a key role in the specification of the olfactory and lens placodes ex vivo. *Dev Cell*. (2007) 13:141–9. doi: 10.1016/j.devcel.2007.04.020

5. Grocott T, Tambalo M, Streit A. The peripheral sensory nervous system in the vertebrate head: a gene regulatory perspective. *Dev Biol*. (2012) 370:3–23. doi: 10.1016/j.ydbio.2012.06.028

6. Schlosser G. Vertebrate cranial placodes as evolutionary innovations–the ancestor's tale. *Curr Top Dev Biol*. (2015) 111:235–300. doi: 10.1016/bs.ctdb.2014.11.008

7. Giannone AA, Li L, Sellitto C, White TW. Physiological mechanisms regulating lens transport. *Front Physiol*. (2021) 12:818649. doi: 10.3389/fphys.2021.818649

8. Greiling TM, Clark JI. New insights into the mechanism of lens development using zebra fish. *Int Rev Cell Mol Biol*. (2012) 296:1–61. doi: 10.1016/B978-0-12-394307-1.00001-1

9. Cvekl A, McGreal R, Liu W. Lens development and crystallin gene expression. *Prog Mol Biol Transl Sci*. (2015) 134:129–67. doi: 10.1016/bs.pmbts.2015.05.001

10. Cvekl A, Zhang X. Signaling and gene regulatory networks in mammalian lens development. *Trends Genet*. (2017) 33:677–702. doi: 10.1016/j.tig.2017.08.001

11. Quinlan RA, Clark JI. Insights into the biochemical and biophysical mechanisms mediating the longevity of the transparent optics of the eye lens. *J Biol Chem*. (2022) 298:102537. doi: 10.1016/j.jbc.2022.102537

12. Beebe DC. Maintaining transparency: a review of the developmental physiology and pathophysiology of two avascular tissues. *Semin Cell Dev Biol*. (2008) 19:125–33. doi: 10.1016/j.semcdb.2007.08.014

13. Brown NP, Brown AJ. *Lens Disorders: A Clinical Manual of Cataract Diagnosis*. Oxford, U.K: Butterworth-Heinemann Ltd (1996).

14. Lovicu FJ, Robinson ML. *Development of the Ocular Lens*. Cambridge, U.K: Cambridge University Press (2004). doi: 10.1017/CBO9780511529825

15. Nowak RB, Fischer RS, Zoltoski RK, Kuszak JR, Fowler VM. Tropomodulin1 is required for membrane skeleton organization and hexagonal geometry of fiber cells in the mouse lens. *J Cell Biol*. (2009) 186:915–28. doi: 10.1083/jcb.200905065

16. Brown NP, Koretz JF, Bron AJ. The development and maintenance of emmetropia. *Eye (Lond)*. (1999) 13:83–92. doi: 10.1038/eye.1999.16

17. Shi Y, Barton K, Maria A, Petrash JM, Shiels A, Bassnett S. The stratified syncytium of the vertebrate lens. *J Cell Sci*. (2009) 122:1607–15. doi: 10.1242/jcs.045203

18. Sikic H, Shi Y, Lubura S, Bassnett S. A full lifespan model of vertebrate lens growth. *R Soc Open Sci*. (2017) 4:160695. doi: 10.1098/rsos.160695

19. Oyster CW. *The Human Eye*. Sunderland, MA, USA: Sinauer Associates (1999).

20. Worgul BV. "Lens". In: Jakobiec FA, editor. *Ocular anatomy, embryology and teratology*. Philadelphia: Harper & Row (1982). p. 355–89.

21. Muralidharan G, Martinez-Enriquez E, Birkenfeld J, Velasco-Ocana M, Perez-Merino P, Marcos S. Morphological changes of human crystalline lens in myopia. *BioMed Opt Express*. (2019) 10:6084–95. doi: 10.1364/BOE.10.006084

22. Kuszak JR, Zoltoski RK, Tiedemann CE. Development of lens sutures. *Int J Dev Biol*. (2004) 48:889–902. doi: 10.1387/ijdb.041880jk

23. Cheng C, Wang K, Hoshino M, Uesugi K, Yagi N, Pierscionek B. EphA2 affects development of the eye lens nucleus and the gradient of refractive index. *Invest Ophthalmol Vis Sci*. (2022) 63:2. doi: 10.1167/iovs.63.1.2

24. Clark JI. Biology of the transparent lens and changes with age. In: Albert JMD, Azar D, Young LH, editors. *Albert and Jakobiec's Principles and Practice of Ophthalmology*. Springer, Cham, Switzerland (2021). p. 188–201.

25. Schachar RA. Central surface curvatures of postmortem- extracted intact human crystalline lenses: implications for understanding the mechanism of accommodation. *Ophthalmology*. (2004) 111:1699–704. doi: 10.1016/S0161-6420(04)00669-4

26. Brown N. The change in lens curvature with age. *Exp Eye Res*. (1974) 19:175–83. doi: 10.1016/0014-4835(74)90034-7

27. Marcos S, Martinez-Enriquez E, Vinas M, Castro A, Dorronsoro C, Bang SP, et al. Simulating outcomes of cataract surgery: important advances in ophthalmology. *Annu Rev BioMed Eng*. (2021) 23:277–306. doi: 10.1146/annurev-bioeng-082420-035827

28. Marcos S, Werner JS, Burns SA, Merigan WH, Artal P, Atchison DA, et al. Vision science and adaptive optics, the state of the field. *Vision Res*. (2017) 132:3–33. doi: 10.1016/j.visres.2017.01.006

29. Cheng C, Fowler VM, Gong X. EphA2 and ephrin-A5 are not a receptor-ligand pair in the ocular lens. *Exp Eye Res*. (2017) 162:9–17. doi: 10.1016/j.exer.2017.06.016

30. Bassnett S, Shi Y, Vrensen GF. Biological glass: structural determinants of eye lens transparency. *Philos Trans R Soc Lond B Biol Sci*. (2011) 366:1250–64. doi: 10.1098/rstb.2010.0302

31. Donaldson PJ, Grey AC, Maceo Heilman B, Lim JC, Vaghefi E. The physiological optics of the lens. *Prog Retin Eye Res*. (2017) 56:e1–e24. doi: 10.1016/j.preteyeres.2016.09.002

32. Pierscionek BK, Regini JW. The gradient index lens of the eye: an opto-biological synchrony. *Prog Retin Eye Res*. (2012) 31:332–49. doi: 10.1016/j.preteyeres.2012.03.001

33. Wang K, Pu Y, Chen L, Hoshino M, Uesugi K, Yagi N, et al. Optical development in the zebrafish eye lens. *FASEB J*. (2020) 34:5552–62. doi: 10.1096/fj.201902607R

34. Cheng C, Nowak RB, Gao J, Sun X, Biswas SK, Lo WK, et al. Lens ion homeostasis relies on the assembly and/or stability of large connexin 46 gap junction plaques on the broad sides of differentiating fiber cells. *Am J Physiol Cell Physiol*. (2015) 308:C835–47. doi: 10.1152/ajpcell.00372.2014

35. Cheng C, Parreno J, Nowak RB, Biswas SK, Wang K, Hoshino M, et al. Age-related changes in eye lens biomechanics, morphology, refractive index and transparency. *Aging (Albany NY)*. (2019) 11:12497–531. doi: 10.18632/aging.v11i24

36. Kuszak JR, Mazurkiewicz M, Jison L, Madurski A, Ngando A, Zoltoski RK. Quantitative analysis of animal model lens anatomy: accommodative range is related to fiber structure and organization. *Vet Ophthalmol*. (2006) 9:266–80. doi: 10.1111/j.1463-5224.2006.00506.x

37. Kuszak JR, Mazurkiewicz M, Zoltoski R. Computer modeling of secondary fiber development and growth: I. Nonprimate lenses. *Mol Vis*. (2006) 12:251–70.

38. Kuszak JR, Zoltoski RK, Sivertson C. Fibre cell organization in crystalline lenses. *Exp Eye Res*. (2004) 78:673–87. doi: 10.1016/j.exer.2003.09.016

39. Kuszak JR, Bertram BA, Macsai MS, Rae JL. Sutures of the crystalline lens: a review. *Scan Electron Microsc*. (1984) 3:1369–78.

40. Kuszak JR. The ultrastructure of epithelial and fiber cells in the crystalline lens. *Int Rev Cytol*. (1995) 163:305–50. doi: 10.1016/S0074-7696(08)62213-5

41. Kuszak JR, Novak LA, Brown HG. An ultrastructural analysis of the epithelial-fiber interface (EFI) in primate lenses. *Exp Eye Res*. (1995) 61:579–97. doi: 10.1016/S0014-4835(05)80052-1

42. Donaldson PJ, Petrova RS, Nair N, Chen Y, Schey KL. Regulation of water flow in the ocular lens: new roles for aquaporins. *J Physiol*. (2024) 602:3041–56. doi: 10.1113/JP284102

43. Huxley JS. *Problems of Relative Growth*. New York, N.Y: Dover Publications (1972).

44. Thompson DW. *On Growth and Form. 2nd*. United Kingdom: Cambridge University Press (1917). doi: 10.5962/bhl.title.11332

45. Donaldson PJ, Chen Y, Petrova RS, Grey AC, Lim JC. Regulation of lens water content: Effects on the physiological optics of the lens. *Prog Retin Eye Res*. (2023) 95:101152. doi: 10.1016/j.preteyeres.2022.101152

46. Shahidullah M, Mandal A, Mathias RT, Gao J, Krizaj D, Redmon S, et al. TRPV1 activation stimulates NKCC1 and increases hydrostatic pressure in the mouse lens. *Am J Physiol Cell Physiol*. (2020) 318:C969–80. doi: 10.1152/ajpcell.00391.2019

47. Petrova RS, Nair N, Bavana N, Chen Y, Schey KL, Donaldson PJ. Modulation of membrane trafficking of AQP5 in the lens in response to changes in zonular tension is mediated by the mechanosensitive channel TRPV1. *Int J Mol Sci*. (2023) 24(10):9080. doi: 10.3390/ijms24109080

48. Robinson KR, Patterson JW. Localization of steady currents in the lens. *Curr Eye Res*. (1982) 2:843–7. doi: 10.3109/02713688209020020

49. Gao J, Sun X, Moore LC, White TW, Brink PR, Mathias RT. Lens intracellular hydrostatic pressure is generated by the circulation of sodium and modulated by gap junction coupling. *J Gen Physiol*. (2011) 137:507–20. doi: 10.1085/jgp.201010538

50. Gao J, Sun X, White TW, Delamere NA, Mathias RT. Feedback regulation of intracellular hydrostatic pressure in surface cells of the lens. *Biophys J*. (2015) 109:1830–9. doi: 10.1016/j.bpj.2015.09.018

51. Gao J, Wang H, Sun X, Varadaraj K, Li L, White TW, et al. The effects of age on lens transport. *Invest Ophthalmol Vis Sci*. (2013) 54:7174–87. doi: 10.1167/iovs.13-12593

52. Candia OA, Mathias R, Gerometta R. Fluid circulation determined in the isolated bovine lens. *Invest Ophthalmol Vis Sci*. (2012) 53:7087–96. doi: 10.1167/iovs.12-10295

53. Patterson JW. Characterization of the equatorial current of the lens. *Ophthalmic Res*. (1988) 20:139–42. doi: 10.1159/000266570

54. Chen Y, Petrova RS, Qiu C, Donaldson PJ. Intracellular hydrostatic pressure regulation in the bovine lens: a role in the regulation of lens optics? *Am J Physiol Regul Integr Comp Physiol*. (2022) 322:R263–79. doi: 10.1152/ajpregu.00309.2021

55. Borchman D, Yappert MC. Lipids and the ocular lens. *J Lipid Res*. (2010) 51:2473–88. doi: 10.1194/jlr.R004119

56. Donaldson PJ, Musil LS, Mathias RT. Point: A critical appraisal of the lens circulation model–an experimental paradigm for understanding the maintenance of lens transparency? *Invest Ophthalmol Vis Sci*. (2010) 51:2303–6. doi: 10.1167/iovs.10-5350

57. Delamere NA, Shahidullah M, Mathias RT, Gao J, Sun X, Sellitto C, et al. Signaling between TRPV1/TRPV4 and intracellular hydrostatic pressure in the mouse lens. *Invest Ophthalmol Vis Sci*. (2020) 61:58. doi: 10.1167/iovs.61.6.58

58. Schey KL, Gletten RB, O'Neale CVT, Wang Z, Petrova RS, Donaldson PJ. Lens aquaporins in health and disease: location is everything! *Front Physiol*. (2022) 13:882550. doi: 10.3389/fphys.2022.882550

59. Zelenka PS. Regulation of cell adhesion and migration in lens development. *Int J Dev Biol*. (2004) 48:857–65. doi: 10.1387/ijdb.041871pz

60. Cheng C, Nowak RB, Biswas SK, Lo WK, FitzGerald PG, Fowler et al. VM. Tropomodulin 1 regulation of actin is required for the formation of large paddle protrusions between mature lens fiber cells. *Invest Ophthalmol Vis Sci*. (2016) 57:4084–99. doi: 10.1167/iovs.16-19949

61. Cheng C, Nowak RB, Fowler VM. The lens actin filament cytoskeleton: Diverse structures for complex functions. *Exp Eye Res*. (2017) 156:58–71. doi: 10.1016/j.exer.2016.03.005

62. Ramaekers FC, Osborn M, Schimid E, Weber K, Bloemendal H, Franke WW. Identification of the cytoskeletal proteins in lens-forming cells, a special epitheloid cell type. *Exp Cell Res*. (1980) 127:309–27. doi: 10.1016/0014-4827(80)90437-1

63. Dubbelman M, van der Heijde GL, Weeber HA, G.F. Vrensen. Changes in the internal structure of the human crystalline lens with age and accommodation. *Vision Res*. (2003) 43:2363–75. doi: 10.1016/S0042-6989(03)00428-0

64. Cvekl A, Camerino MJ. Generation of lens progenitor cells and lentoid bodies from pluripotent stem cells: novel tools for human lens development and ocular disease etiology. *Cells*. (2022) 11(21):3516. doi: 10.3390/cells11213516

65. Al-Ghoul KJ, Lane CW, Taylor VL, Fowler WC, Costello MJ. Distribution and type of morphological damage in human nuclear age-related cataracts. *Exp Eye Res*. (1996) 62:237–51. doi: 10.1006/exer.1996.0029

66. Gong X, Cheng C, Xia CH. Connexins in lens development and cataractogenesis. *J Membr Biol*. (2007) 218:9–12. doi: 10.1007/s00232-007-9033-0

67. FitzGerald PG. Lens intermediate filaments. *Exp Eye Res*. (2009) 88:165–72. doi: 10.1016/j.exer.2008.11.007

68. Song S, Landsbury A, Dahm R, Liu Y, Zhang Q, Quinlan RA. Functions of the intermediate filament cytoskeleton in the eye lens. *J Clin Invest*. (2009) 119:1837–48. doi: 10.1172/JCI38277

69. Beyer EC, Berthoud VM. Connexin hemichannels in the lens. *Front Physiol*. (2014) 5:20. doi: 10.3389/fphys.2014.00020

70. Audette DS, Scheiblin DA, Duncan MK. The molecular mechanisms underlying lens fiber elongation. *Exp Eye Res*. (2017) 156:41–9. doi: 10.1016/j.exer.2016.03.016

71. Rao PV, Maddala R. Ankyrin-B in lens architecture and biomechanics: Just not tethering but more. *Bioarchitecture*. (2016) 6:39–45. doi: 10.1080/19490992.2016.1156284

72. Quinlan RA, Sandilands A, Procter JE, Prescott AR, Hutcheson AM, Dahm R, et al. The eye lens cytoskeleton. *Eye (Lond)*. (1999) 13:409–16. doi: 10.1038/eye.1999.115

73. Prescott AR, Sandilands A, Hutcheson AM, Carter JM, Quinlan RA. The intermediate filament cytoskeleton of the lens: an ever changing network through development and differentiation. A minireview. *Ophthalmic Res*. (1996) 28 Suppl 1:58–61.

74. Ireland M, Maisel H, Bradley RH. The rabbit lens cytoskeletal: an ultrastructural analysis. *Ophthalmic Res*. (1978) 10:231–6. doi: 10.1159/000264960

75. Maisel H, Harding CV, Alcala JR, Kuszak J, Bradley R. Morphology of the lens. In: Bloemendal H, editor. *Molecular and cellular biology of the eye lens*. Wiley and Sons, New York (1981). p. 49–84.

76. Simitian G, Virumbrales-Muñoz M, Sánchez de Diego C, Beebe DJ, Kosoff D. Microfluidics in vascular biology research: a critical review for engineers, biologists, and clinicians. *Lab Chip*. (2022) 22:3618–36. doi: 10.1039/D2LC00352J

77. Beebe DJ, Mensing GA, Walker GM. Physics and applications of microfluidics in biology. *Annu Rev BioMed Eng*. (2002) 4:261–86. doi: 10.1146/annurev.bioeng.4.112601.125916

78. Walker GM, Zeringue HC, Beebe DJ. Microenvironment design considerations for cellular scale studies. *Lab Chip*. (2004) 4:91–7. doi: 10.1039/b311214d

79. Sackmann EK, Fulton AL, Beebe DJ. The present and future role of microfluidics in biomedical research. *Nature*. (2014) 507:181–9. doi: 10.1038/nature13118

80. Fialova S, Pochylý F, Kotek M, Jašíková D. Velocity profiles of fluid flow close to a hydrophobic surface. *EPJ Web Conferences*. (2017) 143:02023. doi: 10.1051/epjconf/201714302023

81. Moller MN, Li Q, Chinnaraj M, Cheung HC, Lancaster JR Jr., Denicola A. Solubility and diffusion of oxygen in phospholipid membranes. *Biochim Biophys Acta*. (2016) 1858:2923–30. doi: 10.1016/j.bbamem.2016.09.003

82. Subczynski WK, Widomska J, Mainali L. Factors determining the oxygen permeability of biological membranes: oxygen transport across eye lens fiber-cell plasma membranes. *Adv Exp Med Biol*. (2017) 977:27–34. doi: 10.1007/978-3-319-55231-6

83. Bernecker C, Kofeler H, Pabst G, Trotzmuller M, Kolb D, Strohmayer K, et al. Cholesterol deficiency causes impaired osmotic stability of cultured red blood cells. *Front Physiol*. (2019) 10:1529. doi: 10.3389/fphys.2019.01529

84. Widomska J, Subczynski WK, Mainali L, Raguz M. Cholesterol bilayer domains in the eye lens health: A review. *Cell Biochem Biophys*. (2017) 75:387–98. doi: 10.1007/s12013-017-0812-7

85. Subczynski WK, Pasenkiewicz-Gierula M, Widomska J, Mainali L, Raguz M. High cholesterol/low cholesterol: effects in biological membranes: A review. *Cell Biochem Biophys*. (2017) 75:369–85. doi: 10.1007/s12013-017-0792-7

86. Subczynski WK, Pasenkiewicz-Gierula M, Widomska J. Protecting the eye lens from oxidative stress through oxygen regulation. *Antioxidants*. (2023) 12(9):1783. doi: 10.3390/antiox12091783

87. Bassnett S, Beebe DC. Coincident loss of mitochondria and nuclei during lens fiber cell differentiation. *Dev Dyn*. (1992) 194:85–93. doi: 10.1002/aja.1001940202

88. Sikic H, Shi Y, Lubura S, Bassnett S. A stochastic model of eye lens growth. *J Theor Biol*. (2015) 376:15–31. doi: 10.1016/j.jtbi.2015.03.021

89. Moncaster JA, Moir RD, Burton MA, Chadwick O, Minaeva O, Alvarez VE, et al. Alzheimer's disease amyloid-beta pathology in the lens of the eye. *Exp Eye Res*. (2022) 221:108974. doi: 10.1016/j.exer.2022.108974

90. Clark JI, Neuringer JR, Benedek GB. Phase separation and lens cell age. *J Gerontol*. (1983) 38:287–92. doi: 10.1093/geronj/38.3.287

91. Latina M, Chylack LT Jr., Fagerholm P, Nishio I, Tanaka T, Palmquist BM. Dynamic light scattering in the intact rabbit lens. Its relation to protein concentration. *Invest Ophthalmol Vis Sci*. (1987) 28:175–83.

92. Nishio I, Weiss JN, Tanaka T, Clark JI, Giblin FJ, Reddy VN, et al. *In vivo* observation of lens protein diffusivity in normal and X-irradiated rabbit lenses. *Exp Eye Res*. (1984) 39:61–8. doi: 10.1016/0014-4835(84)90115-5

93. Klesert TR, Cho DH, Clark JI, Maylie J, Adelman J, Snider L, et al. Mice deficient in Six5 develop cataracts: implications for myotonic dystrophy. *Nat Genet*. (2000) 25:105–9. doi: 10.1038/75490

94. Moncaster JA, Pineda R, Moir RD, Lu S, Burton MA, Ghosh JG, et al. Alzheimer's disease amyloid-beta links lens and brain pathology in Down syndrome. *PloS One*. (2010) 5:e10659. doi: 10.1371/journal.pone.0010659

95. Yuen J, Li Y, Shapiro LG, Clark JI, Arnett E, Sage EH, et al. Automated, computerized, feature-based phenotype analysis of slit lamp images of the mouse lens. *Exp Eye Res*. (2008) 86:562–75. doi: 10.1016/j.exer.2007.11.019

96. Marcos S, Artal P, Atchison DA, Hampson K, Legras R, Lundstrom L, et al. Adaptive optics visual simulators: a review of recent optical designs and applications [Invited]. *BioMed Opt Express*. (2022) 13:6508–32. doi: 10.1364/BOE.473458

97. Kroger RH. Optical plasticity in fish lenses. *Prog Retin Eye Res*. (2013) 34:78–88. doi: 10.1016/j.preteyeres.2012.12.001

98. Coulombre AJ, Herrmann H. Lens development. 3. Relationship between the growth of the lens and the growth of the outer eye coat. *Exp Eye Res*. (1965) 4:302–11. doi: 10.1016/S0014-4835(65)80045-8

99. Yamamoto Y. Growth of lens and ocular environment: role of neural retina in the growth of mouse lens as revealed by an implantation experiment. *Dev Growth Differ*. (1976) 18:273–8. doi: 10.1111/j.1440-169X.1976.00273.x

100. Aose M, Linbo TH, Lawrence O, Senoo T, Raible DW, Clark JI. The occhiolino (occ) mutant Zebrafish, a model for development of the optical function in the biological lens. *Dev Dyn*. (2017) 246:915–24. doi: 10.1002/dvdy.24511

101. Sivak JG. Optics of the eye of the "four-eyed fish" (Anableps anableps). *Vision Res*. (1976) 16:531–4. doi: 10.1016/0042-6989(76)90035-3

102. Perez LN, Lorena J, Costa CM, Araujo MS, Frota-Lima GN, Matos-Rodrigues GE, et al. Eye development in the four-eyed fish Anableps: cranial and retinal adaptations to simultaneous aerial and aquatic vision. *Proc R Soc B Biol Sci*. (2017) 284(1852):20170157. doi: 10.1098/rspb.2017.0157

103. Kanungo J, Swamynathan SK, Piatigorsky J. Abundant corneal gelsolin in Zebrafish and the 'four-eyed' fish, Anableps: possible analogy with multifunctional lens crystallins. *Exp Eye Res*. (2004) 79:949–56. doi: 10.1016/j.exer.2004.04.002

104. Schartau JM, Sjogreen B, Gagnon YL, Kroger RH. Optical plasticity in the crystalline lenses of the cichlid fish Aequidens pulcher. *Curr Biol*. (2009) 19:122–6. doi: 10.1016/j.cub.2008.11.062

105. Beebe D, Garcia C, Wang X, Rajagopal R, Feldmeier M, Kim JY, et al. Contributions by members of the TGFbeta superfamily to lens development. *Int J Dev Biol*. (2004) 48:845–56. doi: 10.1387/ijdb.041869db

106. Brewitt B, Clark JI. Growth and transparency in the lens, an epithelial tissue, stimulated by pulses of PDGF. *Science*. (1988) 242:777–9. doi: 10.1126/science.3187521

107. Cheng C. EphA2 and ephrin-A5 guide eye lens suture alignment and influence whole lens resilience. *Invest Ophthalmol Vis Sci*. (2021) 62:3. doi: 10.1167/iovs.62.15.3

108. Faber SC, Dimanlig P, Makarenkova HP, Shirke S, Ko K, Lang RA. Fgf receptor signaling plays a role in lens induction. *Development*. (2001) 128:4425–38. doi: 10.1242/dev.128.22.4425

109. Lovicu FJ, McAvoy JW. Growth factor regulation of lens development. *Dev Biol*. (2005) 280:1–14. doi: 10.1016/j.ydbio.2005.01.020

110. McAvoy JW, Chamberlain CG, de Iongh RU, Hales and F.J. Lovicu AM. Peter Bishop Lecture: growth factors in lens development and cataract: key roles for fibroblast growth factor and TGF-beta. *Clin Exp Ophthalmol*. (2000) 28:133–9. doi: 10.1046/j.1442-9071.2000.00310.x

111. McAvoy JW, Dawes LJ, Sugiyama Y, Lovicu FJ. Intrinsic and extrinsic regulatory mechanisms are required to form and maintain a lens of the correct size and shape. *Exp Eye Res*. (2017) 156:34–40. doi: 10.1016/j.exer.2016.04.009

112. Reneker LW, Overbeek PA. Lens-specific expression of PDGF-A alters lens growth and development. *Dev Biol*. (1996) 180:554–65. doi: 10.1006/dbio.1996.0328

113. Lovicu FJ, McAvoy JW, de Iongh RU. Understanding the role of growth factors in embryonic development: insights from the lens. *Philos Trans R Soc Lond B Biol Sci*. (2011) 366:1204–18. doi: 10.1098/rstb.2010.0339

114. Li H, Mao Y, Bouaziz M, Yu H, Qu X, Wang F, et al. Lens differentiation is controlled by the balance between PDGF and FGF signaling. *PloS Biol*. (2019) 17:e3000133. doi: 10.1371/journal.pbio.3000133

115. Schatteman GC, Motley ST, Effmann EL, Bowen-Pope DF. Platelet-derived growth factor receptor alpha subunit deleted Patch mouse exhibits severe cardiovascular dysmorphogenesis. *Teratology*. (1995) 51:351–66. doi: 10.1002/tera.1420510602

116. Cvekl A, Eliscovich C. Crystallin gene expression: Insights from studies of transcriptional bursting. *Exp Eye Res*. (2021) 207:108564. doi: 10.1016/j.exer.2021.108564

117. Cheng C, Gao J, Sun X, Mathias RT. Eph-ephrin signaling affects eye lens fiber cell intracellular voltage and membrane conductance. *Front Physiol*. (2021) 12:772276. doi: 10.3389/fphys.2021.772276

118. Zhou Y, Bennett TM, Ruzycki PA, Shiels A. Mutation of the EPHA2 tyrosine-kinase domain dysregulates cell pattern formation and cytoskeletal gene expression in the lens. *Cells*. (2021) 10(10):2606. doi: 10.3390/cells10102606

119. Brewitt B, Clark JI. A new method for study of normal lens development *in vitro* using pulsatile delivery of PDGF or EGF in HL-1 serum-free medium. *Vitro Cell Dev Biol*. (1990) 26:305–14. doi: 10.1007/BF02624462

120. Brewitt B, Talian JC, Zelenka PS. Cell cycle synchrony in the developing chicken lens epithelium. *Dev Biol*. (1992) 152:315–22. doi: 10.1016/0012-1606(92)90138-7

121. Brewitt B, Teller DC, Clark JI. Periods of oscillatory growth in developing ocular lens correspond with cell cycle times. *J Cell Physiol*. (1992) 150:586–92. doi: 10.1002/jcp.1041500320

122. Wang D, Wang E, Liu K, Xia CH, Li S, Gong X. Roles of TGFbeta and FGF signals during growth and differentiation of mouse lens epithelial cell *in vitro*. *Sci Rep*. (2017) 7:7274. doi: 10.1038/s41598-017-07619-5

123. Liu Z, Wang R, Lin H, Liu Y. Lens regeneration in humans: using regenerative potential for tissue repairing. *Ann Transl Med*. (2020) 8:1544. doi: 10.21037/atm

124. Wang Q, McAvoy JW, Lovicu FJ. Growth factor signaling in vitreous humor-induced lens fiber differentiation. *Invest Ophthalmol Vis Sci*. (2010) 51:3599–610. doi: 10.1167/iovs.09-4797

125. Griep AE. Cell cycle regulation in the developing lens. *Semin Cell Dev Biol*. (2006) 17:686–97. doi: 10.1016/j.semcdb.2006.10.004

126. Potts JD, Bassnett S, Kornacker S, Beebe DC. Expression of platelet-derived growth factor receptors in the developing chicken lens. *Invest Ophthalmol Vis Sci*. (1994) 35:3413–21.

127. Wang K, Pierscionek BK. Biomechanics of the human lens and accommodative system: Functional relevance to physiological states. *Prog Retin Eye Res*. (2019) 71:114–31. doi: 10.1016/j.preteyeres.2018.11.004

128. Wang K, Venetsanos DT, Hoshino M, Uesugi K, Yagi N, Pierscionek BK. A modeling approach for investigating opto-mechanical relationships in the human eye lens. *IEEE Trans BioMed Eng*. (2020) 67:999–1006. doi: 10.1109/TBME.10

129. Johnsen S, Widder EA. The physical basis of transparency in biological tissue: ultrastructure and the minimization of light scattering. *J Theor Biol*. (1999) 199:181–98. doi: 10.1006/jtbi.1999.0948

130. Sarangi S, Minaeva O, Ledoux DM, Parsons DS, Moncaster JA, Black CA, et al. *In vivo* quasi-elastic light scattering detects molecular changes in the lenses of adolescents with Down syndrome. *Exp Eye Res*. (2024) 241:109818. doi: 10.1016/j.exer.2024.109818

131. Thurston GM, Hayden DL, Burrows P, Clark JI, Taret VG, Kandel J, et al. Quasielastic light scattering study of the living human lens as a function of age. *Curr Eye Res*. (1997) 16:197–207. doi: 10.1076/ceyr.16.3.197.15410

132. Bettelheim FA. Light scattering in lens research: an essay on accomplishments and promises. *Exp Eye Res*. (2004) 79:747–52. doi: 10.1016/j.exer.2004.06.004

133. Benedek GB, Pande J, Thurston GM, Clark JI. Theoretical and experimental basis for the inhibition of cataract. *Prog Retin Eye Res*. (1999) 18:391–402. doi: 10.1016/S1350-9462(98)00023-8

134. Greiling TM, Clark JI. Early lens development in the zebrafish: a three-dimensional time-lapse analysis. *Dev Dyn*. (2009) 238:2254–65. doi: 10.1002/dvdy.21997

135. Muchowski PJ, Ramsden R, Nguyen Q, Arnett EE, Greiling TM, Anderson SK, et al. Noninvasive measurement of protein aggregation by mutant huntingtin fragments or alpha-synuclein in the lens. *J Biol Chem*. (2008) 283:6330–6. doi: 10.1074/jbc.M709678200

136. Seeberger TM, Matsumoto Y, Alizadeh A, Fitzgerald PG, Clark JI. Digital image capture and quantification of subtle lens opacities in rodents. *J BioMed Opt*. (2004) 9:116–20. doi: 10.1117/1.1630034

137. Koretz JF, Cook CA, Kaufman PL. Aging of the human lens: changes in lens shape at zero-diopter accommodation. *J Opt Soc Am A Opt Image Sci Vis*. (2001) 18:265–72. doi: 10.1364/JOSAA.18.000265

138. Koretz JF, Cook CA, Kuszak JR. The zones of discontinuity in the human lens: development and distribution with age. *Vision Res*. (1994) 34:2955–62. doi: 10.1016/0042-6989(94)90267-4

139. Ehinger B, Grzybowski A. Allvar Gullstrand (1862-1930)–the gentleman with the lamp. *Acta Ophthalmol*. (2011) 89:701–8. doi: 10.1111/aos.2011.89.issue-8

140. Brennan L, Costello MJ, Hejtmancik JF, Menko AS, Riazuddin SA, Shiels A. Autophagy requirements for eye lens differentiation and transparency. *Cells*. (2023) 12 (3):475. doi: 10.3390/cells12030475

141. Costello MJ, Brennan LA, Basu S, Chauss D, Mohamed A, Gilliland KO, et al. Autophagy and mitophagy participate in ocular lens organelle degradation. *Exp Eye Res*. (2013) 116:141–50. doi: 10.1016/j.exer.2013.08.017

142. Morishita H, Mizushima N. Autophagy in the lens. *Exp Eye Res*. (2016) 144:22–8. doi: 10.1016/j.exer.2015.08.019

143. Morishita H, Mizushima N. Autophagy and ageing. *Nihon Rinsho*. (2016) 74:1461–6.

144. Morishita H, Mizushima N. Diverse cellular roles of autophagy. *Annu Rev Cell Dev Biol*. (2019) 35:453–75. doi: 10.1146/annurev-cellbio-100818-125300

145. Bahrami M, Hoshino M, Pierscionek B, Yagi N, Regini J, Uesugi K. Optical properties of the lens: an explanation for the zones of discontinuity. *Exp Eye Res*. (2014) 124:93–9. doi: 10.1016/j.exer.2014.05.009

146. Trokel S. The physical basis for transparency of the crystalline lens. *Invest Ophthalmol*. (1962) 1:493–501.

147. Clark JI. Order and disorder in the transparent media of the eye. *Exp Eye Res*. (2004) 78:427–32. doi: 10.1016/j.exer.2003.10.008

148. Tanaka T, Benedek GB. Observation of protein diffusivity in intact human and bovine lenses with application to cataract. *Invest Ophthalmol*. (1975) 14:449–56.

149. Delaye M, Clark JI, Benedek GB. Identification of the scattering elements responsible for lens opacification in cold cataracts. *Biophys J*. (1982) 37:647–56. doi: 10.1016/S0006-3495(21)00384-2

150. Elbein AD. The metabolism of alpha,alpha-trehalose. *Adv Carbohydr Chem Biochem*. (1974) 30:227–56. doi: 10.1016/S0065-2318(08)60266-8

151. Uwineza A, Kalligeraki AA, Hamada N, Jarrin M, Quinlan RA. Cataractogenic load - A concept to study the contribution of ionizing radiation to accelerated aging in the eye lens. *Mutat Res Rev Mutat Res*. (2019) 779:68–81. doi: 10.1016/j.mrrev.2019.02.004

152. Lampi KJ, Fox CB, David LL. Changes in solvent accessibility of wild-type and deamidated betaB2-crystallin following complex formation with alphaA-crystallin. *Exp Eye Res*. (2012) 104:48–58. doi: 10.1016/j.exer.2012.09.001

153. Lampi KJ, Wilmarth PA, Murray MR, David LL. Lens beta-crystallins: the role of deamidation and related modifications in aging and cataract. *Prog Biophys Mol Biol*. (2014) 115:21–31. doi: 10.1016/j.pbiomolbio.2014.02.004

154. Lou MF. Glutathione and glutaredoxin in redox regulation and cell signaling of the lens. *Antioxid (Basel)*. (2022) 11(10):1973. doi: 10.3390/antiox11101973

155. Benedek GB, Clark JI, Serrallach EN, Young C, Mengel L, Sauke T, et al. Light scattering and reversible cataracts in the calf and human lens. *Philos Trans R Soc London Ser A*. (1979) 293:329–40. doi: 10.1098/rsta.1979.0100

156. Fan X, Monnier VM, Whitson J. Lens glutathione homeostasis: Discrepancies and gaps in knowledge standing in the way of novel therapeutic approaches. *Exp Eye Res*. (2017) 156:103–11. doi: 10.1016/j.exer.2016.06.018

157. Quinlan RA. DRUG DISCOVERY. A new dawn for cataracts. *Science*. (2015) 350:636–7. doi: 10.1126/science.aad6303

frontiers | Frontiers in Ophthalmology

TYPE Original Research
PUBLISHED 15 August 2024
DOI 10.3389/fopht.2024.1407582

OPEN ACCESS

EDITED BY
Catherine Cheng,
Indiana University, United States

REVIEWED BY
Nange Jin,
University of Houston, United States
Barbara Pierscionek,
Anglia Ruskin University, United Kingdom

*CORRESPONDENCE
Julie C. Lim
j.lim@auckland.ac.nz

RECEIVED 26 March 2024
ACCEPTED 22 July 2024
PUBLISHED 15 August 2024

CITATION
Li B, Suzuki-Kerr H, Martis RM, Lim CJJ, Wang Z-a, Nguyen TX, Donaldson PJ, Poulsen RC and Lim JC (2024) Time of day differences in the regulation of glutathione levels in the rat lens. *Front. Ophthalmol.* 4:1407582. doi: 10.3389/fopht.2024.1407582

Time of day differences in the regulation of glutathione levels in the rat lens

Bo Li[1,2], Haruna Suzuki-Kerr[1,2], Renita M. Martis[1,2], Christopher J. J. Lim[1,2], Zhou-ai Wang[1,2], Tai X. Nguyen[1,2], Paul J. Donaldson[1,2], Raewyn C. Poulsen[3] and Julie C. Lim[1,2]*

[1]Department of Physiology, School of Medical Sciences, University of Auckland, Auckland, New Zealand, [2]New Zealand National Eye Centre, University of Auckland, Auckland, New Zealand, [3]Department of Pharmacology, University of Auckland, Auckland, New Zealand

Introduction: Evidence in non-ocular tissues indicate that the antioxidant glutathione (GSH) may be regulated in a circadian manner leading to the idea that GSH levels in the lens may also be controlled in a circadian manner to anticipate periods of oxidative stress.

Methods: Male rat Wistar lenses (6 weeks) were collected every 4 hours over a 24-hour period at 6am, 10am, 2pm, 6pm, 10pm and 2am and quantitative-PCR, western blotting and immunohistochemistry performed to examine the expression of core clock genes and proteins (BMAL1, CLOCK, CRY1-2, PER 1-3) and their subcellular localisation over a 24-hour period. Western blotting of lenses was also performed to examine the expression of NRF2, a transcription factor involved in regulating genes involved in GSH homeostasis and GSH related enzymes (GCLC, GS and GR) over the 24-hour period. Finally, HLPC was used to measure GSH levels in the aqueous humour and lenses every 4 hours over a 24-hour period.

Results: The rat lens contains the core molecular components of a circadian clock with the expression of core clock proteins, NRF2 and GSH related enzymes fluctuating over a 24-hour period. BMAL1 expression was highest during the day, with BMAL1 localised to the nuclei at 10am. NRF2 expression remained constant over the 24-hour period, although appeared to move in and out of the nuclei every 4 hours. GSH related enzyme expression tended to peak at the start of night which correlated with high levels of GSH in the lens and lower levels of GSH in the aqueous humour.

Conclusion: The lens contains the key components of a circadian clock, and time-of-day differences exist in the expression of GSH and GSH related enzymes involved in maintaining GSH homeostasis. GSH levels in the rat lens were highest at the start of night which represents the active phase of the rat when high GSH levels may be required to counteract oxidative stress induced by cellular metabolism. Future work to directly link the clock to regulation of GSH levels in the lens will be important in determining whether the clock can be used to help restore GSH levels in the lens.

KEYWORDS

lens, circadian clock, glutathione, antioxidant, NRF2

1 Introduction

The lens contains high levels of the antioxidant glutathione (GSH) which exceed levels found in other ocular tissues (1, 2). These high levels are important in protecting the lens from oxidative stress and maintaining lens transparency. However, with advancing age, GSH levels decrease initiating a series of events such as loss of protein thiols, an increased in mixed disulfides, an increase in insoluble protein, protein aggregation and ultimately cataract formation (3–6). In the young lens, high GSH levels are maintained by several different pathways including the direct uptake of GSH from the ocular humours, intracellular synthesis of GSH from cysteine, glutamate and glycine by the sequential actions of the enzymes glutamate cysteine ligase (GCL) and glutathione synthetase (GS), regeneration of GSH from oxidised GSH (GSSG) by GSH reductase (GR), and export and degradation of GSH into its precursor amino acids for re-uptake by the lens (7). However, little is known about how GSH levels in the lens are regulated.

Circadian clocks in the body are self-sustaining endogenous oscillators that possess a timekeeper function to generate circadian rhythms which drives mammalian physiological and behavioural processes within a 24- hour cycle (8). Circadian rhythms are generated by the rhythmic expression of clock genes that involve transcriptional-translational feedback loop (9). These loops have a positive arm (BMAL1 and CLOCK) and a negative arm (PER1–3, CRY1&2). BMAL1 and CLOCK form a complex in the nucleus that bind to target gene promoters, resulting in the initiation of transcription of specific genes including genes of the negative arm of the clock. As the negative arm, PER and CRY proteins heterodimerise to repress the transcription of BMAL1 and CLOCK, with the BMAL1/CLOCK and PER/CRY cycle taking ~24 hours. Emerging evidence in non-ocular tissues suggests a connection between antioxidant balance and the circadian clock with antioxidants and antioxidant enzymes displaying daily cycles in their expression or activity levels (10, 11). Previous studies have reported daily fluctuations in levels of GSH in the mouse liver (12, 13), human platelets (14), mouse pancreas (15), and rat cerebral cortex (16). Enzymes involved in the synthesis of GSH, such as GCL and GR also exhibited rhythms in their mRNA expression and activity in rodent tissues (13, 17, 18). However, there is no clear pattern as to when GSH levels or enzyme expression/activity peak or trough between diurnal versus nocturnal animals or between rat and mouse suggesting it may be tissue specific. Time of day differences in GSH levels in *Drosophila* were shown to be controlled by a circadian clock as loss of Cycle (CYC; BMAL1 in mammals) or PER resulted in loss of temporal GSH fluctuations (19). Moreover, mRNA expression and activity of GCL, also displayed circadian rhythms, which were lost with loss of CYC or PER, directly linking GSH synthesis and the circadian clock (19).

NRF2 (nuclear factor erythroid 2-related factor 2) is a transcription factor that drives the transcription of several genes involved in antioxidant protection such as those involved in glutathione synthesis (GCL and GS) and glutathione regeneration (GR) (20). In the rat lung, BMAL1 and CLOCK regulates the transcription of NRF2 which in turn drives the expression of genes involved in GSH synthesis (17). NRF2-deficient mouse embryonic fibroblasts were shown to exhibit loss of GCL mRNA rhythms, which in turn corresponded to reduced GSH levels (17). Moreover, in the lungs of mutant mice in which CLOCK expression is disrupted (*Clock*$^{\Delta 19}$ *mice*), the rhythmic expression of NRF2 protein was lost along with reduced GCL mRNA expression and lower levels of GSH resulting in increased oxidative damage (17), demonstrating a link between the circadian clock, the NRF2/GSH pathways and protection from oxidative stress.

There is evidence that the lens utilises circadian rhythms to regulate important functions such as the synthesis of the antioxidant melatonin (21–23). In rat lenses, activity of melatonin synthesis enzymes and melatonin levels were highest at night and lowest during the day (21). Moreover, in more recent studies, Chhunchha et al. revealed that the rhythmic expression of NRF2 and one of its target genes, peroxiredoxin 6 (PRX6) was disrupted when BMAL1 expression was knocked down in human lens epithelial cells, resulting in increased ROS levels (24). These results demonstrate that BMAL1 is important for the regulation of NRF2-mediated antioxidant protection. Since NRF2 is also known to regulate expression of genes involved in the synthesis and regeneration of GSH, in this study, we examined whether the BMAL1/NRF2 pathway could play a role in the regulation of GSH levels in the lens and help anticipate the need for higher levels of GSH protection at different times of the day.

2 Methods

2.1 Reagents

Phosphate-buffered saline (PBS) was prepared from PBS tablets (Sigma-Aldrich Corp., St. Louis, MO, USA). Primers for Bmal1, Clock, Per 1-3, Cry1-2 and β-actin were synthesised by Integrated DNA Technologies (IDT™, Iowa, USA). Primers were reconstituted in RNase/DNase distilled water to yield a 100μM stock solution, which was diluted to 20μM, for use in PCR reactions. BMAL1, PER1, GCLC and β-actin primary antibodies were purchased from Abcam (Cambridge, UK), CLOCK and GR were purchased from ThermoFisher Scientific (Waltham, Massachusetts, USA) and CRY1, CRY2, PER2, PER3, NRF2 and GS were purchased from ProteinTech (Rosemont, Illinois, USA). The goat anti-rabbit Alexa Fluor 488 secondary antibody, the membrane marker wheat germ agglutinin (WGA) conjugated to Alexa Fluor 594 and 4′,6-diamidino-2-phenylindole (DAPI) were obtained from Life Technologies (Carlsbad, CA, USA). Unless otherwise stated, all other chemicals were obtained from Sigma-Aldrich Corp.

2.2 Animals

All animals were treated in accordance with protocols approved by the University of Auckland Animal Ethics Committee (Ethics number R001413) and in compliance with the Association for Research in Vision and Ophthalmology (ARVO) Statement for the Use of Animals in Ophthalmic and Vision Research. 6-week-old male Wistar rats were

housed in a 12hr/12hr light-dark cycle with the lights turned on at 6am (ZT0) and the lights turned off at 6pm (ZT12), in which ZT refers to Zeitgeber time; a standardised unit of time based on the 12hr/12hr light-dark cycle. Animals were euthanised by CO_2 asphyxiation and eyes nucleated at either 6am (ZT0), 10am (ZT4), 2pm (ZT8), 6pm (ZT12), 10pm (ZT16) or 2am (ZT20). For the 10am and 2pm collection, enucleation was performed under standard lighting conditions, but for the 6am and 6pm time points, enucleation was performed under dimmed lighting conditions. For the 10pm and 2am time point, a cohort of animals were reverse entrained to enable tissue collection during the day. A least 2 weeks prior to tissue collection, a cohort of animals were maintained in a reverse light-dark cycle – in which lights were turned off at 6am and lights were turned on at 6pm. This period of 2 weeks reverse entrainment was reported to be sufficient to ensure adaptation of animals to a reverse light-dark cycle (25) meaning that we were able to collect tissues at 10am and 2pm instead of 10pm and 2am. In these instances, eyes were enucleated under dim conditions.

2.3 Aqueous humour collection

Following enucleation, eyes were transferred immediately to a container prefilled with warm PBS. Eyes were then taken out and placed on a pre-chilled petri dish. A 27- gauge needle was then used to make an initial piercing at the limbus and a 2µL pipette was used to quickly collect the aqueous humour (AH) (roughly 1µL/eye) from both eyes of an animal, pooled together and then placed into a pre-chilled Eppendorf tube (n=6 AH sample for each time point). Tubes were snap frozen immediately in liquid nitrogen and were placed in a -80°C freezer for the quantification of total GSH (GSH + GSSG), reduced GSH and oxidised GSH (GSSG) levels using liquid chromatography tandem mass spectrometry (LC-MS/MS).

2.4 Lens dissection

Following enucleation, lenses were dissected from the eye. Lenses collected for RNA extraction were placed in TRIzol Reagent (Invitrogen, Waltham, Massachusetts, USA) and then stored at -80° C. Lenses collected for western blot analysis were homogenised in homogenising solution and then stored at -80°C. Lenses collected for immunohistochemical analysis were fixed in paraformaldehyde. Lenses collected for LC-MS/MS were homogenised in 200µL of 50mM EDTA, spun at 14,000 rpm for 20 minutes at 4°C, supernatants collected, snap frozen and stored immediately in the -80°C freezer.

2.5 Real time-polymerase chain reaction

Total RNA was isolated from brain (control tissue), or lenses collected at 10am using Trizol according to the manufacturer's protocol (TRIzol reagent; Life Technologies). Genomic DNA was removed by incubation with 10U/µL recombinant DNase I (Roche Diagnostics, Basel, Switzerland). Total brain or lens cDNA were synthesised from 1 µg total RNA mixed with 50µM oligo$(dT)_{20}$. The RNA was denatured at 65°C for 5 minutes, immediately placed on ice to cool, and then combined with 2× First-Strand Reaction Mix and SuperScript III/RNaseOUT Enzyme Mix (Life Technologies) for cDNA amplification. A control reaction (no cDNA synthesis) was also conducted in the absence of SuperScript III/RNaseOUT enzyme. Synthesised cDNA or control reaction (0.5–1µL) were added to separate PCR mixtures containing final concentrations of 5µL PowerUpTM SYBR Green PCR Master Mix (Applied BiosystemsTM, Waltham, Massachusetts, USA) and 3µL RNase-free water to a final volume reaction mixture of 10µL and 2 µM sense and antisense primers[15,16] (Table 1). The qPCR reaction was 95°C for 10 minutes, 40 cycles of denaturation at 95°C for 15 seconds, and a combined annealing/extension at 60°C for one minute. The mRNA relative quantity of target genes was obtained from the method of comparative threshold cycle (CT) and the target gene level of expression were normalised to the β-actin levels as an endogenous control within each group.

2.6 Western blotting

Lenses (n=16 lenses) and positive control tissue (kidney, liver or brain; n=1) were collected at 10am and homogenised in homogenising solution (5mM Tris-HCl, 5mM EDTA, and 5mM EGTA (pH 8.0) containing cOmplete Protease Inhibitors (Roche, Basel, Switzerland). Homogenates were centrifuged at 13,000g for 20 minutes and the supernatant stored at −80°C until further use. Concentrations of proteins were determined using the Direct Detect Infrared Spectrometer (Merck, Millipore). Proteins (20µg/lane) were first separated on a 10% or 15% vol/vol acrylamide separating gel and then transferred onto the Immuno-Blot PVDF membrane (Bio-Rad Laboratories) by electrophoresis. After transfer, membranes were incubated with blocking solution (5% milk powder in 1× Tris-buffered saline with Tween 20, pH7.6) for 1 hour and then incubated with primary antibodies (BMAL1 (1:500), CLOCK (1:200), CRY1 (1:1000), CRY2 (1:500), PER 1 (1: 500), PER 2 (1:500), PER 3 (1: 500), NRF2 (1:500), GCLC (1:500), GS (1:1000) or GR (1:500) overnight at 4°C. Membranes were incubated with donkey anti-rabbit secondary antibodies (1:10,000) for 1 hour. Labelled protein was visualised using enhanced chemiluminescence detection (ECL Prime; GE Healthcare) and developed using the Fujifilm Luminescent Image Analyser LAS-4000 System (GE Healthcare).

To determine if protein expression changed over a 24-hour period, lenses were collected at 6am (ZT0), 10am (ZT4), 2pm (ZT8), 6pm (ZT12), 10pm (ZT16), 2am (ZT20) (n=16 lenses for each time point) and processed as described above. Proteins were electrophoresed and transferred to membranes where the following primary antibodies were used: BMAL1 (1:500), CLOCK (1:200), CRY2 (1:500), NRF2 (1:500), GCLC (1:500), GS (1: 1000) or GR (1:500). Membranes were then incubated with secondary antibodies and labelled protein visualised as described above. Equal protein loading was tested by stripping the membranes with 2% SDS, 100 mM β-mercaptoethanol, 62.5mM Tris (pH 6.7) and then re-probing the membrane with antibodies to detect β-actin (1:1000).

TABLE 1 Primer sequences for target genes.

Gene Name (GenBank Accession #)	Primer Sequence (5′ – 3′)	Amplicon Size (bp)
β-actin (NM_001101.5)	Forward: AGCCATGTACGTAGCCATCC Reverse: TCTCAGCTGTGGTGGTGAAG	171
Bmal1 (NM_024362)	Forward: CCGATGACGAACTGAAACACCT Reverse: TGCAGTGTCCGAGGAAGATAGC	215
Clock (NM_021856)	Forward: TCTCTTCCAAACCAGACGCC Reverse: TGCGGCATACTGGATGGAAT	110
Cry1 (NM_198750)	Forward: TGCTCCTGGAGAGAATGTCC Reverse: TGACTCTCCCACCAACTTCA	271
Cry2 (NM_133405)	Forward: GGATAAGCACTTGGAACGGAA Reverse: ACAAGTCCCACAGGCGGT	155
Per1 (NM_001034125)	Forward: ACACCCAGAAGGAAGAGCAA Reverse: GCGAGAACGCTTTGCTTTAG	164
Per2 (NM_031678)	Forward: GAGAGAGGAACAGGGCTTCC Reverse: TTGACACGCTTGGACTTCAG	195
Per3 (NM_023978)	Forward: ATAGAACGGACGCCAGAGTGT Reverse: CGCTCCATGCTGTGAAGTTT	104
Nrf2 (NM_031789)	Forward: GTTGAGAGCTCAGTCTTCAC Reverse: CAGAGAGCTATCGAGTGACT	56
Gclc Catalytic Subunit (NM_012815)	Forward: ATCTGGATGATGCCAACGAGTC Reverse: CCTCCATTGGTCGGAACTCTACT	129
Gs (NM_012962.1)	Forward: GCAGGAACTGAGCAGGGTG Reverse: GCTTCAGCACAAAGTGGCTAG	169
Gr (NM_053906.2)	Forward: GGGCAAAGAAGATTCCAGGTT Reverse: GGACGGCTTCATCTTCAGTGA	101

2.7 Immunohistochemistry

Whole lenses collected at 10am (ZT4), 2pm (ZT8), 6pm (ZT12) and 10pm (ZT16) (n= 4 lenses for each time point) were fixed in 0.75% wt/vol paraformaldehyde, cryoprotected, and cryosectioned in an axial orientation using standard protocols developed in our laboratory. Sections were washed three times and incubated in blocking solution (3% wt/vol bovine serum albumin and 3% vol/vol normal goat/donkey serum) for 1 hour to reduce nonspecific labelling. The sections were then labelled with either BMAL1 (1:200), CLOCK (1:200) or NRF2 (1:100) antibodies diluted in blocking solution, followed by the goat anti-rabbit Alexa Fluor 488 (1:200) secondary antibody for 2 hours. To highlight cell morphology, cell membranes were labelled with WGA Alexa Fluor 594 (1:100) in PBS and to highlight epithelial and fiber cell nuclei, sections were stained with DAPI (1:10,000). Sections were then washed and mounted with VECTASHIELD HardSet aqueous mountant (Vector Laboratories, Burlingame, CA, USA) and viewed using an Olympus FV1000 confocal laser scanning microscope (Olympus Corporation, Tokyo, Japan). To facilitate comparison between data sets, the same pinhole size was used. Specific emission filter sets were used to detect signals from Alexa Fluor 488, WGA Alexa Fluor 594, and DAPI fluorophores.

2.8 Quantification of GSH levels in aqueous humour and lenses using LC-MS/MS

LC-MS/MS was used to quantify GSH and GSSG in the AH and lens as previously described (26). Samples were collected at six different time points (6am (ZT0), 10am (ZT4), 2pm (ZT8), 6pm (ZT12), 10pm (ZT16) and 2am (ZT20)) over a 24-hour period. Briefly, lens supernatants and AH samples were first thawed on ice. Known concentrations (calibration curve) of GSH and GSSG, internal standards (isotopically labelled GSH (13C 15 N)) and GSSG (13C 15 N) as an internal quality control), and AH and lens samples were immediately treated with monobromobimane (MBrB). Samples were then added to a previously conditioned solid phase extraction cartridge (Strata-X-C, Phenomenex, Torrance, CA, USA) before being eluted in 5% NH4OH. Known and unknown samples were vacuum-concentrated and reconstituted in 5% acetonitrile/0.1% heptafluorobutyric anhydride in H_2O. Separations were then performed by injecting 10µL sample into the LC equipped with a Phenomenex Synergi Hydro-RP C18 4µm 150 × 2mm column (Phenomenex, Torrance, CA, USA) and a 0.2µm in-line filter (Phenomenex, Torrance, CA, USA) in gradient mode. The column effluent was then directed into an Agilent 6460 A Triple Quadrupole mass spectrometer (Agilent Technologies, Santa Clara, California, USA) with parameters set in Table 2. GSH and GSSG were quantified using the calibration curve with known concentrations of CSH (range 0–100µM), CSSC (range 0–50µM), GSH (range 0–400µM) and GSSG (range 0–50µM). Metabolite concentrations were expressed as µM and normalised to lens wet weight as individual fractions, particularly of the epithelium, were too difficult to accurately measure.

2.9 Statistical analysis

All numerical values and graphs are displayed as mean ± standard error of the mean (SEM) unless otherwise stated. To compare gene expression between the brain and lens, for each target gene, a t-test was conducted to determine statistical significance. To compare changes across the 24 hour period, a one-way ANOVA test

10.3389/fopht.2024.1407582

was first conducted to determine statistical significance. Once significance was confirmed, a Tukey's *post-hoc* analysis was conducted to determine significance between groups using GraphPad Prism® Version 8. P values of <0.05 were considered statistically significant. To compare differences between GSH levels in the lens and AH at different time points, GSH concentration in the lens and AH was rescaled against the max concentration in either the lens or AH and tabulated. A two-way ANOVA along with the Bonferroni multiple comparison test was then conducted to determine significance at each time point. P values of *p<0.05, **p<0.01 or ***p<0.001 were considered statistically significant.

TABLE 2 MS/MS ions and parameters.

Analyte	Mass transition	Fragmentation Voltage	Collision Energy
GSH-mBrB	498.2>435.1	185 V	21 V
	498.2>192.1	185V	45 V
GSH-mBrB (13C 15N)	501.2>438.1	185 V	21 V
	501.2>192.1	185 V	45 V
GSSG	613>355	190 V	22 V
	613>484	190 V	15 V
GSSG (13C 15N)	619>361	190 V	22 V
	619>490	190 V	15 V

3 Results

3.1 Identification of clock component genes in the rat lens

Brain (positive control) and lens tissue was collected from the same animal at the same time (10am (ZT4)) and total RNA extracted. Brain or lens cDNA was synthesised and then used as a template for RT-qPCR using isoform specific primers for the clock component genes; Bmal1, Clock, Per1, Per2, Per3, Cry1, and Cry2. The relative expression of each clock component gene was normalised to the internal control β-actin. Lens -RT reactions where reverse transcriptase was omitted produced no amplification plots and therefore no relative expression values were provided. Figure 1A shows the relative expression of clock component genes in the brain compared to the lens (n =4 rats). While the lens expresses all the clock component genes, the levels of expression are significantly lower compared to that of the brain. A closer look at the expression levels in the lens (Figure 1B) revealed some interesting findings compared to the brain. Firstly, for Bmal1 and Clock in the lens, Clock expression appeared higher compared to Bmal1 expression. This was different to the pattern in the brain in which Bmal1 was more highly expressed compared to Clock. However, these differences were not statistically significant. Secondly, in the lens, all three Per isoforms appear to be expressed at similar levels, whereas in the brain Per1 appeared to be the more abundant isoform. Finally, like the brain, Cry1 expression appeared to be slightly higher relative to Cry2 expression in the lens. However, these differences were not statistically significant. Taken together, this is the first time that expression of all these clock component genes have been identified in the rat lens.

3.2 Expression of core clock component proteins in the rat lens

Having established that clock component genes are expressed in the lens, we next investigated whether BMAL1, CLOCK, PER1-3

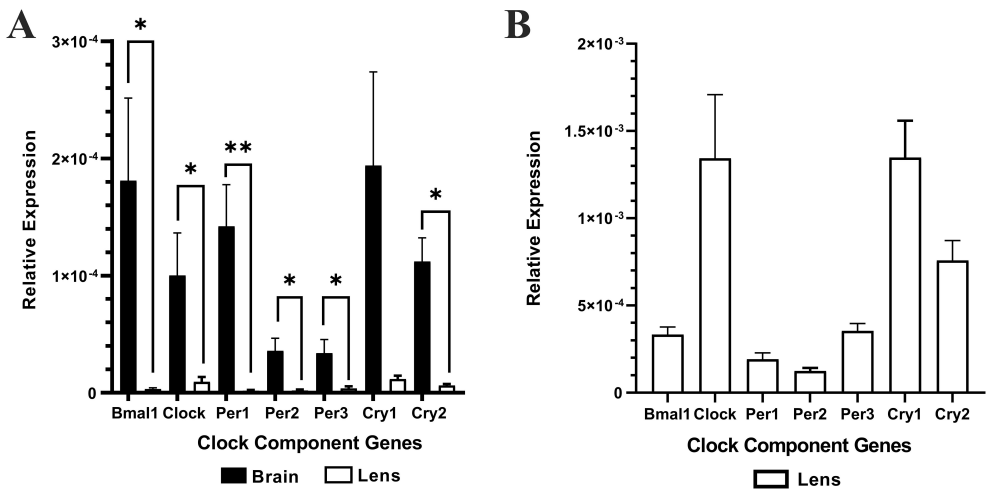

FIGURE 1
The relative expression of the clock component genes in the brain and lens. Brain and lens tissue were harvested at 10am and RNA extracted for cDNA synthesis. RT-qPCR in combination with isoform specific primers for the clock component genes was then performed. **(A)** The relative expression of clock component genes in the brain compared to the lens. **(B)**. Rescaled version of **(A)** to show the relative expression of clock component genes in the lens only. The relative expression for each clock component gene was calculated using the DCt method where the mean Ct value of the target gene is normalised to the b-actin internal control. Data is presented as mean relative expression ± the standard error of the mean (± SEM) from n = 4 rats. *p<0.05; **p<0.01.

and CRY1-2 are expressed at the protein level (Figure 2). Brain, kidney or liver (positive control) and lens tissue was collected at the same time (10am (ZT4)) and protein extracted. We originally used brain tissue as control but found it hard in some cases to identify bands of interest, so opted to test two different control tissues: kidney and liver. Because clock cycling can differ in peripheral tissues versus the brain it was more likely we would detect all of our clock proteins if we used more than one control tissue. As was the case, we were able to detect all core clock proteins in control tissue (kidney, liver or brain). However, in the lens, we only detected bands of the appropriate molecular weight for BMAL1 and CLOCK (Figure 2). While we loaded an equal amount of protein in the kidney and lens, the band for BMAL1 and CLOCK was more intense in the kidney relative to the lens, suggesting these clock proteins are more abundantly expressed in the kidney. While we detected a faint band for CRY2, we were unable to detect bands for CRY1 or PER1-3. This might suggest that time of day differences exist in the expression of these clock proteins in the lens, with BMAL1 and CLOCK expression more abundant during the day (10am) relative to CRY and PER expression.

3.3 Expression and localisation of core clock component proteins in the lens at different times of the day

To determine if time of day differences existed in clock protein expression, we investigated whether the expression of BMAL1, CLOCK and CRY2 oscillated over a 24-hour period. Wistar rats were housed in a 12hr/12hr light-dark cycle with the lights turned on at 6am and the lights turned off at 6pm. Lenses were collected at 4-hour intervals starting at 6am (ZT0) over a 24-hour period and then clock protein expression at 6am (ZT0), 10am (ZT4), 2pm (ZT8), 6pm (ZT12), 10pm (ZT16) and 2am (ZT20) examined by western blotting. BMAL1 expression changed over the course of the 24-hour period, with expression significantly increased at 2pm relative to the 6am time point. BMAL1 expression then declined to reach a significant trough at 10pm relative to the 6am time point (Figure 3A). On the other hand, CLOCK expression remained unchanged over the 24-hour period (Figure 3B). CRY2 expression was also seen to change over the course of the day with expression levels peaking at 6pm which was significantly increased relative to the 6am time point (Figure 3C). Since BMAL1 expression was higher during the day and CRY2 expression lower during the day, this may explain why it was difficult to initially detect CRY2 at 10am (Figure 2).

3.4 Expression of NRF2 and NRF2-regulated GSH related proteins involved in GSH homeostasis

Given that in other tissues, BMAL1 is important in the regulation of NRF2 (17) which drives the transcription of genes involved in the synthesis and regeneration of GSH, we examined the expression patterns of NRF2 over a 24-hour period. While it was expected that NRF2 expression may peak and trough in phase with BMAL1 as had been previously reported in mouse lenses (24), we found that in rat lenses, NRF2 expression remained constant over the 24-hour period (Figure 4A). To determine whether GSH related proteins linked to NFR2 regulated transcription showed time of day differences in their expression patterns, we examined the expression of Glutamate-Cysteine Ligase (GCLC) -the enzyme involved in the first step of GSH synthesis, Glutathione Synthetase (GS) - the enzyme involved in the second step of GSH synthesis, and Glutathione Reductase (GR) -the enzyme involved in the regeneration of GSH (Figures 4B–D). GCLC expression significantly decreased at 10am relative to 6am, and then slowly increased at 2pm and remained constant over the 24-hour period (Figure 4B). On the other hand, GS expression increased from 6am through to 6pm, with expression significantly increased at the start of night (6pm) relative to the 6am time point. (Figure 4C). GR levels fluctuated over the 24-hour period, with expression significantly increased at 10am and at 6pm relative to the 6am time point (Figure 4D). Taken together, it appears that GSH related enzyme expression generally increased at the start of the dark period which would coincide with the start of the active phase of the nocturnal rat.

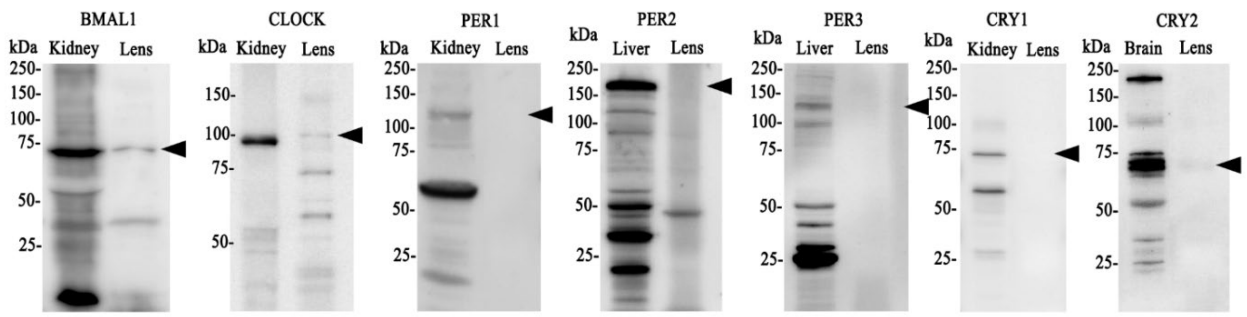

FIGURE 2
Protein expression of clock components of the positive and negative arm of the circadian clock in the rat lens. 20µg/lane of positive control tissue (kidney, liver or brain (n= 1 rat)) and 20µg/lane lens tissue (n=8 rats) was electrophoresed on an SDS-PAGE gel and protein levels analysed by Western blotting. Expression of BMAL1, CLOCK, PER1, PER2, PER3, CRY1 & CRY 2. Arrowheads indicate the predicted size of the target protein. Target proteins were all identified in positive control tissue but not all could be detected in the lens.

10.3389/fopht.2024.1407582

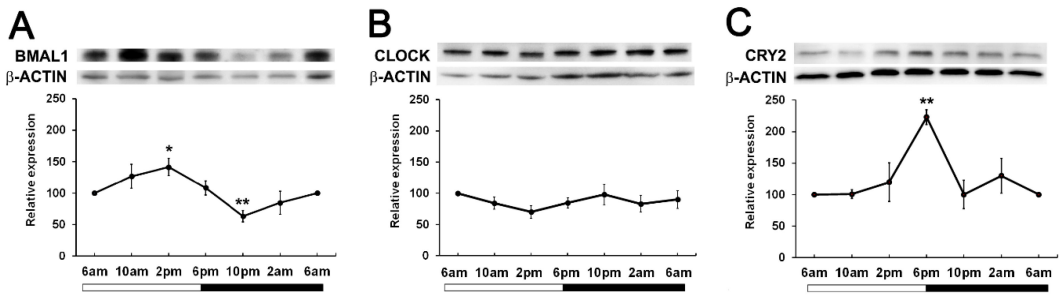

FIGURE 3
Expression of clock component proteins in the rat lens at different times of the day. **(A)** Expression of BMAL1, **(B)** CLOCK and **(C)** CRY2 over a 24-hour time period. Lens tissue (n=8 rats) was harvested at 4-hour intervals over a 24-hour period. 20μg lens protein/lane was electrophoresed on an SDS PAGE gel and protein levels analysed by Western blotting and expressed relative to the β-actin internal control. Relative expression of BMAL1, CLOCK and CRY2 expression in lenses at different times. Data is presented as mean relative expression ± standard error of the mean (SEM) from 5-7 western blots. * Indicates significant differences from the 6am time point; *p<0.01; **p<0.005.

3.5 Time of day differences in the subcellular localisation of BMAL1, CLOCK and NRF2

Given that BMAL1, CLOCK and NRF2 are transcription factors, we investigated the subcellular localisation of these proteins as localisation to the nuclei might suggest active transcription of genes at a particular time of the day. To do this, we labelled axial sections from lenses collected at four different time of the days; 10am (ZT4), 2pm (ZT8), 6pm (ZT12) and 10pm (ZT16) with antibodies specific for BMAL1, CLOCK or NRF2 (*green*), DAPI (*blue*) to visualise the nuclei, and WGA (*red*) to highlight the membranes of the epithelial and fiber cells. These sections were then visualised under a confocal microscope and images taken at the anterior pole (Figures 5A–L) and at the equator region (Figures 5A'–L'). At the anterior pole, BMAL1 labelling was mainly detected in the epithelium, with less labelling evident in the fiber

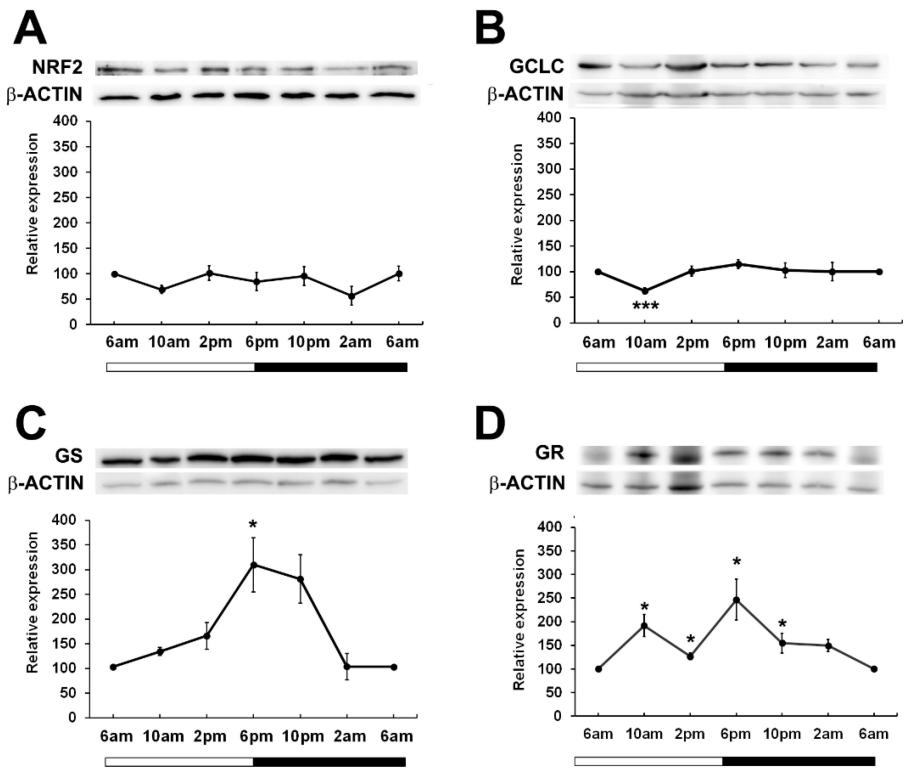

FIGURE 4
Relative expression of NRF2 and NRF2 related proteins in the rat lens over a 24-hour period. Lens tissue (n=8 rats) was harvested at 4-hour intervals over a 24-hour period. 20μg lens protein/lane was electrophoresed on an SDS-PAGE gel and protein levels were analysed by Western blotting and expressed relative to the β-actin internal control. Relative expression of **(A)** NRF2, **(B)** GCLC, **(C)** GS and **(D)** GR in lenses at different time points. Data is presented as mean relative expression ± standard error of the mean (SEM) from 5-7 western blots. * Indicates significant differences from the 6am time point; *p<0.05, ***p<0.001.

cells for each time point (Figures 5A–D). While BMAL1 labelling was mainly cytoplasmic, at 2pm and 10pm, BMAL1 could be seen to be co-localised to the nuclei (Figures 5B, D). At the lens equator, BMAL1 labelling was detected in the epithelial and fibre cells for each time point (Figures 5A'–D'). While BMAL1 was predominantly localised to the cytoplasm for each time point, at 10am BMAL1 was strongly co-localised to the nuclei (Figure 5A'). At the anterior pole and equator region, CLOCK was strongly associated with the nuclei for each time point (Figures 5E–H, E'–H'). Like CLOCK, NRF2 was co-localised to the nuclei of epithelial cells at the anterior pole for each time point (Figures 5I–L), but at the lens equator, NRF2 appeared to translocate in and out of the nuclei at the different timepoints (Figures 5I'–L'). At 10am, NRF2 was absent from the nuclei (Figure 5I'), which was different to what was observed for BMAL1 and CLOCK at this same time point (Figures 5A', E'). However, at 2pm, NRF2 was co-localised to the nuclei, then was absent from the nuclei at 6pm and then reappeared in the nuclei at 10pm (Figures 5J'–L').

3.6 GSH levels fluctuate at different times of the day in the lens and aqueous humour

Having shown that the expression of enzymes involved in GSH synthesis appeared to increase at night, we determined if this corresponded to higher levels of GSH during the dark period. To investigate this, lenses were collected at six different time points (6am (ZT0), 10am (ZT4), 2pm (ZT8), 6pm (ZT12), 10pm (ZT16), 2am (ZT20)) from male Wistar rats over a 24-hour period and GSH/GSSG concentrations measured via LC-MS/MS (Figure 6). In the lens, the majority of GSH was in the reduced form relative to the oxidised form. Reduced GSH levels in the lens appeared high at 6am and to then decrease at 2pm, before increasing at 6pm which correlates to the start of night. From here, GSH levels decrease at 10pm and then levels remain steady overnight (Figure 6A). While an obvious trend was seen, this was not statistically significant. GSSG levels in the lens were almost negligible with no time-of-day differences seen (Figure 6B). While the lens can synthesise GSH, it is known that the lens can take up GSH directly from the aqueous humour (AH). To investigate time-of-day differences in GSH levels in the AH, we collected AH at six different time points (6am, 10am, 2pm, 6pm, 10pm, 2am) over a 24-hour period and GSH/GSSG concentrations measured. Like the lens, the majority of GSH in the AH was in the reduced form relative to the oxidised form. While not statistically significant, there was a trend with low levels of GSH detected at 6am before increasing to a peak at 10am, decreasing from 10am to 6pm, before gradually increasing and then plateauing at 6am (Figure 6C). GSSG levels were low compared to GSH levels and did not appear to change over time (Figure 6D). At 6pm where

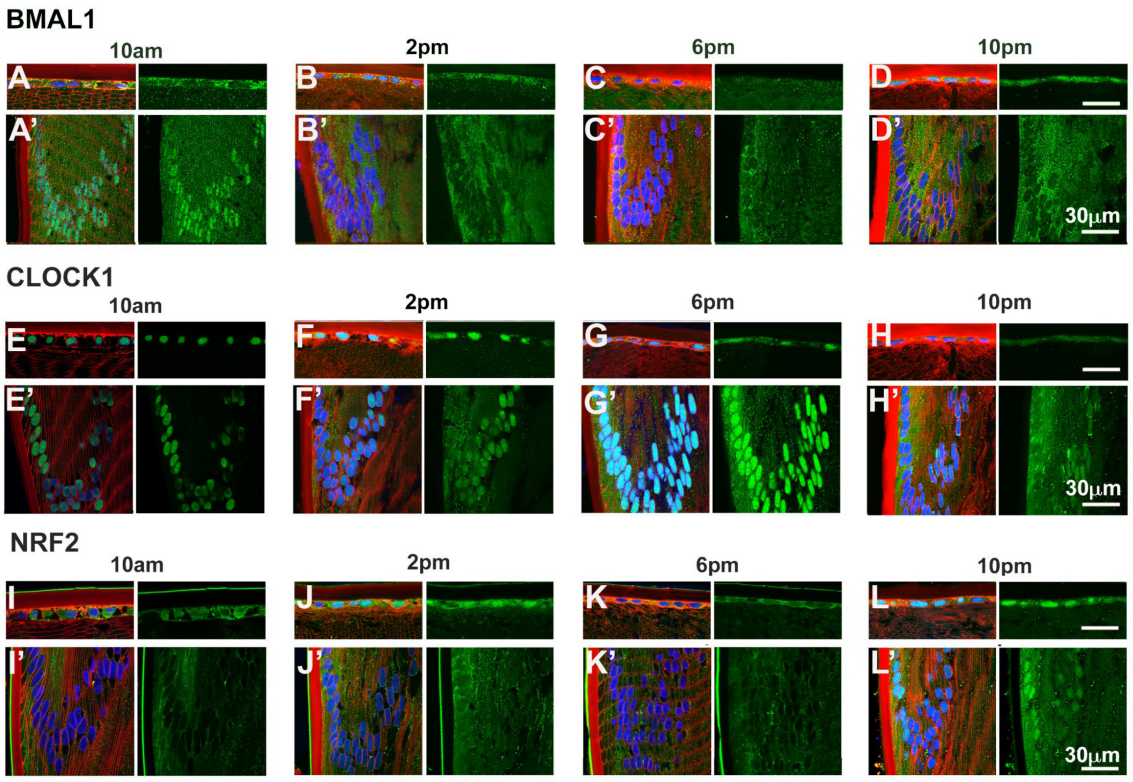

FIGURE 5
Expression of clock component proteins and NRF2 in the rat lens at different times of the day. Subcellular localisation of BMAL1, CLOCK and NRF2 at different times of the day. Lenses were dissected at 10am, 2pm, 6pm or 10pm, fixed, cryoprotected and cryosectioned in an axial orientation. Images were taken at either the anterior pole **(A–L)** or the lens equator **(A'-L')**. **(A–L)** *Left hand panels*-sections labelled with the membrane marker WGA (*red*), DAPI (*blue*) and BMAL1, CLOCK or NRF2 antibodies (*green*). **A'-L'**: *Right hand panels* -sections showing only BMAL1, CLOCK or NRF2 labelling. *n* = 4 lenses.

10.3389/fopht.2024.1407582

GSH levels in the AH are lowest (Figure 6C), GSH levels in the lens appear highest (Figure 6A). To compare these differences, individual GSH concentrations for each time point were rescaled against the max value in either the lens or the AH and plotted (Figure 6E). At 6pm, the levels of GSH in the lens were significantly different to the levels of GSH in the AH (p=0.03). A similar trend was seen at 6am where high levels in GSH in the lens appeared to correspond to low levels of GSH in the AH. However, this was not statistically significant.

4 Discussion

Traditionally there has been a strong bias in basic research on circadian rhythms towards the use of male animals in studies with less than 20% of work in this area including female cohorts (27). To determine in the first instance if the rat lens contained the machinery of a circadian clock, we opted to use a use male rats, so that we could compare our findings to the existing literature. In this study, we confirmed the presence of clock genes from the positive (Bmal1 and Clock) and negative arms (Per1-3, Cry1-2) of the circadian clock in the rat lens (Figure 1). The expression of these core clock genes was significantly lower than that of the brain (Figure 1A). However, it is worth noting that since most cells are anucleate, a homogenate of whole lenses might appear to show less clock gene expression than brain because only a subset of lens cells express those clock genes whereas all brain cells express clock genes. Therefore, it might still be possible that those individual lens cells that are expressing clock components are expressing them to a same level as individual brain cells. Another possibility is that lens and brain clocks may not necessarily be in sync. Nevertheless, the identification of Bmal1 and Clock in the rat lens supports another study that identified Bmal1 and Clock at the mRNA level in human lens epithelial cells and mouse lenses (24). However, to our knowledge, this is the first report of components of the negative arm of the circadian clock being identified in the lens. The detection

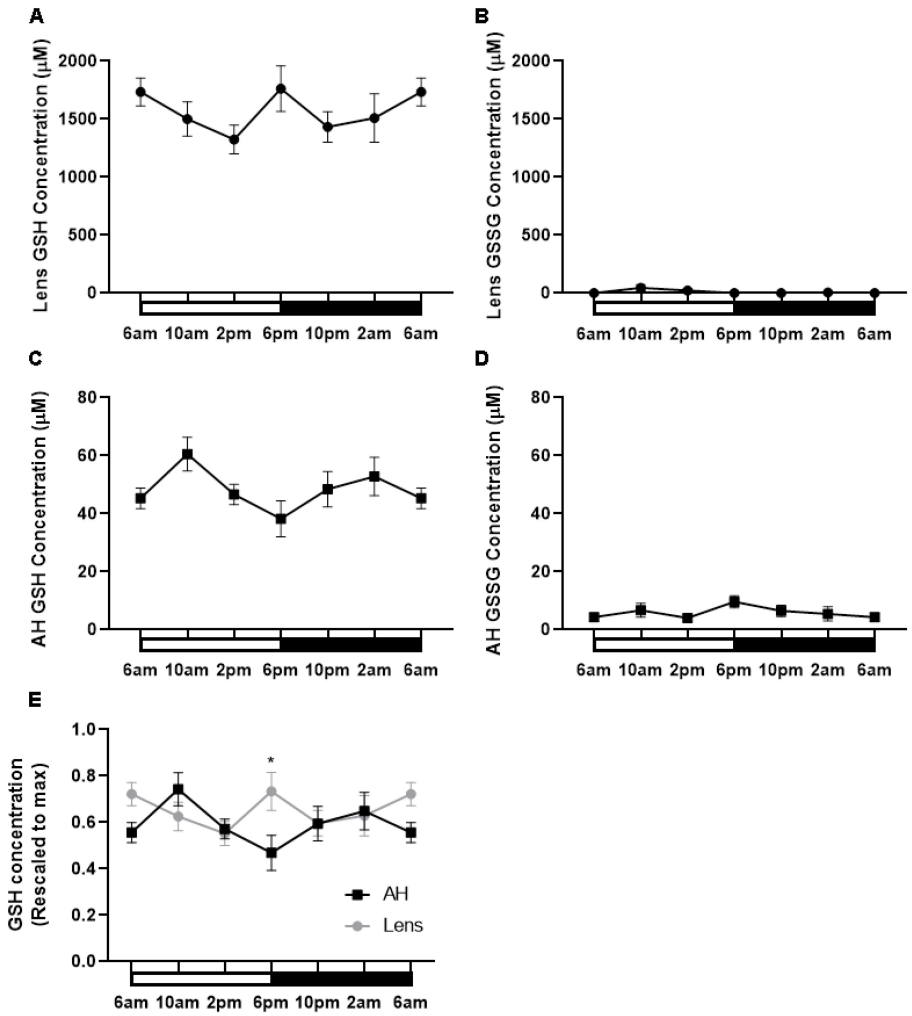

FIGURE 6
GSH levels in the rat lens and aqueous humour over a 24- hour period. **(A, B)** Lenses and **(C, D)** aqueous humour (AH) were collected from six-week-old male Wistar rats at six different time points (6am, 10am, 2pm, 6pm, 10pm and 2am) over a 24-hour period and analysed by LC-MS/MS to quantify the concentration of GSH **(A, C)** and GSSG **(B, D)**. **(E)** Concentration of GSH in the AH and Lens rescaled to max concentration. Each point and error bars represent the mean ± S.E.M. (n=6 animals). *p<0.05.

of all Per and Cry isoforms in the lens is consistent with other studies where it is common for Per 1-3 and Cry 1-2 to be expressed in the same tissue; for example, Per1-3 mRNA are all expressed in the SCN (28, 29), lungs (30), liver (31), and cartilage (32), and Cry 1 and 2 mRNA are expressed in tissues such as the SCN (33), lung (34) and liver (35). Taken together, the detection of both the positive and negative limb of the circadian transcriptional-translational feedback loop supports the idea that the lens may contain its own circadian clock.

At the protein level, BMAL1, CLOCK and CRY2 were detected in the lens, but CRY1 and PER1-3 was undetectable (Figure 2), suggesting that these proteins may be more abundantly expressed during the night compared to during the day. Examining the expression of clock proteins at 4-hour intervals over a 24-hour period and their subcellular localisation during the light (10am) and the start of the dark period (6pm), revealed that BMAL1 expression was highest during the light period (6am-2pm) (Figure 3A), which corresponded with the nuclear localisation of BMAL1 at 10am (Figure 5A'). This is consistent with studies in other peripheral tissue cells, where BMAL1 levels and/or activity have been shown to be highest during the day and lowest at night (36–38). In this study, the pattern of expression for BMAL1 in the lens suggests during the light period, BMAL1 may be actively transcribing genes such as Nrf2 and those related to GSH homeostasis.

In contrast to BMAL1 expression in the lens, CLOCK expression did not fluctuate over the 24-hour period (Figure 3B) and the subcellular localisation of CLOCK remained nuclear during the light vs dark period (Figures 5E–H, E'–H'). This is consistent with the finding in rodent SCN that CLOCK shows stable levels during the 24-hour cycle and is constitutively expressed in the mouse SCN (36, 39). In other tissues, it has been reported that constitutively expressed CLOCK has the potential to make temporally specific associations, alternating between BMAL1 and PER/CRY, thus resulting in transcriptional activation or repression, respectively. In addition, it has also been reported that CLOCK is available to bind to other target proteins such as the p65 subunit of NF-kB (40) which in the lens has been shown to be associated with oxidative-induced damage in human lens epithelial cells (41).

At the protein level, circadian oscillation of clockwork negative factors such as PERs and CRYs were expected to be in anti-phase with BMAL1, and to be more highly expressed during the dark period relative to the night based on studies on mouse SCN (36). In support of this, western blotting of lens samples collected during the day revealed negligible labelling for PER1-3 and CRY 1-2 compared to BMAL1 and CLOCK (Figure 2). When examining CRY2 expression over a 24-hour period, it was revealed that expression was relatively low at all time points except at 6pm (Figure 3C), confirming that at least for CRY2, its peak expression at night was out of phase with peak BMAL1 expression during the day. Unfortunately, we were unable to replicate this with CRY1 or the PER isoforms. Despite testing with different commercial antibodies, our western blot results were inconsistent, and we could not obtain a reliable pattern of expression (see Supplementary Figure 1).

Having established the expression pattern for the core clock protein BMAL1 in the lens, we next examined the expression of NRF2 and GSH related proteins (GCLC, GS and GR) at different times of the day (Figure 4). We expected that if BMAL1 was driving NRF2 expression that BMAL1 and NRF2 expression would be in phase with each other as reported in female mouse lenses (24). However, in our study, using male mouse lenses, NRF2 expression remained relatively steady over the 24-hour period (Figure 4A). The difference may be due to sexual dimorphism in the expression of Nrf2 (13) where it was reported that Nrf2 transcript expression in the liver was highest during the day than at night in female but not males, with Nrf2 transcript levels also higher in females than in males. In the same manner, NRF2 protein expression might also exhibit sexual dimorphism and explain the lack of obvious time of day differences in NRF2 expression in male lenses. Given that is has become increasingly apparent that sex differences exist in terms of antioxidant defence and the regulation of redox homeostasis (42), it is clear that further studies comparing male and female expression of Nrf2 in the lens should be conducted as if there are sex differences in Nrf2 expression, this might impact GSH regulation.

NRF2 is a transcription factor which induces the transcription of various genes involved in redox balance in response to oxidative stress (43–45). These include GCLC which is involved in the first step of GSH synthesis, GS which is involved in the second step of GSH synthesis and GR that is involved in the regeneration of GSH. Given that we did not see any obvious time of time day differences in the expression of NRF2, it was uncertain whether we would observe differences in NRF2 regulated GCLC and GR expression. However, our studies showed that GCLC expression increased during the later part of the day and through to the dark period (2pm-6am) (Figure 4B), while GS and GR levels peaked at the start of the dark period (Figures 4C, D). While we did not measure enzyme activity *per se*, these findings indicate that GSH synthesis and regeneration may be higher during the dark period.

Given that BMAL1/CLOCK has been shown to drive NRF2 expression in other tissues (17, 24), we reasoned that examining their subcellular localisation might give us an idea of what time of day these proteins were transcribing genes (Figure 5), and whether this correlated to specific regions in the lens which contain nucleated cells: the anterior epithelium which is in the direct pathway of light, and the lens equator, which is not in the direct pathway of light as it covered by the iris, but represents nucleated epithelial and fiber cells area that provide the majority of lens GSH via GSH synthesis (46). However, it was difficult to make a correlation. At the anterior pole and lens equator, CLOCK localised to the nuclei at each time point, while BMAL1 and NRF2 appeared to shuttle in and out of the nuclei at different times. While this might suggest a temporal association between BMAL1 driven transcription/translation of NRF2, we cannot be certain since BMAL1 and CLOCK can each separately bind to other proteins (40, 47) and NRF2 can transcribe genes involved in xenobiotic disposition, protection from electrophiles and general stress response (48, 49). As such, the presence of BMAL1 in the nuclei is not solely indicative of Nrf2 transcription nor the presence of NRF2 in the nuclei solely indicative of transcription of genes involved in GSH homeostasis. However, the finding that GSH levels oscillated over a 24-hour period does provide supportive evidence that regulation of GSH levels may be circadian driven. GSH levels were shown to rise towards the start of night (6pm) which correlates with the higher expression of GS and GR

during the dark period. This finding suggests that higher levels of GSH may be required at the start of the active phase of the nocturnal rat. While exogenous ROS sources, such as UV light from sunlight may contribute to the oxidative milieu, endogenous ROS sources such as the mitochondria (50) are likely to be more significant ROS contributors to the nocturnal rat. Therefore, higher levels of GSH can act to directly scavenge ROS or act as a cofactor for antioxidant enzymes such as glutathione peroxidase (GPx), which uses GSH as a cofactor to detoxify hydrogen peroxide (H_20_2) (51).

Measurements of GSH levels in the aqueous humour over a 24-hour period also revealed that GSH levels fluctuate over the course of the day/night. However, the peaks and troughs of GSH in the lens were opposite to that seen in the aqueous humour. GSH levels in the aqueous humour were lowest at the start of the night (6pm) and GSH levels in the lens highest at the start of night. To our knowledge, no other studies have measured GSH levels in the lens and aqueous humour at different times of the day. From our data it is not possible to determine whether GSH levels follow a circadian rhythm per se as since levels peaked at 6am and 6pm this could also indicate the presence of an ultradian rhythm of 12 hours. However, studies have measured intraocular pressure (IOP) where it has been shown that IOP is highest during the day due to increased aqueous humour secretion and lowest at night due to decreased aqueous humour secretion at night (52). Interestingly these patterns of secretion are similar in both nocturnal (rodents) and diurnal (human) studies. In this study, GSH levels in the aqueous humour mirror the same pattern as fluctuations in IOP which makes sense given that GSH is delivered to the lens via the aqueous humour. This suggests that there is some circadian input into the control of lens GSH levels and that GSH availability to the lens differs at different times of the day. In the rat lens, low GSH levels in the aqueous humour and high levels of GSH in the lens may reflect an increase in the uptake of GSH by the lens, and together with GSH synthesis and/or regeneration of GSH may enable the lens to ensure GSH levels are highest towards the start of night. In terms of diurnal animals like humans, it is expected that GSH levels in the human aqueous humour would mirror that of the rat aqueous humour, but that GSH levels in the human lens would be higher during the day versus the night to counteract increased oxidative stress encountered during the day. However, testing using a diurnal animal model would be required to confirm this.

Taken together, our findings demonstrate the lens to contain the molecular machinery of a circadian clock that may be used to ensure high GSH levels in the lens are available to protect against ROS generated through increased metabolic activity and/or exogenous sources. Further work will be aimed at knocking down the expression of BMAL1 to see the effect this has on the other clock component genes as well as NRF2 and GSH levels. Moreover, while our findings implies that there is a rhythmic expression of clock and redox proteins and GSH levels in the lens, further experiments are required to demonstrate that these rhythmic expressions persist in constant darkness and are therefore truly circadian in nature. This will help to establish a direct link between a circadian clock in the lens regulating GSH levels. Since GSH levels in the lens are known to decline with age, understanding these mechanisms may provide a better understanding as to whether the circadian clock can be used to restore GSH levels in the lens with advancing age.

Data availability statement

The original contributions presented in the study are included in the article/Supplementary Material, further inquiries can be directed to the corresponding author/s

Ethics statement

The animal study was approved by University of Auckland Animal Ethics Committee (Ethics number R001413). The study was conducted in accordance with the local legislation and institutional requirements.

Author contributions

BL: Data curation, Formal analysis, Methodology, Supervision, Writing – original draft. HS: Formal analysis, Methodology, Supervision, Writing – review & editing. RM: Data curation, Formal analysis, Methodology, Supervision, Writing – review & editing. CL: Data curation, Writing – original draft. ZW: Data curation, Writing – original draft. TN: Data curation, Writing – original draft. PD: Investigation, Writing – review & editing. RP: Investigation, Supervision, Writing – review & editing. JL: Conceptualization, Formal analysis, Funding acquisition, Investigation, Methodology, Supervision, Writing – original draft, Writing – review & editing.

Funding

The author(s) declare financial support was received for the research, authorship, and/or publication of this article. The Royal Society of New Zealand Marsden Fund provided funding for the project along with postgraduate scholarships for CL and TN.

Acknowledgments

We thank Dr. George Guo for statistical advice.

Conflict of interest

The authors declare that the research was conducted in the absence of any commercial or financial relationships that could be construed as a potential conflict of interest.

Publisher's note

All claims expressed in this article are solely those of the authors and do not necessarily represent those of their affiliated organizations, or those of the publisher, the editors and the

reviewers. Any product that may be evaluated in this article, or claim that may be made by its manufacturer, is not guaranteed or endorsed by the publisher.

Supplementary material

The Supplementary Material for this article can be found online at: https://www.frontiersin.org/articles/10.3389/fopht.2024.1407582/full#supplementary-material

SUPPLEMENTARY FIGURE 1
Expression of negative arm clock component proteins in the rat lens at different times of the day. **(A)** Expression of CRY1, **(B)** PER2 and **(C)** PER3 over a 24-hour time period. Lens tissue (n=8 rats) was harvested at 4-hour intervals over a 24-hour period. 20µg lens protein/lane was electrophoresed on an SDS PAGE gel and protein levels analysed by Western blotting and expressed relative to the β-actin internal control. Antibodies for CRY1 (Protein Tech 13474-1-AP), PER2 (Protein tech 12550-1-AP), PER2 (Abcam, ab179813) and PER3 (Protein Tech 12550-1-AP) were tested. Most western blots revealed no bands or very faint bands with high background with the "best" blots for CRY1, PER2 and PER3 expression shown. While the PER3 blot looks promising, repeated western blots failed to give a similar result making it difficult to obtain a reliable pattern of expression.

References

1. Lou M. Thiol regulation in the lens. *J Ocul Pharmacol Ther*. (2000) 16:137–48. doi: 10.1089/jop.2000.16.137

2. Reddy VN, Giblin FJ. Metabolism and function of glutathione in the lens. *Ciba Found Symp*. (1984) 106:65–87. doi: 10.1002/9780470720875.ch5

3. Giblin FJ. Glutathione: a vital lens antioxidant. *J Ocul Pharmacol Ther*. (2000) 16:121–35. doi: 10.1089/jop.2000.16.121

4. Harding JJ. Free and protein-bound glutathione in normal and cataractous human lenses. *Biochem J*. (1970) 117:957–60. doi: 10.1042/bj1170957

5. Truscott RJ. Age-related nuclear cataract: a lens transport problem. *Ophthalmic Res*. (2000) 32:185–94. doi: 10.1159/000055612

6. Truscott RJ. Age-related nuclear cataract-oxidation is the key. *Exp Eye Res*. (2005) 80:709–25. doi: 10.1016/j.exer.2004.12.007

7. Lim JC, Grey AC, Zahraei A, Donaldson PJ. Age-dependent changes in glutathione metabolism pathways in the lens: New insights into therapeutic strategies to prevent cataract formation-A review. *Clin Exp Ophthalmol*. (2020) 48:1031–42. doi: 10.1111/ceo.13801

8. Takahashi JS. Transcriptional architecture of the mammalian circadian clock. *Nat Rev Genet*. (2017) 18:164–79. doi: 10.1038/nrg.2016.150

9. Cox KH, Takahashi JS. Circadian clock genes and the transcriptional architecture of the clock mechanism. *J Mol Endocrinol*. (2019) 63:R93–R102. doi: 10.1530/JME-19-0153

10. Stangherlin A, Reddy AB. Regulation of circadian clocks by redox homeostasis. *J Biol Chem*. (2013) 288:26505–11. doi: 10.1074/jbc.R113.457564

11. Wilking M, Ndiaye M, Mukhtar H, Ahmad N. Circadian rhythm connections to oxidative stress: implications for human health. *Antioxid Redox Signal*. (2013) 19:192–208. doi: 10.1089/ars.2012.4889

12. White BP, Davies MH, Schnell RC. Circadian variations in hepatic glutathione content, gamma-glutamylcysteine synthetase and gamma-glutamyl transferase activities in mice. *Toxicol Lett*. (1987) 35:217–23. doi: 10.1016/0378-4274(87)90209-8

13. Xu YQ, Zhang D, Jin T, Cai DJ, Wu Q, Lu Y, et al. Diurnal variation of hepatic antioxidant gene expression in mice. *PloS One*. (2012) 7:e44237. doi: 10.1371/journal.pone.0044237

14. Radha E, Hill TD, Rao GH, White JG. Glutathione levels in human platelets display a circadian rhythm in vitro. *Thromb Res*. (1985) 40:823–31. doi: 10.1016/0049-3848(85)90319-6

15. Neuschwander-Tetri BA, Rozin T. Diurnal variability of cysteine and glutathione content in the pancreas and liver of the mouse. *Comp Biochem Physiol B Biochem Mol Biol*. (1996) 114:91–5. doi: 10.1016/0305-0491(96)83706-0

16. Diaz-Munoz M, Hernandez-Munoz R, Suarez J, Chagoya de Sanchez V. Day-night cycle of lipid peroxidation in rat cerebral cortex and their relationship to the glutathione cycle and superoxide dismutase activity. *Neuroscience*. (1985) 16:859–63. doi: 10.1016/0306-4522(85)90100-9

17. Pekovic-Vaughan V, Gibbs J, Yoshitane H, Yang N, Pathiranage D, Guo B, et al. The circadian clock regulates rhythmic activation of the NRF2/glutathione-mediated antioxidant defense pathway to modulate pulmonary fibrosis. *Genes Dev*. (2014) 28:548–60. doi: 10.1101/gad.237081.113

18. Ponce IT, Rezza IG, Delgado SM, Navigatore LS, Bonomi MR, Golini RL, et al. Daily oscillation of glutathione redox cycle is dampened in the nutritional vitamin A deficiency. *Biol Rhythm Res*. (2012) 43:351–72. doi: 10.1080/09291016.2011.593847

19. Beaver LM, Klichko VI, Chow ES, Kotwica-Rolinska J, Williamson M, Orr WC, et al. Circadian regulation of glutathione levels and biosynthesis in Drosophila melanogaster. *PloS One*. (2012) 7:e50454. doi: 10.1371/journal.pone.0050454

20. He F, Ru X, Wen T. NRF2, a transcription factor for stress response and beyond. *Int J Mol Sci*. (2020) 21(13):4777. doi: 10.3390/ijms21134777

21. Abe M, Itoh MT, Miyata M, Ishikawa S, Sumi Y. Detection of melatonin, its precursors and related enzyme activities in rabbit lens. *Exp Eye Res*. (1999) 68:255–62. doi: 10.1006/exer.1998.0601

22. Abe M, Itoh MT, Miyata M, Shimizu K, Sumi Y. Circadian rhythm of serotonin N -acetyltransferase activity in rat lens. *Exp Eye Res*. (2000) 70:805–8. doi: 10.1006/exer.2000.0845

23. Alkozi HA, Wang X, Perez de Lara MJ, Pintor J. Presence of melanopsin in human crystalline lens epithelial cells and its role in melatonin synthesis. *Exp Eye Res*. (2017) 154:168–76. doi: 10.1016/j.exer.2016.11.019

24. Chhunchha B, Kubo E, Singh DP. Clock protein Bmal1 and Nrf2 cooperatively control aging or oxidative response and redox homeostasis by regulating rhythmic expression of Prdx6. *Cells*. (2020) 9(8):1861. doi: 10.3390/cells9081861

25. Nagano M, Adachi A, Nakahama K, Nakamura T, Tamada M, Meyer-Bernstein E, et al. An abrupt shift in the day/night cycle causes desynchrony in the mammalian circadian center. *J Neurosci*. (2003) 23:6141–51. doi: 10.1523/JNEUROSCI.23-14-06141.2003

26. Martis RM, Grey AC, Wu H, Wall GM, Donaldson PJ, Lim JC. N-Acetylcysteine amide (NACA) and diNACA inhibit H(2)O(2)-induced cataract formation ex vivo in pig and rat lenses. *Exp Eye Res*. (2023) 234:109610. doi: 10.1016/j.exer.2023.109610

27. Krizo JA, Mintz EM. Sex differences in behavioral circadian rhythms in laboratory rodents. *Front Endocrinol (Lausanne)*. (2015) 5:234. doi: 10.3389/fendo.2014.00234

28. Hamada T, LeSauter J, Venuti JM, Silver R. Expression of Period genes: rhythmic and nonrhythmic compartments of the suprachiasmatic nucleus pacemaker. *J Neurosci*. (2001) 21:7742–50. doi: 10.1523/JNEUROSCI.21-19-07742.2001

29. Yamaguchi Y, Okada K, Mizuno T, Ota T, Yamada H, Doi M, et al. Real-time recording of circadian Per1 and Per2 expression in the suprachiasmatic nucleus of freely moving rats. *J Biol Rhythms*. (2016) 31:108–11. doi: 10.1177/0748730415621412

30. Liu B, Xu K, Jiang Y, Li X. Aberrant expression of Per1, Per2 and Per3 and their prognostic relevance in non-small cell lung cancer. *Int J Clin Exp Pathol*. (2014) 7:7863–71.

31. Cailotto C, Lei J, van der Vliet J, van Heijningen C, van Eden CG, Kalsbeek A, et al. Effects of nocturnal light on (clock) gene expression in peripheral organs: a role for the autonomic innervation of the liver. *PloS One*. (2009) 4:e5650. doi: 10.1371/journal.pone.0005650

32. Snelling SJ, Forster A, Mukherjee S, Price AJ, Poulsen RC. The chondrocyte-intrinsic circadian clock is disrupted in human osteoarthritis. *Chronobiol Int*. (2016) 33:574–9. doi: 10.3109/07420528.2016.1158183

33. Park K, Kang HM. Cloning and circadian expression of rat Cry1. *Mol Cells*. (2004) 18:256–60. doi: 10.1016/S1016-8478(23)13110-4

34. Song P, Li Z, Li X, Yang L, Zhang L, Li N, et al. Transcriptome profiling of the lungs reveals molecular clock genes expression changes after chronic exposure to ambient air particles. *Int J Environ Res Public Health*. (2017) 14(1):90. doi: 10.3390/ijerph14010090

35. Crew RC, Waddell BJ, Mark PJ. Obesity-induced changes in hepatic and placental clock gene networks in rat pregnancy. *Biol Reprod*. (2018) 98:75–88. doi: 10.1093/biolre/iox158

36. Maywood ES, O'Brien JA, Hastings MH. Expression of mCLOCK and other circadian clock-relevant proteins in the mouse suprachiasmatic nuclei. *J Neuroendocrinol*. (2003) 15:329–34. doi: 10.1046/j.1365-2826.2003.00971.x

37. Rey G, Cesbron F, Rougemont J, Reinke H, Brunner M, Naef F. Genome-wide and phase-specific DNA-binding rhythms of BMAL1 control circadian output functions in mouse liver. *PloS Biol*. (2011) 9:e1000595. doi: 10.1371/journal.pbio.1000595

38. Silver AC, Arjona A, Hughes ME, Nitabach MN, Fikrig E. Circadian expression of clock genes in mouse macrophages, dendritic cells, and B cells. *Brain Behav Immun*. (2012) 26:407–13. doi: 10.1016/j.bbi.2011.10.001

39. von Gall C, Noton E, Lee C, Weaver DR. Light does not degrade the constitutively expressed BMAL1 protein in the mouse suprachiasmatic nucleus. *Eur J Neurosci*. (2003) 18:125–33. doi: 10.1046/j.1460-9568.2003.02735.x

40. Spengler ML, Kuropatwinski KK, Comas M, Gasparian AV, Fedtsova N, Gleiberman AS, et al. Core circadian protein CLOCK is a positive regulator of NF-kappaB-mediated transcription. *Proc Natl Acad Sci U S A*. (2012) 109:E2457–65. doi: 10.1073/pnas.1206274109

41. Jin XH, Ohgami K, Shiratori K, Koyama Y, Yoshida K, Kase S, et al. Inhibition of nuclear factor-kappa B activation attenuates hydrogen peroxide-induced cytotoxicity in human lens epithelial cells. *Br J Ophthalmol*. (2007) 91:369–71. doi: 10.1136/bjo.2006.107037

42. Tiberi J, Cesarini V, Stefanelli R, Canterini S, Fiorenza MT, La Rosa P. Sex differences in antioxidant defence and the regulation of redox homeostasis in physiology and pathology. *Mech Ageing Dev*. (2023) 211:111802. doi: 10.1016/j.mad.2023.111802

43. Reddy NM, Kleeberger SR, Cho HY, Yamamoto M, Kensler TW, Biswal S, et al. Deficiency in Nrf2-GSH signaling impairs type II cell growth and enhances sensitivity to oxidants. *Am J Respir Cell Mol Biol*. (2007) 37:3–8. doi: 10.1165/rcmb.2007-0004RC

44. Malhotra D, Portales-Casamar E, Singh A, Srivastava S, Arenillas D, Happel C, et al. Global mapping of binding sites for Nrf2 identifies novel targets in cell survival response through ChIP-Seq profiling and network analysis. *Nucleic Acids Res*. (2010) 38:5718–34. doi: 10.1093/nar/gkq212

45. Harvey CJ, Thimmulappa RK, Singh A, Blake DJ, Ling G, Wakabayashi N, et al. Nrf2-regulated glutathione recycling independent of biosynthesis is critical for cell survival during oxidative stress. *Free Radic Biol Med*. (2009) 46:443–53. doi: 10.1016/j.freeradbiomed.2008.10.040

46. Fan X, Monnier VM, Whitson J. Lens glutathione homeostasis: Discrepancies and gaps in knowledge standing in the way of novel therapeutic approaches. *Exp Eye Res*. (2017) 156:103–11. doi: 10.1016/j.exer.2016.06.018

47. Timmons GA, Carroll RG, O'Siorain JR, Cervantes-Silva MP, Fagan LE, Cox SL, et al. The circadian clock protein BMAL1 acts as a metabolic sensor in macrophages to control the production of pro IL-1beta. *Front Immunol*. (2021) 12:700431. doi: 10.3389/fimmu.2021.700431

48. Shen G, Kong AN. Nrf2 plays an important role in coordinated regulation of Phase II drug metabolism enzymes and Phase III drug transporters. *Biopharm Drug Dispos*. (2009) 30:345–55. doi: 10.1002/bdd.680

49. Unoki T, Akiyama M, Kumagai Y. Nrf2 activation and its coordination with the protective defense systems in response to electrophilic stress. *Int J Mol Sci*. (2020) 21(2):545. doi: 10.3390/ijms21020545

50. Babizhayev MA. Mitochondria induce oxidative stress, generation of reactive oxygen species and redox state unbalance of the eye lens leading to human cataract formation: disruption of redox lens organization by phospholipid hydroperoxides as a common basis for cataract disease. *Cell Biochem Funct*. (2011) 29:183–206. doi: 10.1002/cbf.1737

51. Ganea E, Harding JJ. Glutathione-related enzymes and the eye. *Curr Eye Res*. (2006) 31:1–11. doi: 10.1080/02713680500477347

52. Goel M, Picciani RG, Lee RK, Bhattacharya SK. Aqueous humor dynamics: a review. *Open Ophthalmol J*. (2010) 4:52. doi: 10.2174/1874364101004010052

frontiers | Frontiers in Ophthalmology

TYPE Review
PUBLISHED 05 September 2024
DOI 10.3389/fopht.2024.1414483

OPEN ACCESS

EDITED BY
Barbara Pierscionek,
Anglia Ruskin University, United Kingdom

REVIEWED BY
Michael Wormstone,
The University of Nottingham Ningbo, China
John I. Clark,
University of Washington, United States

*CORRESPONDENCE
Angus C. Grey
ac.grey@auckland.ac.nz

RECEIVED 09 April 2024
ACCEPTED 12 August 2024
PUBLISHED 05 September 2024

CITATION
MacFarlane ER, Donaldson PJ and Grey AC (2024) UV light and the ocular lens: a review of exposure models and resulting biomolecular changes.
Front. Ophthalmol. 4:1414483.
doi: 10.3389/fopht.2024.1414483

UV light and the ocular lens: a review of exposure models and resulting biomolecular changes

Emily R. MacFarlane, Paul J. Donaldson and Angus C. Grey*

Department of Physiology, School of Medical Sciences, New Zealand National Eye Centre, University of Auckland, Auckland, New Zealand

UV light is known to cause damage to biomolecules in living tissue. Tissues of the eye that play highly specialised roles in forming our sense of sight are uniquely exposed to light of all wavelengths. While these tissues have evolved protective mechanisms to resist damage from UV wavelengths, prolonged exposure is thought to lead to pathological changes. In the lens, UV light exposure is a risk factor for the development of cataract, which is a condition that is characterised by opacity that impairs its function as a focusing element in the eye. Cataract can affect spatially distinct regions of the lens. Age-related nuclear cataract is the most prevalent form of cataract and is strongly associated with oxidative stress and a decrease in the antioxidant capacity of the central lens region. Since UV light can generate reactive oxygen species to induce oxidative stress, its effects on lens structure, transparency, and biochemistry have been extensively investigated in animal models in order to better understand human cataract aetiology. A review of the different light exposure models and the advances in mechanistic understanding gained from these models is presented.

KEYWORDS

lens, UV light, cataract, UV-A, UV-B, oxidative stress, UV filter

1 Introduction

1.1 The cataract epidemic

Our sense of sight is critically dependent on the ability of the ocular lens to maintain its transparent and refractive properties over many decades of life. Failure to maintain lens transparency results in opacification of the lens due to the scattering of transmitted light rays. Lens opacification, or cataracts, are the leading cause of vision impairment and blindness worldwide (1), accounting for around half of all forms of vision loss (2). While cataract is a multi-factorial pathology, with genetics, increasing age, diabetes, and environmental factors such as exposure to cigarette smoking (3) and alcohol use (4) all contributing to its development, exposure to sunlight (UV radiation) is also a major risk factor (5–7), which can exacerbate different types of cataract.

Cortical cataract, the second most prevalent form of cataract, occurs earlier than age-related nuclear (ARN) cataract (8–10), and progresses slowly before manifesting as tissue damage in the outer cortex of the lens (Figure 1A) (11). In contrast, ARN cataract in the human lens (Figure 1B) occurs when the intrinsic repair and protection mechanisms that exist to mitigate the effects of oxidative stress slowly deteriorate or become ineffective (12). Under oxidative stress conditions, thiol groups of proteins are easily oxidised to form protein mixed disulfides with oxidised glutathione (PSSG), cysteine (PSSC), and eventually, protein: protein cross-links (PSSP) (12). This accumulated damage can change protein structure and function, and leads to protein aggregation and insolubilisation (13, 14), which causes the light scattering that is characteristic of ARN cataract. Posterior subcapsular cataracts (Figure 1C) are characterised by dysplasia of the equatorial epithelial cells (15). On their own, they are relatively uncommon (16), and are generally associated with other types of opacities, especially in those aged >80 years old (17).

Currently, the only treatment for human cataract is surgical removal of the opaque lens and implantation of an intra-ocular lens (IOL). Cataract surgery is one of the most commonly performed elective surgical procedures in developed countries (18) and is highly successful. The main outcomes include a marked improvement in visual acuity, decreased risk of falls, and improved quality of life (19, 20). In economically developed countries, cataract blindness in the community is rare, yet across developing countries with low rates of cataract surgery, blindness from unoperated cataract is common (21). Cataract surgery is a substantial cost to global health systems. For example, in the USA, approximately 3 million surgeries are performed each year, with an estimated cost of >$3.4 billion in annual Medicare spending (19, 22). In developing countries, costs associated with cataract surgery can be prohibitive (23, 24). Hence there is a need to develop more cost-effective therapeutic alternatives to cataract surgery to delay, prevent, or reverse cataract formation (25).

Unfortunately, investigating the causes and mechanisms of human cataract formation and the ongoing effort to develop non-surgical anti-cataract therapies has associated difficulties. The use of post-mortem human donor tissue suffers from an inconsistent supply of cataractous lenses (26), as well as variable post-mortem delays between death and tissue processing (27). In addition, lenses obtained from human donors have significant biochemical variability. For example, the lifestyle, genetics, underlying diseases, and causes of death of individual donors will all contribute to this variability, and therefore the consistency of subsequent analysis. Finally, whole, cataractous lenses are now less readily available (28) due to the arrival of the extracapsular cataract surgical extraction (ECCE) method (29), where the nucleus and cortex are now emulsified and removed, leaving the capsule behind that can then be used to hold the IOL implant.

As a consequence of these challenges to utilising human tissue in cataract research, animal models have been used to investigate the underlying mechanisms of cataract formation (26) following a range of cataractous insults. While animal models of cataract aim to recapitulate the characteristics seen in human cataract that take many decades to develop, they are often induced in a laboratory environment over a relatively short time period. Lens parameters that are typically monitored in these models include transparency and morphological changes (that induce light scattering), biochemical changes (such as antioxidant depletion and pigmentation), and biomechanical changes (such as stiffening of the lens) that only manifest as cataract in later in life (30–32).

Animal models that mimic the distinctly different cataract phenotypes observed in ARN cataract (27) and diabetic cortical cataract (33) have previously been reviewed. In this review, animal models used to determine the mechanisms of lens cataract

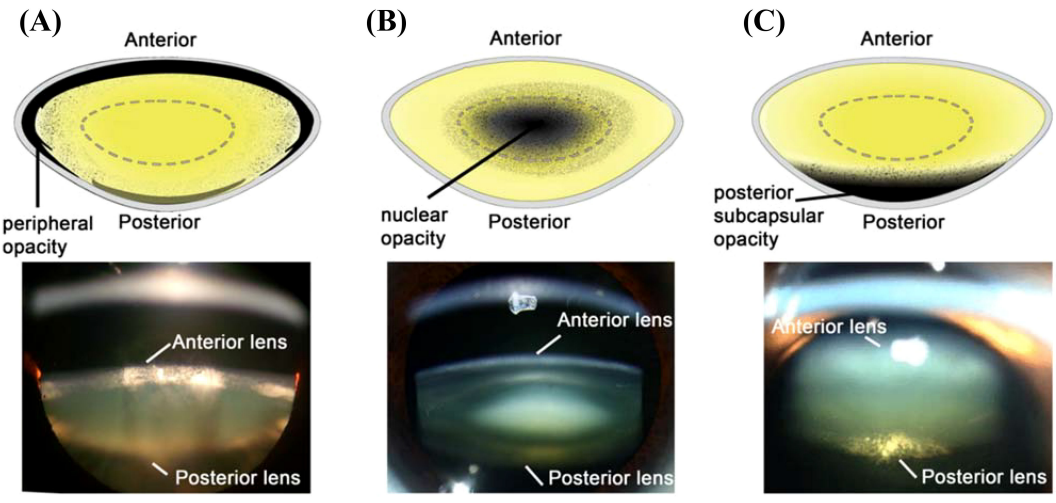

FIGURE 1
Schematic diagrams (Top) and Scheimpflug slit-lamp photographic (bottom) images of the three main types of cataracts. **(A)** cortical cataract, from Uspal NG, Schapiro ES (2011). Cataracts as the initial manifestation of type 1 diabetes mellitus. Paediatric Emergency Care. 27 (2): 132–4. **(B)** Nuclear cataract, from Ophthalmic Atlas Images by EyeRounds.org. **(C)** Posterior subcapsular cataract, from Chaudhary M, Shah DN, Chaudhary, RP (2017). Scleritis and Takayasu's disease. Nepalese Journal of Ophthalmology (18): 170–174. Reproduced with permission from MDPI under Creative Commons Attribution (CC BY 4.0).

formation following exposure to UV radiation are presented and evaluated. We will first review the evidence for the cataractous effects of UV radiation in humans, and the intrinsic properties that the human eye has to protect against cataract formation. This will provide a contextualisation of the animal models used to study the role of UV exposure in cataract formation.

1.2 UV light in human cataract formation: exposure, epidemiology, and effects of aging

UV radiation is a known toxin to biological tissues and is classified as a carcinogen (34). The sun produces UV radiation in the UV-A, -B, and -C ranges. Approximately 97% of the wavelengths of radiation that pass through the atmosphere and reach Earth are UV-A (λ = 315-400nm), while ~3% is UV-B (λ = 280-315nm) (35, 36). Solar UV-C (λ = 200-280nm) is blocked by the Earth's atmosphere (35) and UV-C wavelengths are produced in only a few settings on Earth, such as Arc welding.

Three main types of tissue damage can result from light exposure. While photothermal and photomechanical damage typically result from exposure to the upper end of visible and infrared light wavelengths, photochemical damage is the result of exposure to wavelengths in the UV and visible light range (37). Photochemical damage is further divided into three types. Ablation is utilised extensively in ophthalmology, where high energy wavelengths under 200 nm remove or shape ocular tissue structures. In contrast, both photo-oxidative damage and photosensitised reactions are the result of UV-A and UV-B exposure, typically as a result of long exposure times (37).

Several mechanisms have evolved to protect the eye from the phototoxic effects of UV radiation. For example, the cornea absorbs the majority of incoming UV-B light and a small amount of UV-A (38–41). However, the age of the eye has an impact on UV light penetration and consequently the amount of UV light entering the eye and reaching the lens increases with age (38). Once adulthood is reached, it is assumed that the retina is no longer exposed to UV radiation, due to the decreasing transmission properties of the lens (42). The lens absorbs most of the incoming UV-A, and the small amount of UV-B radiation that is not absorbed by the cornea (Table 1) (39, 40).

Considerable epidemiological evidence shows the harmful effects of different UV wavelengths of light on the lens. The World Health Organization estimates that cataracts in up to 20% of the people who become blind annually may be caused or enhanced by sun exposure (43). Generally, UV-B light has been associated with an increased risk of cortical cataracts (Figure 1A) and subcapsular cataract (Figure 1C) (44–46), but there is less evidence for the effects of UV-B exposure on nuclear cataracts in humans (47, 48). This is possibly due to its limited depth of penetration into the lens in humans (49), monkeys (50), and rats (51). Although once dismissed as a risk factor for cataract, UV-A has since been associated with nuclear cataract formation (Figure 1B) (52, 53), with UV-A light shown to penetrate deep into the lens nucleus of guinea pigs (44).

Epidemiological studies have shown that higher rates of cataract are observed in populations that spend more time outdoors (54) or in the sun (55), in rural as opposed to urban living (56–58), and other specific geospatial relationships (17, 47, 48, 57, 59–73). For example, higher exposure to sunlight significantly increases the risk of age-related cataract, with a slight increased risk of cortical cataract, but no risk effect on nuclear or posterior subcapsular cataract (74). This higher exposure to sunlight can be from reflection of UV from different surfaces in the environment, with snowfields and/or increased altitude (75) having the most reflection, and forest the least (76). Interestingly, prevalence of the type of cataract appears to change with global location. Sasaki and colleagues showed that cortical opacification was more prevalent in Iceland and Japan, while nuclear cataract was more prevalent amongst Singaporeans (77). Furthermore, variations in populations within Japan show an increased prevalence for nuclear cataract formation in Okinawa due to high UV exposure (78).

Brunescence, the process of progressive pigmentation of the aging human lens which turns a young, colourless lens increasingly yellow, brown and even black, has been specifically linked to UV exposure (53). Moreover, brunescent cataracts are particularly prevalent in populations living in tropical regions of the world due to their higher exposure to solar radiation (76, 79, 80). Several of the chromophores and fluorophores (81, 82) responsible for lens colouration have been isolated and identified, including advanced glycation end products (83–86), and tryptophan oxidation products (87–89). Interestingly, some of these tryptophan metabolites are beneficial in young lenses where they play an important role in the intrinsic UV protection mechanism of the eye but become detrimental to the lens following chronic exposure to UV.

TABLE 1 Corneal absorbance of incoming UV light as a function of age, and lenticular absorbance of incoming light.

UV Range	λ (nm)	Cornea (% absorption)		Lens (% absorption)
		Young	Old	
UV-B	280-315	90 (38) – 92 (39)	60 (38)	36 – 52 (39)
UV-A	315-400	18 (39) – 45 (38)	80 (38)	2 (39)

1.3 Lens UV exposure protection mechanisms

The young lens contains several tryptophan metabolites, which act as UV filter compounds that absorb light in the 300 to 400 nm wavelength range (90, 91). Approximately 95% of the light that enters the lens is absorbed by these compounds, with the remaining 5% being absorbed by tryptophan residues on proteins (92). UV filters also decrease chromatic aberration, thus enhancing visual acuity (93), and aid in protecting the retina from induced photo-oxidative damage (92). Synthesis of UV filters occurs between late pregnancy and birth, with some filters

detectable in lenses five months post-natal (94). There are two main types of filters: primary and secondary filters. In young lenses, the ratio of primary to secondary is approximately 10:1, but this decreases with age to 2:1 (91).

When found in their free form, both primary and secondary filters are photochemically inert, and act to dissipate UV energy (95) without the production of harmful radicals (93, 96, 97), that could induce oxidative stress (97) (Figure 2). Photo-oxidative damage occurs when incident light reacts with a tissue chromophore such as a UV filter, which then attains an excited state. Reactive oxygen species (ROS) are generated through interaction of the excited state chromophore with a variety of substrates, which go on to oxidatively damage biomolecules (37). In contrast, photosensitisation reactions occur when oxygen and a photosensitiser molecule absorb the UV to produce hydrogen peroxide (H_2O_2). This can either be detoxified by the action of glutathione peroxidase, or go on to form the hydroxyl radical, which can damage a range of biomolecules, including DNA, proteins, and lipids (37).

While the young lens contains high levels of glutathione (GSH) to protect it from oxidative stress through direct neutralisation of ROS, the age-related decline in this key antioxidant makes the lens vulnerable to cataract formation. This is due to the high concentration of cell membranes in the lens, which make it vulnerable to damage from free radical-mediated lipid peroxidation (37), its high protein concentration which can form irreversible protein-protein cross-links (12), and a variety of naturally occurring small molecules, such as UV filter molecules. While UV filters are highly efficient at dissipating energy, modifications to the filters, and the binding of filters to proteins within the lens, can change their ability to quench UV radiation (95), and instead act as photosensitisers in the aging human lens (98). These filters and their modifications are discussed herein, and their classification summarised (Table 2).

The primary UV filters in the human lens are kynurenine (kyn), 3-hydroxykynurenine (3OHK), and 3-hydroxykynurenine *O*-β-D-glucoside (3OHKG) (99–102). One of the intermediates in the formation of kyn from tryptophan metabolism, N-formyl-kynurenine (NFK), differs from other tryptophan metabolites in its photophysical properties, in that it acts as a photosensitiser to produce singlet oxygen and superoxide (103, 104). In the presence of oxygen, NFK is synthesised enzymatically by indoleamine 2,3-dioxygenase (IDO), which has been found in human lenses (105), or through tryptophan photolysis following *in vitro* exposure to UV light (106). NFK has been shown to bind to crystallin proteins under oxidative stress *in vitro* (107), and during exposure to sunlight (108), suggesting that in the absence of UV filters, it could be a key mediator of UV light induced damage in the lens. 3OHKG is the most abundant filter (109), and is formed via glycosylation of 3OHK (110). Kyn, 3OHK and 3OHKG are found prominently in young lenses (102), but decline at a rate of ~12% per decade, with kyn and 3OHK being nearly undetectable in 80 year old lenses (110).

The amino acid side chain of primary filters is unstable, and is thought to be able to spontaneously deaminate, to form an α-β-ketoalkene (109, 111–113), which is also highly unstable (94). The primary filters are able to form GSH adducts, whereby a molecule of GSH scavenges the deaminated filter, potentially protecting lens proteins from covalent binding of filters (111, 114). NAD(P)H has also been identified as a protective agent, scavenging the deaminated filters (109). High concentrations of GSH, such as those in young lenses, can protect the lens in two ways: by scavenging filter deamination products, and promoting the decomposition of kyn-protein adducts. GSH-conjugated UV filters increase with a corresponding decrease in free GSH, and therefore may contribute to a decreased capacity for nuclear GSH to protect lens proteins from cross-linking and insolubilisation (110). In addition to glutathionylation, all three primary filter compounds can also undergo cyclisation to form 3OHKG-yellow, kyn-yellow, and 3OHK-yellow respectively, although this is thought to be a slow process (109). Enzymatic modification of kyn can result in the formation of kynurenic acid, which acts as a photosensitiser and produces reactive oxygen species (104).

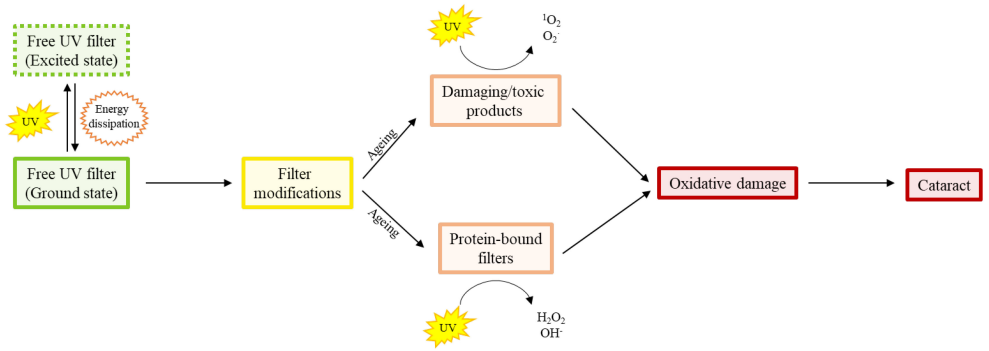

FIGURE 2
Diagram showing the age-related shift in proportion of free human UV filters to modified free and protein bound filters that produce oxidatively damaging species. The free (i.e. not bound to proteins) filters absorb UV light and dissipate the UV energy efficiently. However, with increasing age, there is conversion of filters to different compounds which produce singlet oxygen and superoxide radicals, and the binding of filters to proteins which produce peroxide and hydroxyl radicals, in response to UV light. It is this age-dependent accumulation of oxidative damage that is thought to be responsible for the initiation of ARN cataract.

TABLE 2 Classes of UV filters within the human lens.

Class of filter	Molecules	References
Primary	Kynurenine	(105, 263)
	3-hydroxykynurenine (3OHK)	(93, 102, 217)
	3-hydroxykynurenine glucoside (3OHKG)	(216, 266)
Secondary	GSH-kynurenine	(91, 267)
	GSH-3OHK	(267)
	GSH-3OHKG	(117, 268–270)
	Cys-3OHKG	(118)
	4(2-amino-3-hydroxyphenyl)-4-oxobutanoic acid O-β-D-glucoside	(94, 268)
	4(2-amino-3-hydroxyphenyl)-4-oxobutanoic acid O-β-D-di-glucoside	(99, 115, 267)
Modified	Kynurenine-yellow	(109)
	3OHK-yellow	(109)
	3OHKG-yellow	(109)
	3-hydroxyanthranillic acid	(102, 104)
Damaging/ toxic products	N-formyl-kynurenine	(104)
	Kynurenic acid	(104, 125, 129)
	Xanthurenic acid (XA)	(95, 128)
	Xanthurenic acid glucoside (XAG)	(95, 126)
	Oxo-, dioxo-, XAG	(128)
Protein interacting	Protein-kynurenine	(96, 131)
	Protein-3OHK	(119, 134)
	3OHK crosslinked products	(110)
	Protein-3OHKG	(110)

Primary and secondary filters act to dissipate incoming UV light without the formation of reactive or damaging species. The damaging and toxic products produce singlet oxygen and superoxide when excited by UV light, and protein bound filters produce peroxide and hydroxyl radicals when excited by UV light.

The secondary filters 4-(2-amino-3-hydroxyphenyl)-4-oxobutanoic acid *O*-β-D-glucoside (AHBG) and glutathionyl-3-hydroxykynurenine *O*-β-D-glucoside (GSH-3OHKG) are found predominantly in the lens nucleus (98, 110, 115, 116). The α-β-ketoalkene formed through primary filter deamination undergoes reduction to form AHBG (94), binds to GSH to create GSH-3OHKG (117), or free cysteine (118), and can bind to proteins through lysine, cysteine and histidine (119). 3OHK can also form 3-hydroxyanthranilic acid (3OAA), through the enzyme kynureninase (102). This molecule is also photochemically inert and inhibits the crosslinking of crystallins within the lens (104). High levels of GSH should prevent the autooxidation of 3OAA, but with falling GSH levels in aging lens, autooxidation can occur, producing H_2O_2 that can damage crystallins (120). For secondary filters, AHBG can undergo additional glycosylation to create 4-(2-amino-3-hydroxyphenyl)-4-oxobutanoic acid *O*-β-D-di-glucoside (AHBGD), but neither of these filters can bind to lens proteins. This is because neither compound is able to undergo deamination, in contrast to the other filters (121).

With increasing age, the levels of free UV filters decrease markedly (110), to the point where protein-bound UV filters and free UV filters are equal in concentration in the centre of normal lenses (122). UV filters, however, are present in cataractous tissue at higher concentrations than aged-matched controls (123). Deamination of the UV filters appears to be more pronounced in the nuclear region of the lens (110). This, in combination with the age-related decrease in nuclear GSH (124), would make the nuclear region more susceptible to the covalent linkage of UV filters to crystallin proteins.

In addition to binding to proteins, UV filters also create some damaging products. Xanthurenic acid (XA) is proposed to be one of the damaging products created through filter modification, although there are conflicting findings on whether or not XA is present in normal human lenses (103). However, it is present in cataractous lenses (125), with its glucoside (XAG), being present in brunescent cataracts (95, 126). XA could be formed enzymatically within the lens, from 3OHK, or through oxidation of 3OHK-yellow (127, 128), or through 3OHKG (95, 129). In addition to its glucoside, XA can be oxidised to form oxo-xanthurenic acid (OXA) and subsequently dioxo-xanthurenic acid (DOXA). DOXA may induce oxidative stress by generating oxygen free radicals, and also denature proteins through the crosslinking of crystallin proteins within the lens (128).

It is hypothesised that instead of protecting the lens from oxidative damage, the protein-bound UV filters may initiate oxidative damage, or act as an oxidant (130), resulting in the formation of proteins with altered physical and chemical properties (96, 98). These alterations include cross-linking, oxidation, fragmentation, peroxide formation, amino acid isomerisation, unfolding, and alterations to protein solubility (96–98, 131–134). The coloration or brunescence seen in the cataractous lenses is thought to be a result of accumulated oxidative reactions involving protein bound UV filters (121).

In summary, it has been shown that the human lens has developed a collection of filters to absorb the UV-A and UV-B light that passes through the cornea and penetrates into the different regions of the lens. UV light causes the degradation of these filters, with GSH preventing some of these damaged filters from binding to proteins. With age, the amount of UV light reaching the lens increases as the UV filtering capacity of the cornea declines. This increase in the incidence of UV light, plus a reduction in the efficacy of the filters and a parallel age-related decrease in the GSH availability in the lens, produces oxidative stress that leads to cataract formation. In the next sections, we review what we have learnt about the effects of UV light on lens transparency from a variety of different animal models and critically assess whether these models accurately model the effects of UV exposure seen in the human lens.

1.4 The use of animal models to mimic UV-induced cataract in humans

To understand how UV radiation induces lens cataract, a considerable number of studies have exposed animal lenses, either *in vivo* or *ex vivo*, to UV light (Supplementary Table 1). For *in vivo* models, sub-threshold doses can be applied over many days as

cumulative, chronic doses, whereas *ex vivo* models are subject to tissue degradation, and therefore often use acute, super-threshold doses. While *in vivo* models can better mimic the processes that occur in a whole system than an *ex vivo* lens, this comes at added time and financial cost. In addition, the penetration of UV light through the cornea changes depending on the animal model used. Hence, *ex vivo* models that use the lens alone must also consider that the dose given to the lens may be different to what the lens would experience *in vivo*, due to the lack of protection from the cornea. While both *in vivo* and *ex vivo* models can be used to assess recovery of lens tissue post-exposure, *ex vivo* models are again constrained by tissue degradation and time post-mortem. Despite these limitations, *ex vivo* models can be exposed to large doses of UV without concerns for animal welfare. In addition, lenses from larger animals, such as pigs and cows, can often be obtained as a by-product from abattoirs and are more cost effective than tissue derived from smaller laboratory animals. The downside of this, however, is that the exact age and other potential confounding factors such as disease, sex, and post-mortem time is less precise than small laboratory animals sourced in-house.

Despite the above factors, both *in vivo* and *ex vivo* models have been very effective in elucidating the mechanisms underlying cataract initiation and progression following UV exposure (Table 3). However, the relevance of the chosen animal model to the level of exposure and cataract development in the human lens is often not critically assessed. In each section of this review, we have assessed the relative merits of the existing animal models of UV cataract and have assigned the models to one of two categories: 1) Nocturnal animal models where "non-environmental" UV exposure serves as an oxidative stress that compromises lens transparency, and 2) UV light exposure in crepuscular and diurnal animals that could act as more relevant models that mimic the effects of UV light on cataract development in humans. While many of these animal studies investigated alterations in gene expression (135–140) and DNA damage (141, 142) upon irradiation, in this review we focus on the morphological, biochemical, metabolic, and protein changes that characterise the cataract phenotype induced as a result of UV-A or UV-B exposure.

2 Nocturnal animal models of UV as an oxidative stress

Due to their size and ease of housing, mice and rats have proven to be popular choices for the development of models of UV cataract formation. However, the most widely used rodent animal models are nocturnal and not naturally exposed to the high levels of UV light experienced by diurnal animals. Moreover, rodent models are often exposed to UV light at much higher doses than diurnal animals experience environmentally in order to shorten the experimental time course required for the development of cataract. Due to their low natural exposure to UV radiation nocturnal animals do not express the same system of UV filters seen in the human lens. Therefore, the same radiation energy dissipation that occurs in the human lens does not occur in mice and rat lenses that do not have UV filters.

2.1 Mice

Mice have been used as models for many types of cataract (see (27)). Important differences between the mouse and human lens include a different distribution of β-crystallins (143) and crystallin proteins that are modified differently (144). Critically, however, mice see in the ultraviolet range (145), and thus their lenses contain no UV filters to absorb UV radiation (32). Despite these differences, mice have been used to study the effects of both UV-A and UV-B radiation on lens protein content, as well as the morphological and biochemical status of UV-exposed lens. Murine tissue has also been used to assess the efficacy of external agents, such as caffeine and ascorbate, in preventing UV cataract *in vivo* (146, 147).

2.1.1 Cataract phenotypes induced by UV light exposure

To establish the relative toxicity of UV light exposure to lenses, mice have been exposed to UV-A or UV-B for up to 39 weeks. UV-A exposure was found to be weakly cataractogenic when compared to UV-B in albino mice *in vivo* (148, 149). *In vivo* exposure of mice to UV-B has not only induced subcapsular cataract, but also cortical and nuclear cataract (150). Further development of this model showed that when only one eye was exposed to UV-B, the non-exposed eye suffered intraocular inflammation and an increase in lens light scattering also, perhaps due to a co-cataractogenic inflammatory response (151).

2.1.2 Effects of UV light on metabolism, antioxidant pathways and protein function

Changes to lenticular protein concentration of albino mice in response to UV-A has been investigated *in vivo* (152, 153). Following long-term exposure to UV-A (up to 87 weeks), insoluble protein levels rose to 46% higher than controls (153), which is similar to the accumulation of insoluble proteins observed in ARN cataracts in humans (124, 154). Subcapsular and cortical opacities were observed between 30 and 50 weeks, after which anterior cortical cloudiness was observed. While the cataract phenotype observed here was different to that observed in humans, these results confirmed that long-term *in vivo* exposure to UV-A light leads to cataract in an albino mouse model.

Morphological and biochemical alterations produced as a result of *in vivo* exposure of mice to UV-B radiation have been investigated (155). Within two days of exposure, the mice had developed anterior subcapsular cataracts, similar to results from another study (156), with the onset of morphological changes beginning at 24 hours post-exposure. Importantly, older mice showed more prominent macroscopic changes compared to younger mice, and GSH depletion was more prominent in the older lenses than the younger lenses, again reflecting changes observed in human lenses. Glyceraldehyde-3-phosphate dehydrogenase (G3PD) inactivation was more exaggerated in the older lenses, diminishing ATP production and having a direct impact on lens transparency.

In addition, the enzymes thioltransferase (TTase) and thioredoxin (Trx) were upregulated following UV exposure, likely providing oxidative damage repair in the younger mice. Trx has

TABLE 3 Key features of UV cataract in humans - a comparison to animal models of UV exposure.

		Antioxidants			Protein changes			Impaired enzymatic function	Lens colouration	Cataract phenotype	
		Total	COR	NUC	↑ mixed disulfide	↑ WI fraction	Aggregation			COR	NUC
Human	*In vivo*	↓	NC	↓	✓	✓	✓	✓	✓	✓	✓
Mouse	*In vivo*	↓ ↓	- -	- -	✓ ✓	- -	- -	✓ ✓	- -	✓ ✓	✓ -
Rat	*In vivo*	- -	- -	- -	- -	- -	- -	x ✓	- -	✓ -	✓ -
	Ex vivo	- -	- -	- -	- -	- -	- -	✓ -	- -	✓ -	- -
Guinea pig	*In vivo*	- ↓	- NC	- ↓	- ✓	- ✓	- ✓	- -	- ✓	- ✓	- ✓
	Ex vivo	- -	- -	- -	- ✓	- -	- -	- -	- -	✓ -	- -
Rabbit	*In vivo*	↓ -	- -	- -	- -	- -	- -	- -	- ✓	✓ x	x x
	Ex vivo	- -	- -	- -	- -	- -	- -	- -	- -	✓ x	- -
Cow	*Ex vivo*	- -	- -	- -	- -	- -	- ✓	- ✓	- -	✓ ✓	- -
Pig	*Ex vivo*	- -	- -	- -	- -	- -	- -	- -	- -	✓ ✓	- -
Squirrel	*In vivo*	- -	- -	- -	- ✓	- ✓	- ✓	- -	- -	- -	- -
	Ex vivo	↓ -	- -	- -	- -	- -	- ✓	- -	- -	✓ ✓	- ✓

Blue symbols = UV-B, Green symbols = UV-A, COR, cortex; NUC, nucleus; ↓, decrease; -, not reported; ✓, present; x, absent; NC, no change.

been shown to play an important role in defending against UV-A light in cultured human epithelial cells (157). The decrease in G3PD function, which can be restored by dethiolation of TTase, was thought to be a result of suppressed enzyme activity by UV exposure, rather than a direct effect on protein expression levels. While there are differences in how deep UV will penetrate into the mouse eye versus the human eye, the same age-related deterioration in enzyme function is seen in humans (158), suggesting that a similar response to UV-B exposure may occur in the human lens.

In summary, while prolonged UV-A exposure to mice *in vivo* induces a variety of cataract morphologies that differ to those observed in humans, these studies showed that elevated protein insolubility and impaired enzyme function are caused by UV-B irradiation. In addition, older lens tissue appears to have a reduced capacity for repair compared to younger lens tissue.

2.2 Rats

Rats are one of the most commonly used laboratory animals. However in comparison to human lenses, rat lenses have different protein distributions (159). Relative to body size, rats have larger lenses and thinner corneas than humans (49, 160). Rat corneas attenuate less UV-B and more UV-A radiation than the human cornea (49). Rat lenses also do not accommodate, due to poorly developed ciliary muscles (161). In addition, rat lenses transmit almost all incoming UV-A, which can damage the rat retina (162), suggesting that rats lack UV-A absorbing compounds (32). Despite these fundamental difference to human lenses, numerous studies have investigated the effects of UV light exposure on lens morphology and biochemistry.

2.2.1 Cataract phenotypes induced by UV light exposure

Acute exposure of rat lenses *in vivo* to both UV-A and UV-B cause a variety of cataract phenotypes (163, 164). Results from these studies have suggested that the lens epithelium exhibits an ability for regenerative repair, which is not observed in cortical fibre cells. Dose accumulation of UV-B radiation was assessed in a chronic exposure rat lens model (160). Lenses that were exposed to UV irradiation developed cataracts on the anterior surface. In addition, the anterior lens opacities intensified in all exposure period groups with the increasing cumulative dose. However, the sensitivity of the lens to UV-B radiation decreased with the number of days during

which the dose was accumulated, suggesting that repeated exposure to UV-B decreases the lenses ability to recover and repair damage (160).

2.2.2 Effects of UV light on metabolism, antioxidant pathways and protein function

The localised cell swelling induced in the anterior surface of the rat lens induced by *in vitro* UV-A exposure appears to be due to an effect of UV-A on Na^+/K^+ ATPase activity, which decreased in both the lens epithelium and cortex (164). Low Na^+/K^+ ATPase activity may also underly cataract formation following exposure to UV-B, where lactate dehydrogenase (LDH) activity, and therefore ATP production, was lower predominantly in the anterior lens regions (epithelium and outer cortex), which was consistent with the pattern of exposure (51). While the decrease was relatively small (20%), this suggested a role for decreased ATPase activity in UV-B-induced cataract formation. However, this mechanism is yet to be confirmed in human lenses exposed to UV-B.

Changes in the metabolic profile of lenses exposed to UV-B radiation may also be anticipated if ATP production is affected as shown by Löfgren and Söderberg (51). Decreases in phenylalanine, GSH, and succinate, have been detected, potentially due to their leakage from the lens following membrane damage from UV irradiation (165). Metabolite levels can be restored following UV-B exposure, although the timeframe of metabolite decrease and restoration can vary (166). It would be interesting to apply this approach to study UV-B exposure in human lenses, and whether similar changes to metabolites and LDH are observed, whether metabolite levels can be restored, and whether this exposure would produce similar cataract phenotypes to those observed in the rat.

The effect of UV-B irradiation on lens glycolysis has been investigated in Sprague-Dawley rats (167). Lactate (produced by LDH) is an end product of anaerobic glycolysis and is often used as an indicator for activity of the glycolytic pathway (168). Lactate production was reduced initially, however, six hours after exposure, the lactate level in the exposed lenses was greater than contralateral lenses (167).

In vitro, irradiation of both intact and homogenised rat lenses has shown decreased activity of enzymes involved in the major metabolic pathways. For example, hexokinase, G6PD, aldose reductase, and Na^+/K^+ ATPase showed decreased activity of up to 57% compared to the control lenses, although UV-B exposure did not result in cataract formation (169). Interestingly, physiologically relevant levels of antioxidants (vitamins C and E, and β-carotene) that were added to the lens incubation medium during irradiation prevented the perturbation of enzymatic activity detected in UV-B-exposed lenses in a concentration dependent manner (169), suggesting that the damage to enzymes was through an oxidative stress mechanism. While enzyme activity changes may be involved in UV-B-induced lens opacity, the therapeutic potential of antioxidant supplementation for human lenses remains unclear since it has already been shown that both vitamin C and E have little to no effect on the prevention of human ARN cataracts when consumed as a dietary supplement (170–172).

Interestingly, albino rats are more sensitive to UV-B radiation than pigmented rats *in vivo* (173), possibly due to differences in corneal, aqueous humour, or iris transmission of light. The same trend is also seen with *in vitro* irradiation of lenses extracted from albino and pigmented rats (174). However, it is difficult to say whether the pigmented or albino rat is more suitable as a model for UV cataract.

In summary, rat models have shown that both UV-A and UV-B can impact cation homeostasis through Na^+/K^+ ATPase, and both ranges of wavelengths can create anterior subcapsular cataracts in the rat lens. The rat lens has been shown to be most susceptible to UV-B at 300 nm (175), with most of these models employing this wavelength. UV-B increases light scattering, and also decreases water soluble metabolites, enzyme activities, and cellular respiration.

3 Crepuscular animal models of human age-related cataract

Crepuscular animals are active during twilight hours of dawn and dusk. The UV index at twilight is approximately 200 μJ cm^{-2} (176), and therefore considerably less than the average 2 J cm^{-2} experienced during the day. However, the dose of UV that these animals would be exposed to in their natural environment is more than nocturnal animals and more similar to humans. Thus, crepuscular animals have been used as animal models of human age-related cataract. Crepuscular animals can be used *in vivo* as they are relatively small and easy to keep, and *ex vivo* tissue is readily available.

3.1 Guinea pigs

Guinea pigs have previously been used for models of ARN cataracts (177–180), and galactose-induced cataract (181, 182). Due to high levels of a UV-A chromophore in the lens (122) that mimics that of the human UV filter, a similar pattern of lens GSH distribution with lower levels of GSH in the nucleus relative to the cortex (183), and a similar age-dependent pattern of nuclear disulfide formation (184), it is proposed that guinea pigs are the best non-primate model currently available for the study of UV-A exposure and cataract (32).

However, while there are many benefits to the use of guinea pigs as a model of human UV exposure, it is also important to consider inconsistencies between humans and guinea pigs. For example, there is conflicting evidence for the formation of brunescence in the guinea pig lens (185, 186), unlike the characteristic time dependent increase in colouration observed in the human lens (187).

3.1.1 Cataract phenotypes induced by UV light

Chronic exposure of guinea pigs to a low level of UV-A light *in vivo* produces protein aggregation and cataract in the centre of the lens (188). In contrast, the anterior lens cortex showed no difference

between UV-A exposed and control guinea pigs, perhaps due to the higher metabolic activity, and therefore antioxidant capacity of the lens cortex. The mechanism of nuclear cataract formation in the guinea pig nucleus may be due to the binding of the UV-A chromophore NADPH to zeta crystallin. This is proposed to mimic the binding of kynurenine to crystallin proteins in the human lens (122). NADPH is known to cause the formation of superoxide ions (189), and H_2O_2 (190), when it absorbs UV-A (see Figure 2). Interestingly, the guinea pig is over 10-fold more tolerant to UV-B than pigmented rabbits, rats, and mouse (191). Very high doses of UV-B are required to produce cortical cataracts in the anterior subcapsular region of the lens *in vivo*. The exact mechanism for this enhanced protection is unclear, although perhaps it is because the guinea pig lens contains more ascorbate than rat lenses, with levels similar to the human lens (191), as well as high levels of free NADPH (44, 192) and zeta-crystallins (193).

3.1.2 Effects of UV light on metabolism, antioxidant pathways and protein function

Interestingly, UV-A light produced deleterious effects on the nucleus of guinea pig lenses, when compared to age-matched controls (44). There was an increase in light scattering, distention of intracellular spaces, a decrease in GSH, increased lipid peroxidation, and a loss of water-soluble proteins in the lens nucleus. Results from UV-A exposure of guinea pig lenses *in vivo* strongly support the role of oxidative stress in cataract formation following UV exposure. For example, lenses show up to a 50% reduction in free sulfhydryl, with a concomitant 100% increase in disulphide formation (185). This is possibly due to the formation of protein mixed disulphides (44), or reduction in activity of glutathione reductase, such as that suggested from studies of squirrel lenses (194). The guinea pig has also been used to test if ascorbate delivered by the diet (195–197) can protect against photooxidative damage to the lens induced by UV exposure. While this work showed promise, more recent investigations showed that ascorbate does not prevent human ARN cataract formation when consumed as a dietary supplement (170, 171).

In summary, *in vivo* guinea pig models show that UV-A can penetrate deep into the lens nucleus and cause dense nuclear opacification, as well as brunescence of lens tissue. In addition, ROS may be generated, which may contribute to changes to the lens after exposure that are characteristic of oxidative stress. Nuclear opacification, protein aggregation, loss of free GSH, and increased levels of disulphides within UV-A exposed lenses show how potentially damaging UV-A radiation can be *in vivo*. Guinea pigs appear to be quite tolerant to UV-B radiation, with very high doses required to produce cataracts.

3.2 Rabbits

Rabbits have previously been used as *ex vivo* models for ARN cataract formation (198) and oxygen-induced protein changes (199, 200). Cultured rabbit lens epithelial cells have also been used to investigate the effects of UV-A and/or UV-B (201–206), as well as the efficacy of UV blocking contact lenses (207, 208). While rabbit lenses lack kynurenine-based UV filters (32), they contain high levels of NADH and NADPH (207) which absorb UV-A light and may therefore act as a human UV filter analogue. Rabbit lenses are also more similar in size and sphericity to human lenses than other commonly used rodent lenses and have been used in both *ex vivo* and *in vivo* studies.

3.2.1 Cataract phenotypes induced by UV light

The rabbit cornea absorbs radiation completely at wavelengths at, and below 290 nm (209), and therefore the lens is more susceptible to damage at wavelengths greater than 290 nm. UV-A irradiation of rabbit lenses (210) produced opacification, potentially due to the tight bundling of actin filaments, or other morphological effects indicating cell cytotoxicity, including the breakdown of plasma membranes. Relatively low exposures of UV-B can produce anterior subcapsular lenticular opacities *in vivo*, although these opacities are not permanent and resolve within three months (209).

After *in vivo* irradiation of rabbit lenses, the lenses exhibit a pale yellow colour, although the reason for this colouration is unclear (207). Given that human lenses show colouration with aging, this is an interesting finding and suggests the potential of the rabbit lens for investigating the effects of UV light on lens colouration, despite differences in UV absorbing compounds.

3.2.2 Effects of UV light on metabolism, antioxidant pathways and protein function

Changes to the metabolic profile of *in vivo* albino rabbit lenses with either a single dose, or repeated exposures adding up to a single dose, of UV-B has been investigated (211). Interestingly, repeated exposure to a small dose had more of an impact on the lenticular metabolic profile than a single dose (equal to cumulative repeated dose) did, demonstrating the cumulative effect of repeated UV-B irradiations. No lenticular opacification was reported, therefore, combined with the results of Pitts (209), it is unclear whether UV-B irradiation produces permanent cataracts in rabbit lenses *in vivo*. In contrast, exposure of *ex vivo* albino rabbit lenses to UV-B does produce lens opacification. This appears to confirm that impairment of Na^+/K^+ ATPase function is a common mechanism for UV-induced lens cataract (212), while highlighting that *in vivo* and *ex vivo* exposure systems can produce conflicting results.

Cultured lenses from rabbits four to five weeks old are not sensitive to UV-A irradiation alone (213), which contradicts previous findings (210), although the age of the rabbit may influence the extent of UV-A sensitivity. However, a combination of UV-A and UV-B has been shown to be more damaging to the cultured rabbit lens than UV-A alone (213). *In vivo* exposure to combinations of UV-A and UV-B using a variety of protocols have not consistently produced changes to rabbit lens metabolites (211, 214), proteins or malondialdehyde as a marker of oxidative stress (215). Taken together it appears that the rabbit lens *in vivo* is relatively well protected from UV-induced damage.

4 Diurnal animal models of human age-related cataract

Diurnal animals are active during the day, and sleep at night and therefore more closely resemble the activity of the average human than nocturnal and crepuscular animals. Moreover, UV filters have been identified in diurnal animal lenses. Like humans, primate lenses have been found to contain 3OHKG (216–218). 3OHKG is the main absorbing species in young primate lenses, and both UV-A and UV-B have been shown to penetrate, and be absorbed by, the young lens nucleus (219). Primate lenses have similar optical and biometric properties to human lenses (220), but tissue can be difficult to obtain. Primate lenses have been used to investigate changes in UV absorption and transmission with age (219, 221), and effects of UV radiation on the cornea (222). However, to our knowledge, primate lenses have not been used experimentally to assess the impact of UV radiation on the lens, and thus will not be discussed further. Grey squirrels (223, 224), thirteen-lined ground squirrels (225, 226), cows (227), fish (228–230), and other mammalian lenses (231), have been shown to contain tryptophan metabolites or UV sensitive pigments. While smaller diurnal animals (e.g. squirrels) can be studied *in vivo*, most diurnal animal models generally use *ex vivo* tissue.

4.1 Cows

Bovine lenses are thought to express limited UV filter compounds, such as 3OHK (227), but share a similar predominance of α-crystallin (232, 233). Bovine lenses also do not undergo significant accommodation (234). There are UV models that utilise isolated bovine proteins (235–238), and epithelial cell cultures (239), however they will not be discussed.

4.1.1 Effect of UV light on cataract phenotype

Daily exposure of *ex vivo* bovine lenses to UV-A results in no significant changes to transmittance or focal length, when compared to controls (240). Mild subcapsular opacity is also observed. When *ex vivo* bovine lenses were exposed to UV-B, the results show that weekly doses of UV-B prevented lens repair, but these changes should not be considered to be cumulative, since the damage did not worsen with subsequent doses (240).

The effect of varying low-level UV-B exposure on light scattering and lens focal length *ex vivo* has also been investigated (241). Although not statistically significant, the second lowest dose (0.06 J cm^{-2}) appeared to have the greatest impact on the measurement parameters. Slight anterior subcapsular opacities became apparent as soon as two hours after irradiation, but in most cases, the damage cleared and only a very small area of damage remained on the anterior surface of the lens. Most of the exposed lenses showed measurable increases in light scatter and focal length but were able to recover. Thus, low doses of UV-B radiation do not permanently damage *ex vivo* bovine lenses, similar to findings in rabbit lenses (209).

4.1.2 Effects of UV light on metabolism, antioxidant pathways and protein function

The effect of UV-A irradiation and subsequent recovery on the biochemical and optical properties of *ex vivo* bovine eyes has been investigated (242). The activity of hexokinase, catalase, and G6PD enzymes is perturbed by UV-A in a dose-dependent manner. Hexokinase appears to be the most sensitive to UV-A exposure, similar to the observation for rat lens hexokinase in response to UV-B radiation (243). In addition, the activity of Na^+/K^+ ATPase in lens epithelial cells is impaired in response to UV-A exposure (244). However, repair mechanisms exist within the bovine lens that remain intact *ex vivo*, which were able to repair damage done to optical quality and Na^+/K^+ ATPase activity in the central region of the lens epithelium.

The effect of UV-A irradiation on the chaperone-like properties of α-crystallin has been investigated in bovine lenses, showing differences between the response of α-crystallin from young, and old lenses (245). In comparison to young lenses, α-crystallin from old lenses had a decreased ability to inhibit protein denaturation *in vitro*. There was an increase in the molecular weight of α-crystallin fractions, and a loss of tryptophan fluorescence which barely recovered following irradiation. This suggested that older lens proteins are more susceptible to damage from irradiation, which has also been observed in mice exposed to UV-B (155). This is perhaps due to a cumulative effect of UV-A radiation, and potentially similar to the UV-B effects observed in rats (160), and rabbits (211). When the lenses began to recover (indicated by focal length repair), chaperone-like activity recovered and tryptophan fluorescence increased predominantly in young lenses, suggesting that conformational changes to α-crystallin which had occurred during irradiation had resolved.

In summary, UV-A irradiation can cause anterior subcapsular opacities in the bovine lens and older lens proteins appear to be more susceptible to UV-A damage. Permanent damage to lenticular enzyme activities can occur with sufficiently high doses of UV-A and may be implicated in UV-A induced cataract. UV-B can induce small subcapsular opacities in the bovine lens, although low doses do not appear to permanently damage the lens. However, lens repair may be prevented with repeated UV-B exposure.

4.2 Pigs

In comparison to humans, pigs have a similar lens protein concentration (32, 246), lens shape (247, 248), light transmission (249), and protein content (250). While pig lenses are thought not to accommodate (251), and differences in the UV filter composition of pigs and humans exist (252), some inferences on human lens response to UV radiation may be made from porcine studies. While the impact of UV-A light on protein isolates (253, 254), and lens

tissue sections (255) have been investigated, we will only focus on changes induced in *ex vivo* organ cultured lenses.

4.2.1 Cataract phenotypes induced by UV light

The effectiveness of different wavelengths of light has been assessed using *ex vivo* porcine lenses (256). Mid-range UV-B (295 nm) was 25 times more effective than tail-end UV-B (315 nm) radiation at producing anterior subcapsular lesions. To assess for the ability of porcine lenses to recover from exposure to UV, lenses were exposed to five times UV-B threshold exposure, resulting in the appearance of the lens sutures, suggesting the radiation had inflicted permanent damage to the lens. At two times threshold for UV-A, there was no full recovery of the lens, confirming that UV-A is cataractogenic in the porcine lens. This study concluded that the most damaging wavelengths are 270 to 315 nm, due to the low dosages required to produce visible damage. Without the protection provided by the cornea *in vivo*, the UV-B radiation was able to have a substantial impact on the lens tissue. Wavelengths shorter than 285 nm would be expected to be more damaging, since shorter wavelength photons are also higher energy (257), but this was not the case.

In addition, the same group utilised *ex vivo* porcine lenses to investigate the effect of a combination exposure of both UV-A and UV-B radiation (252). This model demonstrated the synergistic effects of low, subsolar UV-A and UV-B, with significant inhibition of cellular metabolic activity and no indication of recovery. Some recovery of plasma membrane damage was observed; however, optical quality did not recover in the study period. UV-A radiation alone required high doses (λ = 365 nm, 86 J/cm^2) to produce significant decreases in cellular and optical integrity, in accordance with the previous study (256).

In summary, there are numerous similarities between porcine and human lenses, making them a more popular animal model of choice in recent UV exposure investigations. High doses of UV-A are required to produce anterior subcapsular opacities in porcine lenses, compared to the lower doses of UV-B required to produce the same phenotype. However, a combination of UV-A and UV-B incurs significant damage to the cellular metabolic activity and optical quality of the lens. Further experiments using porcine lenses could monitor changes to the cellular systems that are known to be involved in UV-induced damage which have been established in other models, and to investigate whether porcine lenses would become brunescent with age and/or UV exposure.

4.3 Squirrels

Squirrel lenses share several features in common with humans, suggesting they may be a good model animal for understanding the effects of UV exposure on lens transparency. For example, they contain UV filters (226) which have a similar structure and concentration to those found in humans (225), and display brunescence (224, 225). Squirrels have similar levels of GSH in the nucleus as a young human lens (225), but the total GSH is approximately twice that of humans (258). While cultured squirrel lens epithelial cells have been used to study the use of vitamin E as a protective agent against UV-induced damage (202, 205), only *in vivo* and *ex vivo* experiments that utilised whole squirrel lenses will be discussed here.

4.3.1 Cataract phenotypes induced by UV light

The effects of ambient exposure to UV-A have been investigated in grey squirrels *in vivo* (194). Following chronic UV-A (λ = 365nm), well defined lens opacities (cortical and subcapsular) were observed, and histological analysis showed swelling of the superficial cortical fibre cells and some degenerating fibres post UV-A exposure. Anterior opacities that increase in severity with exposure time have also been observed using *ex vivo* squirrel lenses (259). The type of cataract formed from exposure to UV-B is not documented, but UV-B exposed lenses have been used for biochemical analyses (260).

4.3.2 Effects of UV light on metabolism, antioxidant pathways and protein function

UV-A exposure was associated with an increase in crosslinking and degradation of crystallin proteins, and small changes in the levels of soluble crystallin proteins (194). A major loss of GSH in the outer and inner cortex was detected, while levels in the nucleus remained the same, which is opposite to the pattern seen in the aging human lens (183). Although apparent in the lens cortex, this study showed that chronic exposure of UV-A light can induce cataract formation.

Furthermore, UV-A exposure causes significant damage to phosphorous metabolites, such as ATP, in the *ex vivo* squirrel lens (259). Changes to ATP levels appear to scale with dose, whereby a lower dose causes a smaller decrease in ATP. Crystallin proteins have been shown to undergo crosslinking when exposed to UV-A in the squirrel lens (261). *In vivo*, increases in proteins with greater molecular weights occurred in the outer layers of the lens, but not the nucleus (261). This is similar to the pattern of altered lens protein distribution in cataractous human lenses (262). Crosslinking of soluble crystallins was seen in both *in vivo* and *ex vivo* exposed lenses. A link was also made between squirrel lens pigment and protein crosslinking, indicating that lens pigment stimulates the photosensitised crosslinking of lens proteins *in vitro* (261) which may provide some insight into the protein changes that occur during human cataract formation.

Indoleamine 2,3-dioxygenase (IDO) is an antioxidant enzyme, and the first-rate limiting enzyme of tryptophan catabolism. Exposure of squirrel lenses to UV-B led to an increase in IDO activity within the lens, and thus an increase in tryptophan metabolites (i.e. kyn and 3OHK) (260). Irradiation also led to increased lipid peroxidation and a decrease in GSH, suggesting UV-B had caused oxidative stress within the lens. Long durations of UV-B exposure had a small but suppressive effect on the activity of superoxide dismutase (SOD), an antioxidant protein that reduces intracellular levels of superoxide radicals. Human lenses rely on IDO for the formation of UV filters (105, 263, 264), and these findings in squirrel lenses may have parallels in human lenses.

In summary, squirrel models have been used to show the damaging effect UV-A has on proteins, initiating crosslinking and degradation. Although it is unclear if UV-B induces opacification of

squirrel lenses, it does cause oxidative stress, shown through increasing lipid peroxidation and a reduction in antioxidant.

5 Conclusions

The paucity and significant biochemical variability of human lens tissue necessitates the use of animal tissue to model and characterise the effect that UV light has on tissue transparency and its role in cataract formation. While conclusions drawn from animal studies cannot always be directly translated to human cataract due to the morphological and biochemical differences between species, animal models have revealed several changes that take place in lenses exposed to different wavelengths of UV light with both UV-A and UV-B light appearing to play a role in cataract formation, albeit by different mechanisms. It remains clear that the same wavelength and dose of UV-A or UV-B can produce an array of different biochemical and metabolic changes, as well as cataract phenotypes, and is dependent on the animal model used. Similarly, different cataract phenotypes can result from the same underlying mechanism. While mice and rats are convenient laboratory animal models, the fact that they are nocturnal animals that normally experience completely different UV exposure levels to humans means that the role of UV light exposure in cataract development in rodents must be carefully interpreted with respect to cataract formation in the human lens. Nevertheless, these models have helped to identify oxidative stress via photooxidation, and photosensitisation as major factors involved in UV cataract development. Specifically, the Na/K ATPase activity is impaired in several UV exposure models, which is likely to impair the specialised transport system known to maintain lens tissue transparency (265).

Although crepuscular animals experience higher levels of UV radiation than nocturnal animals, they still do not experience the same levels of exposure as humans. In addition, both classes of animal lack the same range of UV filters found in the lens. However, in both types of animals the application of "non-environmental" UV exposures to these laboratory animals does provide information on UV-A and UV-B as cataractous stressors that can differentially activate oxidative defence pathways in different regions of the lens that normally act to maintain lens structure and function. Guinea pigs, however, appear to recapitulate many of the characteristics of UV cataract in humans, including lens brunescence.

Diurnal animals share more similarities with humans than nocturnal or crepuscular animals with respect to UV exposure levels, the presence of UV filters, and the characteristic brunescence of lens tissue at least in the case of the squirrel lens (225). This suggests that mechanisms of UV damage observed in squirrel lenses could be directly applicable to UV cataract formation in humans. However, not all laboratories have access to these animals.

In contrast, porcine and bovine lenses are more readily available and easily utilised in organ culture experiments. The use of these diurnal *ex vivo* animal models has shown that UV-A radiation has the potential to be more harmful than UV-B radiation, possibly due to the absorption of this longer wavelength energy in deeper lens cell layers that inactivates enzymatic activity involved in the protection against oxidative stress. They have also shown that in younger lenses at low doses this UV induced damage can be repaired; but that older lenses are more susceptible to UV damage and showed impaired recovery compared to young lenses receiving the same dose. The lack of evidence surrounding yellowing of the lens tissue with age (or UV exposure) in these larger animals, however, means that while they are useful for understanding potential changes to proteins resulting from photooxidation and photosensitisation, they lack a key characteristic of human UV cataract.

Despite this substantial body of work, gaps in our understanding of the extent of the impact that exposure to UV light has on the lens remain. To close this gap continued development of UV light exposure models that utilise diurnal animals, especially guinea pig and squirrel lenses, will further enhance our understanding of the role that UV light exposure plays in the development of human lens opacities. In addition, models that combine stressors, for example oxidative and photooxidative stress, may prove useful to further investigate human cataract development.

Author contributions

EM: Writing – original draft, Writing – review & editing. PD: Writing – review & editing. AG: Writing – review & editing.

Funding

The author(s) declare financial support was received for the research, authorship, and/or publication of this article. The authors acknowledge support from the Health Research Council of New Zealand.

Conflict of interest

The authors declare that the research was conducted in the absence of any commercial or financial relationships that could be construed as a potential conflict of interest.

Publisher's note

Supplementary material

The Supplementary Material for this article can be found online at: https://www.frontiersin.org/articles/10.3389/fopht.2024.1414483/full#supplementary-material

References

1. Pascolini D, Mariotti S. Global estimates of visual impairment: 2010. *Br J Ophthalmol*. (2012) 96:614–8. doi: 10.1136/bjophthalmol-2011-300539

2. Bourne RRA, Stevens GA, White RA, Smith JL, Flaxman SR, Price H, et al. Causes of vision loss worldwide, 1990-2010: a systematic analysis. *Lancet*. (2013) 1:339–49. doi: 10.1016/S2214-109X(13)70113-X

3. Liu Y-C, Wilkins M, Kim T, Malyugin B, Mehta JS. Cataracts. *Lancet*. (2017) 390:600–12. doi: 10.1016/S0140-6736(17)30544-5

4. Wolff SP. Cataract and UV radiation. *Doc Ophthalmol*. (1995) 88:201–4. doi: 10.1007/BF01203674

5. Hollows F, Moran D. Cataract - the ultraviolet risk factor. *Lancet*. (1981) 2:1249–50. doi: 10.1016/S0140-6736(81)91490-2

6. Taylor HR. Ultraviolet radiation and the eye: an epidemiologic study. *Trans Am Ophthalmol Soc*. (1989) 87:802–53.

7. Wittenberg S. Solar radiation and the eye: a review of knowledge relevant to eye care. *Am J Opto Physiol Opt*. (1985) 63:676–89. doi: 10.1097/00006324-198608000-00012

8. Javadi M-A, Zarei-Ghanavati S. Cataracts in diabetic patients: A review article. *J Ophthal Vision Res*. (2008) 3:62–5.

9. Klein BEK, Klein R, Moss SE. Incidence of cataract surgery in the Wisconsin epidemiologic study of diabetic retinopathy. *Am J Ophthalmol*. (1995) 119:295–300. doi: 10.1016/S0002-9394(14)71170-5

10. Klein BEK, Klein R, Moss SE. Prevalence of cataracts in a population-based study of persons with diabetes mellitus. *Ophthalmology*. (1985) 92:1191–6. doi: 10.1016/S0161-6420(85)33877-0

11. Chan AWH, Ho Y-S, Chung SK, Chung SSM. Synergistic effect of osmotic and oxidative stress in slow-developing cataract formation. *Exp Eye Res*. (2008) 87:454–61. doi: 10.1016/j.exer.2008.08.001

12. Lou MF. Redox regulation in the lens. *Prog Retinal Eye Res*. (2003) 22:657–82. doi: 10.1016/S1350-9462(03)00050-8

13. Lim JC, Vaghefi E, Li B, Nye-Wood MG, Donaldson PJ. Characterization of the effects of hyperbaric oxygen on the biochemical and optical properties of the bovine lens. *Invest Opthalmol Visual Sci*. (2016) 57:1961–73. doi: 10.1167/iovs.16-19142

14. Lou MF. Glutathione and glutaredoxin in redox regulation and cell signalling of the lens. *Antioxidants*. (2022) 11:1973–2003. doi: 10.3390/antiox11101973

15. Vasavada AR, Mamidipudi PR, Sharma PS. Morphology of and visual performance with posterior subcapsular cataract. *J Cataract Refractive Surge*. (2004) 30:2097–104. doi: 10.1016/j.jcrs.2004.02.076

16. Shun-Shin GA, Brown NAP, Bron AJ, Sparrow JM. Dynamic nature of posterior subcapsular cataract. *Br J Ophthalmol*. (1989) 73:522–7. doi: 10.1136/bjo.73.7.522

17. Delcourt C, Cristol J-P, Tessier F, Leger CL, Michel F, Papoz L, et al. Risk factors for cortical, nuclear, and posterior subcapsular cataracts. *POLA Study Am J Epidemiol*. (2000) 151:497–504. doi: 10.1093/oxfordjournals.aje.a010235

18. OECD. Health Care Utilisation: Surgical procedures : Stat technology; OECD Stat (2023). Available online at: https://stats.oecd.org/index.aspx?queryid=30167. (AccessedJune 19, 2023).

19. Brown GC, Brown MM, Menezes A, Busbee BG, Lieske HB, Lieske PA. Cataract surgery cost utility revisited in 2012. *Am Acad Ophthalmol*. (2013) 120:2367–76. doi: 10.1016/j.ophtha.2013.04.030

20. Heemraz BS, Lee CN, Hysi PG, Jones CA, Hammond CJ, Mahroo OA. Changes in quality of life shortly after routine cataract surgery. *Can J Ophthalmol*. (2016) 51:282–7. doi: 10.1016/j.jcjo.2016.02.004

21. Wang W, Yan W, Fotis K, Prasad NM, Lansingh VCL, Taylor HR, et al. Cataract surgical rate and socioeconomics: A global study. *Invest Ophthalmol Visual Sci*. (2017) 57:5872–81. doi: 10.1167/iovs.16-19894

22. Schein OD, Cassard SD, Tielsch JM, Gower EW. Cataract surgery among medicare beneficiaries. *Ophthal Epidemiol*. (2012) 19:257–64. doi: 10.3109/09286586.2012.698692

23. Kessy JP, Lewallen S. Poverty as a barrier to accessing cataract surgery: a study from Tanzania. *Br J Ophthalmol*. (2007) 91:1114–6. doi: 10.1136/bjo.2006.112474

24. Nirmalan PK. Utilisation of eye care services in rural south India: the Aravind Comprehensive Eye Survey. *Br J Ophthalmol*. (2004) 88:1237–41. doi: 10.1136/bjo.2004.042606

25. Semmens JB, Li J, Morlet N, Ng J. Trends in cataract surgery and postoperative endophthalmitis in Western Australia (1980–1998): the Endophthalmitis Population Study of Western Australia. *Clin Exp Ophthalmol*. (2003) 31:312–219. doi: 10.1046/j.1442-9071.2003.00647.x

26. Zigler JS. Animal models for the study of maturity-onset and hereditary cataract. *Exp Eye Res*. (1990) 50:651–7. doi: 10.1016/0014-4835(90)90109-8

27. Lim JC, Umapathy A, Donaldson PJ. Tools to fight the cataract epidemic: A review of experimental animal models that mimic age related nuclear cataract. *Exp Eye Res*. (2016) 145:432–43. doi: 10.1016/j.exer.2015.09.007

28. Duncan G, Wormstone IM, Davies PD. The aging human lens: structure, growth, and physiological behaviour. *Br J Ophthalmol*. (1997) 81:818–23. doi: 10.1136/bjo.81.10.818

29. Apple DJ, Solomon KD, Tetz MR, Assia EI, Holland EY, Legler UFC, et al. Posterior capsule opacification. *Survey Ophthalmol*. (1992) 37:73–116. doi: 10.1016/0039-6257(92)90073-3

30. Bron AJ, Vrensen GFJM, Koretz J, Maraini G, Harding JJ. The ageing lens. *Ophthalmologica*. (2000) 214:86–104. doi: 10.1159/000027475

31. Michael R, Bron AJ. The ageing lens and cataract: a model of normal and pathological ageing. *Philos Trans R Soc B*. (2011) 366:1728–292. doi: 10.1098/rstb.2010.0300

32. Truscott RJ. Age-related nuclear cataract-oxidation is the key. *Exp Eye Res*. (2005) 80:709–25. doi: 10.1016/j.exer.2004.12.007

33. Lim JC, Vorontsova I, Martis RM, Donaldson PJ. Animal Models in Cataract Research. In: *Animal Models for the Study of Human Disease* (2017) United Kingdom: Elsevier, Academic Press. p. 103–16.

34. Organization WH. World report on vision. Switzerland: World Health Organisation (2019), ISBN: . Contract No.: Licence: CC BY-NC-SA 3.0 IGO.

35. Frederick JE, Snell HE, Haywood EK. Solar ultraviolet radiation at the Earth's surface. *Photochem Photobiol*. (1989) 50:443–50. doi: 10.1111/j.1751-1097.1989.tb05548.x

36. Nunez M, Forgan B, Roy C. Estimating ultraviolet radiation at the Earth's surface. *Int J Biometerol*. (1994) 38:5–17. doi: 10.1007/BF01241798

37. Ivanov IV, Mappes T, Schaupp P, Lappe C, Wahl S. Ultraviolet radiation oxidative stress affects eye health. *J Biophoton*. (2018) 11:e201700377. doi: 10.1002/jbio.201700377

38. Mallet JD, Rochette PJ. Wavelength-dependent ultraviolet induction of cyclobutane pyrimidine dimers in the human cornea. *Photochem Photobiol Sci*. (2013) 12:1310. doi: 10.1039/c3pp25408a

39. Boettner EA, Reimer Wolter J. Transmission of the ocular media. *Invest Ophthalmol Visual Sci*. (1962) 1:776–83.

40. Organization WH. *The Effects of Solar UV Radiation on the Eye*. Switzerland: World Health Organisation (1993). Report No.: Who/PBL/EHG/94.1.

41. Kamari F, Hallaj S, Dorosti F, Alinezhad F, Taleschian-Tabrizi N, Farhadi F, et al. Phototoxicity of environmental radiations in human lens: revisiting the pathogenesis of UV-induced cataract. *Graefe's Arch Clin Exp Ophthalmol*. (2019) 257:2065–77. doi: 10.1007/s00417-019-04390-3

42. Saßmannshausen M, Ach T. Influence of ultraviolet radiation exposure to the retina. *Ophthalmol*. (2022) 119:240–7. doi: 10.1007/s00347-021-01506-1

43. Murray CJL, Lopez AD, Organisation WH, Bank WHealth HSoP. *The Global burden of disease: a comprehensive assessment of mortality and disability from diseases, injuries, and risk factors in 1990 and projected to 2020*. Boston, MA, USA: Harvard School of Public Health (1996).

44. Giblin FJ, Leverenz VR, Padgaonkar VA, Unakar NJ, Dang L, Lin L-R, et al. UVA light *in vivo* reaches the nucleus of the Guinea pig lens and produces deleterious, oxidative effects. *Exp Eye Res*. (2002) 75:445–58. doi: 10.1006/exer.2002.2039

45. Beebe DC, Holekamp NM, Shui Y-B. Oxidative damage and the prevention of age-related cataracts. *Ophthal Res*. (2010) 44:155–65. doi: 10.1159/000316481

46. McCarty CA, Taylor HR. A review of the epidemiologic evidence linking ultraviolet radiation and cataracts. *Develop Ophthalmol*. (2002) 35:21–31. doi: 10.1159/000060807

47. Dolin PJ. Ultraviolet radiation and cataract: a review of the epidemiological evidence. *Br J Ophthalmol*. (1994) 78:478–82. doi: 10.1136/bjo.78.6.478

48. Taylor HR, West SK, Rosenthal FS, Muñoz B, Newland HS, Abbey H, et al. Effect of ultraviolet radiation on cataract formation. *New Engl J Med*. (1988) 319:1429–33. doi: 10.1056/NEJM198812013192201

49. Dillon JP, Zheng L, Merriam JC, Gaillard ER. The optical properties of the anterior segment of the eye: implications for cortical cataract. *Exp Eye Res*. (1999) 68:785–95. doi: 10.1006/exer.1999.0687

50. Maher EF. Transmission and absorption coefficients for ocular media of the Rhesus Monkey. Brooks Air Force Base, San Antonio, Texas: USAF School of Aerospace Medicine (1978). Contract No.: Report SAM-TR-78-32.

51. Löfgren S, Söderberg PG. Lens lactate dehydrogenase inactivation after UV-B irradiation: an *in vivo* measure of UVR-B penetration. *Invest Ophthalmol Visual Sci*. (2001) 42:1833–6.

52. Neale RE, Purdie JL, Hirst LW, Green AC. Sun exposure as a risk factor for nuclear cataract. *Int J Biochem Cell Biol*. (2003) 35:1500–4. doi: 10.1097/01.ede.0000086881.84657.98

53. Zigman S, Datiles M, Torczynski E. Sunlight and human cataract. *Assoc Res Vision Ophthalmol*. (1979) 18:462–7.

54. Sasaki K, Sasaki H, Kojima M, Shui YB, Hockwin O, Jonasson F, et al. Epidemiological studies on UV-related cataract in climatically different countries. *J Epidemiol*. (1999) 9:33–8. doi: 10.2188/jea.9.6sup_33

55. Rosmini F, Stazi MA, Milton RC, Sperduto RD, Pasquini P, Maraini G, et al. A dose response effect between a sunlight index and age related cataracts annals of epidemiology. *Annals of Epidemiology*. (1994) 4:266–70. doi: 10.1016/1047-2797(94)90081-7

56. Hiller R, Giacometti L, Yuen K. Sunlight and cataract: an epidemiologic investigation. *Am J Epidemiol*. (1977) 105:450–9. doi: 10.1093/oxfordjournals.aje.a112404

57. Hiller R, Sperduto RD, Ederer F. EPIDEMIOLOGIC ASSOCIATIONS WITH CATARACT IN THE 1971–1972 NATIONAL HEALTH AND NUTRITION EXAMINATION SURVEY1. *Am J Epidemiol*. (1983) 118:239–49. doi: 10.1093/oxfordjournals.aje.a113631

58. Said M-E, Goldstein H, Korra A, El-Kashlan K. Prevalence and causes of blindness in urban and rural areas of Egypt. *Public Health Rep*. (1970) 85:587–99. doi: 10.2307/4593913

59. Schein OD, West SK, Munoz B, Vitale S, Maguire M, Taylor HR, et al. Cortical lenticular opacification: distribution and location in a longitudinal study. *Invest Ophthalmol Visual Sci*. (1994) 35:263–366.

60. Brilliant LB, Grasset NC, Pokhrel RP, Kolstad A, Lepkowski JM, Brilliant G,E, et al. Associations among cataract prevalence, sunlight hours, and altitude in the Himalayas. *Am J Epidemiol*. (1983) 118:250–64. doi: 10.1093/oxfordjournals.aje.a113632

61. Hu T-s, Lao Y-x. An epidemiologic survey of senile cataract in China. In: Sasaki K, Hockwin O, Leske MC, editors. *Cataract Epidemiology: International Meeting*. Noto/Japan: S. Karger AG (1987).

62. Hu T-S. Age-related cataract in the Tibet eye study. *Arch Ophthalmol*. (1989) 107:666. doi: 10.1001/archopht.1989.01070010684027

63. Miyashita H, Hatsusaka N, Shibuya E, Mita N, Yamazaki M, Shibata T, et al. Association between ultraviolet radiation exposure dose and cataract in Han people living in China and Taiwan: A cross-sectional study. *PloS One*. (2019) 14:e0215338. doi: 10.1371/journal.pone.0215338

64. Hatsusaka N, Yamamoto N, Miyashita H, Shibuya E, Mita N, Yamazaki M, et al. Association among pterygium, cataracts, and cumulative ocular ultraviolet exposure: A cross-sectional study in Han people in China and Taiwan. *PloS One*. (2021) 16:1–15. doi: 10.1371/journal.pone.0253093

65. Garzon-Chavez DR, Quentin E, Harrison SL, Parisi AV, Butler HJ, Downs NJ. The geospatial relationship of pterygium and senile cataract with ambient solar ultraviolet in tropical Ecuador. *Photochem Photobiol Sci*. (2018) 17:1075–83. doi: 10.1039/c8pp00023a

66. Mitchell BD, Lepkowski JM. The epidemiology of cataract in Nepal. *Hum Biol*. (1986) 58:975–90.

67. Cruickshanks KJ, Klein BE, Klein R. Ultraviolet light exposure and lens opacities: the Beaver Dam Eye Study. *Am J Public Health*. (1992) 82:1658–62. doi: 10.2105/AJPH.82.12.1658

68. Prokofyeva E, Wegener A, Zrenner E. Cataract prevalence and prevention in Europe: a literature review. *Acta Ophthalmol*. (2013) 91:395–405. doi: 10.1111/j.1755-3768.2012.02444.x

69. Sasaki H, Jonasson F, Kojima M, Katoh N, Ono M, Takahashi N, et al. The Reykjavik eye study – prevalence of lens opacification with reference to identical Japanese studies. *Ophthalmologica*. (2000) 214:412–20. doi: 10.1159/000027535

70. West SK, Duncan DD, Muñoz B, Rubin GS, Fried LP, Bandeen-Roche K, et al. Sunlight exposure and risk of lens opacities in a population-based study. *JAMA*. (1998) 280:714. doi: 10.1001/jama.280.8.714

71. Javitt JC, Taylor HR. Cataract and latitude. *Doc Ophthalmol*. (1995) 88:307–25. doi: 10.1007/BF01203684

72. Collman GW, Shore DL, Shy CM, Checkoway H, Luria AS. Sunlight and other risk factors for cataracts: an epidemiologic study. *Am J Public Health*. (1988) 78:1459–62. doi: 10.2105/AJPH.78.11.1459

73. Tang Y, Ji Y, Ye X, Wang X, Cai L, Xu J. The association of outdoor activity and age-related cataract in a rural population of Taizhou eye study: phase 1 report. *Public Library Sci*. (2015) 10:1–13. doi: 10.1371/journal.pone.0135870

74. Li X, Cao X, Yu Y, Bao Y. Correlation of sunlight exposure and different morphological types of age-related cataract. *BioMed Res Int*. (2021) 2021:10. doi: 10.1155/2021/8748463

75. Goldsmith RI, Rothhammer F, Schull WJ. The multinational Andean genetic and health program: III. Ophthalmic disease and disability among the Aymara. *Bull Pan Am Health Organ*. (1979) 13:58–65. doi: 10665.2/27562

76. Sliney DH. Physical factors in cataractogenesis: ambient ultraviolet radiation and temperature. *Invest Ophthalmol Visual Sci*. (1986) 27:781–90.

77. Sasaki K, Sasaki H, Jonasson F, Kojima M, Cheng HM. Racial differences of lens transparency properties with aging and prevalence of age-related cataract applying a WHO classification system. *Ophthal Res*. (2004) 36:332–40. doi: 10.1159/000081636

78. Sasaki K, Ono M, Aoki K, Katou N, Morine M, Nakaizumi H, et al. Cataract epidemiology survey in the three climatically different areas in Japan–prevalence of cataracts and types of lens opacification. *Nippon Ganka Gakksi Zasshi*. (1995) 99:204–11.

79. Mohan M, Sperduto RD, Angra SK, Milton RC, Mathur RL, Underwood BA, et al. India-US case-control study of age-related cataracts. *Arch Ophthalmol*. (1989) 107:670–6. doi: 10.1001/archopht.1989.01070010688028

80. Halpern P, Dave JV, Braslau N. Sea-level solar radiation in the biologically active spectrum. *Science*. (1974) 186:1204–8. doi: 10.1126/science.186.4170.1204

81. Manabe S, Wada O, Urban RC. A fluorescent carcinogen, 2-amino-1-methyl-6-phenylimidazo[4,5-b]pyridine (PhlP) in human lens. *Exp Eye Res*. (1993) 57:319–24. doi: 10.1006/exer.1993.1130

82. Ranjan M, Beedu SR. Spectroscopic and biochemical correlations during the course of human lens aging. *BMC Ophthalmol*. (2006) 6. doi: 10.1186/1471-2415-6-10

83. Cheng R, Lin B, Lee K-W, Ortwerth BJ. Similarity of the yellow chromophores isolated from human cataracts with those from ascorbic acid-modified calf lens proteins: Evidence for ascorbic acid glycation during cataract formation. *Biochem Biophys Acta*. (2001) 1537:14–26. doi: 10.1016/S0925-4439(01)00051-5

84. Ahmed MU, Thorpe SR, Baynes JW. Identification of N(ε)-carboxymethyllysine as a degradation product of fructoselysine in glycated protein. *J Biol Chem*. (1986) 261:4889–94. doi: 10.1016/S0021-9258(19)89188-3

85. Nagaraj RH, Monnier VM. Isolation and characterization of a blue fluorophore from human eye lens crystallins: *In vitro* formation from Maillard reaction with ascorbate and ribose. *Biochem Biophys Acta*. (1992) 1116:34–42. doi: 10.1016/0304-4165(92)90125-E

86. Tessier F, Obrenovich M, Monnier VM. Structure and mechanism of formation of human lens fluorophore LM-1. *J Biol Chem*. (1999) 274:20796–804. doi: 10.1074/jbc.274.30.20796

87. Manabe S, Wada O. Carcinogenic tryptophan pyrolysis products in human lens. *Exp Eye Res*. (1989) 48:351–3. doi: 10.1016/S0014-4835(89)80004-1

88. Dillon J, Spector A, Nakanishi K. Identification of β carbolines isolated from fluorescent human lens proteins. *Nature*. (1976) 259:422–3. doi: 10.1038/259422a0

89. Spector A, Roy D, Stauffer J. Isolation and characterization of an age-dependednt polypeptide from human lens with non-tryptophan fluorescence. *Exp Eye Res*. (1975) 21:9–24. doi: 10.1016/0014-4835(75)90053-6

90. Truscott RJW. Human cataract: the mechanisms responsible; light and butterfly eyes. *Int J Biochem Cell Biol*. (2003) 35:1500–4. doi: 10.1016/S1357-2725(03)00145-6

91. Tsentalovich YP, Sherin PS, Kopylova LV, Cherepanov IV, Grilj J, Vauthey E. Photochemical properties of UV filter molecules of the human eye. *Invest Opthalmol Visual Sci*. (2011) 52:7687. doi: 10.1167/iovs.11-8120

92. Dillon J, Atherton SJ. Time resolved spectroscopic studies on the intact human lens. *Photochem Photobiol*. (1990) 51:465–8. doi: 10.1111/j.1751-1097.1990.tb01738.x

93. van Heyningen R. Photo-oxidation of lens proteins by sunlight in the presence of fluorescent derivatives of kynurenine, isolated from the human lens. *Exp Eye Res*. (1973) 17:137–47. doi: 10.1016/0014-4835(73)90203-0

94. Bova LM, Wood AM, Jamie JF, Truscott RJW. UV filter compounds in human lenses: the origin of 4-(2-amino-3-hydroxyphenyl)-4-oxobutanoic acid O-β-d-glucoside. *Invest Opthalmol Visual Sci*. (1999) 40:3237–44.

95. Thiagarajan G, Shirao E, Ando K, Inoue A, Balasubramanian D. Role of xanthurenic acid 8-O-β-d-glucoside, a novel fluorophore that accumulates in the brunescent human eye lens. *Photochem Photobiol*. (2002) 76:368. doi: 10.1562/0031-8655(2002)076<0368:ROXAOD>2.0.CO;2

96. Parker NR, Jamie JF, Davies MJ, Truscott RJW. Protein-bound kynurenine is a photosensitizer of oxidative damage. *Free Radical Biol Med*. (2004) 37:1479–89. doi: 10.1016/j.freeradbiomed.2004.07.015

97. Tweeddale HJ, Hawkins CL, Janmie JF, Truscott RJW, Davies MJ. Cross-linking of lens crystallin proteins induced by tryptophan metabolites and metal ions: implications for cataract development. *Free Radical Res*. (2016) 50:1116–30. doi: 10.1080/10715762.2016.1210802

98. Mizdrak J, Hains PG, Truscott RJW, Jamie JF, Davies MJ. Tryptophan-derived ultraviolet filter compounds covalently bound to lens proteins are photosensitizers of oxidative damage. *Free Radical Biol Med*. (2008) 44:1108–19. doi: 10.1016/j.freeradbiomed.2007.12.003

99. Taylor LM, Aquilina JA, Willis RH, Jamie JF, Truscott RJW. Identification of a new human lens UV filter compound. *FEBS Letters*. (2001) 509:6–10. doi: 10.1016/S0014-5793(01)03102-7

100. van Heyningen R. Experimental studies on cataract. *Invest Ophthalmol Vis Sci*. (1976) 15:685–97.

101. van Heyningen R. What happens to the human lens in cataract. *Sci American*. (1975) 233:70–83. doi: 10.1038/scientificamerican1275-70

102. Wood AM, Truscott RJW. UV filters in human lenses: tryptophan catabolism. *Exp Eye Res*. (1993) 56:317–25. doi: 10.1006/exer.1993.1041

103. Hains PG, Gao L, Truscott RJW. The photosensitiser xanthurenic acid is not present in normal human lenses. *Exp Eye Res*. (2003) 77:547–53. doi: 10.1016/S0014-4835(03)00194-5

104. Luthra M, Balasubramanian D. 3-hydroxykynurenine and 3-hydroxyanthranilic acid may act as endogenous antioxidants in the eye lens. *Exp Eye Res*. (1992) 55:641–3. doi: 10.1016/S0014-4835(05)80177-0

105. Takikawa O, Littlejohn TK, Truscott RJW. Indoleamine 2,3-dioxygenase in the human lens, the first enzyme in the synthesis of UV filters. *Exp Eye Res*. (2001) 72:271–7. doi: 10.1006/exer.2000.0951

106. Borkman RF, Hibbard LB, Dillon J. The photolysis of tryptophan with 337.1 nm laser radiation. *Photochem Photobiol*. (1986) 43:13–9. doi: 10.1111/j.1751-1097.1986.tb05585.x

107. Finley EL, Dillon J, Crouch RK, Schey KL. Identification of tryptophan oxidation products in bovine α-crystallin. *Protein Sci*. (1998) 7:2391–7. doi: 10.1002/pro.5560071116

108. Pirie A. Formation of N-formylkynurenine in proteins from lens and other sources by exposure to sunlight. *Biochem J*. (1971) 125:203–8. doi: 10.1042/bj1250203

109. Taylor LM, Aquilina JA, Jamie JF, Truscott RJW. UV filter instability: consequences for the human lens. *Exp Eye Res*. (2002) 75:165–75. doi: 10.1006/exer.2002.2012

110. Bova LM, Sweeney MHJ, Jamie JF, Truscott RJW. Major changes in human ocular UV protection with age. *Invest Ophthalmol Visual Sci*. (2001) 42:200–5.

111. Taylor LM, Aquilina JA, Jamie JF, Truscott RJW. Glutathione and NADH, but not Ascorbate, Protect Lens Proteins from Modification by UV Filters. *Exp Eye Res*. (2002) 74:503–11. doi: 10.1006/exer.2001.1165

112. Tsentalovich YP, Snytnikova OA, Forbes MDE, Chernyak EI, Morozov SV. Photochemical and thermal reactivity of kynurenine. *Exp Eye Res*. (2006) 83:1439–45. doi: 10.1016/j.exer.2006.07.022

113. Tsentalovich YP, Snytnikova OA, Sagdeev RZ. Photochemical and thermal reactions of kynurenines. *Russian Chem Rev*. (2008) 77:189–97. doi: 10.1070/RC2008v077n09ABEH003880

114. Stutchbury GM, Truscott RJW. The modification o proteins by 3-hydroxykynurenine. *Exp Eye Res*. (1993) 57:149–55. doi: 10.1006/exer.1993.1110

115. Demarais NJ, Donaldson PJ, Grey AC. Age-related spatial differences of human lens UV filters revealed by negative ion mode MALDI imaging mass spectrometry. *Exp Eye Res*. (2019) 184:146–51. doi: 10.1016/j.exer.2019.04.016

116. Tamara SO, Yanshole LV, Yanshole VV, Fursova AZ, Stepakov DA, Novoselov VP, et al. Spatial distribution of metabolites in the human lens. *Exp Eye Res*. (2016) 143:68–74. doi: 10.1016/j.exer.2015.10.015

117. Garner B, Vazquez S, Griffith R, Lindner RA, Carver JA, Truscott RJW. Identification of glutathionyl-3-hydroxykynurenine glucoside as a novel fluorophore associated with aging of the human lens. *J Biol Chem*. (1999) 274:20847–54. doi: 10.1074/jbc.274.30.20847

118. Hains PG, Mizdrak J, Streete IM, Jamie JF, Truscott RJW. Identification of the new UV filter compound cysteine-L-3-hydroxykynurenine O-B-D-glucoside in human lenses. *FEBS Letters*. (2006) 580:5071–6. doi: 10.1016/j.febslet.2006.08.026

119. Korlimbinis A, Truscott RJW. Identification of 3-hydroxykynurenine bound to proteins in the human lens. A possible role in age-related nuclear cataract†. *Biochemistry*. (2006) 45:1950–60. doi: 10.1021/bi051744y

120. Truscott RJ, Martin F. The reaction of proteins with 3-hydroxyanthranilic acid as a possible model for senile nuclear cataract in man. *Exp Eye Res*. (1989) 49:927–40. doi: 10.1016/S0014-4835(89)80017-X

121. Hood BD, Garner B, Truscott RJW. Human lens coloration and aging. *J Biol Chem*. (1999) 274:32547–50. doi: 10.1074/jbc.274.46.32547

122. Korlimbinis A, Aquilina JA, Truscott RJ. Protein-bound and free UV filters in cataract lenses. *concent UV filters is much lower than normal lenses Exp Eye Res*. (2007) 85:21–225. doi: 10.1016/j.exer.2007.04.004

123. Streete IM, Jamie JF, Truscott RJW. Lenticular levels of amino acids and free UV filters differ significantly between normals and cataract patients. *Invest Opthalmol Visual Sci*. (2004) 45:4091. doi: 10.1167/iovs.04-0178

124. Truscott RJW, Augusteyn RC. The state of sulphydryl groups in normal and cataractous human lenses. *Exp Eye Res*. (1977) 25:139–48. doi: 10.1016/0014-4835(77)90126-9

125. Roberts JE, Wishart JF, Martinez L, Chignell CF. Photochemical studies on xanthurenic acid. *Photochem Photobiol*. (2000) 72:467–71. doi: 10.1562/0031-8655(2000)072<0467:PSOXA>2.0.CO;2

126. Shirao E, Ando K, Inoue A, Shirao Y, Balasubramanian D. Identification of a novel fluorophore, xanthurenic acid 8-O-D-glucoside in human brunescent cataract. *Exp Eye Res*. (2001) 73:421–31. doi: 10.1006/exer.2001.1051

127. Hains PG, Truscott RJ. Proteomic analysis of the oxidation of cysteine residues in human age-related nuclear cataract lenses. *Biochim Biophys Acta*. (2008) 1784:1959–64. doi: 10.1016/j.bbapap.2008.07.016

128. Malina HZ, Martin XD. Xanthurenic acid derivative formation in the lens is responsible for senile cataract in humans. *Graefe's Arch Clin Exp Ophthalmol*. (1996) 234:723–30. doi: 10.1007/BF00189352

129. Roberts JE, Finley EL, Patat SA, Schey KL. Photooxidation of lens proteins with zanthurenic acid: A putative chromophore for cataractogenesis. *Photochem Photobiol*. (2001) 74:740–4. doi: 10.1562/0031-8655(2001)074<0740:POLPWX>2.0.CO;2

130. Linetsky M, Raghavan CT, Johar K, Fan X, Monnier VM, Vasavada AR, et al. UVA light-excited kynurenines oxidize ascorbate and modify lens proteins through the formation of advanced glycation end products. *Implic Hum lens Aging cataract form J Biol Chem*. (2014) 289:17111–23. doi: 10.1074/jbc.M114.554410

131. Garner MH, Spector A. Selective oxidation of cysteine and methionine in normal and senile cataractous lenses. *Proc Natl Acad Sci USA*. (1980) 77:1274–7. doi: 10.1073/pnas.77.3.1274

132. Spector A, Wang G-M, Wang R-H, Li W-C, Kleiman NJ. A brief photochemically induced oxidative insult causes irreversible lens damage and cataract II. *Mech action Exp Eye Res*. (1995) 60:483–93. doi: 10.1016/S0014-4835(05)80063-6

133. Finley EL, Busman M, Dillon J, Crouch RK, Schey KL. Identification of photooxidation sites in bovine α-crystallin. *Photochem Photobiol*. (1997) 66:635–41. doi: 10.1111/j.1751-1097.1997.tb03200.x

134. Korlimbinis A, Hains PG, Truscott RJW, Aquilina JA. 3-hydroxykynurenine oxidizes alpha-crystallin: potential role in cataractogenesis. *Biochemistry*. (2006) 45:1852–60. doi: 10.1021/bi051737+

135. Breadsell RO, Wegener A, Breipohl W, Hirst LW. UV-B radiation-induced cataract in the royal college of surgeons rat. *Ophthal Res*. (1994) 26:84–9. doi: 10.1159/000267522

136. Chauss D, Brennan LA, Bakina O, Kantorow M. Integrin aV5-mediated Removal of Apoptotic Cell Debris bythe Eye Lens and Its Inhibition by UV Light Exposure. *J Biol Chem*. (2015) 290:30253–66. doi: 10.1074/jbc.M115.688390

137. Lv J, Xing Y. Effects of UV on apoptotic factors in lens epithelial cells of an animal model. *Exp Ther Med*. (2018) 16:2309–12. doi: 10.3892/etm

138. Xiang J-W, Xiao Y, Gan Y, Chen H, Liu Y, Wang L, et al. Glucose oxidase- and UVA-induced changes in the expression patterns of seven de-sumoylation enzymes (SENPs) are associated with cataract development. *Curr Mol Med*. (2019) 19:48–53. doi: 10.2174/1566524019666190311094313

139. Jiang Y, Fu R, Zhao J, Wu D, Qiao G, Li R. Effects of ELL-associated factor 2 on ultraviolet radiation-induced cataract formation in mice. *Mol Med Rep*. (2015) 12:6605–11. doi: 10.3892/mmr.2015.4281

140. Ayala M, Strid H, Jacobsson U, Söderberg PG. p53 expression and apoptosis in the lens after ultraviolet radiation exposure. *Invest Opthalmol Visual Sci*. (2007) 48:4187. doi: 10.1167/iovs.06-0660

141. Michael R, Vrensen GFJM, van Marle J, Gan L, Söderberg PG. Apoptosis in the rat lens after *in vivo* threshold dose ultraviolet irradiation. *Invest Ophthalmol Visual Sci*. (1998) 39:2681–7.

142. Li W-C, Spector A. Lens epithelial cell apoptosis is an early event in the development of UVB-induced cataract. *Free Radical Biol Med*. (1995) 20:301–11. doi: 10.1016/0891-5849(96)02050-3

143. Ueda Y, Duncan MK, David LL. Lens proteomics: the accumulation of crystallin modifications in the mouse lens with age. *Invest Ophthalmol Visual Sci*. (2002) 43:205–15.

144. Bloemendal H, De Jong W, Jaenicke R, Lubsen NH, Slingsby C, Tardieu A. Ageing and vision: structure, stability and function of lens crystallins. *Prog Biophys Mol Biol*. (2004) 86:407–85. doi: 10.1016/j.pbiomolbio.2003.11.012

145. Gouras P, Ekesten B. Why do mice have ultra-violet vision? *Exp Eye Res*. (2004) 79:887–92. doi: 10.1016/j.exer.2004.06.031

146. Varma SD, Hegde KR, Kovtun S. UV-B-induced damage to the lens *in vitro* prevention by caffeine. *J Ocular Pharmacol Ther*. (2008) 24:439–44. doi: 10.1089/jop.2008.0035

147. Varma SD, Kovtun S, Hegde KR. Role of ultraviolet irradiation and oxidative stress in cataract formation—Medical prevention by nutritional antioxidants and metabolic agonists. *Eye Contact Lens: Sci Clin Pract*. (2011) 37:233–45. doi: 10.1097/ICL.0b013e31821ec4f2

148. Jose JG. Posterior cataract induction by UV-B radiation in albino mice. *Exp Eye Res*. (1986) 42:11–20. doi: 10.1016/0014-4835(86)90013-8

149. Jose JG, Pitts DG. Wavelength dependency of cataracts in albino mice following chronic exposure. *Exp Eye Res*. (1985) 41:545–63. doi: 10.1016/S0014-4835(85)80011-7

150. Meyer LM, Söderberg P, Dong X, Wegener A. UVR-B induced cataract development in C57 mice. *Exp Eye Res*. (2005) 81:389–94. doi: 10.1016/j.exer.2005.02.009

151. Meyer LM, Löfgren S, Holz FG, Wegener A, Söderberg P. Bilateral cataract induced by unilateral UVR-B exposure - evidence for an inflammatory response. *Acta Ophthalmol*. (2013) 91:236–42. doi: 10.1111/j.1755-3768.2012.02384.x

152. Zigman S, Schultz J, Yulo T. Possible roles of near UV light in the cataractous process. *Exp Eye Res*. (1973) 15:201–8. doi: 10.1016/0014-4835(73)90120-6

153. Zigman S, Yulo T, Schultz J. Cataract induction in mice exposed to near UV light. *Ophthal Res*. (1974) 6:259–70. doi: 10.1159/000264710

154. Pirie A. Color and solubility of the proteins of human cataracts. *Invest Ophthalmol Visual Sci*. (1968) 7:634–50.

155. Zhang J, Yan H, Löfgren S, Tian X, Lou MF. Ultraviolet radiation–induced cataract in mice: the effect of age and the potential biochemical mechanism. *Invest Opthalmol Visual Sci*. (2012) 53:7276. doi: 10.1167/iovs.12-10482

156. Meyer LM, Löfgren S, Ho Y-S, Lou MF, Wegener A, Holz F, et al. Absence of glutaredoxin1 increases lens susceptibility to oxidative stress induced by UVR-B. *Exp Eye Res*. (2009) 89:833–9. doi: 10.1016/j.exer.2009.07.020

157. Padgaonkar VA, Leverenz VR, Bhat AV, Pelliccia SE, Giblin FJ. Thioredoxin Reductase Activity may be More Important than GSH Level in Protecting Human Lens Epithelial Cells against UVA Light. *Photochem Photobiol*. (2015) 91:387–96. doi: 10.1111/php.12404

158. Xing K-Y, Lou MF. Effect of age on the thioltransferase (Glutaredoxin) and thioredoxin systems in the human lens. *Invest Ophthalmol Visual Sci*. (2010) 51:6598. doi: 10.1167/iovs.10-5672

159. Ramaekers F, Dodemont H, Vorstenbosch P, Bloemendal H. Classification of rat lens crystallins and identification of proteins encoded by rat lens mRNA. *Eur J Biochem*. (1982) 128:503–8. doi: 10.1111/j.1432-1033.1982.tb06993.x

160. Galichanin K, Löfgren S, Söderberg PG. Cataract after Repeated Daily *in vivo* Exposure to Ultraviolet Radiation. *Health Phys*. (2014) 107:523–9. doi: 10.1097/HP.0000000000000152

161. Levere TE. The primary visual system of the rat: A primer of its anatomy. *Physiol Psychol*. (1978) 6:142–69. doi: 10.3758/BF03326707

162. Gorgels TG, van Norren D. Ultraviolet and green light cause different types of damage in rat retina. *Invest Ophthalmol Visual Sci*. (1995) 36:851–63.

163. Galichanin K, Löfgren S, Bergmanson J, Söderberg PG. Evolution of damage in the lens after *in vivo* close to threshold exposure to UV-B radiation: Cytomorphological study of apoptosis. *Exp Eye Res*. (2010) 91:369–77. doi: 10.1016/j.exer.2010.06.009

164. Torriglia A, Zigman S. The effect of near-UV light on Na-K-ATPase of the rat lens. *Curr Eye Res*. (1988) 7:539–48. doi: 10.3109/02713688809031809

165. Risa Ø, Sæther O, Löfgren S, Söderberg PG, Krane J, Midelfart A. Metabolic changes in rat lens after *in vivo* exposure to ultraviolet irradiation: measurements by high resolution MAS1H NMR spectroscopy. *Invest Opthalmol Visual Sci*. (2004) 45:1916. doi: 10.1167/iovs.03-1292

166. Risa Ø, Sæther O, Kakar M, Mody VC, Löfgren S, Söderberg PG, et al. Time dependency of metabolic changes in rat lens after *in vivo* UVB irradiation analysed by HR-MAS 1H NMR spectroscopy. *Exp Eye Res*. (2005) 81:407–24. doi: 10.1016/j.exer.2005.02.012

167. Löfgren S, Söderberg PG. Rat lens glycolysis after *in vivo* exposure to narrow band UV or blue light radiation. *J Photochem Photobiol B: Biol*. (1995) 30:145–51. doi: 10.1016/1011-1344(95)07183-3

168. Hightower KR, Harrison SE. The influence of calcium on glucose metabolism in the rabbit lens. *Invest Ophthalmol Visual Sci*. (1987) 28:1433–6.

169. Reddy B, Bhat S. Protection against UVB inactivation (*in vitro*) of rat lens enzymes by natural antioxidants. *Mol Cell Biochem*. (1999) 194:41–5. doi: 10.1023/a:1006966318403

170. Christen WG, Glynn RJ, Sesso HD, Kurth T, MacFadyen J, Bubes V, et al. Age-related cataract in a randomized trial of vitamins E and C in men. *Arch Ophthalmol*. (2010) 128:1397. doi: 10.1001/archophthalmol.2010.266

171. Mathew MC, Ervin A-M, Tao J, Davis RM. Antioxidant vitamin supplementation for preventing and slowing the progression of age-related cataract. *Cochrane Database Systema Rev*. (2012) 6:1–62. doi: 10.1002/14651858

172. Lim JC, Caballero Arredondo M, Braakhuis AJ, Donaldson PJ. Vitamin C and the lens: new insights into delaying the onset of cataract. *Nutrients*. (2020) 12:3142. doi: 10.3390/nu12103142

173. Löfgren S, Michael R, Söderberg P. Impact of iris pigment and pupil size in ultraviolet radiation cataract in rat. *Acta Ophthalmol*. (2010) 90:44–8. doi: 10.1111/j.1755-3768.2010.01871.x

174. Löfgren S. Lenses from Brown-Norway pigmented rats are more tolerant to *in vitro* ultraviolet irradiation than lenses from Fischer-344 albino rats. *Acta Ophthalmol*. (2012) 90:179–83. doi: 10.1111/j.1755-3768.2010.01903.x

175. Merriam JC, Löfgren S, Michael R, Söderberg PG, Dillon JP, Zheng L, et al. An action spectrum for UV-B radiation and the rat lens. *Invest Ophthalmol Visual Sci*. (2000) 41:2642–7.

176. Negelspach DC, Kaladchibachi S, Fernandez F. The circadian activity rhythm is reset by nanowatt pulses of ultraviolet light. *Proc R Soc B: Biol Sci*. (2018) 285:20181288. doi: 10.1098/rspb.2018.1288

177. Borchman D, Giblin FJ, Leverenz VR, Reddy VN, Lin L-R, Yappert MC, et al. Impact of aging and hyperbaric oxygen *in vivo* on Guinea pig lens lipids and nuclear light scatter. *Invest Ophthalmol Visual sci*. (2000) 41:3061–73.

178. Giblin FJ, Anderson DM, Han J, Rose KL, Wang Z, Schey KL. Acceleration of age-induced proteolysis in the Guinea pig lens nucleus by *in vivo* exposure to hyperbaric oxygen: a mass spectrometry analysis. *Exp Eye Res*. (2021) 210:1–8. doi: 10.1016/j.exer.2021.108697

179. Giblin FJ, Padgaonkar VA, Leverenz VR, Lin L-R, Lou MF, Unakar NJ, et al. Nuclear light scattering, disulfide formation and membrane damage in lenses of older Guinea pigs treated with hyperbaric oxygen. *Exp Eye Res*. (1995) 60:219–35. doi: 10.1016/S0014-4835(05)80105-8

180. Padgaonkar VA, Leverenz VR, Rinke A, Reddy VN, Giblin FJ. Hyperbaric oxygen *in vivo* accelerates the loss of cytoskeletal proteins and MIP26 in Guinea pig lens nucleus. *Exp Eye Res*. (1999) 68:493–505. doi: 10.1006/exer.1998.0630

181. Kosegarten DC, Maher TJ. Use of Guinea pigs as model to study galactose-induced cataract formation. *J Pharma Sci*. (1978) 67:1478–9. doi: 10.1002/jps.2600671045

182. Yokoyama T, Sasaki H, Giblin FJ, Reddy VN. A physiological level of ascorbate inhibits galactose cataract in Guinea pigs by decreasing polyol accumulation in the lens epithelium: a dehydroascorbate-linked mechanism. *Exp Eye Res*. (1994) 58:207–18. doi: 10.1006/exer.1994.1009

183. Giblin FJ. Glutathione: A vital lens antioxidant. *J Ocular Pharmacol Ther*. (2000) 16:121–35. doi: 10.1089/jop.2000.16.121

184. Yu N-T, DeNagel DC, Pruett PL, Kuck JFR. Disulfide bond formation in the eye lens. *Proc Natl Acad Sci*. (1985) 82:7965–8. doi: 10.1073/pnas.82.23.7965

185. Barron BC, Yu N-T, Kuck JFRJ. Raman spectroscopic evaluation of aging and long-wave UV exposure in the Guinea pig lens: A possible model for human aging. *Exp Eye Res*. (1988) 46:249–58. doi: 10.1016/S0014-4835(88)80082-4

186. Bergbauer KL, Kuck JFR, Su KC, Yu N-T. Use of a UV-Blocking contact lens in evaluation of UV-induced damage to the Guinea pig lens. *Int Contact Lens Clinic*. (1991) 18:182–7. doi: 10.1016/0892-8967(91)90005-K

187. Truscott RJW, Augusteyn RC. Changes in human lens proteins during nuclear cataract formation. *Exp Eye Res*. (1977) 24:159–70. doi: 10.1016/0014-4835(77)90256-1

188. Simpanya MF, Ansari RR, Leverenz VR, Giblin FJ. Measurement of lens protein aggregation *in vivo* using dynamic light scattering in a Guinea pig/UVA model for nuclear cataract. *Photochem Photobiol*. (2008) 84:1589–95. doi: 10.1111/j.1751-1097.2008.00390.x

189. Cunningham ML, Johnson JS, Giovanazzi SM, Peak MJ. Photosensitized production of superoxide anion by monochromatic (290-405 nm) ultraviolet irradiation of NADH and NADPH coenzymes. *Photochem Photobiol*. (1985) 42:125–8. doi: 10.1111/j.1751-1097.1985.tb01549.x

190. Czochralska B, Kawczynski W, Bartosz G, Shugar D. Oxidation of excited-state NADH and NAD dimer in aqueous medium involvement of O2 as a mediator in the presence of oxygen. *Biochem Biophys Acta*. (1984) 801:403–9. doi: 10.1016/0304-4165(84)90145-4

191. Mody VC, Kakar M, Söderberg PG, Löfgren S. High lenticular tolerance to ultraviolet radiation-B by pigmented Guinea pig; application of a safety limit strategy for UVR induced cataract. *Acta Ophthalmol*. (2012) 90:226–30. doi: 10.1111/j.1755-3768.2010.01931.x

192. Rao CM, Zigler JS. Levels of reduced pyridine nucleotides and lens photodamage. *Photochem Photobiol*. (1992) 56:523–8. doi: 10.1111/j.1751-1097.1992.tb02196.x

193. Rao PV, Gonzalez P, Persson B, Jörnvall H, Garland D, Zigler JS. Guinea pig and bovine ζ-crystallins have distinct functional characteristics highlighting replacements in otherwise similar structures. *Biochemistry*. (1997) 36:5353–62. doi: 10.1021/bi9622985

194. Zigman S, Paxhia T, McDaniel T, Lou MF, Yu N-T. Effect of chronic near-ultraviolet radiation on the gray squirrel lens *in vivo*. *Invest Ophthalmol Visual Sci*. (1991) 32:1723–32.

195. Blondin J, Baragi V, Schwartz E, Sadowski JA, Taylor A. Delay of UV induced eye lens protein damage in Guinea pigs by dietary ascorbate. *J Free Radicals Biol Med*. (1986) 2:275–81. doi: 10.1016/S0748-5514(86)80010-1

196. Malik A, Kojima M, Sasaki K. Morphological and biochemical changes in lenses of Guinea pigs after vitamin-C-deficient diet and UV-B radiation. *Ophthal Res*. (1995) 27:189–96. doi: 10.1159/000267704

197. Reddy VN, Giblin FJ, Lin L-R, Chakrapani B. The effect of aqueous humor ascorbate on ultraviolet B-induced DNA damage in lens epithelium. *Invest Ophthalmol Visual Sci*. (1998) 39:344–50.

198. Giblin FJ, Schrimscher L, Chakrapani B, Reddy VN. Exposure of rabbit lens to hyperbaric oxygen *in vitro*: regional effects on GSH level. *Invest Ophthalmol Visual Sci*. (1988) 29:1312–9.

199. Padgaonkar VA, Giblin FJ, Reddy VN. Disulfide cross-linking of urea-insoluble proteins in rabbit lenses treated with hyperbaric oxygen. *Exp Eye Res*. (1989) 49:887–99. doi: 10.1016/s0014-4835(89)80047-8

200. Padgaonkar VA, Giblin FJ, Reddan JR, Dziedzic DC. Hyperbaric oxygen inhibits the growth of cultured rabbit lens epithelial cells without affecting glutathione level. *Exp Eye Res*. (1993) 56:443–52. doi: 10.1006/exer.1993.1057

201. Rogers CS, Chan L-M, Sims YS, Byrd KD, Hinton DL, Twining SS. The effects of sub solar levels of UV-A and UV-B on rabbit corneal and lens epithelial cells. *Exp Eye Res*. (2004) 78:1007–14. doi: 10.1016/j.exer.2003.12.011

202. Zigman S, McDaniel T, Schultz JB, Reddan J, Meydani M. Damage to cultured lens epithelial cells of squirrels and rabbits by UV-A (99.9%) plus UV-B (0.1%) radiation and alpha tocopherol protection. *Mol Cell Biochem*. (1995) 143:35–46. doi: 10.1007/bf00925924

203. Sidjanin D, Grdina D, Woloschak GE. UV-induced changes in cell cycle and gene expression within rabbit lens epithelial cells. *Photochem Photobiol*. (1996) 63:79–85. doi: 10.1111/j.1751-1097.1996.tb02995.x

204. Sidjanin D, Zigman S, Reddan J. DNA damage and repair in rabbit lens epithelial cells following UVA radiation. *Curr Eye Res*. (1993) 12:773–81. doi: 10.3109/02713689309020382

205. Zigman S, Reddan J, Schultz JB, McDaniel T. Structural and functional changes in catalase induced by near-UV radiation. *Photochem Photobiol*. (1996) 63:818–24. doi: 10.1111/j.1751-1097.1996.tb09637.x

206. Andley UP, Lewis RM, Reddan JR, Kochevar IE. Action spectrum for cytotoxicity in the UVA- and UVB-wavelength region in cultured lens epithelial cells. *Invest Ophthalmol Visual Sci*. (1994) 35:367–73.

207. Giblin FJ, Lin L-R, Simpanya MF, Leverenz VR, Fick CE. A Class I UV-blocking (senofilcon A) soft contact lens prevents UVA-induced yellow fluorescence and NADH loss in the rabbit lens nucleus *in vivo*. *Exp Eye Res*. (2012) 102:17–27. doi: 10.1016/j.exer.2012.06.007

208. Chandler HL, Reuter KS, Sinnott LT, Nichols JJ. Prevention of UV-induced damage to the anterior segment using class I UV-absorbing hydrogel contact lenses. *Invest Ophthalmol Visual Sci*. (2010) 51:172–8. doi: 10.1167/iovs.09-3996

209. Pitts DG, Cullen AP, Hacker PD. Ocular effects of ultraviolet radiation from 295 to 365 nm. *Invest Ophthalmol Visual Sci*. (1977) 16:932–9.

210. Rafferty NS, Zigman S, McDaniel T, Scholz DL. Near-UV radiation disrupts filamentous actin in lens epithelial cells. *Cell Motil Cytoskeleton*. (1993) 26:40–8. doi: 10.1002/cm.970260105

211. Fris M, Čejková J, Midelfart A. The effect of single and repeated UVB radiation on rabbit lens. *Graefe's Arch Clin Exp Ophthalmol*. (2008) 246:551–8. doi: 10.1007/s00417-007-0747-6

212. Hightower KR, McCready J. Physiological effects of UVB irradiation on cultured rabbit lens. *Invest Ophthalmol Visual Sci*. (1992) 33:1783–7.

213. Hightower K, McCready J. Comparative effect of UVA and UVB on cultured rabbit lens. *Photochem Photobiol*. (1993) 58:827–30. doi: 10.1111/j.1751-1097.1993.tb04978.x

214. Tessem M-B, Midelfart A, Čejková J, Bathen TF. Effect of UVA and UVB irradiation on the metabolic profile of rabbit cornea and lens analysed by HR-MAS 1H NMR spectroscopy. *Ophthal Res*. (2006) 38:105–14. doi: 10.1159/000090511

215. Čejka Č, Pláteník J, Buchal R, Guryca V, Širc J, Vejražka M, et al. Effect of two different UVA doses on the rabbit cornea and lens. *Photochem Photobiol*. (2009) 85:794–800. doi: 10.1111/j.1751-1097.2008.00478.x

216. van Heyningen R. Fluorescent glucoside in the human lens. *Nature*. (1971) 230:393–4. doi: 10.1038/230393a0

217. van Heyningen R. Fluorescent derivatives of 3-hydroxy-L-kynurenine in the lens of man, the baboon and the grey squirrel. *Biochem J*. (1971) 123:30P–1P. doi: 10.1042/bj1230030P

218. Manthey MK, Jamie JF, Truscott RJW. Synthesis of human ultraviolet filter compounds: O-β-d-glucopyranosides of 3-hydroxykynurenine and 2-amino-3-hydroxy-γ-oxobenzenebutanoic acid. *J Organ Chem*. (1999) 64:3930–3. doi: 10.1021/jo982321n

219. Gaillard ER, Zheng L, Merriam JC, Dillon JP. Age-related changes in the absorption characteristics of the primate lens. *Invest Ophthalmol Visual Sci*. (2000) 41:1454–9.

220. Borja D, Manns F, Ho A, Ziebarth NM, Acosta AC, Arrieta-Quintero E, et al. Refractive power and biometric properties of the nonhuman primate isolated crystalline lens. *Invest Ophthalmol Visual Sci*. (2010) 51:2118–25. doi: 10.1167/iovs.09-3905

221. Gaillard ER, Merriam JC, Zheng L, Dillon J. Transmission of light to the young primate retina: possible implicationsfor the formation of lipofuscin. *Photochem Photobiol*. (2011) 87:18–21. doi: 10.1111/j.1751-1097.2010.00837.x

222. Pitts DG, Bergmanson JPG, Chu LWF. Ultrastructural analysis of corneal exposure to UV radiation. *Acta Ophthalmol*. (1987) 65:263–73. doi: 10.1111/j.1755-3768.1987.tb08504.x

223. Collier R, Zigman S. The grey squirrel lens protects the retina from near-UV radiation damage. *Prog Clin Biol Res*. (1987) 247:571–85.

224. Zigman S, Paxhia T. The nature and properties of squirrel lens yellow pigment. *Exp Eye Res*. (1988) 47:819–24. doi: 10.1016/0014-4835(88)90065-6

225. Hains PG, Simpanya MF, Giblin F, Truscott RJW. UV filters in the lens of the thirteen lined ground squirrel (Spermophilus tridecemlineatus). *Exp Eye Res*. (2006) 82:730–7. doi: 10.1016/j.exer.2005.09.014

226. Lyons B, Karuso P, Jamie JF, Simpanya MF, Giblin FJ, Truscott RJW. Characterisation of a novel UV filter in the lens of the thirteen-lined ground squirrel (*Ictidomys tridecemlineatus*). *Exp Eye Res*. (2014) 121:114–20. doi: 10.1016/j.exer.2014.01.022

227. Malina HZ, Martin XD. Deamination of 3-hydroxykynurenine in bovine lenses: a possible mechanism of cataract formation in general. *Graefe's Arch Clin Exp Ophthalmol*. (1995) 233:38–44. doi: 10.1007/BF00177784

228. Thorpe A, Truscott RJW, Douglas RH. Kynurenine identified as the short-wave absorbing lens pigment in the deep-sea fish stylephorus chordatus. *Exp Eye Res*. (1992) 55:53–7. doi: 10.1016/0014-4835(92)90091-6

229. Truscott RJ, Carver JA, Thorpe A, Douglas RH. Identification of 3-hydroxykynurenine as the lens pigment in the gourami Trichogaster trichopterus. *Exp Eye Res*. (1992) 54:1015–7. doi: 10.1016/0014-4835(92)90167-Q

230. Zigman S. Special features of the lens relative to the environment. *Lens Eye Toxic Res*. (1989) 6:807–21.

231. Douglas RH, Jeffery G. The spectral transmission of ocular media suggests ultraviolet sensitivity is widespread among mammals. *Proc R Soc B: Biol Sci*. (2014) 281:20132995. doi: 10.1098/rspb.2013.2995

232. Grey AC, Schey KL. Distribution of bovine and rabbit lens α-crystallin products by MALDI imaging mass spectrometry. *Mol Vision*. (2008) 14:171–9.

233. Selivanova OM, Galzitskaya OV. Structural and functional peculiarities of α-crystallin. *Biology*. (2020) 9:85. doi: 10.3390/biology9040085

234. Marussich L, Manns F, Nankivil D, Maceo Heilman B, Yao Y, Arrieta-Quintero E, et al. Measurement of crystalline lens volume during accommodation in a lens stretcher. *Invest Ophthalmol Visual Sci*. (2015) 56:4239–48. doi: 10.1167/iovs.15-17050

235. Hott JL, Borkman RF. Concentration dependence of transmission losses in UV-laser irradiated bovine α-, βH-,βL- and γ-crystallin solutions. *Photochem Photobiol*. (1993) 57:312–7. doi: 10.1111/j.1751-1097.1993.tb02293.x

236. Krivandin AV, Muranov KO, Yakovlev FY, Poliansky NB, Wasserman LA, Ostrovsky MA. Resistance of α-crystallin quaternary structure to UV irradiation. *Biochem (Moscow)*. (2009) 74:633–42. doi: 10.1134/S0006297909060078

237. Ostrovsky MA, Sergeev YV, Atkinson DB, Soustov LV, Hejtmancik JF. Comparison of ultraviolet induced photo-kinetics for lens-derived and recombinant β-crystallins. *Mol Vision*. (2002) 8:72–8.

238. Chelnokov E, Soustov L, Sapogova N, Ostrovsky M, Bityurin N. Nonreciprocal XeCl laser-induced aggregation of β -crystallins in water solution. *Opt Express*. (2008) 16:18798. doi: 10.1364/OE.16.018798

239. Kleiman NJ, Wang R-R, Spector A. Ultraviolet induced DNA damage and repair in bovine lens epithelial cells. *Curr Eye Res*. (1990) 9:1185–93. doi: 10.3109/02713689009003475

240. Stuart DD, Cullen AP, Sivak JG, Doughty MJ. Optical effects of UV-A and UV-B radiation on the cultured bovine lens. *Curr Eye Res*. (1994) 13:371–6. doi: 10.3109/02713689409167301

241. Stuart DD, Sivak JG, Cullen AP, Weerheim JA, Monteith CA. UV-B radiation and the optical properties of cultured bovine lenses. *Curr Eye Res*. (1991) 10:177–84. doi: 10.3109/02713689109001746

242. Dovrat A, Weinreb O. Recovery of lens optics and epitehlial enzymes after ultraviolet A radiation. *Invest Ophthalmol Visual Sci*. (1995) 36:2417–24.

243. Reddy B, Bhat S. UVB irradiation alters the activities and kinetic properties of the enzymes of energy metabolism in rat lens during aging. *J Photochem Photobiol B: Biol*. (1998) 42:40–6. doi: 10.1016/S1011-1344(97)00114-0

244. Dovrat A, Weinreb O. Effects of UV-A radiation on lens epithelial NaK-ATPase in organ culture. *Invest Ophthalmol Visual Sci*. (1999) 40:1616–20.

245. Weinreb O, Adrianus M, van Boekel M, Dovrat A, Bloemendal H. Effect of UV-A light on the chaperone-like properties of young and old lens α-crystallin. *Invest Ophthalmol Visual Sci*. (2000) 41:191–8.

246. van Heyningen R. The human lens III some observations on the post-mortem lens. *Exp Eye Res*. (1972) 13:155–60. doi: 10.1016/0014-4835(72)90028-0

247. Evans JW. Anatomy and histology of the eye and orbit in domestic animals. *Arch Neurol*. (1961) 5:693–. doi: 10.1001/archneur.1961.00450180115017

248. Olsen TW, Sanderson S, Feng X, Hubbard WC. Porcine sclera: thickness and suface area. *Invest Ophthalmol Visual Sci*. (2002) 43:2529–32.

249. Artigas CN, López-Murcia M-M, Felipe A, Desco C, Artigas J-M. Spectral transmission of the pig lens: effect of ultraviolet A+B radiation. *J Francais d'Ophtalmol*. (2014) 37:773–9. doi: 10.1016/j.jfo.2014.06.006

250. Keenan J, Orr DF, Pierscionek BK. Patterns of crystallin distribution in porcine eye lenses. *Mol Vision*. (2008) 14:1245–53.

251. Heys KR, Friedrich MG, Truscott RJW. Presbyopia and heat: changes associated with aging of the human lens suggest a functional role for the small heat shock protein, α-crystallin, in maintaining lens flexibility. *Aging Cell*. (2007) 6:807–15. doi: 10.1111/j.1474-9726.2007.00342.x

252. Oriowo OM, Cullen AP, Sivak JG. Impairment of eye lens cell physiology and optics by broadband ultraviolet A-ultraviolet B radiation. *Photochem Photobiol*. (2002) 76:361–7. doi: 10.1562/0031-8655(2002)076<0361:IOELCP>2.0.CO;2

253. Lee J-S, Liao J-H, Wu S-H, Chiou S-H. a-crystallin acting as a molecular chaperonin against photodamage by UV irradiation. *J Protein Chem*. (1997) 16:283–9. doi: 10.1023/A:1026305025816

254. Honisch C, Donadello V, Hussain R, Peterle D, De Filippis V, Arrigoni G, et al. Application of circular dichroism and fluorescence spectroscopies to assess photostability of water-soluble porcine lens proteins. *ACS Omega*. (2020) 5:4293–301. doi: 10.1021/acsomega.9b04234

255. Zhang TO, Alperstein AM, Zanni MT. Amyloid β-sheet secondary structure identified in UV-induced cataracts of porcine lenses using 2D IR spectroscopy. *J Mol Biol*. (2017) 429:1705–21. doi: 10.1016/j.jmb.2017.04.014

256. Oriowo OM, Cullen AP, Chou BR, Sivak JG. Action spectrum and recovery for *in vitro* UV-induced cataract using whole lenses. *Invest Ophthalmol Visual Sci*. (2001) 42:2596–602.

257. Yuan D, Liu Q. Photon energy and photon behaviour discussions. *Energy Rep*. (2022) 8:22–42. doi: 10.1016/j.egyr.2021.11.034

258. Lou MF, Dickerson JE. Protein-thiol mixed disulfides in human lens. *Exp Eye Res*. (1992) 55:889–96. doi: 10.1016/0014-4835(92)90015-K

259. Thomas DM, Papadopoulou O, Mahendroo PP, Zigman S. Phosphorous-31 NMR study of the effects of UV on squirrel lenses. *Exp Eye Res*. (1993) 57:59–65. doi: 10.1006/exer.1993.1099

260. Nagalaxmi V, Praveen KM, Sashidhar R, Turlapati NR. UV-B exposure increases the activity of indoleamine 2, 3-dioxygenase (Ido) and alters the levels of tryptophan metabolites in Indian ground squirrel (Funambulus palmarum) lens. *J Diabetic Complic Med*. (2015) 1:6. doi: 10.4172/2475-3211.1000102

261. Zigman S, Paxhia T, Waldron W. Effects of near-UV radiation on the protein of the grey squirrel lens. *Curr Eye Res*. (1988) 7:531–7. doi: 10.3109/02713688809031808

262. Horwitz J, Neuhaus R, Dockstader J. Analysis of microdissected cataractous human lenses. *Invest Ophthalmol Visual Sci*. (1981) 21:616–9.

263. Takikawa O, Truscott RJW, Fukao M, Miwa S. *Age-Related Nuclear Cataract and Indoleamine 2,3-Dioxygenase-Initiated Tryptophan Metabolism in the Human Lens*. Boston, MA, USA: Springer US (2003) p. 277–85.

264. Malina HZ, Martin XD. Indoleamine 2,3-dioxygenase: Antioxidant enzyme in the human eye. *Graefe's Arch Clin Exp Ophthalmol*. (1996) 234:457–62. doi: 10.1007/BF02539413

265. Donaldson PJ, Grey AC, Maceo Heilman B, Lim JC, Vaghefi E. The physiological optics of the lens. *Prog Retinal Eye Res*. (2016) 56:1–24. doi: 10.1016/j.preteyeres.2016.09.002

266. Wood AM, Truscott RJW. Ultraviolet filter compounds in human lenses: 3-hydroxykynurenine glucoside formation. *Vision Res*. (1994) 34:1369–74. doi: 10.1016/0042-6989(94)90135-X

267. Tsentalovich YP, Verkhovod T, Yanshole VV, Kiryutin A, Yanshole LV, Fursova AZ, et al. Metabololmic composition of normal aged and cataractous human lenses. *Exp Eye Res*. (2015) 164:15–23. doi: 10.1016/j.exer.2015.03.008

268. Snytnikova OA, Fursova AZ, Chernyak EI, Vasiliev VG, Morozov SV, Kolosova NG, et al. Deaminated UV filter 3-hydroxykynurenine O-B-D-glucoside is found in cataractous human lenses. *Exp Eye Res*. (2008) 86:951–6. doi: 10.1016/j.exer.2008.03.013

269. Mizdrak J, Hains PG, Kalinowski D, Truscott RJW, Davies MJ, Jamie JF. Novel human lens metabolites from normal and cataractous human lenses. *Tetrahedron*. (2007) 63:4990–9. doi: 10.1016/j.tet.2007.03.133

270. Parker NR, Korlimbinis A, Jamie JF, Davies MJ, Truscott RJW. Reversible binding of kynurenine to lens proteins: potential protection by glutathione in young lenses. *Invest Opthalmol Visual Sci*. (2007) 48:3705. doi: 10.1167/iovs.06-1061

frontiers | Frontiers in Ophthalmology

TYPE Original Research
PUBLISHED 02 December 2024
DOI 10.3389/fopht.2024.1508779

OPEN ACCESS

EDITED BY
Barbara Pierscionek,
Anglia Ruskin University, United Kingdom

REVIEWED BY
Velia Fowler,
University of Delaware, United States
Juliet Moncaster,
Boston University, United States

*CORRESPONDENCE
Matthew A. Reilly
Reilly.196@osu.edu

RECEIVED 09 October 2024
ACCEPTED 12 November 2024
PUBLISHED 02 December 2024

CITATION
Crews M, Rich W and Reilly MA (2024) Influence of zonular tension on molecular transport in the porcine ocular lens.
Front. Ophthalmol. 4:1508779.
doi: 10.3389/fopht.2024.1508779

Influence of zonular tension on molecular transport in the porcine ocular lens

Morgan Crews[1], Wade Rich[1] and Matthew A. Reilly[1,2]*

[1]Department of Biomedical Engineering, The Ohio State University, Columbus, OH, United States, [2]Department of Ophthalmology and Visual Sciences, The Ohio State University, Columbus, OH, United States

Introduction: Accommodation is the process of changing the ocular lens' refractive power and focal distance. This process involves application of biomechanical forces on the lens by the surrounding musculature. Previous studies have demonstrated that the lens epithelium demonstrates mechanotransduction and that tension influences its chemical activity. It is not yet known how these forces affect the structure and permeability of the lens. This study aimed to identify the influence of tension on molecular transport of dyes through the lens.

Methods: Paired porcine eyes were incubated in each of four dyes for three time periods with no stretch (null), static, or cyclic stretching using a bespoke mechanical lens stretcher. After incubation, the lenses were frozen and cryosectioned sagittally through the optic axis. Photographs of the stretched and unstretched lenses were compared and qualitatively assessed.

Results: None of the four dyes showed drastic stretch-induced differences in dye penetration depth. However, the dye neutral red showed dramatic stretch-induced changes in the dye uptake color behind lens anterior surfaces, with unstretched lenses appearing far more orange than their stretched counterparts. Three of four dyes showed notable differences between anterior and posterior diffusion patterns. One dye, methylene blue, demonstrated unexpected intensity in the lens nucleus compared to the lower intensity shown in the cortex, suggesting active transport rather than a linearly graded passive diffusion regardless of stretching condition.

Discussion: All this taken together suggests that lens transport is more complex than simple passive diffusion and that active transport of some molecules may be affected by stretching. Future work should assess the mechanisms of transport for the various dyes and attempt to explain the dye permeation patterns observed here, including the effects of stretching.

KEYWORDS

crystalline lens, tension, diffusion, stretching, lens circulation

1 Introduction

Accommodation is the ability of the crystalline ocular lens to change shape, resulting in a wider range of focal distances. During accommodation and disaccomodation, the ciliary muscle constricts and relaxes which modulates tension in the zonular fibers that connect the lens to the ciliary body and attached sclera (Figure 1). Recent studies have indicated that the causes and/or treatments of multiple lenticular pathologies, such as Presbyopia and cataract, are likely to be biomechanical in nature (1–6). There are no efficient preventative therapies for these pathologies, and current treatments can only help symptoms rather than restore accommodative function. A more comprehensive understanding of ocular biomechanics will reveal the root causes of lenticular disease, lead to effective preventative treatments, and improve the accuracy of ocular modeling.

The optical changes caused by accommodation can be mimicked ex vivo by varying radially applied mechanical forces (1–8). While there have been many variations in the methodology, all studies use the principle of radial stretching and transmission of forces through the zonules onto the lens capsule. The lens capsule is a basement membrane composed of extracellular matrices of lens epithelial cells (LECs) and has been shown to exhibit mechanotransduction (6). When force is applied through the zonules, the lens capsule, deforms the lens fiber cells changing the curvature of the biconvex lens (9). The mechanical properties of the lens capsule are also yet to be fully illuminated.

The chemical properties of the lens capsule have been more thoroughly studied than the lens mechanical properties. The lens capsule is known to be permeable to small molecules such as water, carbon dioxide, and oxygen (10, 11). Studies have additionally shown the lens capsule has selective permeability to nutrients and proteins needed for cortical fiber cells development and metabolism (9, 12, 13). The current understanding in the field is that lens capsule permeability varies greatly depending on molecule size, polarity, hydrogen bond affinity, and other chemical properties (12–15). Additionally, zonular tension has been shown to influence both aquaporin activity and hydrostatic pressure gradient, which are intrinsically linked to lens capsule properties (16).

The geometry, physical properties, chemical properties, and tissue composition of the anterior and posterior lens differ significantly. The anterior lens houses a monolayer of LECs that are most metabolically active just anterior of the equator where LECs continually proliferate throughout life. The lens is biconvex, meaning that each side has a distinct convexity throughout all accommodative conditions (17). The posterior has a larger curvature, resulting in larger lens volume posterior to the equator.

In 1997, Mathias et al. proposed the lens Fluid Circulation Model (FCM), which theorized a pattern of transport going inward at the poles and outward at the equator (18, 19). Since then, multiple studies have supported this model, and it is becoming foundational in lens transport research (20–23). It has yet to be investigated whether this pattern of microcirculation holds true for all molecules or in various accommodative/stretched conditions.

It is thus hypothesized that LEC mechanotransduction and chemical effects of tension are likely to be observed after the lens is exposed to tensile stretching force. Few studies to date have analyzed the effects of stretching on transport in the lens. In theory, application of mechanical force will alter the structure of the lens capsule and thus influence permeability. Stretching could also affect permeability of LECs and fiber cells even deep within the lens cortex. Variations in dye permeation under different stretching conditions may elucidate the structural behavior of the lens capsule and underlying cells under accommodative conditions.

2 Materials and methods

Fresh, paired porcine eyes were obtained from a local abattoir. Pig sex was unknown, and age was 6 months. The lenses were dissected less than four hours after the whole eyes were extracted to maximize tissue viability. The dissection involved removing the cornea, iris, vitreous humor, and the posterior sclera (6). The zonules and ciliary body were left intact to allow force

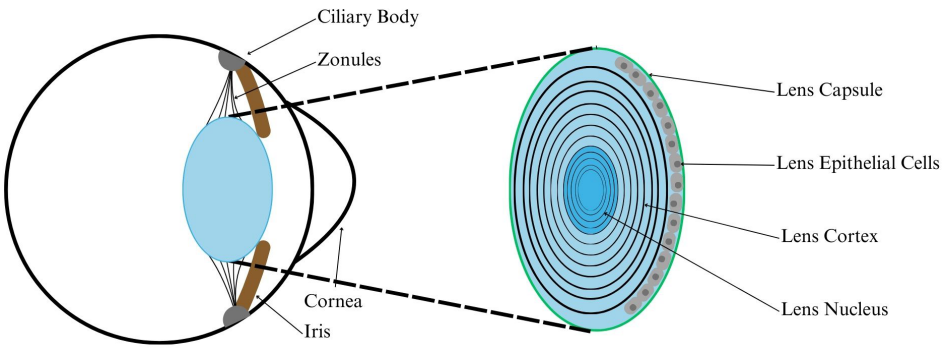

FIGURE 1
Diagram showing ocular lens anatomy. The lens is comprised of many layers of transparent matrix, with metabolically active lens epithelial cells along the anterior surface. The lens is held in place behind the iris by zonules, which are connective fibers extending from the ciliary body. The ciliary body contains the ciliary muscle, which exerts force on the zonules and lens capsule to change the shape of the lens.

distribution onto the lens capsule. The anterior cup (sans cornea, iris, and vitreous humor) was mounted to a silicone elastomer ring via staples in the equatorial sclera, as shown in Figure 2.

The paired eyes were incubated with 4 different dyes, 3 durations of incubation, and one of three stretching conditions: cyclic, static, or control (null), as shown in Figure 3. The silicone rings attached to experimental eye cups were attached using 8 bolts to the stretching apparatus shown in Figure 4, which allowed for equally distributed stretching along the eye cup's circumference (6). A single motor was used to impart equibiaxial stretching using a

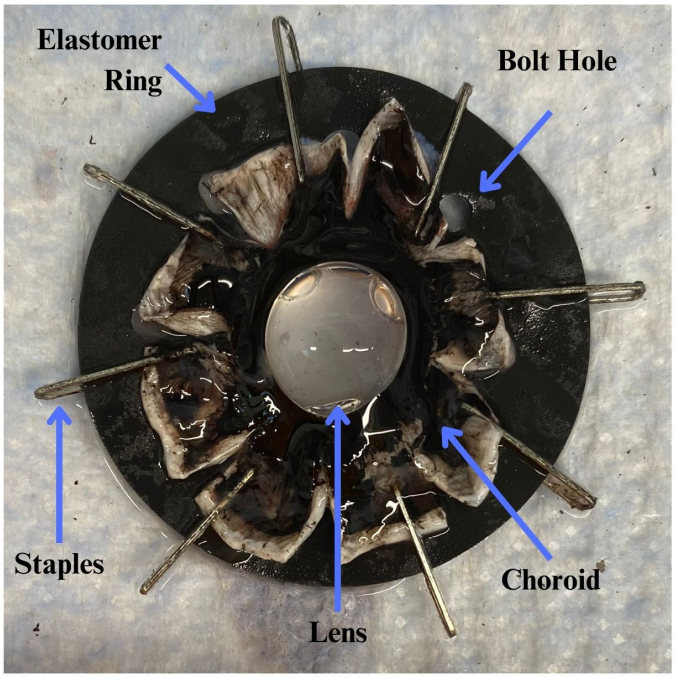

FIGURE 2
After the porcine eyes were cleared of cornea, iris, and vitreous humor, they were bisected and the posteriors discarded. The sclera was then cut into 8 flaps to allow the anterior cup to lay flat. The equatorial sclera was stapled to a silicone elastomer ring via 8 equally spaced staples. The ring's 8 bolt holes were used to affix the sample to the stretching device. The sample photo was oriented with its anterior facing into the page and posterior lens closest to the reader.

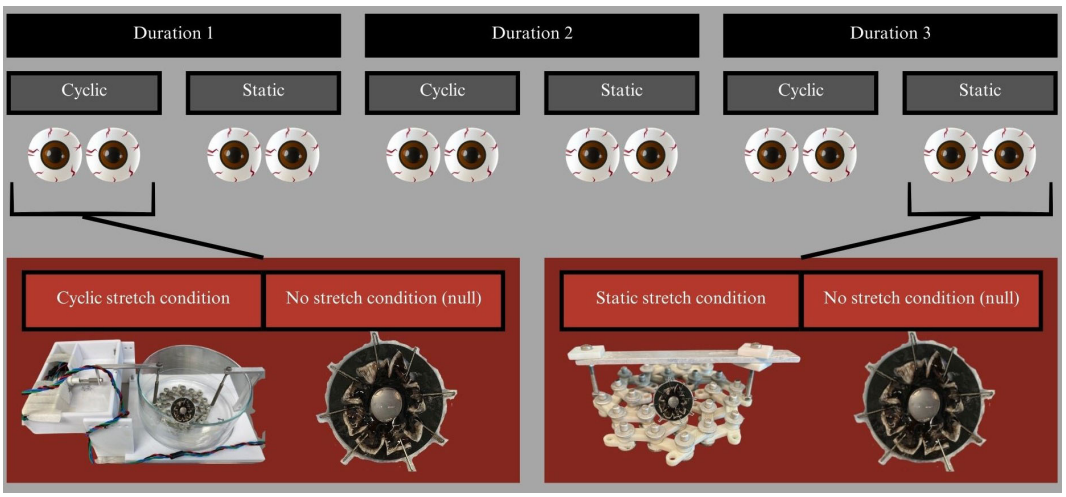

FIGURE 3
Experimental design showing how paired eyes were divided into experimental conditions. Each dye was incubated for 3 time points and each time point had a cyclic and a static experiment. Each stretch condition had one eye of the pair stretched and the other not. This system was replicated for 4 dyes, though one of the dyes could not survive the 2nd or 3rd time point.

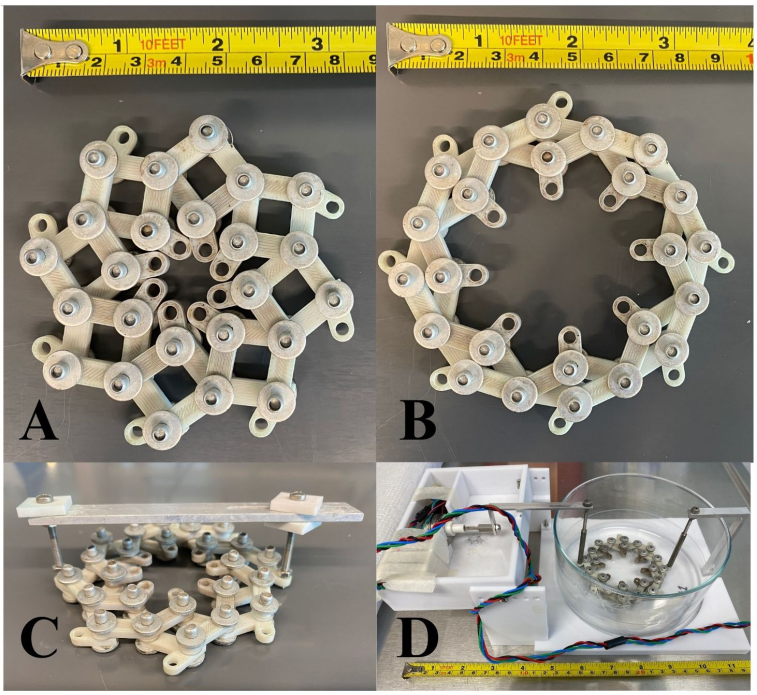

FIGURE 4
(A) Bespoke stretching apparatus in the unstretched and **(B)** stretched positions. The eye was stapled to an elastomer ring, which was bolted into the center of the device. Force on the stretcher's outer edge caused the sample to be stretched equally in all directions, similarly to accommodation. **(C)** Stretcher in its static stretching apparatus. The metal bar across the top held opposite sides of the stretcher a fixed distance apart to continuously stretch the sample in a radial fashion. The whole stretcher and its sample were submerged in a large dish of dyed media. **(D)** Cyclic stretching apparatus inside its glass dish for submersion in media and dye. The right side of the stretcher was affixed to the plastic base plate while the left side was attached to an Arduino-powered oscillating motor.

3D-printed lens stretcher as discussed further in 6. The statically stretched eye cups were placed in the stretcher and the equatorial radius increased by 6-12% using the rigid bar shown in Figure 4C. The cyclically stretched cups were connected to the stretcher in the same manner (Figure 4D). The cyclic stretcher was then fixed on one side and attached to an Arduino controlled motor on the opposite side. The motor caused the stretcher to continually oscillate between the stretched and unstretched positions throughout the incubation period at about 0.25 Hz.

Once set up in their respective stretching apparatus, each system was placed in a 10:1 media to dye solution covering the entire eye cup and put in an incubator at 37°C and 5% CO2. This experiment used four dyes, chosen to represent a variety of molecular weights and hydrogen bond affinities, which were Neutral Red (NR) (Sigma Aldrich, 72210-5G), Methylene Blue (MB) (Millipore Sigma, M4159-25G), Crystal Violet (CV) (Sigma Aldrich, 61135-25G), and Erythrosin Extra Bluish (EB) (Sigma Aldrich, 45690-10G-F). Table 1 shows some relevant properties of each dye. All dyes were used at a concentration of 1mg dye powder to 1mL deionized water and 1mL liquid concentrate to 10mL media. All tests used media 199 without phenol red to eliminate confounding color effects (Gibco, 11043-023). Each stretch/dye combination was incubated for 3 time periods before imaging. Eyes were incubated for 24, 48, and 72 hours for MB, CV, and EB dyes. In preliminary testing, NR had a particular affinity for the lens cortex and was therefore incubated at 1, 3, and 6 hours.

Once incubated, the lenses were removed from the eye cups and frozen in Optimal Cutting Temperature (OCT) compound for at least 12 hours at -80°C. The OCT Blocks were mounted into a cryotome and cut to reveal sagittal planes of the lenses. The sagittal

TABLE 1 Chemical properties of 4 dyes used.

	H-bond Acceptor	H-bond Donor	Molecular Weight (g/mol)	Polar Surface Area (Å^2)
Methylene Blue	4	0	319.9	43.9
Crystal Violet	3	0	408	9.5
Neutral Red	4	2	288.77	55
Erythrosin Extra Bluish	5	0	879.9	81.6

midline or optic axis was assumed to be the cross section that had the largest area within the lens outline. Photos were taken using a dSLR camera at a standardized angle and distance (Figure 5). Photographs were organized into figures to allow direct visual comparison between experimental conditions within each dye.

3 Results

The cryotome sectioning process yielded images like those seen in Figure 6. All photos were oriented with the anterior lens toward the left and the posterior lens toward the right.

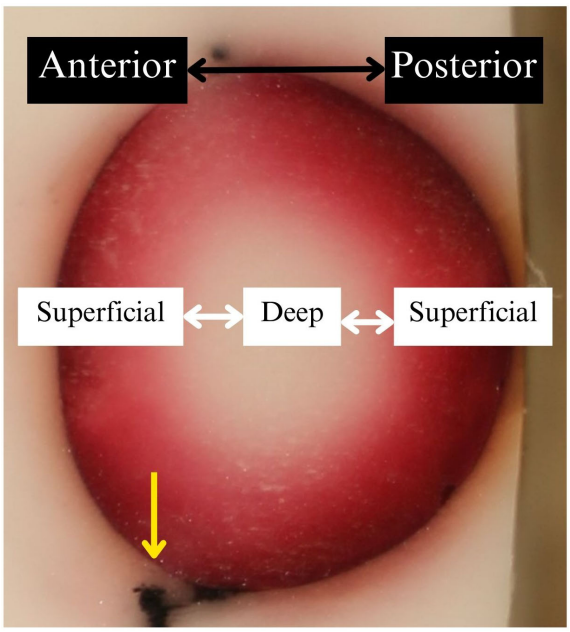

FIGURE 5
Representative experimental result of a lens embedded in frozen OCT compound after submersion in dyed media. Photos were oriented with the anterior facing left and superficial aspects closest to the photo's edges. The lighter colored/white background was frozen OCT. The brown line was the outline of the lens, most likely caused by dye particles adhering to the outer surface of the lens capsule. The center of the photo showed dye uptake in the lens cortex via color intensity. The yellow arrow indicates black zonule tissue that remained at the lens equator.

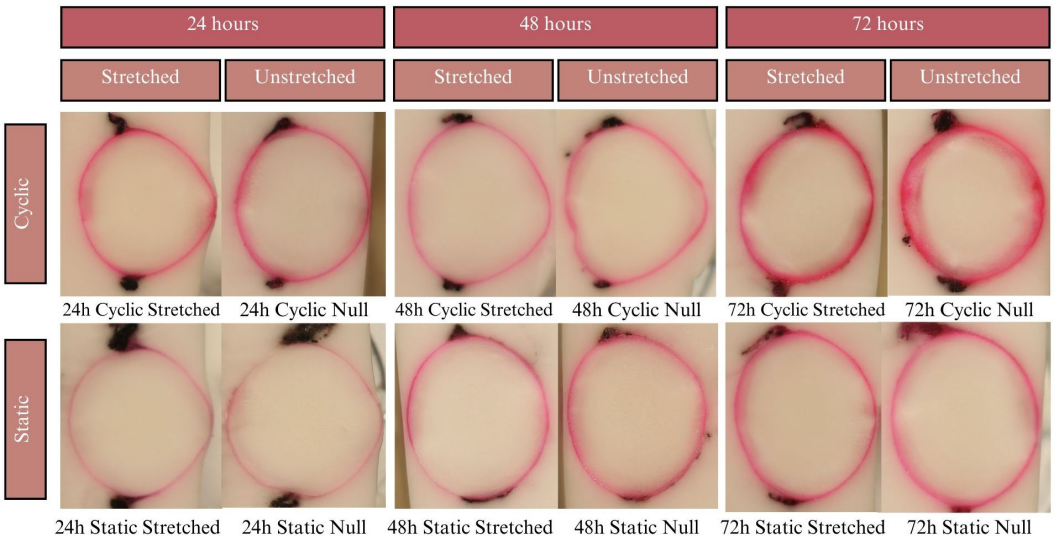

FIGURE 6
Results of the EB experiments after 24, 48, and 72 hours of incubation. Dye uptake manifests as bright pink, while freezing medium and areas of no dye uptake appear white. The pink outlines of the lenses are relatively thin, covering only the lens capsule with little to no penetration into the cortex.

Lenses were incubated for up to 24 hours in CV, but beyond that showed considerable degradation of the zonules, in all cases causing detachment of the lens from the sclera. Due to zonular failure, this subset of CV lenses was unable to be assessed. The results of the 24-hour duration can be seen in Figure 7A. Lenses were incubated for 24, 48, and 72 hours in solution containing EB. As seen in Figure 6, EB did not permeate past the lens capsule even at the longest incubation duration. The EB samples did not show any visual differences between stretch conditions or anterior vs. posterior surfaces. The intensity of the dye adherence to the superficial lens capsule was, as expected, greater after longer exposure. The concavity of the anterior and posterior lenses was as expected and relatively consistent. In preliminary experiments, NR dye showed a much higher affinity for the lens than other dyes, such that the lens was fully colored before 24 hours. This led to alteration of the incubation duration to 1, 3, and 6 hours. As seen in Figure 8A, NR experiments showed the expected gradual increase in concentration over time and the expected intensity gradient going from superficial penetration to complete penetration into the lens nucleus. Differences between stretch conditions were not perceptible for 1 or 3 hours. However, for both cyclic and static stretching, lenses stretched for 6 hours showed different coloring on the anterior side when compared to their unstretched controls. As seen in Figure 8B, unstretched NR 6h lens anterior regions were noticeably more orange than unstretched NR 6h lens posteriors, unstretched NR lenses at all other time points, and stretched NR 6h lens anterior sections. MB did not show consistent observable changes between stretching conditions (Figure 9). The overall presence of dye was greater at longer time points, as expected, but its distribution pattern was distinct from other dyes. While NR showed a high intensity superficially which decreased gradually as depth increased, MB exhibited a more piecewise distribution of dye. The outermost ring of tissue had a sharp rather than gradual drop in intensity, then a ring of little to no dye uptake, and finally a moderate intensity in the deepest region. There existed a non-monotonic concentration gradient within the lens. Nine of twelve MB samples showed disparity in anterior-posterior dye distribution. Posterior sides of both the whole lens and the nucleus tended to have higher intensity concentration than the respective anterior.

Additionally, MB seemed to induce shape changes in the lens, making its overall shape more ovular than the typical biconvex. Future work should analyze the curvature changes quantitatively and elucidate the reasoning for such changes.

4 Discussion

The mechanism by which the zonules degraded in CV solution was not evident in this study's results nor the literature due to CV's novel use in the lens. Since the tissue cannot be cultured beyond 24 hours with CV, it is not an ideal dye to use in lens stretching research. Notably, all samples showed a slightly decreased permeation on the anterior surface closest to the equator, as shown in Figure 7B. This may be due to the lens anterior having

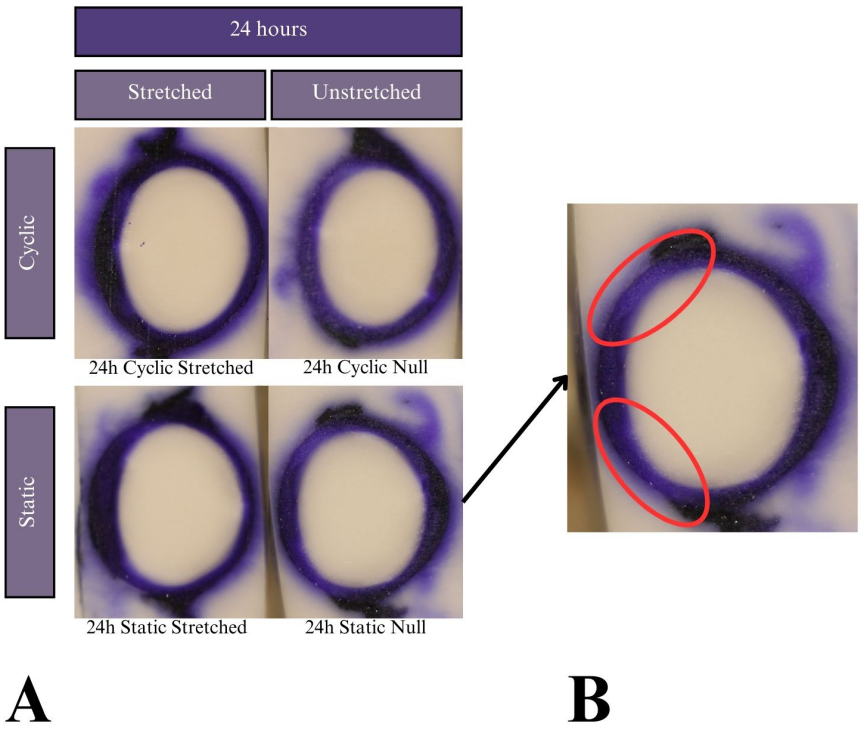

FIGURE 7
(A) Results of the CV experiments after 24 h of incubation. Tissue samples did not keep tension for 48- or 72-hour tests, so the results are not reported. Dye uptake manifests as dark purple, while freezing medium and areas of no dye uptake appear white. **(B)** Expanded image of the 24 hour-incubated null eye of the static test. Red ovals indicate areas of lower dye uptake on the lens anterior towards the equators compared to higher uptake on the anterior pole.

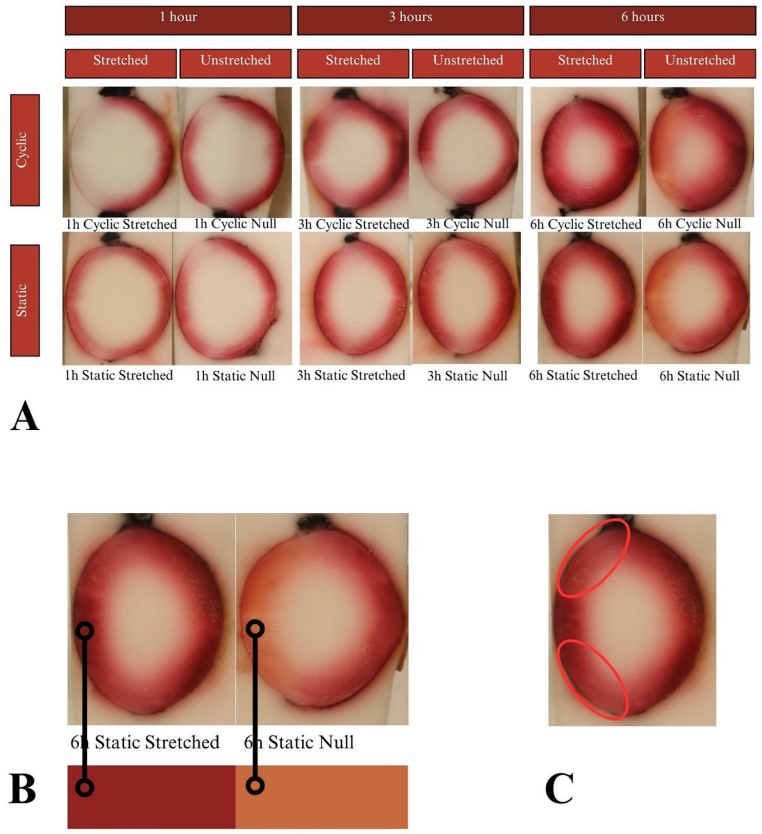

FIGURE 8
(A) Results of the NR experiments after 1, 3, and 6 hours of incubation. Dye uptake manifests as red, while freezing medium and areas of no dye uptake appear white. All photos show simple linear gradients appearing the darkest at superficial areas and decreasing intensity going deep. **(B)** Analysis of 6-hour NR samples. The anterior sides of the unstretched samples showed a more orange color compared to their own posterior sides and compared to the paired anteriors. NR being a pH indicator, this result suggests that stretching has a physiological impact on acidity. **(C)** All samples showed regions of decreased intensity at the anterior equators, which are known to be LEC proliferation sites.

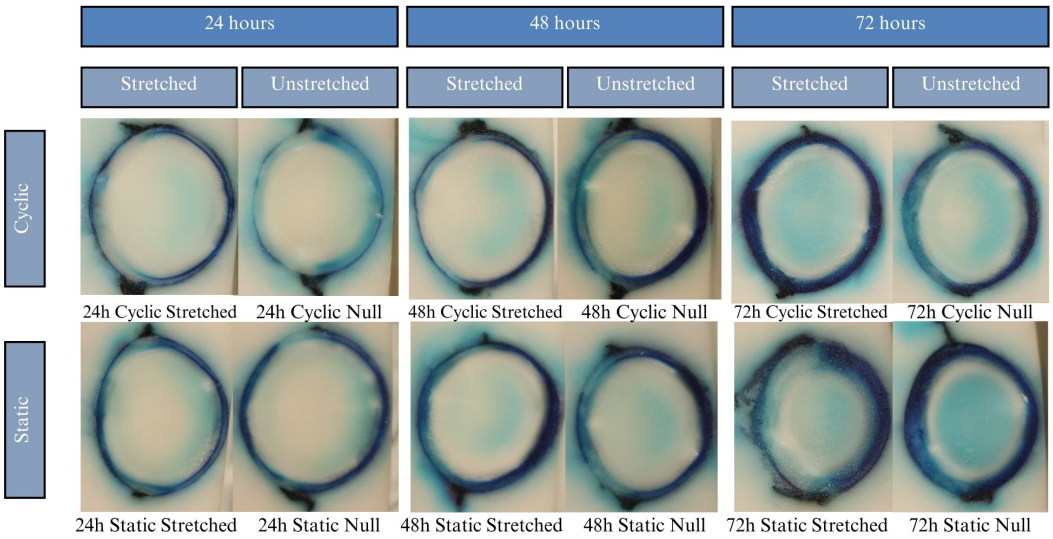

FIGURE 9
Results of the MB experiments after 24, 48, and 72 hours of incubation. Dye uptake manifests as blue, while freezing medium and areas of no dye uptake appear white. All samples show a dark ring deep to the lens outline, which abruptly decreases intensity in the lens cortex. Samples incubated for 48 hours show a mild patch of dye uptake in the lens center. For 72-hour samples the central mass of dye is darker and more heavily contrasts with the white just superficial to it. This pattern of nonlinear dye uptake indicates that lens microcirculation of MB is influenced by active transport rather than mere passive diffusion.

a layer of lens epithelial cells (LECs) that is known to be metabolically active.

EB's lack of penetration could be due, in part, to its large polar surface area, which indicates the molecule is highly polarized. More importantly, EB molecules have a molecular weight of nearly 880 g/mol, which is 2-3 times as large as the other dyes. This shortcoming prevents any visualization of changes from stretch condition, and as such we were able to determine that EB is an unsuitable dye with which to visually assess lens transport in these culture conditions.

NR is known to act as a pH indicator from 6.8 to 8 as red to yellow, respectively (Sigma Aldrich n.d.). This indicates unstretched NR 6h anteriors had a higher pH and lower acidity than all other test conditions. The mechanism by which stretching preserves the physiological pH in this case is unknown and warrants further inquiry. Perhaps LECs are dependent upon a certain level of tension to remain healthy, and absence of tension led to a buildup of acidic byproducts which manifested in the NR uptake color. This correlation between tension and lens activity would be a natural sequitur from the research suggesting LECs experience mechanotransduction. Additionally, NR lenses showed a similar decrease to CV in absorption at the areas of active cell proliferation on the lens anterior, again suggesting metabolic influence.

The lower permeation of dye at the LEC proliferation sites seen in CV and NR (Figures 7B, 8C) could be due to several factors. The metabolic activity itself or the phenotype of the LECs could have resulted in less uptake. Alternatively, these cells may have absorbed the same amount of dye but processed or degraded it more quickly or more thoroughly than other tissues did. A difference in molecular breakdown chemistry may also relate to the observed color change between NR 6h stretched vs. unstretched.

MB's irregular concentration gradient strongly supports that the lens has pathways of active transport for certain molecules and does not merely rely on passive diffusion. The increased central concentration of MB seems to occur within the outline of the lens nucleus, which is of a much higher cell density than the surrounding cortex. The ring of low dye concentration between the outer cortex and the outer nucleus defies the expected gradation pattern. That is, where we expect the lens to be darkest on the periphery and lightest in the innermost region, it appears lightest in the central concentric layer and moderate at the nucleus core. Standard fluid dynamics declares that unaided diffusion occurs in a concentration gradient going predominantly from areas of high to low concentration, which we do not see here. As such, a more complex process like active transport must be at work. The pathways illustrated by the dye concur with predicted models of lens diffusion. Full analysis of the chemical differences between the dyes and how this manifested in differing patterns was outside the scope of this paper but should be further explored.

MB samples containing higher posterior concentrations is unusual due to the posterior's larger area, which intuitively should result in a more diffuse dispersion. This result may suggest that the epithelium of the anterior provides a protective barrier against certain molecules used in this study.

CV and EB were ineffective at visualizing lens transport, in this particular application, due to induced tissue degradation and low penetration depth, respectively. NR dye showed stretch-induced pH differences between anterior and posterior surfaces at 6 hours. Future work should inspect the mechanism of this pH change and how stretching contributes. MB demonstrated clear pathways of active transport with significant anterior-posterior differences, though stretching effects were not apparent within this sample. These findings are in agreement with the microcirculation or FCM by Mathias et al., though CV and MB require more chemical characterization in the lens to be situated in the literature.

This study was limited by both small sample size and lack of statistical quantification. Quantification is possible using image analysis software to convert RBG images into vectors of intensity values, which correlate to dye uptake throughout the lens and could then be compared between experimental conditions. This approach yielded a massive amount of data, best visualized using surface plots, but meaningful statistical analysis was beyond the scope of this study. The raw data were, therefore, not reported. However, this pilot study revealed topics for the focus of future research and eliminated certain ineffective routes of study.

In summary, we investigated the potential role of biomechanical stretching in driving lens transport. The findings generally indicated that lens transport was not significantly altered by stretching, at least on the timescales investigated in this study. It may be that any stretch-induced changes are very transient in nature, acting on the order of seconds rather than hours or days. Studying such brief events is infeasible with the current protocol owing to the lengthy processing of tissue to mount it on the stretcher; it seems likely that the biomechanical manipulations during the mounting process would overwhelm those of the stretching and would confound the effects. Still, it is certainly interesting that stretching may alter the pH of the lens' anterior and that the distribution of MB within the lens is governed by some active process. Future work should focus on developing a more real-time monitoring of dye uptake, such as in calcium imaging.

Data availability statement

The original contributions presented in the study are included in the article/supplementary material. Further inquiries can be directed to the corresponding author.

Ethics statement

Ethical approval was not required for the studies on animals in accordance with the local legislation and institutional requirements because only postmortem tissues were used.

Author contributions

MC: Conceptualization, Data curation, Investigation, Methodology, Software, Visualization, Writing – original draft, Writing – review & editing. WR: Writing – review & editing, Conceptualization. MR: Funding acquisition, Software, Supervision, Writing – review & editing.

Funding

The author(s) declare financial support was received for the research, authorship, and/or publication of this article. This project was funded by NIH grant NIH 1R01EY035278.

Acknowledgments

The authors would like to thank Dr. Benjamin Walter's lab for the use of their equipment. The authors also acknowledge content consultations from Dr. Sara McBride-Gagyi and Dr. Heather Chandler.

Conflict of interest

The authors declare that the research was conducted in the absence of any commercial or financial relationships that could be construed as a potential conflict of interest. One author was an editorial board member of Frontiers, at the time of submission. This had no impact on the peer review process and the final decision.

The author(s) declared that they were an editorial board member of Frontiers, at the time of submission. This had no impact on the peer review process and the final decision.

Generative AI statement

The author(s) declare that no Generative AI was used in the creation of this manuscript.

Publisher's note

References

1. Manns F, Parel J-M, Denham D, Billotte C, Ziebarth N, Borja D, et al. Optomechanical response of human and monkey lenses in a lens stretcher. *Invest Ophthalmol Visual Sci.* (2007) 48:3260–8. doi: 10.1167/iovs.06-1376

2. Wei H, Wolffsohn JS, de Oliveira OG, Davies L. An artificial lens capsule with a lens radial stretching system mimicking dynamic eye focusing. *Polymers*. (2021) 13:3552. doi: 10.3390/polym13203552

3. Michael R, D'Antin JC, Cortés LP, Burd HJ, Sheil B, Barraquer RI. Deformations and ruptures in human lenses with cortical cataract subjected to ex vivo simulated accommodation. *Invest Ophthalmol Visual Sci.* (2021) 62:12. doi: 10.1167/iovs.62.1.12

4. Cortés LP, Burd HJ, Montenegro GA, D'Antin CJ, Marek M, Barraquer RI, et al. Experimental protocols for ex vivo lens stretching tests to investigate the biomechanics of the human accommodation apparatus. *Invest Ophthalmol Visual Sci.* (2015) 56:2926–32. doi: 10.1167/iovs.14-15744

5. Nankivil D, Heilman BM, Durkee H, Manns F, Ehrmann K, Kelly S, et al. The zonules selectively alter the shape of the lens during accommodation based on the location of their anchorage points. *Invest Ophthalmol Visual Sci.* (2015) 56:1751–60. doi: 10.1167/iovs.14-16082

6. Kumar B, Chandler HL, Plageman T, Reilly MA. Lens stretching modulates lens epithelial cell proliferation via YAP regulation. *Invest Ophthalmol Visual Sci.* (2019) 60:3920–9. doi: 10.1167/iovs.19-26893

7. Ziebarth NM, Borja D, Arrieta E, Aly M, Manns F, Dortonne I, et al. Role of the lens capsule on the mechanical accommodative response in a lens stretcher. *Invest Ophthalmol Visual Sci.* (2008) 49:4490–6. doi: 10.1167/iovs.07-1647

8. Reilly MA, Hamilton PD, Perry G, Ravi N. Comparison of the behavior of natural and refilled porcine lenses in a robotic lens stretcher. *Exp Eye Res.* (2009) 88:483–94. doi: 10.1016/j.exer.2008.10.021

9. Roberts CJ, Dupps WJ, Downs JC. *Biomechanics of the Eye*. Kugler Publications, Amsterdam, The Netherlands (2018).

10. Fisher RF. Changes in the permeability of the lens capsule in senile cataract. *Trans Ophthalmological Societies United Kingdom*. (1977) 97:100–3.

11. Friedenwald JS. The permeability of the lens capsule to water, dextrose, and other sugars. *Transaction Am Ophthalmological Soc.* (1930) 28:195–211. doi: 10.1001/archopht.1930.00810110052009

12. Danysh BP, Duncan MK. The lens capsule. *Exp Eye Res.* (2009) 88:151–64. doi: 10.1016/j.exer.2008.08.002

13. Boyle DL, Carman P, Takemoto L. Translocation of macromolecules into whole rat lenses in culture. *Mol Vision*. (2002) 10:226–34.

14. Winkler J, Wirbelauer C, Frank V, Laqua H. Quantitative distribution of glycosaminoglycans in young and senile (cataractous) anterior lens capsules. *Exp Eye Res.* (2001) 72:311–8. doi: 10.1006/exer.2000.0952

15. Lo WK, Harding CV. Tight junctions in the lens epithelia of human and frog: freeze-fracture and protein tracer studies. *Invest Ophthalmol Visual Sci.* (1983) 24:396–402.

16. Petrova RS, Bavana N, Zhao R, Schey KL, Donaldson PJ. Changes to zonular tension alters the subcellular distribution of AQP5 in regions of influx and efflux of water in the rat lens. *Invest Ophthalmol Visual Sci.* (2020) 61:36. doi: 10.1167/iovs.61.11.36

17. Ruan X, Liu Z, Luo L, Liu Y. Structure of the lens and its associations with the visual quality. *BMJ Open Ophthalmol.* (2020) 5:e000459. doi: 10.1136/bmjophth-2020-000459

18. Mathias RT, Rae JL, Baldo GJ. Physiological properties of the normal lens. *Physiol Rev.* (1997) 77:21–50. doi: 10.1152/physrev.1997.77.1.21

19. Quinlan RA, Clark JI. Insights into the biochemical and biophysical mechanisms mediating the longevity of the transparent optics of the eye lens. *J Biol Chem*. (2022) 298(11):102537.

20. Mathias RT, Kistler J, Donaldson P. The lens circulation. *J Membrane Biol.* (2007) 216:1–16. doi: 10.1007/s00232-007-9019-y

21. Chen Y, Petrova RS, Qui C, Donaldson P. Intracellular hydrostatic pressure regulation in the bovine lens: a role in the regulation of lens optics? *Am J Physiology: Regulatory Integr Comp Physiol*. (2022) 322(3):R263–79. doi: 10.1152/ajpregu.00309.2021

22. Cao L, Liu J, Collinson JM, Forrester JV, McCaig C. Endogenous bioelectric currents promote differentiation of the mammalian lens. *J Cell Physiol*. (2018) 233:2202–12. doi: 10.1002/jcp.v233.3

23. Giannone AA, Li L, Sellitto C, White TW. Physiological mechanisms regulating lens transport. *Front Physiol.* (2021) 12. doi: 10.3389/fphys.2021.818649

frontiers | Frontiers in Ophthalmology

TYPE Original Research
PUBLISHED 19 February 2025
DOI 10.3389/fopht.2025.1502836

OPEN ACCESS

EDITED BY
Catherine Cheng,
Indiana University, United States

REVIEWED BY
Justin Parreno,
University of Delaware, United States
Barbara Pierscionek,
Anglia Ruskin University, United Kingdom
Peter N. Huynh,
Indiana University Bloomington, United States

*CORRESPONDENCE
Thomas W. White
thomas.white@stonybrook.edu

RECEIVED 27 September 2024
ACCEPTED 03 February 2025
PUBLISHED 19 February 2025

CITATION
Sellitto C and White TW (2025) Combinatorial genetic manipulation of Cx50, PI3K and PTEN alters postnatal mouse lens growth and homeostasis. *Front. Ophthalmol.* 5:1502836. doi: 10.3389/fopht.2025.1502836

Combinatorial genetic manipulation of Cx50, PI3K and PTEN alters postnatal mouse lens growth and homeostasis

Caterina Sellitto and Thomas W. White*

Department of Physiology and Biophysics, Stony Brook University School of Medicine, Stony Brook, NY, United States

Introduction: Phosphoinositide 3-kinase (PI3K), Phosphatase and tensin homolog (PTEN) and connexin50 (Cx50) have individually been shown to play critical roles in the growth, development and maintenance of the lens and to functionally interact *in vitro*. To elucidate how gap junctional coupling mediated by Cx50 and intracellular signaling mediated by PI3K and PTEN synergistically interact to regulate lens homeostasis *in vivo*, we generated and characterized double knockout animal models lacking the p110α subunit of PI3K and Cx50, or PTEN and Cx50.

Methods: We interbred lens specific p110α and PTEN conditional knockout animals with Cx50 deficient mice to generate double knockouts. Animals and eyes were weighed, lenses were dissected, photographed, measured, fixed and sectioned for histological analysis. Lens epithelial cell proliferation was determined using 5-ethynyl-2'-deoxyuridine (EdU) labeling.

Results: Double knockout of p110α and Cx50 led to a significant reduction in lens and eye size, and a high rate of lens rupture. The individual cell proliferation defects of the Cx50 and p110α single knockout lenses both persisted in the double KO. Double deletion of Cx50 and PTEN produced severe lens defects, including cataract, aberrant cell migration, altered cell proliferation, vacuole formation and lens rupture.

Conclusion: The severe phenotypes in p110α/Cx50 and PTEN/Cx50 double deficient lenses suggest that PI3K, PTEN and Cx50 participate in both distinct and common regulatory pathways that are necessary to maintain normal lens growth and homeostasis.

KEYWORDS

lens, growth, cataract, connexin, PTEN, PI3K, mouse model

1 Introduction

Multicellular organisms utilize several mechanisms to provide the intercellular communication needed between cells to achieve the normal growth, differentiation and maintenance of organs. These mechanisms can include communication being directly mediated by the connexin channels present in gap junctions (1–3), or driven by extracellular growth factors binding to receptors and activating intracellular signal transduction cascades (4, 5). Both signal transduction pathways and connexin mediated communication have been shown to play critical roles in the development of the eye lens by numerous laboratories (5–23), however, less is known about the potential interplay between them (24).

Gap junction channels facilitate the direct transport of ions, metabolites, and small signaling molecules between cells of the lens (25). Gap junctions are comprised of hexameric oligomers of connexin proteins (26). When two of these complexes from neighboring cells dock, they form a channel that directly connects the cytoplasm of two cells (27). Three connexins are present in the lens with different patterns of expression: Connexin43 (Cx43) is present in the lens epithelium (28), Connexin46 (Cx46) is expressed in the lens fiber cells (29), and Connexin50 (Cx50) is highly abundant in both cell types (13, 30, 31). Knockout of Cx43 in the lens had no detectable phenotype, while loss of Cx46 resulted in cataract (32–34). By contrast, deletion of Cx50 significantly reduced postnatal lens cell proliferation, particularly in the central epithelium, resulting in deficient lens growth, micropthalmia and cataract (13, 15, 17, 35).

Phosphoinositide 3-kinases (PI3Ks) act downstream of cell receptors to phosphorylate the 3′-hydroxyl group of phosphatidylinositol- (4, 5)P_2. This generates phosphatidylinositol-(3–5)P_3 (PIP_3), which then activates signaling pathways to regulate cell growth, proliferation, and survival (36). PI3Ks are separated into different classes depending upon sequence homology and substrate specificity (37). Class IA enzymes are heterodimers composed of 110kD catalytic and 85kD regulatory subunits. The p110α catalytic subunit is widely expressed, and responds to input from receptor tyrosine kinases (38), generating PIP_3, whose most prominent biological function is the activation of the AKT signaling pathway (39–42). PI3K signaling is antagonized by phosphatase and tensin homolog (PTEN), a ubiquitously expressed lipid phosphatase that dephosphorylates PIP_3 (43, 44). Regulatory control mediated by the interplay between PI3K and PTEN governs numerous cellular processes in many organs, including the lens (45–47).

The lens contains a monolayer of epithelial cells covering the anterior surface, with fiber cells derived from epithelial precursors filling its core (48). Epithelial proliferation drives lens growth, which predominantly occurs near the equator in the germinative zone (49–51). Lens growth and development are regulated by growth factor signaling, such as that provided by the fibroblast growth factors (FGFs) and fibroblast growth factor receptors (FGFRs) that control lens induction, epithelial cell proliferation and fiber differentiation (5, 18, 52). FGFRs are receptor tyrosine kinases that stimulate the mitogen-activated protein kinase (MAPK, or Ras-Raf-Mek-ErK) or PI3K-AKT intracellular signaling pathways (45, 53, 54). Components of the MAPK pathway have been extensively studied in the lens by genetic dissection using transgenic mice (9, 10, 55–59).

Elucidation of the role(s) played by components of the PI3K/PTEN branch of the intracellular signaling pathway has also been explored using genetically engineered mice. Lens specific deletion of PTEN induced elevated levels of phosphorylated AKT, with distinct consequences depending upon the developmental timing of deletion (6, 60). Deletion at the lens placode stage rescued a cell death phenotype caused by knockout of FGFR2 (6), whereas deletion at the lens vesicle stage inhibited Na^+/K^+-ATPase activity, leading to lens rupture and cataract (60). Lens specific conditional knockouts of the p110α and p110β catalytic subunits of PI3K alone, or in combination, have also been generated (16). Deletion of p110α significantly reduced eye and lens growth due to altered spatial organization, and a reduced magnitude of lens epithelial cell proliferation on postnatal day 0 (P0). Deletion of p110β did not induce a detectable phenotype, and mice with double knockout of p110α and p110β had the same lens phenotype as p110α single knockout animals (16).

We have previously shown that both Cx50 and PI3K individually regulate postnatal lens cell proliferation and growth *in vivo* (15, 16, 35). We have also demonstrated that PI3K can specifically modulate the functional activity of Cx50 *in vitro* (61). We have further established that PI3K/PTEN signaling critically regulates the activity of a broad network of lens ion channels and transporters, including Cx50 (60, 62–64). We do not currently know if Cx50, PI3K and PTEN operate independently, or in a common pathway, in the regulation of lens cell proliferation. We also do not understand the mechanism(s) whereby PI3K/PTEN signaling leads to Cx50 dependent changes in lens differentiation and homeostasis. To address how Cx50 and PI3K/PTEN signaling work together in the lens to maintain clarity, preserve integrity and regulate postnatal mitosis, we have examined the *in vivo* functional interactions between PI3K, PTEN, and Cx50 using double knockout mouse models.

2 Materials and methods

2.1 Generation of double knockout animals

The Stony Brook University Institutional Animal Care and Use Committee approved all animal experimentation. Mice with a global knockout of Cx50 (17) and lens-specific conditional knockouts of the p110α catalytic subunit of PI3K (16), or PTEN (60), were mated to generate double knockout animals (p110/Cx50α dKO, or PTEN/Cx50 dKO). Briefly, Cx50 KO and p110α floxed (65) mice were interbred to homozygosity. Cx50 KO and PTEN floxed mice (66) were also interbred to homozygosity. MLR10-Cre mice, whose Cryaa driven Cre expression is limited to the lens epithelium and fibers (67), were interbred with both strains to heterozygosity, maintaining the homozygous floxed p110α and PTEN alleles, in addition to the homozygous Cx50 KO alleles. Animal genotypes were confirmed by PCR of DNA from tail biopsies as previously described (16, 17, 60). Due to the mixed genetic background that resulted from the interbreeding of the

different strains of original mice, littermate controls (Cx50 KO Cre negative) were used for all experiments. All animals used for breeding had homozygous Cx50 KO and homozygous floxed alleles for either PTEN or p110α, while one member of the breeding pair carried a heterozygous copy of the MLR10-cre transgene. The resulting litters contained half of the animals with no Cre (Cx50 KO controls) and half with a double knockout of p110α/Cx50, or a double knockout of PTEN/Cx50 (dKOs).

2.2 Lens photography and growth measurement

Littermate mice between birth and 24 weeks of age were euthanized by CO_2 asphyxia and weighed. Eyes were dissected, weighed, and transferred to 37°C Tyrode solution on a warmed stage. Lenses were removed, transferred to 35mm glass bottom culture dishes and photographed with a SZX16 dissecting microscope attached to a digital camera (Olympus, Waltham, MA). Diameters of lenses were measured from the images, and lens volume was calculated assuming a spherical shape. The incidences of the presence of blood vessels associated with the lens and lens rupture were also recorded (16, 17, 60).

2.3 5-ethynyl-2′-deoxyuridine labeling

Postnatal day 0 (P0) or postnatal day 2 (P2) mice were subcutaneously injected with 50 μg/gm EdU (Click-iT, Thermo Fisher Scientific, Waltham, MA) and then returned to their mothers for 2 hours. Subsequently, lenses were removed and fixed in a 4% formaldehyde in PBS for 1 hour at room temperature (~22°C) and photographed for measurement. Permeabilization and Click-iT staining were performed as described in the manufacturer's instructions and previously published protocols (16, 68, 69). Z-stacks of fluorescent images were acquired on an Axiovert 200M microscope (Zeiss, Thornwood, NY) and processed using ImageJ. For line-scan analysis, the flattened fluorescent image of EdU staining was manually thresholded, and the plot profile function in ImageJ was used to measure fluorescent intensity across the entire lens diameter as described previously (16, 68). For central epithelial cell counts, a circular region with a diameter equal to the lens radius was drawn over the central region, fluorescent values were thresholded using the color threshold fuction in ImageJ, and EdU stained cells were quantified using the analyze particles function in ImageJ. The number of labeled cells was divided by the circular area to calculate the density of labeled cells.

2.4 Histological staining

Eyes from postnatal day 2 mice were dissected and fixed in 4% formaldehyde in phosphate-buffered saline (PBS) overnight at room temperature. Eyes were rinsed with PBS, dehydrated through increasing ethanol concentrations (50, 70, 70, 80, 95, 100%), and then embedded in paraffin. 2.5 μm sections were cut using a diamond knife, mounted on glass slides and deparaffinized. Slides were stained with hematoxylin-eosin as previously described (16, 60), and histological sections were observed on a BX51 microscope and photographed with a DP72 digital camera (Olympus).

2.5 Statistical analysis

Data were plotted as the mean ± SD, or SEM, as described in each figure. Statistical significance was determined using one-way ANOVA in the Origin software program (OriginLab Corporation, Northampton, MA) with Tukey's *post hoc* test. P values less than 0.05 were considered significant.

3 Results

3.1 Double knockout of p110α/Cx50 or PTEN/Cx50 altered lens size, clarity and integrity

Cx50 KO mice (17) containing homozygous floxed p110α, or PTEN alleles (65, 66) were interbred with MLR10-Cre transgenic mice (67) to obtain double knockout animals. All comparisons in this manuscript are made between animals lacking Cx50. As described in the introduction, loss of Cx50 reduced postnatal lens cell proliferation, causing deficient lens growth, micropthalmia and cataract (13, 15, 17, 35). Please see Table 1, and the original knockout papers (16, 17, 60) for a comparison of the single KO mouse phenotypes with wild-type lenses. Lenses isolated from homozygous floxed p110α/Cx50, or PTEN/Cx50 animals lacking the MLR10-Cre transgene (i.e. Cx50 KO) remained intact at all ages examined (Figures 1A–D), with a mild nuclear cataract as previously described (70). By contrast, lenses dissected between 1 and 24 weeks of age from homozygous floxed p110α/Cx50 animals expressing the MLR10-Cre transgene (i.e. p110α/Cx50 dKO) showed a distinct dual pathology. Intact lenses formed the first group, which were noticeably smaller than their Cx50 KO littermates, and no longer displayed the mild nuclear cataract phenotype of the Cx50 KO (Figures 1E–H). The second group of p110α/Cx50 dKO lenses displayed a partial posterior rupture, leaving a small transparent anterior lens fragment attached to posterior lens debris (Figures 1I–L). Lenses dissected between 1 and 24 weeks of age from homozygous floxed PTEN/Cx50 mice expressing the MLR10-Cre transgene (i.e. PTEN/Cx50 dKO) showed a progressive pathology that also included lens rupture. A dense central cataract, the presence of vacuoles, and progressively worsening cortical opacities, characterized the PTEN/Cx50 dKO lenses that remained intact (Figures 1M–P). Lens rupture was not detected at 1 week of age for PTEN/Cx50 dKO lenses, however from 5 weeks of age onward, ruptured lenses were observed with an increasing frequency leaving behind a dense nuclear cataract attached to cortical fragments (Figures 1Q–T). Thus, lens size,

TABLE 1 Summary of phenotypic differences between single and double knockout animals.

knockout(s)	eye mass	lens volume	epithelial cell proliferation	lens rupture	reference(s)
Cx50	reduced 32%	reduced 44%	reduced on P2 in central zone	none	(15, 17)
p110α	reduced 22%	reduced 27%	reduced on P0 in germinative zone	none	(16, 68)
PTEN	increased 19%	increased 29%	no change	> 50% at 24 weeks	(60, 68)
p110α/PTEN	normal	increased 22%	no change	> 50% at 12 weeks	(68)
p110α/Cx50	reduced 55%	reduced 62%	reduced on P0 in germinative zone	> 50% at 1 week	present work
PTEN/Cx50	reduced 27%	reduced 40%	reduced on P2 in central zone	> 50% at 24 weeks	present work

Comparisons of body mass, organ mass, organ volume, cell proliferation and organ rupture are all made to aggregate wild-type data from previous publications (15–17, 60, 68).

clarity, and integrity were all differentially impacted by the double deletion of Cx50 with p110α, or PTEN. p110α/Cx50 dKO lenses were prone to lens rupture, however, intact p110α/Cx50 dKO lenses were much smaller than Cx50KOs, and had lost the central cataract. PTEN/Cx50 dKO lenses had more severe cataracts that either Cx50, or PTEN single KOs, and displayed frequent lens rupture.

3.2 Double deletion of p110α/Cx50 resulted in reduced eye and lens growth

Previous studies reported that individual knockouts of either Cx50, or p110α, resulted in the lens volume being reduced by 44% and 27%, respectively with a corresponding decrease in eye mass (13, 16, 17). By contrast, single knockout of PTEN resulted in a small increase in lens volume and eye mass (60). To determine the effect of double knockout of Cx50 and p110α or PTEN, changes in animal mass, eye mass and lens volume were quantified over time by weighing mice, weighing eyes, and photographing lenses between postnatal day 0 (P0) and 24 weeks of age in Cx50 KO, p110α/Cx50 dKO and PTEN/Cx50 dKO animals. Lens diameters were measured, and then used to calculate lens volumes as previously described (16, 17, 60, 68). There were no significant differences in body mass between Cx50 KO, p110α/Cx50 dKO and PTEN/Cx50 dKO animals between birth and 24 weeks of age (Figure 2A). By contrast, eye mass in the p110α/Cx50 dKO was significantly reduced ($p < 0.05$, one-way ANOVA) compared to Cx50 KO and PTEN/Cx50 dKO mice (Figure 2B). At 1 week old, the mass of p110α/Cx50 dKO eyes was reduced 23% and by 12 weeks of age, the eyes were 40% smaller than Cx50 KO mice. By contrast, eyes from PTEN/Cx50 dKO animals were 8-15% larger than Cx50 KO littermates at 5 and 12 weeks of age ($p < 0.05$). The eye mass data includes all eye samples, regardless of lens rupture status. Similar to eye mass, lens volume in the p110α/Cx50 dKO animals was significantly reduced ($p < 0.05$) compared to either the Cx50 KO or PTEN/Cx50 dKO (Figure 2C). At P0, the volume of p110α/Cx50 dKO lenses was reduced 35% and at 12 weeks of age the lenses were 37% smaller than those of Cx50 KOs. The lenses from PTEN/Cx50 dKO animals were 8-18% larger than Cx50 KO littermates between 12 and 24 weeks of age ($p < 0.05$). The lens volume data was calculated from lenses that had not ruptured. These data show that the eye and lens growth deficiencies induced by individual knockout of Cx50 or p110α were compounded in the p110α/Cx50 dKO. The modest effect of single PTEN KO on lens and eye size (60) was not notably altered in the PTEN/Cx50 dKO animals.

3.3 Double knockout of Cx50 and p110α or PTEN increased lens rupture

Previous studies have shown that single Cx50, or p110α, KO lenses never displayed lens rupture (16, 17, 68). By contrast, single PTEN KO lenses displayed an increasing propensity to rupture with age (60). To quantify changes in lens integrity over time, dissected lenses from Cx50 KO, p110α/Cx50 dKO and PTEN/Cx50 dKO animals between birth and 24 weeks were scored for the incidence of lens rupture (Figure 3). Reduced viability or anophthalmia were never observed in either dKO strain. Lenses from p110α/Cx50 dKO mice were intact between P0 and P2, but displayed 65% to 81% rupture between 1 week and 24 weeks of age. Lenses from PTEN/Cx50 dKO mice were intact between P0 and 1 week of age. By 5 weeks of age, PTEN/Cx50 dKO animals had an 18% incidence of lens rupture, which increased to 32% at 12 weeks, and 73% at 24 weeks of age. These data show that loss of either p110α or PTEN from Cx50 KO lenses produced a loss of lens integrity and high incidences of lens rupture. However, the kinetics of lens ruptured differed dramatically between the p110α/Cx50 dKO and PTEN/Cx50 dKO mice.

3.4 Double deletion of PTEN/Cx50 alters the association of blood vessels with the early postnatal lens

In the early mouse eye, the hyaloid artery grows out from the optic nerve head ensheathing the lens as the tunica vasculosa lentis (71, 72). This structure persists during the first postnatal week before regressing prior to eye opening on P14 (73, 74). In PTEN/Cx50 dKO mice, this process appeared to be compromised in a subset of lenses dissected between P2 and P7. All of the postnatal lenses from Cx50 KO and p110α/Cx50 dKO, and the majority of lenses from PTEN/Cx50 dKO animals could be easily dissected

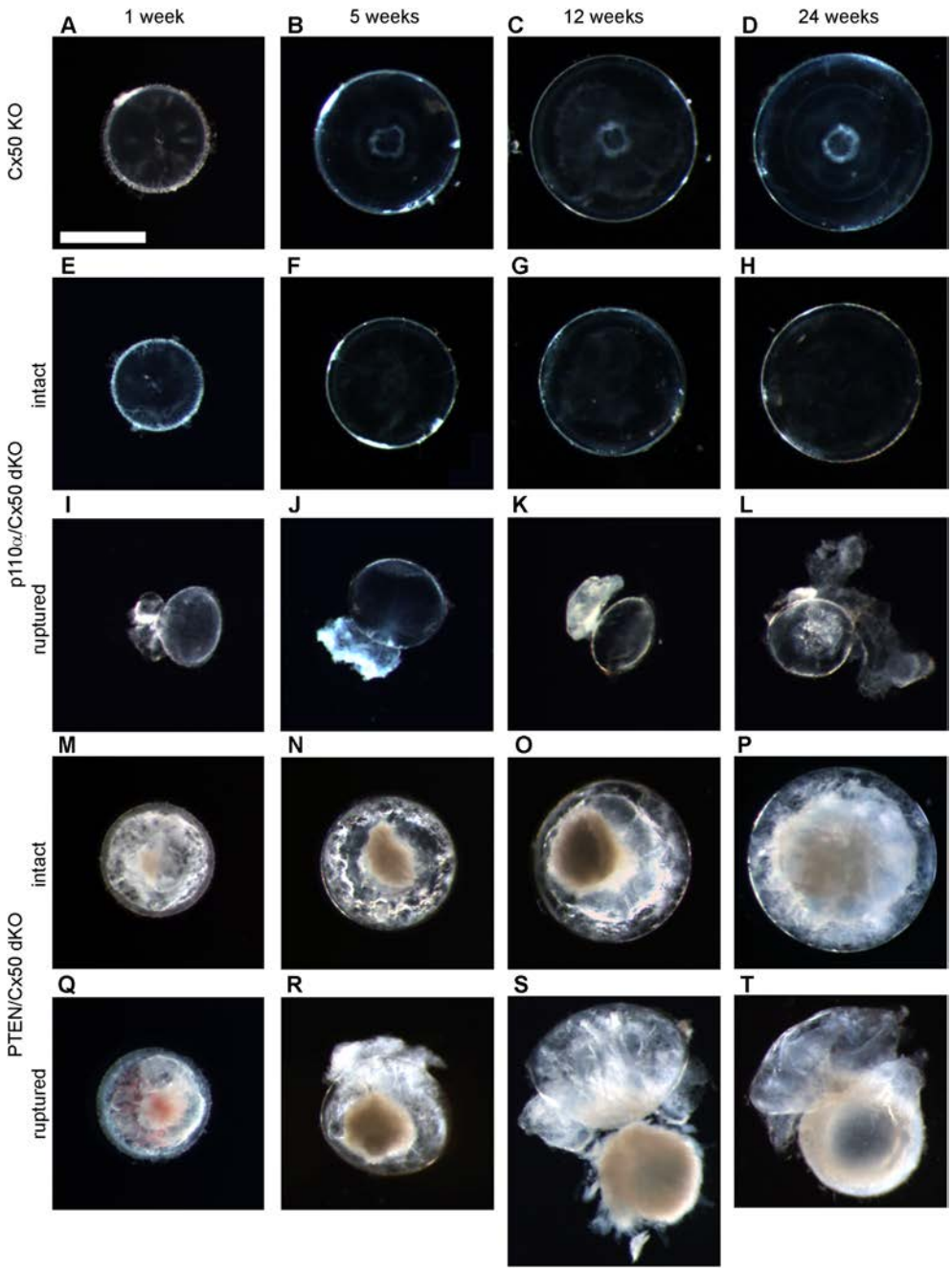

FIGURE 1
p110α/Cx50 dKO and PTEN/Cx50 dKO mice show altered lens size, clarity and integrity. Lenses were dissected and photographed at 1, 5, 12, and 24 weeks of age. Cx50 KO lenses **(A–D)** were intact at all ages studied and contained a mild nuclear cataract. p110α/Cx50 dKO lenses that did not rupture **(E–H)** were smaller than single Cx50 KOs, and lacked the mild nuclear cataract. Most p110α/Cx50 double KO lenses **(I–L)** displayed a partial posterior rupture, leaving a transparent anterior lens fragment attached to posterior lens debris. PTEN/Cx50 dKO lenses displayed a more severe phenotype than single Cx50 KO or PTEN KO lenses. Intact lenses **(M–P)** displayed a dense nuclear cataract and abundant cortical vacuoles. The incidence of total lens rupture increased with age **(Q–T)**. Bar = 1mm, all panels are at the same magnification.

away from the tunica vasculosa on P2 (Figures 4A–C). However, 29% (n = 14) of the P2 lenses (Figures 4D–F) and 13% (n = 16) of the P7 lenses (Figures 4G–I) from PTEN/Cx50 dKO could not be separated from highly adherent/penetrant blood vessels that presumably originated from the tunica vasculosa lentis. This phenomenon was not previously observed in wild-type, single Cx50 KO, or single PTEN KO eyes (13, 17, 60).

3.5 The P0 proliferation defect present in single p110α KO lenses persisted in p110α/Cx50 dKO mice

The pattern of mitosis in p110α single KO lenses was altered on P0, with a large reduction in cell division in the equatorial germinative zone of the lens epithelium (16, 68). To examine

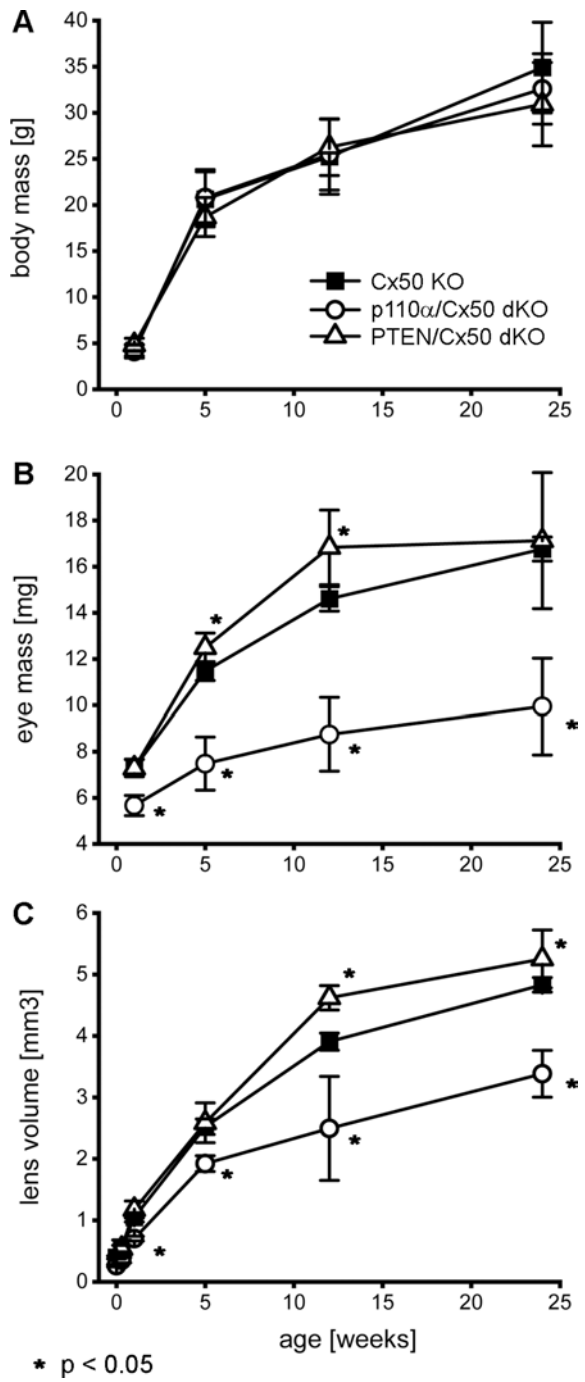

FIGURE 2
Double knockout of p110α/Cx50 reduced eye and lens growth. Changes in animal mass, eye mass and lens volume were quantified between P0 and 24 weeks of age. Body mass **(A)** for Cx50 KO, p110α/Cx50 dKO, and PTEN/Cx50 dKO animals was similar at all ages (n = 8-27 animals/genotype/age). Eye mass **(B)** in the p110α/Cx50 dKO was significantly reduced at all ages (23-40% smaller, $p < 0.05$, one-way ANOVA, n = 16-42 eyes/genotype/age) compared to either the Cx50 KO or PTEN/Cx50 dKO mice. Between 5 and 12 weeks, eyes from PTEN/Cx50 dKO animals were slightly larger than Cx50 KO (8-15% increase, $p < 0.05$). Lens volume **(C)** in the p110α/Cx50 dKO was significantly reduced (up to 37% smaller, $p < 0.05$, n = 6-36 lenses/genotype/age). Lens volume in the PTEN/Cx50 dKO animals were increased between 12 and 24 weeks of age (8-18% larger, $p < 0.05$). Data are plotted as mean ± SD. Asterisks indicate significantly different values compared to the Cx50 KO.

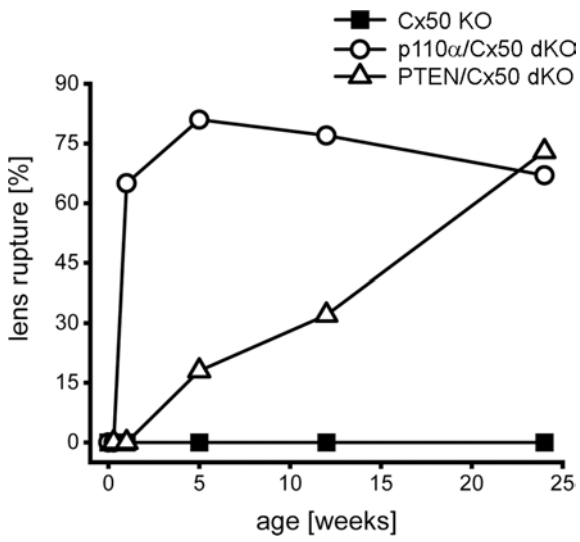

FIGURE 3
Lens rupture increased in p110α/Cx50 and PTEN/Cx50 dKO mice. The incidence of lens rupture was plotted against age between P0 and 24 weeks. No lens rupture was observed in Cx50 KO animals. Lenses from p110α/Cx50 dKO mice were intact up until P2, but then displayed high rates (65-81%) of rupture after 1 week. PTEN/Cx50 dKO lenses displayed an increasing propensity to rupture with age, than was accelerated compared to single PTEN KO mice (60). n = 16-42 lenses/genotype/age.

postnatal mitosis in p110α/Cx50 mice, lenses from Cx50 KO and p110α/Cx50 dKO mice were labeled with EdU on P0. Cx50 KO lenses showed strong EdU labeling, with the highest level of fluorescence in the germinative zone near the lens equator (Figures 5A, B). By contrast, p110α/Cx50 dKO lenses lacked the ring of increased labeling near the equatorial germinative zone, and showed a more uniform pattern of EdU incorporation across the lens epithelium (Figures 5D, E). Line scans of the mean fluorescent intensity taken across the lens diameter (black lines, ± the SEM green bars) confirmed this change in mitotic pattern between EdU labeled images from P0 Cx50 KO (Figure 5C) and p110α/Cx50 dKO lenses (Figure 5F, arrowheads). All P0 Cx50 KO lenses displayed large peaks of EdU fluorescent intensity in the equatorial germinative zone (n = 5). By contrast, all P0 p110α/Cx50 dKO lenses lacked the equatorial peaks, and had maximum mean values of fluorescence that ranged from 35% to 39% lower than Cx50 KO lenses (n =4). These data show that further deletion of Cx50 from p110α knockout lenses did not restore normal P0 epithelial cell proliferation.

3.6 PTEN/Cx50 dKO lenses did not rescue central epithelial proliferation and displayed altered distribution of nuclei on P2

Single PTEN KO lenses were previously shown to display robust postnatal EdU labeling with a pattern similar to wild-type animals with the highest level of fluorescence in the germinative zone near

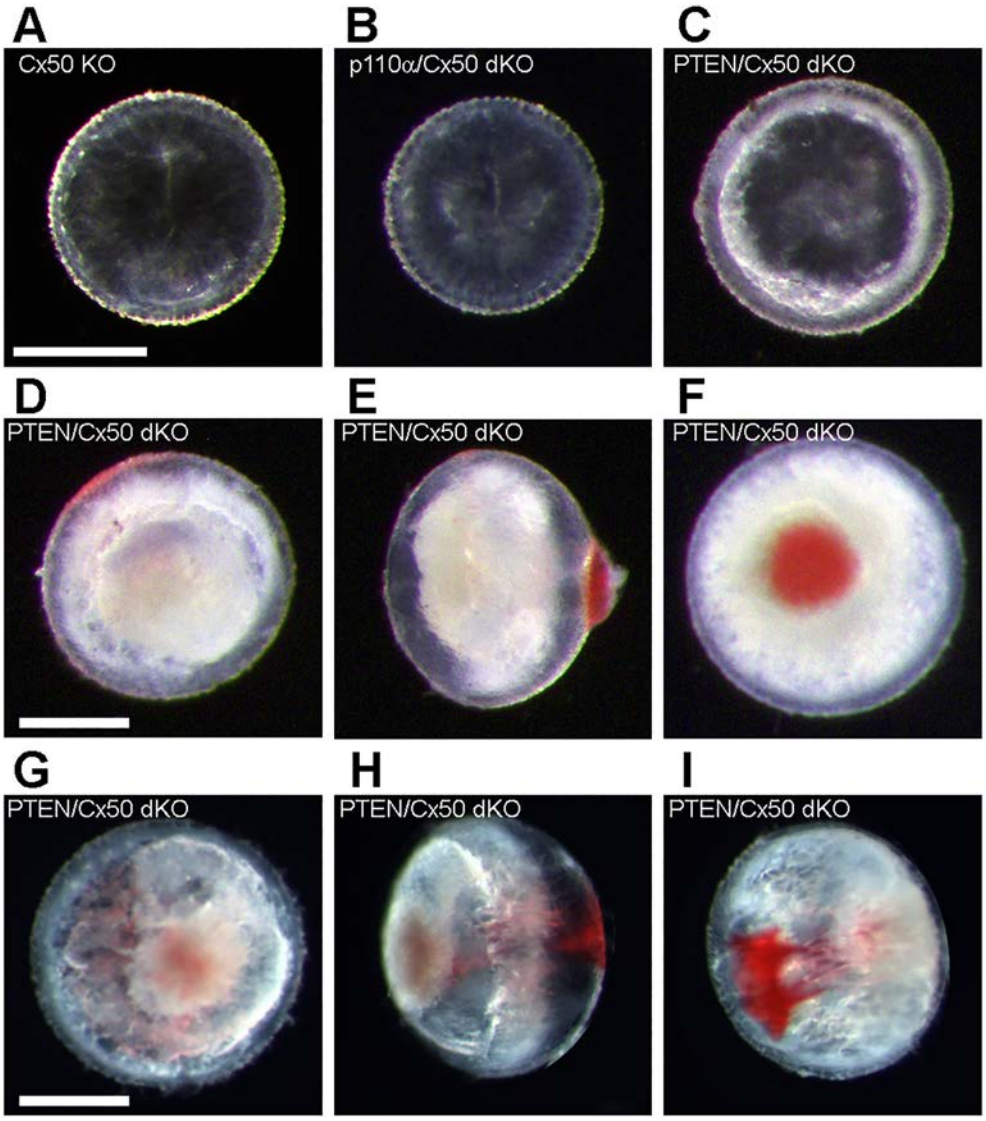

FIGURE 4
Postnatal PTEN/Cx50 dKO lenses show altered interaction with blood vessels. The tunica vasculosa lentis provides a blood supply to the developing lens during the first postnatal week (71–74). All P2 lenses from Cx50 KO **(A)** and p110α/Cx50 dKO **(B)** could be dissected away from the blood vessels of the tunica vasculosa. Most lenses (71%, n = 14) from PTEN/Cx50 dKO animals could also be separated from the tunica vasculosa on P2 **(C)**. However, 29% of P2 PTEN/Cx50 dKO lenses could not be separated from highly adherent/penetrant blood vessels (**D**, anterior view, **E** side view, **F** posterior view). On P7, 13% (n = 16) of PTEN/Cx50 dKO lenses were associated with tunica vasculosa blood vessels (**G**, anterior view, **H** side view, **I** posterior view). Bars = 0.5 mm.

the lens equator (68). By contrast, single Cx50 KO lenses previously showed decreased DNA replication on P2, especially within the central anterior epithelium (15). To examine mitosis on P2 in in p110α/Cx50 and PTEN/Cx50 dKO animals, lenses from Cx50 KO, p110α/Cx50 dKO and PTEN/Cx50 dKO mice were labeled with EdU. On postnatal day 2, Cx50 KO (Figures 6A, B), p110α/Cx50 dKO (Figures 6E, F), and PTEN/Cx50 dKO (Figures 6I, J) lenses all displayed the greatest levels of proliferation in the equatorial germinative zone. Similar to p110α KO mice (16), P2 p110α/Cx50 dKO lenses had recovered the deficit of proliferation in this region that was evident on P0. The mean values of line scans (black lines, ± the SEM green bars) of EdU fluorescence taken across the lens diameter confirmed that the p110α/Cx50 dKO lenses had recovered peak proliferation in the equatorial germinative zone on P2 (Figure 6H). All three of the Cx50 deficient lenses also showed decreased EdU incorporation in the central lens epithelium (Figures 6M–O), consistent with prior studies (15, 35), with the lowest levels observed in the Cx50 KO and PTEN/Cx50 dKO animals (Figure 6P). The Hoechst staining of nuclei in the PTEN/Cx50 dKO lenses (Figures 6J, K) further illustrated a loss of organization of nuclei in the equatorial bow region, compared with the dense band of nuclear staining seen in both Cx50 KO and p110α/Cx50 dKO mice where new fiber cells become internalized (Figures 6B, C, F, G, white arrowheads). Lens nuclei in the P2 PTEN/Cx50 dKO animals failed to internalize in the bow region and were diffusely distributed and displaced toward the

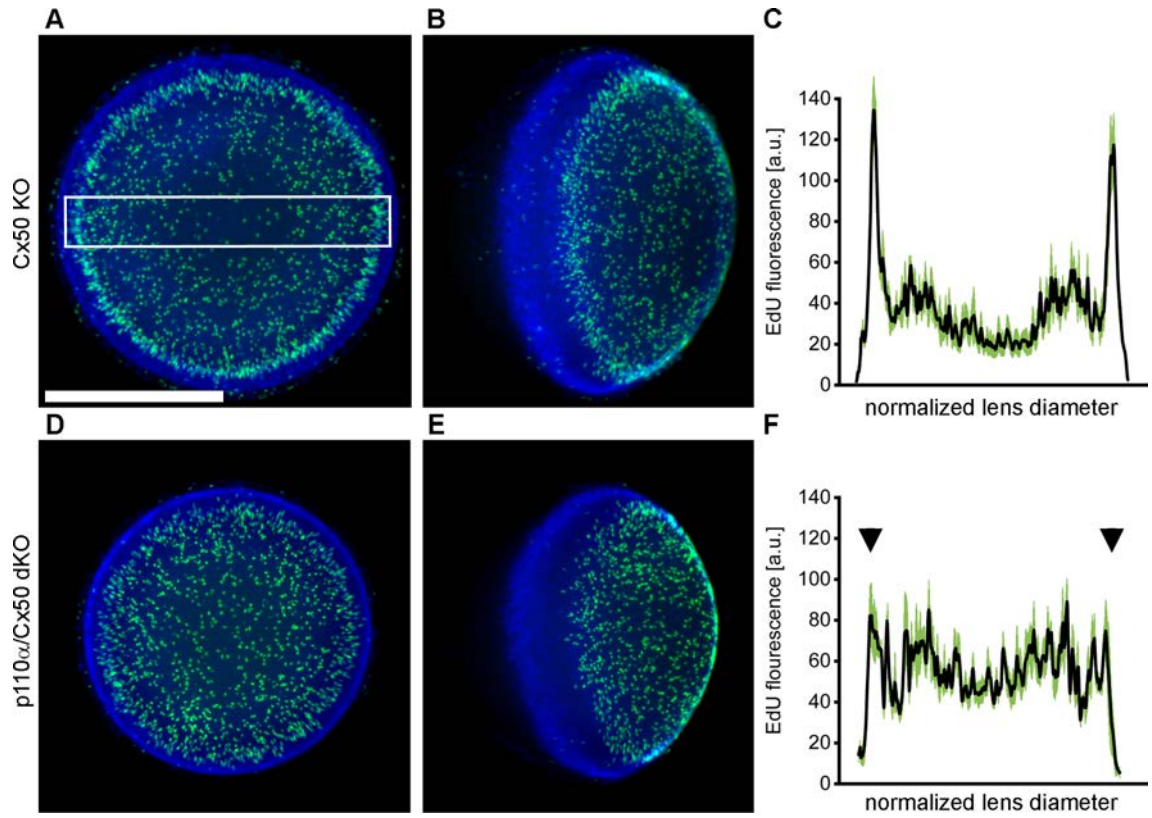

FIGURE 5
P0 p110α/Cx50 dKO lenses showed a large reduction in cell division in the equatorial germinative zone of the lens epithelium. Lenses from Cx50 KO **(A, B)** and p110α/Cx50 dKO **(D, E)** animals were labeled with EdU (green **A, B, D, E**) and Hoechst (blue **A, B, D, E**) on P0. Z-stack images were created looking onto the epithelial surface **(A, D)**, or onto the lens edge **(B, E)**. Plots of mean values of line scans (black lines, ± the SEM green bars) of EdU fluorescence taken across the lens diameter **(C, F)** showed that the p110α/dKO lenses **(F)** had reduced peak proliferation in the equatorial germinative zone (black arrowheads) compared to Cx50 KO lenses **(C)**. n = 4-5 lenses per genotype. White boxed area in A depicts a representative scan region. Bar = 0.5 mm.

posterior pole. These data suggest that the independent additive effects of transient loss of proliferating epithelial cells in the germinative zone on P0 and in the central zone on P2, as seen previously in the single p110α and Cx50 KO mice respectively could cause the significant reduction in lens size following p110α/Cx50 double deletion. They further show that double deletion of PTEN/Cx50 disrupted the spatial organization of lens nuclei.

3.7 Double deletion of PTEN/Cx50 resulted in histological abnormalities in the lens

To compare the histology of Cx50 KO, p110α/Cx50 dKO and PTEN/Cx50 dKO lenses, eyes from mouse pups on P2 were dissected, fixed, sectioned and stained with hematoxylin and eosin. Sagittal sections through the central region of Cx50 KO lenses (Figure 7A) contained a central zone where the lens fibers displayed reduced eosinophilic staining as previously described (17). The bow region of Cx50 KO lenses was normal (Figure 7B), although there was evidence of delayed denucleation of differentiated fiber cells as formerly reported (13). Consistent with the absence of nuclear cataract shown in Figure 1, the p110α/Cx50 dKO lenses lacked the central zone of reduced eosinophilic staining (Figures 7C, D). In addition, p110α/Cx50 dKO lenses often displayed posterior defects that may represent early stages of lens rupture. By contrast, PTEN/Cx50 dKO lenses showed severe histological anomalies (Figures 7E, F). The bow region failed to form properly, with shortened lens fibers and their associated nuclei displaced toward the posterior lens, consistent with the Hoechst staining described above (Figures 6J, K). This equatorial area also contained large vacuoles, and additional histological defects were present in the anterior and posterior regions of PTEN/Cx50 dKO lenses. Thus, double deletion of PTEN/Cx50 from the lens induced several histological defects in the lens.

4 Discussion

We have generated and characterized p110α/Cx50 and PTEN/Cx50 double knockout mice with the goal of improving our understanding of the integration of gap junctional communication mediated by Cx50 with the intracellular signaling activity of PI3K and PTEN in the pathophysiology and normal physiology of the lens. As summarized in Table 1, double deletion of Cx50 and p110α resulted in a unique phenotype compared to both of the respective single knockouts. The microphthalmia, proliferation defects, and smaller

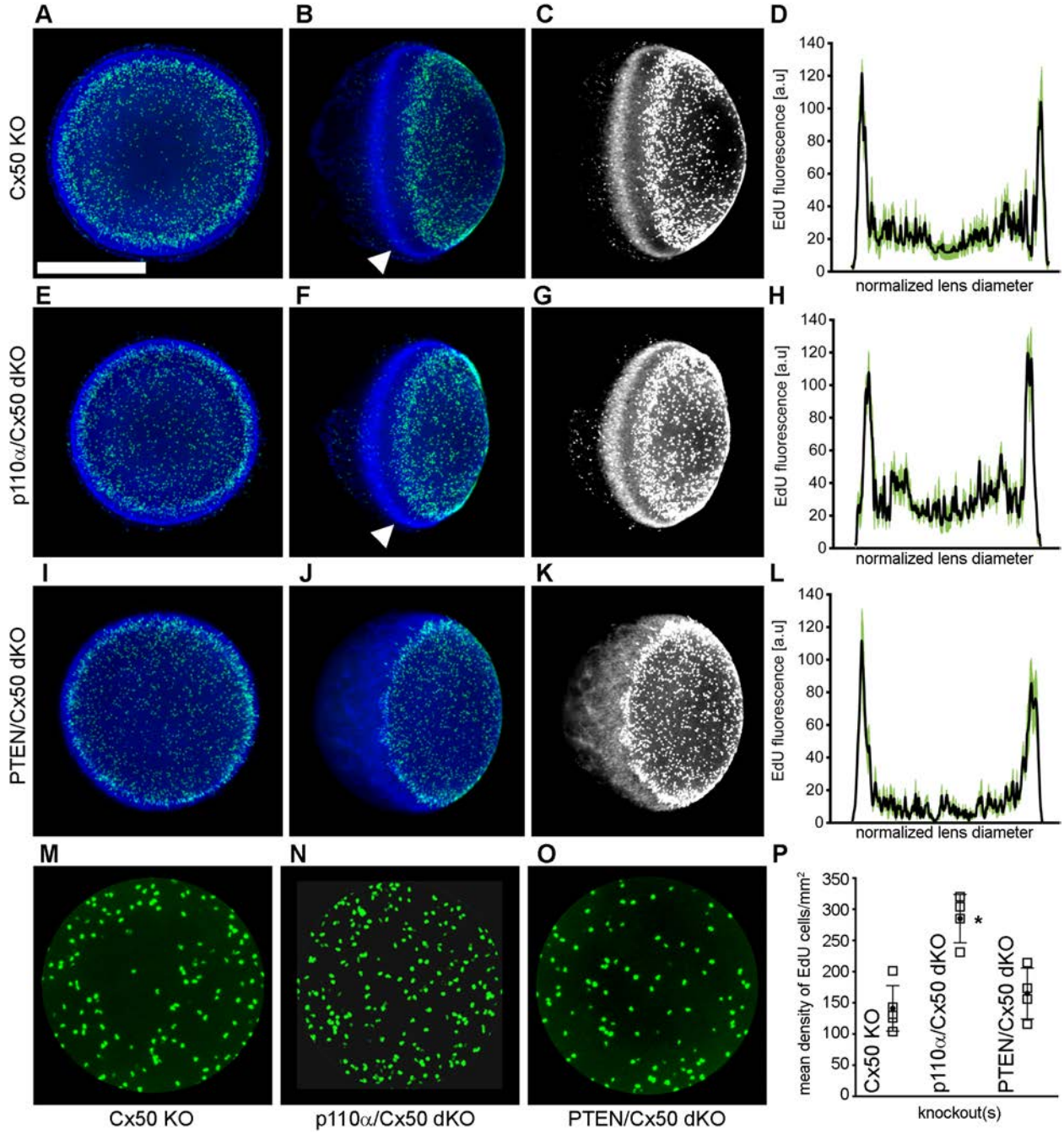

FIGURE 6
PTEN/Cx50 dKO lenses did not rescue central epithelial proliferation and displayed altered distribution of nuclei on P2. Lenses from Cx50 KO **(A–C)**, p110α/Cx50 dKO **(E–G)** and PTEN/Cx50 dKO **(I–K)** animals were labeled with EdU (green **A, B, E, F, I, J**) and Hoechst (blue **A, B, E, F, I, J**) on P2. High contrast grayscale images of stained nuclei **(C, G, K)** were generated to highlight changes in distribution between genotypes. Z-stack images were created looking onto the epithelial surface **(A, E, I)**, or onto the lens edge **(B, C, F, G, J, K)**. Plots of mean values of line scans (black lines, ± the SEM green bars) of EdU fluorescence taken across the lens diameter **(D, H, L)** showed that p110α/Cx50 dKO lenses had recovered peak proliferation in the equatorial germinative zone **(H)**, and that PTEN/Cx50 dKO lenses displayed EdU incorporation that peaked in the germinative zone **(L)**. Hoechst staining in the PTEN/Cx50 dKO lenses **(J, K)** illustrated that equatorial nuclei were diffusely distributed and displaced toward the posterior pole, compared to the dense band of nuclear staining seen in Cx50 KO and p110α/Cx50 dKO mice where new fiber cells become internalized (**B, C, F, G**, white arrowheads). Quantitation of central proliferation **(M–O)** revealed an elevated mean density of EdU positive lens epithelial cells in p110α/Cx50 dKO **(P)** mice compared to Cx50 KO or PTEN/Cx50 dKO animals ($p < 0.05$). n = 4-5 lenses per genotype. Bar = 0.5 mm. Open squares are raw data, filled circles are the mean ± SD. Asterisk indicates significantly different values compared to the Cx50 KO.

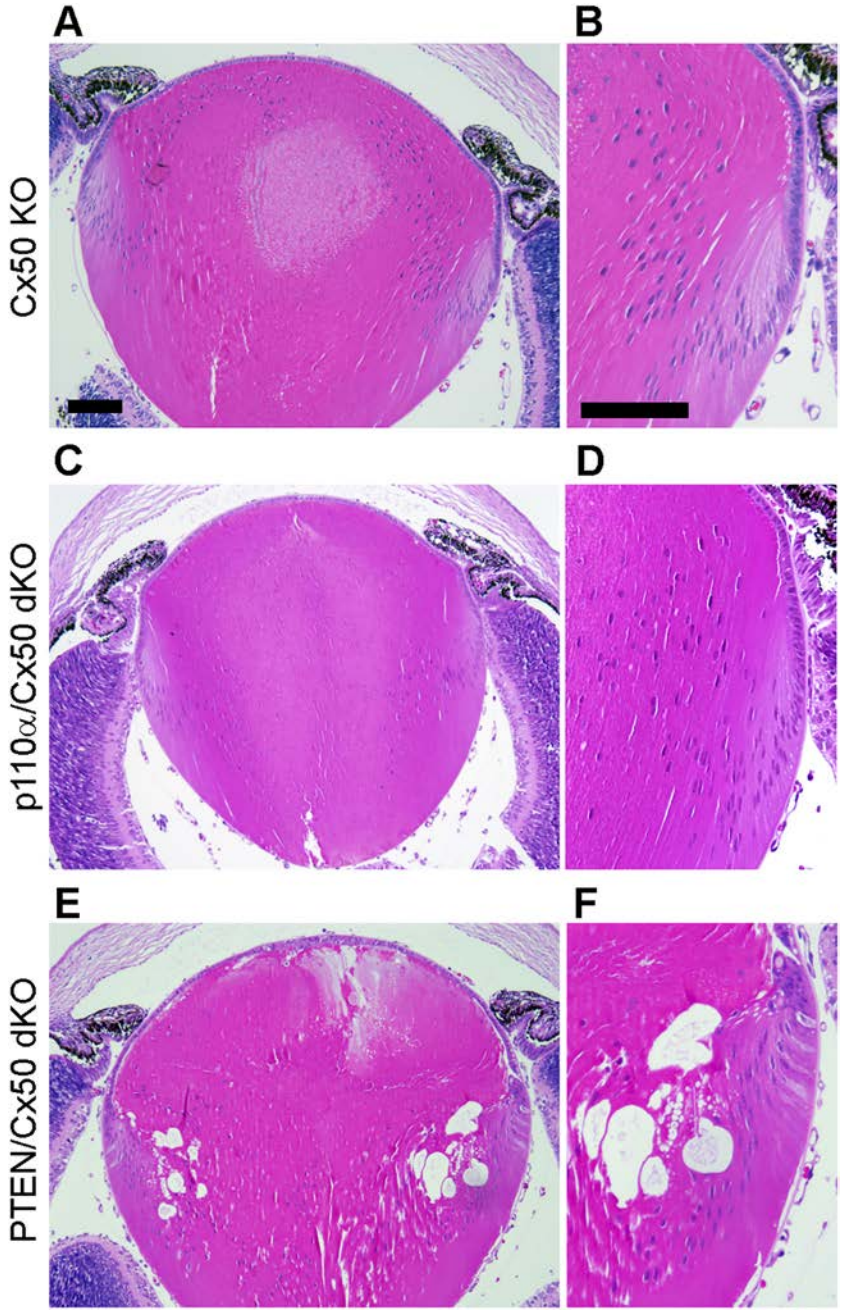

FIGURE 7
PTEN/Cx50 dKO lenses showed histological abnormalities. P2 eyes were fixed, embedded in paraffin and sectioned. Sagittal sections through the central region were stained with hematoxylin and eosin. Cx50 KO lenses **(A)** contained a central zone of reduced eosinophilic staining. The bow region of Cx50 KO lenses **(B)** showed delayed denucleation of differentiated fiber cells. p110α/Cx50 dKO lenses **(C, D)** were similar to Cx50 KOs, but had normal eosinophilic staining, and often displayed posterior defects. PTEN/Cx50 dKO lenses **(E, F)** had several histological anomalies. The bow region failed to form properly, with shortened lens fibers and their associated nuclei displaced toward the posterior lens. The equatorial area also contained large vacuoles, and additional histological defects were present in the anterior and posterior regions. Bars = 100 μm.

sizes of single Cx50 KO and p110α KO lenses (15–17) were additively intensified in the p110α/Cx50 dKO. In addition, a novel rupture phenotype, never observed in the single KOs, appeared in the p110α/Cx50 dKO with a rapid time course of development. Double knockout of PTEN and Cx50 produced lenses with some features similar to each of the respective single knockouts. The smaller eye and lens size of the Cx50 KO was not notably altered by further removal of PTEN in the dKO. By contrast, the cataract and rupture phenotype seen in single PTEN KO lenses (60) was more severe and had a faster time course in the PTEN/Cx50 dKO mice. Two novel phenotypes also emerged, that were absent in the respective single KOs. PTEN/Cx50 dKO animals had postnatal lens fiber differentiation defects that resulted in disorganized and anteriorly displaced cell nuclei. Finally, a subset of PTEN/Cx50 dKO lenses displayed an anomalous association with blood vessels of the tunica vasculosa lentis during the first postnatal week.

The lens growth pattern in rodents undergoes a change at P0, the time point where we observed a large decrease in dividing epithelial cells in the germinative zone of p110α/Cx50 dKO lenses. During embryonic development, the diameter of the lens increases linearly while the lens volume grows exponentially (75, 76). During the first postnatal week, lens growth occurs in an oscillatory manner corresponding to epithelial cell cycle timing that can be simulated by pulsatile administration of growth factors to organ-cultured lenses (77, 78). In single p110α KOs, peak lens epithelial cell proliferation in the germinative zone vanished at P0, despite being clearly evident on E17 and P2 (16). In p110α/Cx50 dKO lenses, germinative zone peak proliferation also transiently vanished at P0, but returned by P2. This suggests that both embryonic and postnatal growth mechanisms can produce maximum cell division in the germinative zone that do not require the activity of p110α. However, the transition period between these two distinct growth mechanisms on P0 was affected by the absence of p110α activity, in a manner that was independent of the presence of Cx50.

Loss of Cx50 activity was also correlated with discrete temporal changes in epithelial cell proliferation linked to significant reductions in lens size. Knockout of Cx50, or its replacement with Cx46 by genetic knocking, resulted in significantly smaller lenses that failed to generate a single pulse of postnatal epithelial cell proliferation on P2 (15, 17, 23, 35). Cx50 functional activity reaches a peak in early postnatal epithelial cells when lens mitosis switches to the pulsatile growth pattern, and Cx50 conductance can be significantly upregulated by p110α activity (35, 61). The finding that the two distinct lens growth defects persisted independently in the p110α/Cx50 dKO, and resulted in a much smaller lens that either single KO, suggests that there was no functional epistasis between the Cx50 and p110α growth deficits, despite their ability to functionally interact *in vitro* (61).

The vast majority of p110α/Cx50 dKO lenses underwent a posterior rupture within 1 week of age. This was unexpected, as neither Cx50, nor p110α, single KO lenses ever displayed lens rupture (16, 17, 68). Both p110α and Cx50 play a central role in the regulation of intracellular hydrostatic pressure in the lens (62–64), so it is possible that the combined loss of their activities led to a catastrophic loss of homeostasis. PTEN antagonism of p110α signaling is critical to maintain lens homeostasis (68). In single PTEN KO lenses, unchecked p110α activity reduced epithelial cell Na^+/K^+-ATPase activity (60), causing reduced sodium and water efflux mediated by the lens circulation (79, 80), and resulted in increased intracellular hydrostatic pressure and lens rupture. The incidence and kinetics of lens rupture in the PTEN/Cx50 dKO was also accelerated compared to the single PTEN KO (60), highlighting the importance of Cx50 and PTEN in regulation of the lens circulation. Elucidation of the precise mechanisms whereby Cx50, PI3K and PTEN collaboratively preserve lens homeostasis will require additional investigation.

The PTEN/Cx50 dKO mice displayed two additional defects that were not previously observed in wild-type mice or the respective single KOs (13, 17, 60). First, blood vessels, presumably from the tunica vasculosa lentis, became highly adherent to a subset of PTEN/Cx50 dKO lenses between P2 and P7. The reasons for this alteration in tunica vasculosa structure, and how these changes were driven by the combined loss of Cx50 and PTEN in the lens are not known. Second, newly differentiated fiber cells in the bow region failed to elongate properly and migrated posteriorly, leading to displaced and disordered cell nuclei. The cytopathology in PTEN/Cx50 dKO animals was amplified when compared to the specific and limited histological defects present in either PTEN or Cx50 single KO lenses (17, 60). PTEN/Cx50 dKO lenses also showed a less organized band of new fiber nuclei in the bow region. Examination of the nuclear distribution by Hoechst staining showed that Cx50 single KOs had a clearly demarcated transition zone where the anterior epithelium ended and fiber differentiation began. By contrast, disordered surface nuclei persisted well toward the posterior pole in PTEN/Cx50 dKO lenses. Fiber cell differentiation is largely regulated by FGF signaling (5, 6, 81), although in the absence of PTEN the differentiation process can be influenced by non-FGF signaling pathways (7). Cx50 also affects lens fiber differentiation (13, 21, 82), and it is possible that the loss of both modes of communication could not be compensated for in the PTEN/Cx50 dKO lenses.

We have examined interaction between Cx50 mediated gap junctional communication and PI3K/PTEN signaling in the lens using an *in vivo* methodology involving mice with multiple gene knockouts. Double knockout of p110α and Cx50 significantly reduced eye and lens size, and resulted in a high rate of lens rupture starting in the first postnatal week. Cell proliferation defects identified in the single Cx50 and p110α knockouts were maintained in the p110α/Cx50 dKO lenses. Double deletion of Cx50 and PTEN produced severe lens defects, including cataract, aberrant cell migration, vacuole formation and lens rupture. Taken together, these observations suggest that interaction between PI3K/PTEN signaling and Cx50 mediated intercellular communication may participate in the regulation of lens cell proliferation, differentiation and homeostasis, and that loss of this regulation may contribute to a variety of developmental defects. Further study of how lens gap junction channels and PI3K/PTEN signaling work together to maintain clarity, preserve integrity and regulate postnatal mitosis could provide broad insights into the regulation of channel/transport activity in other tissues.

Data availability statement

The raw data supporting the conclusions of this article will be made available by the authors, without undue reservation.

Ethics statement

The animal study was approved by Stony Brook University Institutional Animal Care and Use Committee. The study was conducted in accordance with the local legislation and institutional requirements.

Author contributions

CS: Conceptualization, Data curation, Formal analysis, Investigation, Methodology, Resources, Validation, Writing – original draft, Writing – review & editing. TW: Conceptualization, Formal analysis, Funding acquisition, Investigation, Methodology, Project administration, Supervision, Writing – original draft, Writing – review & editing.

Funding

The author(s) declare financial support was received for the research, authorship, and/or publication of this article. This research was funded by National Institutes of Health, grant number EY026911.

Acknowledgments

We thank Dr. Leping Li for assistance with histological analysis.

Conflict of interest

The authors declare that the research was conducted in the absence of any commercial or financial relationships that could be construed as a potential conflict of interest.

Generative AI statement

The author(s) declare that no Generative AI was used in the creation of this manuscript.

Publisher's note

References

1. Berthoud VM, Minogue PJ, Osmolak P, Snabb JI, Beyer EC. Roles and regulation of lens epithelial cell connexins. *FEBS Lett*. (2014) 588:1297–303. doi: 10.1016/j.febslet.2013.12.024

2. Jiang JX. Gap junctions or hemichannel-dependent and independent roles of connexins in cataractogenesis and lens development. *Curr Mol Med*. (2010) 10:851–63. doi: 10.2174/156652410793937750

3. White TW, Bruzzone R. Intercellular communication in the eye: clarifying the need for connexin diversity. *Brain Res Brain Res Rev*. (2000) 32:130–7. doi: 10.1016/S0165-0173(99)00072-7

4. Lovicu FJ, McAvoy JW, de Iongh RU. Understanding the role of growth factors in embryonic development: insights from the lens. *Philos Trans R Soc Lond B Biol Sci*. (2011) 366:1204–18. doi: 10.1098/rstb.2010.0339

5. Robinson ML. An essential role for FGF receptor signaling in lens development. *Semin Cell Dev Biol*. (2006) 17:726–40. doi: 10.1016/j.semcdb.2006.10.002

6. Chaffee BR, Hoang TV, Leonard MR, Bruney DG, Wagner BD, Dowd JR, et al. Fgfr and pten signaling interact during lens development to regulate cell survival. *Dev Biol*. (2016) 410:150–63. doi: 10.1016/j.ydbio.2015.12.027

7. Padula SL, Sidler EP, Wagner BD, Manz CJ, Lovicu FJ, Robinson ML. Lens fiber cell differentiation occurs independently of fibroblast growth factor receptor signaling in the absence of Pten. *Dev Biol*. (2020) 467:1–13. doi: 10.1016/j.ydbio.2020.07.017

8. Boswell BA, Lein PJ, Musil LS. Cross-talk between fibroblast growth factor and bone morphogenetic proteins regulates gap junction-mediated intercellular communication in lens cells. *Mol Biol Cell*. (2008) 19:2631–41. doi: 10.1091/mbc.E08-02-0124

9. Le AC, Musil LS. A novel role for FGF and extracellular signal-regulated kinase in gap junction-mediated intercellular communication in the lens. *J Cell Biol*. (2001) 154:197–216. doi: 10.1083/jcb.200101057

10. Le AC, Musil LS. FGF signaling in chick lens development. *Dev Biol*. (2001) 233:394–411. doi: 10.1006/dbio.2001.0194

11. McAvoy JW, Chamberlain CG, de Iongh RU, Richardson NA, Lovicu FJ. The role of fibroblast growth factor in eye lens development. *Ann N Y Acad Sci*. (1991) 638:256–74. doi: 10.1111/j.1749-6632.1991.tb49036.x

12. Lovicu FJ, McAvoy JW. Growth factor regulation of lens development. *Dev Biol*. (2005) 280:1–14. doi: 10.1016/j.ydbio.2005.01.020

13. Rong P, Wang X, Niesman I, Wu Y, Benedetti LE, Dunia I, et al. Disruption of Gja8 (Alpha8 connexin) in mice leads to microphthalmia associated with retardation of lens growth and lens fiber maturation. *Development*. (2002) 129:167–74. doi: 10.1242/dev.129.1.167

14. Wang E, Geng A, Seo R, Maniar A, Gong X. Knock-in of Cx46 partially rescues fiber defects in lenses lacking Cx50. *Mol Vis*. (2017) 23:160–70.

15. Sellitto C, Li L, White TW. Connexin50 is essential for normal postnatal lens cell proliferation. *Invest Ophthalmol Vis Sci*. (2004) 45:3196–202. doi: 10.1167/iovs.04-0194

16. Sellitto C, Li L, Vaghefi E, Donaldson PJ, Lin RZ, White TW. The phosphoinosotide 3-kinase catalytic subunit P110alpha is required for normal lens growth. *Invest Ophthalmol Vis Sci*. (2016) 57:3145–51. doi: 10.1167/iovs.16-19607

17. White TW, Goodenough DA, Paul DL. Targeted ablation of connexin50 in mice results in microphthalmia and zonular pulverulent cataracts. *J Cell Biol*. (1998) 143:815–25. doi: 10.1083/jcb.143.3.815

18. Garcia CM, Yu K, Zhao H, Ashery-Padan R, Ornitz DM, Robinson ML, et al. Signaling through FGF receptor-2 is required for lens cell survival and for withdrawal from the cell cycle during lens fiber cell differentiation. *Dev Dyn*. (2005) 233:516–27. doi: 10.1002/dvdy.20356

19. Garcia CM, Huang J, Madakashira BP, Liu Y, Rajagopal R, Dattilo L, et al. The function of FGF signaling in the lens placode. *Dev Biol*. (2011) 351:176–85. doi: 10.1016/j.ydbio.2011.01.001

20. Tjahjono N, Xia CH, Li R, Chu S, Wang J, Gong X. Connexin 50-R205g mutation perturbs lens epithelial cell proliferation and differentiation. *Invest Ophthalmol Vis Sci*. (2020) 61:25. doi: 10.1167/iovs.61.3.25

21. Hu Z, Shi W, Riquelme MA, Shi Q, Biswas S, Lo WK, et al. Connexin 50 functions as an adhesive molecule and promotes lens cell differentiation. *Sci Rep*. (2017) 7:5298. doi: 10.1038/s41598-017-05647-9

22. Gu S, Biswas S, Rodriguez L, Li Z, Li Y, Riquelme MA, et al. Connexin 50 and AQP0 are essential in maintaining organization and integrity of lens fibers. *Invest Ophthalmol Vis Sci*. (2019) 60:4021–32. doi: 10.1167/iovs.18-26270

23. White TW. Unique and redundant connexin contributions to lens development. *Science*. (2002) 295:319–20. doi: 10.1126/science.1067582

24. Wei CJ, Xu X, Lo CW. Connexins and cell signaling in development and disease. *Annu Rev Cell Dev Biol*. (2004) 20:811–38. doi: 10.1146/annurev.cellbio.19.111301.144309

25. Donaldson P, Kistler J, Mathias RT. Molecular solutions to mammalian lens transparency. *News Physiol Sci*. (2001) 16:118–23. doi: 10.1152/physiologyonline.2001.16.3.118

26. Harris AL. Emerging issues of connexin channels: biophysics fills the gap. *Q Rev Biophys*. (2001) 34:325–472. doi: 10.1017/S0033583501003705

27. Bruzzone R, White TW, Paul DL. Connections with connexins: the molecular basis of direct intercellular signaling. *Eur J Biochem*. (1996) 238:1–27. doi: 10.1111/j.1432-1033.1996.0001q.x

28. Beyer EC, Kistler J, Paul DL, Goodenough DA. Antisera directed against connexin43 peptides react with a 43-kD protein localized to gap junctions in myocardium and other tissues. *J Cell Biol*. (1989) 108:595–605. doi: 10.1083/jcb.108.2.595

29. Paul DL, Ebihara L, Takemoto LJ, Swenson KI, Goodenough DA. Connexin46, a novel lens gap junction protein, induces voltage-gated currents in nonjunctional plasma membrane of xenopus oocytes. *J Cell Biol*. (1991) 115:1077–89. doi: 10.1083/jcb.115.4.1077

30. White TW, Bruzzone R, Goodenough DA, Paul DL. Mouse Cx50, a functional member of the connexin family of gap junction proteins, is the lens fiber protein MP70. *Mol Biol Cell*. (1992) 3:711–20. doi: 10.1091/mbc.3.7.711

31. Dahm R, van Marle J, Prescott AR, Quinlan RA. Gap junctions containing alpha8-connexin (Mp70) in the adult mammalian lens epithelium suggests a re-evaluation of its role in the lens. *Exp Eye Res*. (1999) 69:45–56. doi: 10.1006/exer.1999.0670

32. White TW, Sellitto C, Paul DL, Goodenough DA. Prenatal lens development in connexin43 and connexin50 double knockout mice. *Invest Ophthalmol Vis Sci*. (2001) 42:2916–23.

33. DeRosa AM, Mese G, Li L, Sellitto C, Brink PR, Gong X, et al. The cataract causing Cx50-S50p mutant inhibits Cx43 and intercellular communication in the lens epithelium. *Exp Cell Res*. (2009) 315:1063–75. doi: 10.1016/j.yexcr.2009.01.017

34. Gong X, Li E, Klier G, Huang Q, Wu Y, Lei H, et al. Disruption of alpha3 connexin gene leads to proteolysis and cataractogenesis in mice. *Cell*. (1997) 91:833–43. doi: 10.1016/S0092-8674(00)80471-7

35. White TW, Gao Y, Li L, Sellitto C, Srinivas M. Optimal lens epithelial cell proliferation is dependent on the connexin isoform providing gap junctional coupling. *Invest Ophthalmol Vis Sci*. (2007) 48:5630–7. doi: 10.1167/iovs.06-1540

36. Ilic N, Roberts TM. Comparing the roles of the P110alpha and P110beta isoforms of PI3k in signaling and cancer. *Curr Top Microbiol Immunol*. (2010) 347:55–77. doi: 10.1007/82_2010_63

37. Domin J, Waterfield MD. Using structure to define the function of phosphoinositide 3-kinase family members. *FEBS Lett*. (1997) 410:91–5. doi: 10.1016/S0014-5793(97)00617-0

38. Vanhaesebroeck B, Guillermet-Guibert J, Graupera M, Bilanges B. The emerging mechanisms of isoform-specific PI3k signalling. *Nat Rev Mol Cell Biol*. (2010) 11:329–41. doi: 10.1038/nrm2882

39. Cantley LC. The phosphoinositide 3-kinase pathway. *Science*. (2002) 296:1655–7. doi: 10.1126/science.296.5573.1655

40. Engelman JA, Luo J, Cantley LC. The evolution of phosphatidylinositol 3-kinases as regulators of growth and metabolism. *Nat Rev Genet*. (2006) 7:606–19. doi: 10.1038/nrg1879

41. Fruman DA, Meyers RE, Cantley LC. Phosphoinositide kinases. *Annu Rev Biochem*. (1998) 67:481–507. doi: 10.1146/annurev.biochem.67.1.481

42. Hawkins PT, Anderson KE, Davidson K, Stephens LR. Signalling through class I PI3ks in mammalian cells. *Biochem Soc Trans*. (2006) 34:647–62. doi: 10.1042/BST0340647

43. Cantley LC, Neel BG. New insights into tumor suppression: PTEN suppresses tumor formation by restraining the phosphoinositide 3-kinase/AKT pathway. *Proc Natl Acad Sci U.S.A*. (1999) 96:4240–5.

44. Waite KA, Eng C. Protean PTEN: form and function. *Am J Hum Genet*. (2002) 70:829–44. doi: 10.1086/340026

45. Martinez G, de Iongh RU. The lens epithelium in ocular health and disease. *Int J Biochem Cell Biol*. (2010) 42:1945–63. doi: 10.1016/j.biocel.2010.09.012

46. Teo ZL, McQueen-Miscamble L, Turner K, Martinez G, Madakashira B, Dedhar S, et al. Integrin linked kinase (Ilk) is required for lens epithelial cell survival, proliferation and differentiation. *Exp Eye Res*. (2014) 121:130–42. doi: 10.1016/j.exer.2014.01.013

47. Weber GF, Menko AS. Phosphatidylinositol 3-kinase is necessary for lens fiber cell differentiation and survival. *Invest Ophthalmol Vis Sci*. (2006) 47:4490–9. doi: 10.1167/iovs.06-0401

48. Piatigorsky J. Lens differentiation in vertebrates. A review of cellular and molecular features. *Differentiation*. (1981) 19:134–53. doi: 10.1111/j.1432-0436.1981.tb01141.x

49. McAvoy JW, Chamberlain CG, de Iongh RU, Hales AM, Lovicu FJ. Lens development. *Eye (Lond)*. (1999) 13:425–37. doi: 10.1038/eye.1999.117

50. McAvoy JW. Cell division, cell elongation and the co-ordination of crystallin gene expression during lens morphogenesis in the rat. *J Embryol Exp Morphol*. (1978) 45:271–81. doi: 10.1242/dev.45.1.271

51. Sikic H, Shi Y, Lubura S, Bassnett S. A stochastic model of eye lens growth. *J Theor Biol*. (2015) 376:15–31. doi: 10.1016/j.jtbi.2015.03.021

52. Lovicu FJ, McAvoy JW. FGF-induced lens cell proliferation and differentiation is dependent on MAPK (ERK1/2) signalling. *Development*. (2001) 128:5075–84. doi: 10.1242/dev.128.24.5075

53. Wang Q, Stump R, McAvoy JW, Lovicu FJ. MAPK/ERK1/2 and PI3-kinase signalling pathways are required for vitreous-induced lens fibre cell differentiation. *Exp Eye Res*. (2009) 88:293–306. doi: 10.1016/j.exer.2008.08.023

54. Iyengar L, Patkunanathan B, Lynch OT, McAvoy JW, Rasko JE, Lovicu FJ. Aqueous humour- and growth factor-induced lens cell proliferation is dependent on MAPK/ERK1/2 and AKT/PI3-K signalling. *Exp Eye Res*. (2006) 83:667–78. doi: 10.1016/j.exer.2006.03.008

55. Xie L, Overbeek PA, Reneker LW. Ras signaling is essential for lens cell proliferation and lens growth during development. *Dev Biol*. (2006) 298:403–14. doi: 10.1016/j.ydbio.2006.06.045

56. Upadhya D, Ogata M, Reneker LW. MAPK1 is required for establishing the pattern of cell proliferation and for cell survival during lens development. *Development*. (2013) 140:1573–82. doi: 10.1242/dev.081042

57. Gong X, Wang X, Han J, Niesman I, Huang Q, Horwitz J. Development of cataractous macrophthalmia in mice expressing an active MEK1 in the lens. *Invest Ophthalmol Vis Sci*. (2001) 42:539–48.

58. Shakespeare TI, Sellitto C, Li L, Rubinos C, Gong X, Srinivas M, et al. Interaction between connexin50 and mitogen-activated protein kinase signaling in lens homeostasis. *Mol Biol Cell*. (2009) 20:2582–92. doi: 10.1091/mbc.E08-12-1257

59. Iyengar L, Wang Q, Rasko JE, McAvoy JW, Lovicu FJ. Duration of erk1/2 phosphorylation induced by FGF or ocular media determines lens cell fate. *Differentiation*. (2007) 75:662–8. doi: 10.1111/j.1432-0436.2007.00167.x

60. Sellitto C, Li L, Gao J, Robinson ML, Lin RZ, Mathias RT, et al. Akt activation promotes pten hamartoma tumor syndrome-associated cataract development. *J Clin Invest*. (2013) 123:5401–9. doi: 10.1172/JCI70437

61. Martinez JM, Wang HZ, Lin RZ, Brink PR, White TW. Differential regulation of connexin50 and connexin46 by PI3k signaling. *FEBS Lett*. (2015) 589:1340–5. doi: 10.1016/j.febslet.2015.04.029

62. Gao J, Sun X, White TW, Delamere NA, Mathias RT. Feedback regulation of intracellular hydrostatic pressure in surface cells of the lens. *Biophys J*. (2015) 109:1830–9. doi: 10.1016/j.bpj.2015.09.018

63. Chen Y, Gao J, Li L, Sellitto C, Mathias RT, Donaldson PJ, et al. The ciliary muscle and zonules of zinn modulate lens intracellular hydrostatic pressure through transient receptor potential vanilloid channels. *Invest Ophthalmol Vis Sci*. (2019) 60:4416–24. doi: 10.1167/iovs.19-27794

64. Delamere NA, Shahidullah M, Mathias RT, Gao J, Sun X, Sellitto C, et al. Signaling between TRPV1/TRPV4 and intracellular hydrostatic pressure in the mouse lens. *Invest Ophthalmol Vis Sci*. (2020) 61:58. doi: 10.1167/iovs.61.6.58

65. Lu Z, Jiang YP, Wang W, Xu XH, Mathias RT, Entcheva E, et al. Loss of cardiac phosphoinositide 3-kinase P110 alpha results in contractile dysfunction. *Circulation*. (2009) 120:318–25. doi: 10.1161/CIRCULATIONAHA.109.873380

66. Suzuki A, Yamaguchi MT, Ohteki T, Sasaki T, Kaisho T, Kimura Y, et al. T cell-specific loss of Pten leads to defects in central and peripheral tolerance. *Immunity*. (2001) 14:523–34. doi: 10.1016/S1074-7613(01)00134-0

67. Zhao H, Yang Y, Rizo CM, Overbeek PA, Robinson ML. Insertion of a Pax6 consensus binding site into the alphaa-crystallin promoter acts as a lens epithelial cell enhancer in transgenic mice. *Invest Ophthalmol Vis Sci*. (2004) 45:1930–9. doi: 10.1167/iovs.03-0856

68. Sellitto C, Li L, White TW. Double deletion of PI3k and PTEN modifies lens postnatal growth and homeostasis. *Cells*. (2022) 11(17):2708. doi: 10.3390/cells11172708

69. Wiley LA, Shui YB, Beebe DC. Visualizing lens epithelial cell proliferation in whole lenses. *Mol Vis*. (2010) 16:1253–9.

70. Gerido DA, Sellitto C, Li L, White TW. Genetic background influences cataractogenesis, but not lens growth deficiency, in Cx50-knockout mice. *Invest Ophthalmol Vis Sci*. (2003) 44:2669–74. doi: 10.1167/iovs.02-1311

71. Selvam S, Kumar T, Fruttiger M. Retinal vasculature development in health and disease. *Prog Retin Eye Res*. (2018) 63:1–19. doi: 10.1016/j.preteyeres.2017.11.001

72. Mutlu F, Leopold IH. The structure of fetal hyaloid system and tunica vasculosa lentis. *Arch Ophthalmol*. (1964) 71:102–10. doi: 10.1001/archopht.1964.00970010118019

73. Ito M, Yoshioka M. Regression of the hyaloid vessels and pupillary membrane of the mouse. *Anat Embryol (Berl)*. (1999) 200:403–11. doi: 10.1007/s004290050289

74. Giannone AA, Sellitto C, Rosati B, McKinnon D, White TW. Single-cell RNA sequencing analysis of the early postnatal mouse lens epithelium. *Invest Ophthalmol Vis Sci*. (2023) 64:37. doi: 10.1167/iovs.64.13.37

75. Foster FS, Zhang M, Duckett AS, Cucevic V, Pavlin CJ. *In vivo* imaging of embryonic development in the mouse eye by ultrasound biomicroscopy. *Invest Ophthalmol Vis Sci*. (2003) 44:2361–6. doi: 10.1167/iovs.02-0911

76. Mu J, Slevin JC, Qu D, McCormick S, Adamson SL. *In vivo* quantification of embryonic and placental growth during gestation in mice using micro-ultrasound. *Reprod Biol Endocrinol*. (2008) 6:34. doi: 10.1186/1477-7827-6-34

77. Brewitt B, Clark JI. Growth and transparency in the lens, an epithelial tissue, stimulated by pulses of PDGF. *Science*. (1988) 242:777–9. doi: 10.1126/science.3187521

78. Brewitt B, Teller DC, Clark JI. Periods of oscillatory growth in developing ocular lens correspond with cell cycle times. *J Cell Physiol*. (1992) 150:586–92. doi: 10.1002/jcp.1041500320

79. Giannone AA, Li L, Sellitto C, White TW. Physiological mechanisms regulating lens transport. *Front Physiol*. (2021) 12:818649. doi: 10.3389/fphys.2021.818649

80. Mathias RT, Kistler J, Donaldson P. The lens circulation. *J Membr Biol*. (2007) 216:1–16. doi: 10.1007/s00232-007-9019-y

81. Boswell BA, Overbeek PA, Musil LS. Essential role of BMPS in FGF-induced secondary lens fiber differentiation. *Dev Biol*. (2008) 324:202–12. doi: 10.1016/j.ydbio.2008.09.003

82. Li Z, Quan Y, Wang G, Ma B, Gu S, Jiang JX. The second extracellular domain of connexin 50 is important for in cell adhesion, lens differentiation, and adhesion molecule expression. *J Biol Chem*. (2023) 299:102965. doi: 10.1016/j.jbc.2023.102965

Frontiers in Ophthalmology

Research with a vision for the future of ophthalmology and eye health

An exciting new journal which advances our knowledge of the mechanisms underlying eye diseases and disorders, to aid in diagnosis and best management, thereby aiming to prevent visual loss.

Discover the latest Research Topics

See more →

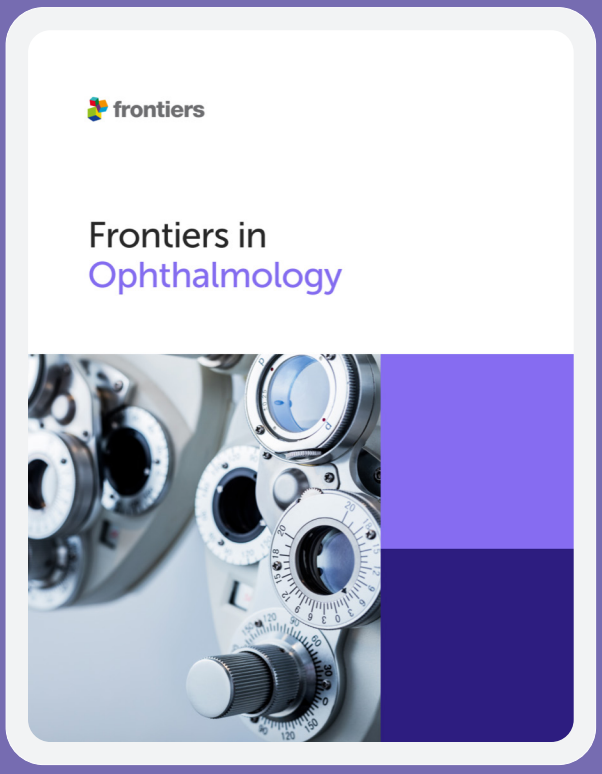

Frontiers

Avenue du Tribunal-Fédéral 34
1005 Lausanne, Switzerland
frontiersin.org

Contact us

+41 (0)21 510 17 00
frontiersin.org/about/contact